LANTHANIDES AND THEIR COMPLEXES FOR THE TREATMENT OF BONE DENSITY DISORDERS

by

YASMIN JENNY MAWANI

B.Sc., McGill University, 2006

A THESIS SUBMITTED IN PARTIAL FULFILLMENT OF

THE REQUIREMENTS FOR THE DEGREE OF

DOCTOR OF PHILOSOPHY

in

THE FACULTY OF GRADUATE STUDIES

(Chemistry)

THE UNIVERSITY OF BRITISH COLUMBIA

(Vancouver)

August 2012

Abstract

Lanthanides are of interest in the treatment of bone density disorders because they are found to accumulate preferentially in bone (*in vivo*), have a stimulatory effect on bone formation, and exhibit an inhibitory effect on bone degradation (*in vitro*), altering the homeostasis of the bone cycle. In an effort to develop an orally active lanthanide drug, a series of 3-hydroxy-4-pyridinone ligands were synthesized and eight of these ligands (H**1** = 3-hydroxy-2-methyl-1-(2-hydroxyethyl)-4-pyridinone, H**2** = 3-hydroxy-2-methyl-1-(3-hydroxypropyl)-4-pyridi-none, H**3** = 3-hydroxy-2-methyl-1-(4-hydroxybutyl)-4-pyridinone, H**4** = 3-hydroxy-2-methyl-1-(2-hydroxypropyl)-4-pyridinone, H**5** = 3-hydroxy-2-methyl-1-(1-hydroxy-3-methylbutan-2-yl)-4-pyridinone, H**6** = 3-hydroxy-2-methyl-1-(1-hydroxybutan-2-yl)-4-pyridinone, H**8** = 1-carboxymethyl-3-hydroxy-2-methyl-4-pyridinone, H**9** = 1-carboxyethyl-3-hydroxy-2-methyl-4-pyridinone) were coordinated to Ln^{3+} (Ln = La, Eu, Gd, Lu) forming stable *tris*-ligand complexes (Ln**L**$_3$, L = **1**$^-$, **2**$^-$, **3**$^-$, **4**$^-$, **5**$^-$, **6**$^-$, **8**$^-$ and **9**$^-$). The dissociation (pK_{an}) and metal ligand stability constants ($\log \beta_n$) of the 3-hydroxy-4-pyridinones with La^{3+} and Gd^{3+} were determined by potentiometric titrations, which demonstrated that the 3-hydroxy-4-pyridinones form stable *tris*-ligand complexes with the lanthanide ions. One phosphinate-EDTA derivative (H$_5$**XT** = bis[[bis(carboxymethyl)amino]methyl]phosphinate) was also synthesized and coordinated to Ln^{3+} (Ln = La, Eu, Lu), forming the potassium salt of $[Ln(\mathbf{XT})]^{2-}$. Lastly, the naturally occurring curcuminoids found in turmeric were separated into the three naturally occurring components (H**Curc** = (1*E*,6*E*)-1-(4-hydroxy-3-methoxyphenyl)-7-(4-hydroxyphenyl)hepta-1,6-diene-3,5-dione, H**DMC** = (1*E*,6*E*)-1,7-bis(4-hydroxy-3-methoxy-phenyl)hepta-1,6-diene-3,5-dione, H**BDMC** = (1*E*,6*E*)-1,7-bis(4-hydroxy-phenyl)hepta-1,6-diene-3,5-dione); H**Curc** was then coordinated to Ln^{3+} (Ln = Eu, Gd, Yb, Lu), forming Ln(**Curc**)$_3$ complexes. The free ligands and metal complexes were studied for their *in vitro* efficacy. Cytotoxicity assays were carried out in MG-63 cells; with the exception of the curcuminoids, all the ligands and metal complexes tested were observed to be non-toxic to this cell line. Further studies to investigate the toxicity, cellular uptake and

apparent permeability (P_{app}) of the lanthanide ions were conducted in Caco-2 cells and it was observed that [La(**XT**)]$^{2-}$ had the greatest cell uptake. Investigation into the binding affinities of free lanthanide ions (Ln = La, Gd and Lu), metal complexes and free 3-hydroxy-4-pyridinones with the bone mineral (HAP) indicate a strong binding affinity of the lanthanide ions for HAP, as well as a moderate to strong interaction of the free ligand with the bone mineral depending on the functional group.

Preface

Portions of Chapter 1 have been published as part of a book chapter: Mawani, Y.; Orvig, C. Essential Metal Related Metabolic Disorders. In *Bioinorganic Medicinal Chemistry*; Alessio, E., Ed.; Wiley: New York, 2011; p 311. I researched and wrote the manuscript, prepared the figures, and formatted the chapter; edits were carried out by myself and Dr. Chris Orvig.

Portions of the content in Chapter 2 pertaining to the synthesis of the compounds H**4**, H**5** and H**6** were performed with the aid of Mr. Stanley Chang. Likewise, the synthesis of compounds Bn**13**, Bn**14** and Bn**15** were performed in collaboration with Mr. Michael Lacasse. I was responsible for the ligand design and directly supervised Mr. Chang and Mr. Lacasse in the synthesis and characterization of the ligands and ligand precursors. With the exception of the help provided by Mr. Chang and Mr. Lacasse (both undergraduates), I synthesized the remaining ligands and metal complexes.

The association and dissociation constant studies reported in Chapter 2 were performed in collaboration with Dr. Jacqueline Cawthray. I was responsible for performing the titrations and Dr. Cawthray performed the data analysis. All discussion pertaining to the stability constants was written by myself.

In Chapter 3, the Caco-2 cell studies (toxicity, uptake and bidirectional transport) were performed in collaboration with Dr. Kristina Sachs-Barrable. Dr. Sachs-Barrable was responsible for growth, maintenance and treatment of the cells, along with the analyses of the TEER values, MTS toxicity studies and BCA protein analysis. I was responsible for the synthesis of the compounds, acid digestion of samples and analyses of Ln(III) content by ICP-MS. All calculations for cell uptake and apparent permeability were conducted by me, as was writing the discussion pertaining to these assays. The determination of the partition coefficients as well as the growth, maintenance and treatment and toxicity studies in MG-63 cells along with the data analysis were carried out by myself.

The isothermal titration calorimetry studies reported in Chapter 4 were conducted in the Michael Smith Laboratories in collaboration with Dr. Louise Creagh and Dr. Jacqueline Cawthray. The sample preparation was performed by Dr. Jacqueline Cawthray, and the titrations were performed by Dr. Creagh. All data was analyzed by Dr. Creagh and all discussion in this thesis was written by myself. The analysis of the PXRDs obtained for the La-rhabdophane was done in collaboration with Dr. Anita Lam, UBC Chemistry X-ray services. Dr. Lam helped identify the production of La-rhabdophane from hydroxyapatite using TOPAS. With the exception of the calorimetry studies, all other hydroxyapatite studies were performed by myself.

I was responsible for the isolation of the curcuminoids, along with the synthesis of the metal complexes reported in Chapter 5.

Table of Contents

List of Tables

List of Figures

List of Schemes

List of Equations

List of Abbreviations

°	degree(s); standard state
°C	degrees Celsius
Å	angstrom, 1×10^{-10} meter
β_n	overall metal ligand stability constant
δ	chemical shift in part per million (ppm)
Δ	change, clockwise handedness (chelate isomers)
$\Delta Q/\Delta t$	flow rate (nmol/s)
Λ	counterclockwise handedness (chelate isomers)
μ	micro (10^{-6})
A	apical, surface area of insert membrane (cm^2)
AA	atomic absorption
ADH	antidiuretic hormone
AHO	Albright's hereditary osteodystrophy
alendronate	4-amino-1-hydroxybutane-1,1-diphosphonic acid
Anal.	analytical
AP-1	activator protein-1
ATCC	American Type Culture Collection
ATP	adenosine triphosphate
ATPase	adenosine triphosphatase

B	basolateral
B.M.	Bohr magneton
BCA	bicinchoninic acid protein assay
benzylmaltol	3-benzyloxy-2-methyl-4-pyrone
BET	Brunauer-Emmett-Teller
bisdemethoxycurcumin	(1E,6E)-1,7-bis(4-hydroxyphenyl)hepta-1,6-diene-3,5-dione
Bn	benzyl
Bn**1**	3-benzyloxy-2-methyl-1-(2-hydroxyethyl)-4-pyridinone
Bn**2**•HCl	3-benzyloxy-2-methyl-1-(3-hydroxypropyl)-4-pyridinone hydrochloride
Bn**3**•HCl	3-benzyloxy-2-methyl-1-(4-hydroxybutyl)-4-pyridinone hydrochloride
Bn**4**	3-benzyloxy-2-methyl-1-(2-hydroxypropyl)-4-pyridinone
Bn**5**	3-benzyloxy-2-methyl-1-(1-hydroxy-3-methylbutan-2-yl)-4-pyridinone
Bn**6**	3-benzyloxy-2-methyl-1-(1-hydroxybutan-2-yl)-4-pyridinone
Bn**7**	3-benzyloxy-2-methyl-1-(2,3-dihydroxypropyl)-4-pyridinone
Bn**9**	1-carboxyethyl-3-benzyloxy-2-methyl-4-pyridinone
Bn**10**	(4-(3-(benzyloxy)-2-methyl-4-oxopyridin-1-yl)-1-hydroxybutane-1,1-diyl)diphosphonic acid
Bn**11**	2-(3-(benzyloxy)-2-methyl-4-oxopyridin-1-yl)ethyl dihydrogen phosphate
Bn**12**	3-(3-(benzyloxy)-2-methyl-4-oxopyridin-1-yl)propyl dihydrogen phosphate

Bn**13**	4-(3-(benzyloxy)-2-methyl-4-oxopyridin-1-yl)butyl dihydrogen phosphate
Bn**14**	1-(3-(benzyloxy)-2-methyl-4-oxopyridin-1-yl)propan-2-yl dihydrogen phosphate
Bn**15**	2-(3-(benzyloxy)-2-methyl-4-oxopyridin-1-yl)butyl dihydrogen phosphate
Bn**L**	3-benzyloxy-2-methyl-4-pyridinone
Bn**ma**	3-benzyloxy-2-methyl-4-pyrone
BP	bisphosphonate or diphosphonic acid
BP-**DOTA**	(3-(2-(4,7,10-tris(carboxymethyl)-1,4,7,10-tetraazacyclododecan-1-yl)acetamido)propane-1,1-diyl)bis(phosphonate).
BP-OH	hydroxyl-bisphosphonate or hydoxyl-disphosphonic acid
br.	broad (NMR)
BSA	bovine serum albumin
Caco-2	cell line derived from a human colon adenocarcinoma
Calc.	calculated
calcitriol	1,25-dihydroxycholecalciferol or 1,25-dihydroxyvitamin D_3
cAMP	cyclic adenosine monophosphate
CCC	countercurrent chromatography
cisplatin	*cis*-diamminedichloroplanitum(II)
CKD	chronic kidney disease
cm	centimeters
CN	coordination number

C_o	initial concentration (µM)
curcumin	(1E,6E)-1,7-bis(4-hydroxy-3-methoxyphenyl)hepta-1,6-diene-3,5-dione
d	doublet (NMR); day(s)
dd	doublet of doublets (NMR)
deferiprone	3-hydroxy-1,2-dimethyl-4-pyridinone
demethoxycurcumin	(1E,6E)-1-(4-hydroxy-3-methoxyphenyl)-7-(4-hydroxyphenyl)hepta-1,6-diene-3,5-dione
DMEM	Dulbecco's modified Eagle's medium
DMSO	dimethylsulfoxide
DNA	deoxyribonucleic acid
DPG	diphosphoglycerate
DTPP	diethylenetriaminepenta(methylene phosphonate)
EA	elemental analysis
EC_{50}	half maximal effective concentration
ECF	extracellular fluid
EDTA	ethylenediaminetetraacetic acid
EDTMP	ethylenediaminetetra(methylene phosphonate)
ENRD	end stage renal disease
EPR	electron paramagnetic resonance
ESI-MS	electrospray ionization mass spectrometry
ethyl maltol	3-hydroxy-2-ethyl-4-pyrone
equiv	equivalent

fac	facial
FBS	fetal bovine serum
FDA	Food and Drug Administration
Ferriprox[TM]	3-hydroxy-2-methyl-4-pyrone
Flammacerium[TM]	cerium nitrate
Fosrenol[TM]	lanthanum carbonate, $La_2(CO_3)_3$
FTIR	Fourier transform infrared spectroscopy
g	gram
G	Gibbs free energy
GI	gastrointestinal
G_s	GTP (guanosine triphosphate) binding protein
h	hour(s)
H	enthalpy
H. pylori	Helicobacter pylori
H**1**	3-hydroxy-2-methyl-1-(2-hydroxyethyl)-4-pyridinone
H**2**•HCl	3-hydroxy-2-methyl-1-(3-hydroxypropyl)-4-pyridinone hydrochloride
H**3**•HCl	3-hydroxy-2-methyl-1-(4-hydroxybutyl)-4-pyridinone hydrochloride
H**4**	3-hydroxy-2-methyl-1-(2-hydroxypropyl)-4-pyridinone
H**5**	3-hydroxy-2-methyl-1-(1-hydroxy-3-methylbutan-2-yl)-4-pyridinone
H**6**	3-hydroxy-2-methyl-1-(1-hydroxybutan-2-yl)-4-pyridinone

H**7**	3-hydroxy-2-methyl-1-(2,3-dihydroxypropyl)-4-pyridinone
H**8**	1-carboxymethyl-3-hydroxy-2-methyl-4-pyridinone
H**9**	1-carboxyethyl-3-hydroxy-2-methyl-4-pyridinone
H**10**	(4-(3-(hydroxy)-2-methyl-4-oxopyridin-1-yl)-1-hydroxybutane-1,1-diyl)diphosphonic acid
H**11**	2-(3-hydroxy-2-methyl-4-oxopyridin-1-yl)ethyl dihydrogen phosphate
H**12**	3-(3-hydroxy-2-methyl-4-oxopyridin-1-yl)propyl dihydrogen phosphate
H**13**	4-(3-hydroxy-2-methyl-4-oxopyridin-1-yl)butyl dihydrogen phosphate
H**14**	1-(3-hydroxy-2-methyl-4-oxopyridin-1-yl)propan-2-yl dihydrogen phosphate
H**15**	2-(3-hydroxy-2-methyl-4-oxopyridin-1-yl)butyl dihydrogen phosphate
H**16**	3-hydroxy-2-methyl-1-propyl-4-pyridinone
H$_4$**DOTA**	1,4,7,10-tetrazacyclododecane-1,4,7,10-tetraacetic acid.
H$_4$**EDTA**	ethylenediaminetetraacetic acid
H$_5$**DTPA**	diethylenetriaminepentaacetic acid
H$_5$**XT**	bis[[bis(carboxymethyl)amino]methyl]phosphinate
HAP	hydroxyapatite, $Ca_5(PO_4)_3OH$
H**BDMC**	(1E,6E)-1,7-bis(4-hydroxyphenyl)hepta-1,6-diene-3,5-dione
HBSS	Hank's balanced salt solution
H**Curc**	(1E,6E)-1,7-bis(4-hydroxy-3-methoxyphenyl)hepta-1,6-diene-3,5-dione

H**DMC**	(1*E*,6*E*)-1-(4-hydroxy-3-methoxyphenyl)-7-(4-hydroxyphenyl)hepta-1,6-diene-3,5-dione
H**ema**	3-hydroxy-2-ethyl-4-pyrone
HEPES	4-(2-hydroxyethyl)-1-piperazineethanesulfonic acid
H**L**	3-hydroxy-2-methyl-4-pyridinone
H**L1**	3-hydroxy-1,2-dimethyl-4-pyridinone
H**ma**	3-hydroxy-2-methyl-4-pyrone
H**mpp**	3-hydroxy-2-methyl-4-pyridinone
HPLC	high-performance liquid chromatograph
HPT	hyperparathyroidism
HPTLC	high-performance thin layer liquid chromatography
HRMS	high resolution mass spectrometry
Hz	hertz (s^{-1})
ICP	inductively coupled plasma
IR	infrared spectroscopy
ITC	isothermal titration calorimetry
IUPAC	International Union of Pure and Applied Chemistry
IV	intravenous
K	Kelvin
K_{app}	apparent binding affinity
K_{eq}	equilibrium constant
K_n	stepwise metal ligand stability constant, n = integer

kojic acid	5-hydroxy-2-(hydroxymethyl)-4-pyrone
L	litre
Ln	lanthanide(s)
Ln(**L**)$_3$	*tris*(3-oxy-2-methyl-4-pyridinonato)lanthanide(III)
log K	stability constant (formation constant)
m	meter, milli (10^{-3})
M	mega (10^6)
M	molarity (mol/L)
m/z	mass-to-charge ratio
MALDI-TOF	matrix-assisted laser desorption/ionization-time of flight
maltol	3-hydroxy-2-methyl-4-pyrone
MEEKC	microemulsion electrokinetic chromatography
Me**L**	3-methoxy-2-methyl-4-pyridinone
MEM-α	minimum essential medium alpha
mer	meridional
methylmaltol	3-hydroxy-2-methyl-4-pyrone
MG-63	cell line derived from a human osteosarcoma
MHz	megahertz
Miacalcin^{TM}	salmon calcitonin
min	minute(s)
mol	mole (6.02 x 10^{23} molecules)
MRI	magnetic resonance imaging

mRNA	messenger ribonucleic acid
MS	mass spectrometry
MTS	3-(4,5-dimethylthiazol-2-yl)-5-(3-carboxymethoxyphenyl)-2-(4-sulfophenyl)-2H-tetrazolium
MTT	3-(4,5-dimethylthiazol-2-yl)-2,5-diphenyltetrazolium bromide
n	nano; integer
Na_2H_2EDTA	disodium ethylenediaminetetraacetic acid
n.d.	not determined
NFκB	nuclear factor κB
NMR	nuclear magnetic resonance
NO	not observed
NSAIDs	non-steroidal anti-inflammatory drugs
octanol	1-octanol
OPG	osteoprotegerin
OVX	ovariectomized
P	partition coefficient
P_{app}	apparent permeability
$P_{o/w}$	octanol-water partition coefficient
PBS	phosphate buffer solution
Pd on C	palladium on carbon
Pd/C	palladium on carbon
Pen-Strep	penicillin-streptomycin-neomycin 100X

PET	positron emission tomography
pH	potential hydrogen, $-\log[H^+]$
PHP	pseudohypoparathyroidism
pK_a	acid dissociation constant
PPH	pseudopseudohypoparathyroidism
ppm	part per million, mg/L
prep-TLC	preparative thin layer chromatography
PTH	parathyroid hormone
PXRD	powder X-ray diffraction
pyromeconic acid	3-hydroxy-4-pyrone
Quadramet^{TM}	samarium (^{153}Sm) lexidronam
R	gas constant
R	*Rectus*, right handedness (clockwise)
RANKL	RANK ligand
RIPA	radioimmunoprecipitation assay
RNA	ribonucleic acid
ROD	renal osteodystrophy
RPM	revolutions per minute
RT	room temperature, 20–25 °C
s	Second; singlet (NMR)
S	total spin angular momentum quantum number; entropy
S	*Sinister*, left handedness (counterclockwise)

SD	standard deviation
SERM	selective estrogen receptor modulator
SPECT	single photon emission computed tomography
STP	standard temperature and pressure (273.15 K, 100 kPa)
t	triplet (NMR)
T	temperature (K)
TEER	transepithelial electrical resistance
TGA	thermogravimetric analysis
THF	tetrahydrofuran
TLC	thin layer chromatography
TLS	tumor-lysis syndrome
TNSALP	tissue-nonspecific of alkaline phosphatase
Torr	torr, pressure unit (1 Torr = 133.322 Pascals)
UV	ultraviolet
UV-vis	ultraviolet-visible
V_o	initial volume (titration, Gran plot)
V_t	volume of titrant added (Gran plot)
vis	visible
vitamin D_2	ergocalciferol
vitamin D_3	cholecalciferol
w/v	weight by volume
w/w	weight by weight

w   weak (FTIR)

Acknowledgments

Shukran Allah. Thank you to my parents and brother for their unwavering emotional support over the course of this degree; Salim, a big thank you for letting me use your condo and car for the last few years. Thank you to all of my family here in Vancouver, my mamas Kayber, Munir and Riyaz, my aunties Ruzmin, Naz and Bilkis, my Nanima and all of my cousins, for all of your help and especially for keeping me well fed. A big thanks to all my friends here in Vancouver for all their support and encouragement.

I would like to acknowledge my supervisor, Chris Orvig, for being so supportive and allowing me to take the project in the direction of my choice. Thank you to my three wonderful undergrads, Stan, Scott and Mike. Cheri, thank you for giving me a great project to continue; Meryn, Lauren, Jacquie, Lisa, Christoph and Paloma, thank you for helping me in lab and thank you for being such a wonderful labmates and friends. Dave, Maria, Eric, Caterina, Cristina and Katja thank you for all your support, encouragement, friendship and the wonderful laughs in lab. Kristina Sachs-Barrable, Kishor Wasan, Rizhi Wang, Louise Creagh, Robin Stoodley, Vivian Lai, Anita Lam, Elena Polishcuk and Jessie Chen, thank you for all of your help and knowledge about cells, ITC, ICP-MS and hydroxyapatite.

None of the work in this thesis would have been possible with the aforementioned people. *Wal Hamduliallah.*

To my mom, the strongest person I know. I pray that one day I can possess half your strength, courage and perseverance.

Chapter 1. Introduction

1.1　Electrolyte Disturbances and Metabolic Bone Density Disorders

The physiological importance of metals in humans, especially in blood, is well known. At low concentrations, essential metals play an important role in metabolism and enzymatic processes, and as functional components of proteins. At high concentrations, these metals can lead to serious health problems and even death.[1] The ability of our bodies to maintain a constant internal state with varying external conditions is essential for survival. This is called homeostasis, a state in which the nutrient flow within an organism is at a steady state. The importance of this steady state can be seen in Figure 1.1, where extreme deficiency or overload of the essential metal, if untreated, can lead to death.
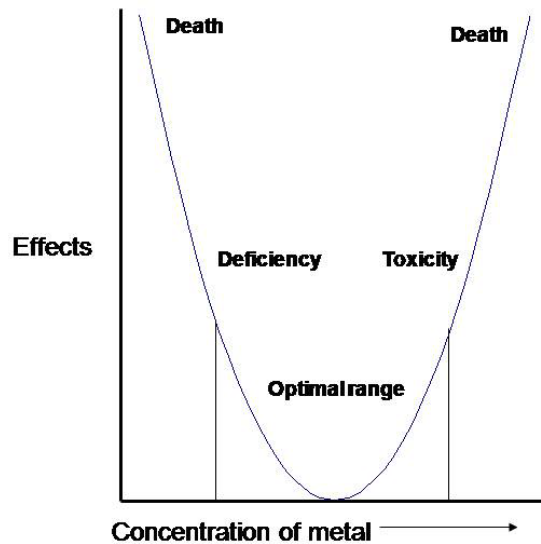
Figure 1.1. Dose-effect curve demonstrating the biological effect of essential metals.[2]

Maintenance of fluid and electrolyte homeostasis intra- and extracellularly is critical for normal muscular function, nerve function, hydration, and pH balance. The kidneys play a key role in maintaining homeostasis of electrolyte and fluid balance in a wide variety of environments. Renal disease thus almost always leads to a number of electrolytic disorders.[3]

The role of alkali and alkaline earth metals in clinical medicine, nutrition and physiology is of interest; for example, calcium and phosphorus make up the structural component of our bones, potassium has a potent protective effect against cardiovascular disease, and magnesium deficiency causes cardiac arrhythmia and disruption of the nervous system.[1] Maintenance of fluid and electrolyte balance is especially important as the homeostasis of these metals is inter-related. Magnesium deficiency causes potassium deficiency; vitamin D affects the serum concentrations of both phosphorus and calcium. Many diseases cause a multitude of electrolyte disorders and are all related to the renal and kidney function, as shown schematically in Figure 1.2. A summary of diseases that cause an imbalance in electrolyte homeostasis can be found in Table 1.1.[4-7]

As bone is primarily made up of calcium and phosphorus, understanding the homeostasis of these two electrolytes is essential to understanding what makes bones healthy. In the following sections the homeostasis of the electrolytes calcium, magnesium, phosphates, sodium, and potassium will be discussed. The focus will be on the effect of disturbances of calcium, phosphorus, and the two hormones that control calcium and phosphorus metabolism, vitamin D and the parathyroid hormone, along with metabolic disorders that can cause imbalances of the aforementioned electrolytes.

Table 1.1. Causes of deficiency and overload of electrolytes of Ca, K, Mg, and P.[4,5,7]

Hypocalcemia	Hypomagnesemia	Hypophosphatemia	Hypokalemia
Factitious: 　Sample contamination with EDTA *Normal plasma ionized with reduced total calcium:* 　Hypoalbuminemia 　Reduced plasma ionized with normal total calcium 　Respiratory alkalosis *Reduced plasma ionized with normal total calcium* 　Hypoparathyroidism 　Malabsorption of vitamin D 　Vitamin D resistant rickets 　Rhabdomyolysis 　Pancreatitis *Hyperphosphatemia*	*Redistribution:* 　Hungry bone syndrome 　Catecholamine excess 　Massive blood transfusion *Gastrointestinal disorders (GI):* 　Malabsorption 　Short-bowel syndrome 　GI tract fistulas, diarrhea 　Pancreatitis *Renal losses:* 　Reduced sodium reabsorption 　Bartter's and Gitleman's syndromes *Endocrine disorders:* 　Hypercalcemia 　Hyperparathyroidism 　Hyperthyroidism 　Hyperaldosteronism *Alcoholism, Diuretics*	*Redistribution:* 　Malnutrition 　Diabetic ketoacidosis 　Respiratory alkalosis 　Hormones 　Rapid cell proliferation (hungry bone syndrome, acute leukemia, Burkitt's lymphoma) *Increased urinary excretion:* 　Hyperparathyroidism 　Vitamin D and PTH deficiency 　Fanconi syndrome 　Alcoholsim 　Drugs - diuretics 　Glucocorticoids 　Kidney transplant *Decreased intestinal absorption:* 　Phosphate binders 　Diarrhea, vomiting	*Inadequate intake* *Increased excretion:* 　Diarrhea, laxative abuse *Renal losses:* 　Loop, thiazide diuretics 　Metabolic alkalosis 　Osmotic dieresis 　Bartter's and Gitleman's syndromes 　Glucocorticoids *Magnesium depletion* *Renal tubular acidosis*

Hypercalcemia	Hypermagnesemia	Hyperphosphatemia	Hyperkalemia
Factitious	Acidosis	*Factitious*	*Factitious:*
Carcinomas:	Hemolysis	*Redistribtution:*	Thrombocytosis
Primary (lymphoma)	Excessive administration of Mg^{2+} salts	Trauma	Leukocytosis
Secondary (breast,	(enemas, cathartics) in the presence of renal	Rhabdomyolysis	Hemolysis
renal)	failure	Acidosis (keto and lactic)	*Impaired potassium excretion:*
Paget's disease		Tumor lysis	Renal insufficiency or
Hyperparathyroidism		Bisphosphonate therapy	failure
Renal failure		*Vitamin D toxicity*	Mineralocorticoid
Vitamin A & D toxicity		*Renal retention:*	deficiency
Drugs - lithium, diuretics		Renal failure	*Drugs:*
Endocrine		Hypoparathyroidism	Non-steroidal anti-
Addison's disease		Pseudohypoparathyrodism	inflammatory drugs
			(NSAIDs)
			Diuretics
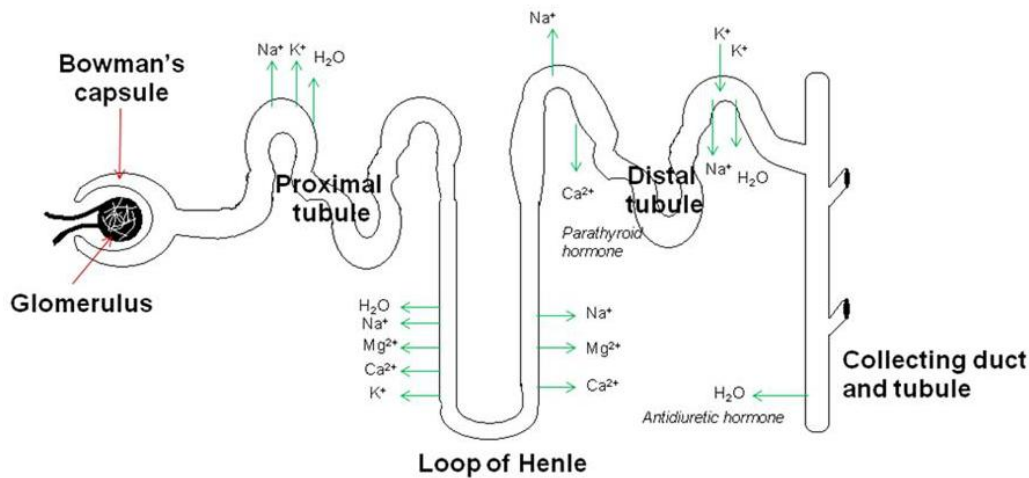
Figure 1.2. Renal physiology and electrolyte reabsorption.[2]

1.1.1   Parathyroid Hormone

The expression of the parathyroid hormone (PTH) gene that synthesizes the parathyroid hormone is regulated by a number of factors, most importantly the concentration of serum calcium, but vitamin D and serum phosphate levels also regulate PTH synthesis. The active form of vitamin D_3, calcitriol (see Chapter 1.1.3), decreases the transcription of the PTH gene.[8] When there is a decrease in ionized calcium levels in the blood, there is an increase in PTH. The PTH receptor is expressed by osteoblasts (which build bone), osteocytes and bone-lining cells, but not osteoclasts (which remodel bone). A decrease in extracellular calcium leads to a rapid increase in PTH secretion, whereas an increase in calcium concentration inhibits the secretion of PTH. The surface of the calcium-sensing receptor of the parathyroid cell contains a large extracellular domain for the binding of cations.[9]

The primary function of PTH is maintenance of plasma calcium levels, as seen in Figure 1.3. This occurs by withdrawing the calcium from bone tissue, reabsorbing it from the glomerular filtrate (intestine), and indirectly increasing its intestinal absorption by stimulating calcitriol production.[10]
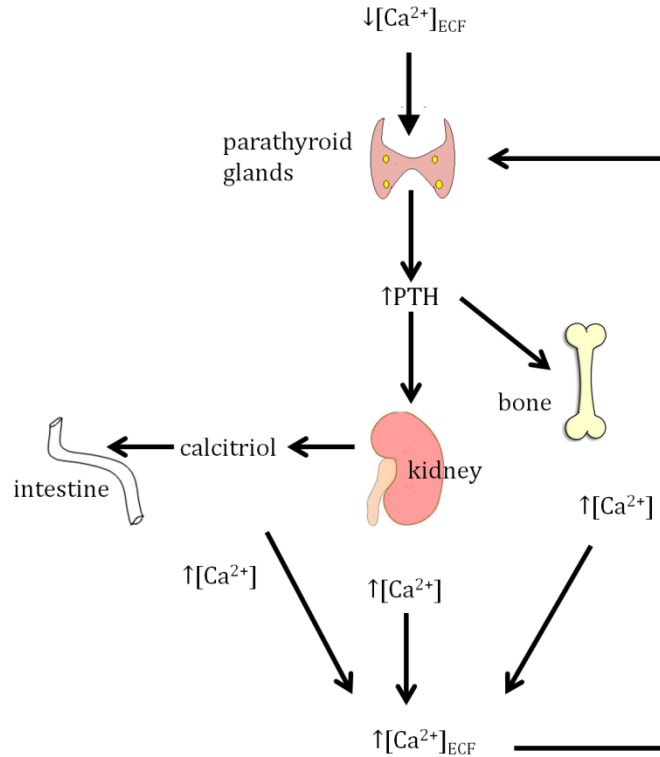
Figure 1.3. Endocrine regulation of extracellular fluid (ECF) calcium ion concentration $[Ca^{2+}]_{ECF}$. The two hormones that are responsible for maintaining calcium levels are parathyroid hormone (PTH) and active form of vitamin D_3 (calcitriol). Hypocalcemia (low ECF calcium levels) stimulates the secretion of the parathyroid hormone (PTH) from the parathyroid glands. PTH then stimulates the release of Ca^{2+} from the bone, promoting bone resorption, it stimulates the reabsorption of Ca^{2+} in the small intestine, decreasing calcium ion loss from the urine and it stimulates the synthesis of calcitriol by the kidneys, thus indirectly increasing absorption of Ca^{2+} in the small intestine. This increase in ECF calcium feeds back on the parathyroid glands, decreasing the secretion of PTH.[11]

1.1.2   Diseases Related to the Parathyroid Hormone

Hypoparathyroidism

Hypoparathyroidism is caused by a decrease in the function of the parathyroid glands, leading to a decrease in the level of PTH, which can lead to hypocalcemia. Two mechanisms

may alter the function of the parathyroid hormone, limiting its control on calcium: 1) insufficient PTH production by the parathyroid glands, called hypoparathyroidism, and 2) a resistance against its action in target tissues called pseudohypoparathyroidism, which is discussed below. Both cases result in significantly reduced levels of plasma calcium associated with hyperphosphatemia (see Chapter 1.1.5).[10]

Causes of low PTH include destruction of the parathyroid by surgery, auto-immune disorders, reduction in parathyroid function caused by hypomagnesemia (see Chapter 1.1.4), PTH gene defects and calcium sensing receptor mutations or parathyroid agenesis caused by DiGeorge Syndrome, isolated x-linked hypoparathyroidism and mitochondrial neuropathies.[10] Laboratory measurements present as hypocalcemia (see Chapter 1.1.7), hyperphosphatemia (see Chapter 1.1.5), low PTH levels and generally calcitriol levels are low as well. Symptoms of hypoparathyroidism are the same as for that of hypocalcemia; hypomagnesemia may also cause hypoparathyroidism because it promotes PTH secretion levels to drop, in addition to causing renal and bone resistance to PTH action.

Pseudohypoparathyroidism

Pseudohypoparathyroidism (PHP) is a group of abnormalities characterized by clinical indications of hypoparathyroidism (hypocalcemia, hyperphosphatemia), but with the presence of high levels of PTH in the absence of chronic renal failure or magnesium deficiency.[10] In 1942, Fuller Albright reported seeing a patient with seizures, hypocalcaemia and hyperphosphatemia, who did not respond to treatment with parathyroid extract.[12] It was concluded that the patient was resistant to PTH and the disease was called pseudohypoparathyroidism or PHP. Pseudohypoparathyroidism manifests as short stocky build, round face and cutaneous ossification. This physical appearance is known as Albright's hereditary osteodystrophy (AHO). A decade later, Fuller Albright described a patient with typical features of AHO, but who manifested with normal serum calcium and phosphate levels and the absence of PTH resistance. This disease was called pseudopseudohypoparathyroidism (PPHP).[12]

PTH exerts itself by stimulating the intracellular formation of cAMP. The signal-transducing protein known as G_s (a GTP binding protein), comprised of α, β and γ subunits, helps to stimulate cAMP formation by coupling to receptors for hormones, such as PTH. The $G_{s\alpha}$ subunit activity in patients with PHP has been shown to be reduced significantly (~50%). Thus patients suffering from AHO show resistance to other hormones, such as TSH (thyroid-stimulating hormone). Surprisingly, individuals suffering from PPHP do not lack the activity of the $G_{s\alpha}$ protein, despite the lack of PTH resistance.[12,13] The gene presents with parental imprinting phenomenon, which explains the phenotypic variations of the disease, depending whether the mutation origin is maternal or paternal.[10] The gene is present as a single copy per haploid, and heterozygous loss of function is present in both PHP and PPHP patients.[12] Patients who manifest with PHP were found to result exclusively from maternal transmission and patients with PPHP from paternal.[10,12]

Hyperparathyroidism (HPT)

Primary hyperparathyroidism

Primary hyperparathyroidism is a disease caused by excessive secretion of the parathyroid hormone, manifesting as hypercalcemia (see Chapter 1.1.7). Adenoma, hyperplasia and carcinoma have all been attributed to primary HPT.[14] When extracellular calcium binds to the calcium receptor in the parathyroid cell, PTH secretion is inhibited. At the kidneys this interaction between calcium and the calcium receptor inhibits the production of the active form of vitamin D_3.[15]

In primary hyperparathyroidism, mutations of the calcium receptor gene have not been identified; however, significant reductions in calcium receptor messenger ribonucleic acid (mRNA) levels have been detected in parathyroid adenomas, a benign glandular tumor. The pathophysiological significance of this observation is unclear because the reductions could be secondary to the chronic hypercalcemia and not the primary case.[15]

Primary HPT is associated with a reduction in bone mineral density, generally a silent symptom.[15] Symptomatic patients with primary HPT presented with nephrolithiasis (kidney stones), osteitis fibrosa cystica, muscle atrophy, hyperreflexia, gait abnormalities and other neuromuscular signs and present with hypercalcemia and its associated symptoms. When primary HPT occurs in the absence of hypercalcemia, patients tend to be asymptomatic. Nephrolithiasis is its major clinical manifestation of primary HPT (formation of kidney stones, calcification).[14]

For patients whose serum calcium levels are > 3mM, the recommended course of treatment is a parathyroidectomy. Hormone replacement therapy has seen some success. Bisphosphonates (see Chapter 1.6) have also seen some use, as they decrease serum calcium levels and decrease bone loss, but do not affect PTH levels.[14]

Secondary hyperparathyroidism

Secondary hyperparathyroidism is caused by an increase in PTH because of hypocalcemia (see Chapter 1.1.7), without disturbances to the production of calcitriol, or calcium and phosphorus metabolism and is usually caused by chronic kidney disease (CKD). PTH levels begin to rise in the course of CKD when normal serum levels of phosphorus, calcitriol and calcium are observed. A decrease in calcitriol leads to a decrease in calcium absorption which leads to a decrease in ionized calcium. This leads to an increase in PTH (because of decreased ionized Ca levels), which normalizes calcitriol and restores serum calcium values. As loss of kidney function progresses, phosphorus is retained and calcitriol production decreases.[14,16] Symptoms include many of those seen in primary HPT: arthritis, bone pain, myopathy, tendon rupture, extraskeletal calcifications and low bone turnover. Secondary HPT is easier to prevent than to treat; vitamin D replacement and the administration of phosphate binders, are the mainstays of prevention.[14]

1.1.3 Vitamin D

Vitamin D has two main forms, vitamin D_2 (ergocalciferol) and vitamin D_3 (cholecalciferol) as seen in Figure 1.4. Vitamin D_2 is synthesized by plants while D_3 is synthesized in humans. Vitamin D_3 is synthesized in the skin by direct exposure to UV B radiation from the sun or is obtained directly from the diet. The use of sunscreen, darker skin or lack of exposure to sunlight can lead to vitamin D deficiency.[17]

Vitamin D_3 is metabolized by the liver to 25-hydroxyvitamin D_3, which is then metabolized by the kidneys to the active form of vitamin D_3, 1,25-dihydroxyvitamin D_3, also known as calcitriol. The production of calcitriol is stimulated by the PTH (see Chapter 1.1.1), and is regulated by the serum concentrations of calcitriol, PTH, calcium (see Chapter 1.1.7) and phosphate (see Chapter 1.1.5).[17]

vitamin D_2
ergocalciferol

vitamin D_3
cholecalciferol
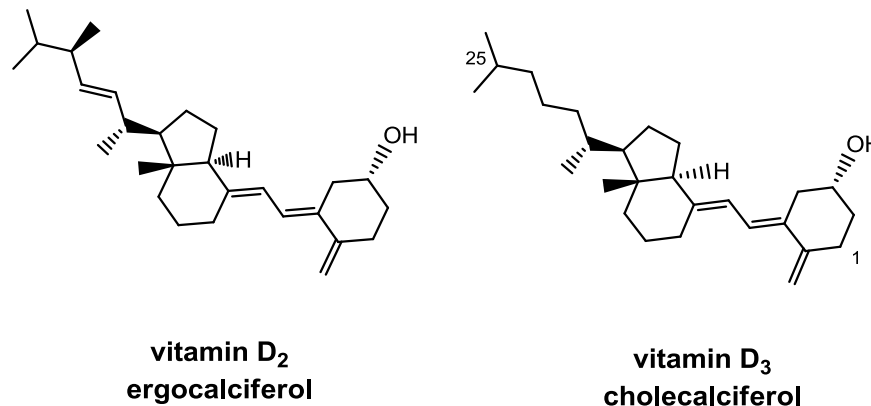
Figure 1.4. The two forms of vitamin D: vitamin D_2 (ergocalciferol) and vitamin D_3 (cholecalciferol). The 1- and 25- positions of vitamin D_3 are marked to indicate the sites that undergo metabolism to form the active metabolite of vitamin D_3 (1,25-dihydroxyvitamin D_3) generally referred to as calcitriol.[17]

Vitamin D helps the intestinal absorption of calcium and phosphate. Calcium enters the cell through membrane proteins, in the intestinal cell, calcitriol enters, binds to the vitamin D

receptor and the calcium binding protein is synthesized, regulating the active transport of calcium through the cell.[17] There is a negative feedback through calcium which decreases PTH and a direct negative feedback from calcitriol to PTH.

1.1.4 The Role and Metabolism of Sodium, Potassium and Magnesium in the Body

Sodium is the most abundant cation in the body and is generally found in the extracellular compartment, with the exception of blood cells, which have a high intracellular sodium concentration. Sodium is critical for osmoregulation, nerve function and muscle function. Absorption of sodium occurs through the jejunum and ileum of the small intestine, and is excreted through sweat and urine.[18]

Healthy kidneys maintain a constant sodium level by adjusting the amount of sodium excreted in urine, thus disorders of sodium metabolism are generally only seen in patients whose kidney function is impaired. The kidneys help maintain sodium balance by stimulating adrenal glands to secrete aldosterone, which causes the kidneys to retain sodium and excrete potassium. Urinary dilution is determined by arginine vasopressin, also known as antidiuretic hormone (ADH), which is produced by the pituitary gland. ADH causes the kidneys to conserve fluid and increase blood volume, helping to regulate the body's retention of water.[19] When ADH is produced, concentrated urine is produced by water reabsorption across the renal collecting ducts, as seen in Figure 1.2.

Despite many foods being high in sodium, and dietary variations in salt and water intake, plasma sodium concentration is finely tuned within a small range of 135–145 mM.[20] Disorders of sodium balance are a common clinical manifestation, seen in hospitalized patients and the elderly. In mild cases sodium disorders generally are symptomless, but in extreme cases can lead to morbidity. Most cases of sodium balance disorders are iatrogenic—meaning they are unavoidable in certain medical treatments. Disorders of sodium balance—hyponatremia (low sodium) and hypernatremia (high sodium)—are the

11

most common electrolytic disturbances seen in hospitalized patients and clinical medicine, and are discussed below.[20]

Potassium is the most abundant intracellular cation—with only 2% found in the extracellular fluid.[21] Potassium plays a vital role in maintaining intracellular osmotic pressure by polarizing membranes. These polarized membranes help conduct nerve impulses and muscle cell contraction. β-Adrenergic activity and insulin levels affect the concentration of potassium in and out of cells. Insulin and β-adrenergic stimulation move potassium into cells; the mechanism by which β-adrenergic activity moves K^+ into cells has not been identified. Small changes in serum potassium concentration can have detrimental clinical manifestations.[7]

In a healthy individual, serum potassium levels are between 3.5–5 mM.[22] Potassium intake is unregulated, with the average adult consuming between 40-100 mmol/day; however excretion increases with intake, so homeostasis of potassium is usually easily maintained. Once potassium is absorbed insulin is released, stimulating N^+/K^+ ATPase activity, which helps facilitate its entrance into cells. A rise in potassium also stimulates aldosterone secretion, stimulating its excretion within thirty minutes of ingestion. Ninety percent of potassium is excreted by the kidneys and the other 10% by the stool.[7] Hypokalemia (low potassium) and hyperkalemia (high potassium) can result from an impairment in renal activity or in a perturbation of transcellular homeostasis. A summary of causes of disturbances in potassium homeostasis can be seen in Table 1.1.

Magnesium is the fourth most abundant cation in the body and the second most prevalent intracellular cation.[23] Magnesium is an essential trace metal that is primarily found in bone and intracellularly bound as a metallo-cofactor; the total distribution of magnesium in the body is reported in Table 1.2.[24,25] Magnesium is essential for over 300 phosphate transfer reactions as well as energy transfer, as it plays a vital role in the production of adenosine triphosphate (ATP); it is also involved in protein and nucleic acid synthesis. Unlike serum calcium and phosphate levels, PTH and vitamin D do not regulate magnesium metabolism.[23]

Table 1.2. Distribution of magnesium in the body of a 70 kg individual.[24]

	mmol
Bone	60 – 65
Intracellular (bound)	365
(free)	25
Extracellular fluid (ECF)	10

Normal serum levels of total magnesium are 0.8–1.2 mM (with ionic magnesium plasma levels of 0.7–0.96 mM), where ionic concentration of magnesium is approximately the same in the extra- and intracellular compartments.[22,24] Intracellular magnesium homeostasis is well managed, thus changes in magnesium homeostasis are caused by extracellular disturbances.[25] Average daily magnesium intake is approximately 8–20 mmol (300–350 mg), and total body magnesium levels depend on kidney function and gastrointestinal (GI) absorption.[23] Of this, 40% is absorbed in the jejunum and ileum of the small intestine by passive absorption. Urinary loss accounts for 2.5–8 mmol/day, filtration by the glomerulus (Figure 1.2) is 100 mmol/day in the kidney. Of this only 10–15% is absorbed into the proximal tubule, 60–70% is reabsorbed in the cortical thick ascending limb of the loop of Henle, 10–15% in the distal tube and 5% is excreted.[24,25] There is a large abundance in our diet, however, there is no indication that magnesium homeostasis is under specific tight hormonal control, despite its importance to many physiological processes in the body.[25]

As the metabolism of sodium, potassium and magnesium are not controlled by the parathyroid hormone or vitamin D synthesis, no further discussion will be made on these electrolytes. Table 1.1 is a summary of the causes of the metabolic disorders of magnesium and potassium: hypomagnesemia (low magnesium), hypermagnesemia (high magnesium), hypokalemia (low potassium) and hyperkalemia (high potassium). Figure 1.2 shows the renal

loss and absorption of sodium, potassium and magnesium. The reader is referred to Chapter 11: Essential Metal Related Metabolic Disorders in Bioinorganic Medicinal Chemistry by Mawani and Orvig[2] for an exhaustive review of the metabolic disorders of sodium, potassium and magnesium.

1.1.5   The Role, Metabolism and Metabolic Disorders of Phosphorus

Phosphorus is ubiquitous in the body; in a healthy 70 kg adult the total body phosphorus content is 700 g, with serum phosphate levels between 0.89–1.44 mM.[23] Phosphorus is an essential element that is found bound to oxygen as phosphate. Most of this phosphorus, approximately 80%, is found in bone and teeth, 9% in skeletal muscle, ~11% in other tissues and approximately 0.1% in the extracellular fluid.[6,23]

Phosphate is a vital component of nucleic acids forming the backbone of DNA and RNA and constitutes an important component of the lipid bilayer. Most intracellular phosphate is bound to ATP and phosphocreatine. Phosphocreatine is an important energy store for skeletal muscle and the brain. Most of the inorganic phosphorus found in the body is as free phosphate, existing as $H_2PO_4^-$, HPO_4^{2-} and PO_4^{3-}. Approximately 10% is found complexed to proteins, and 5% to calcium, magnesium and sodium.[6]

Phosphorus, as mentioned above, is an essential component of energy stores in the form of ATP and phosphocreatine. Adenosine triphosphatases (ATPases) are a class of enzymes that catalyzes the decomposition of adenosine triphosphate (ATP) to adenosine diphosphate (ADP), releasing a free phosphate ion and energy. The Na^+/K^+–ATPase, or sodium–potassium pump, is responsible for active transport of potassium into cells and sodium out of cells against respective concentration gradients. This is extremely important in maintaining resting potential and the regulation of cellular volume.

Phosphorus is found abundantly in protein-rich foods such as meat, dairy and eggs, but is also high in cereal grains; the average dietary intake is 800–1400 mg/day. It is absorbed in the GI tract in the duodenum and jejunum mostly through passive transport as phosphates. The absorption of phosphate in the intestine is mediated by the production of calcitriol, which is produced by the kidneys; calcitriol synthesis is regulated by the PTH.[23] Hypophosphatemia, hypophosphatasia and hyperphosphatemia are all disorders of phosphate metabolism discussed below.

Hypophosphatemia

Hypophosphatemia is an electrolytic disorder defined as a phosphate plasma level below 0.65 mM, with normal phosphate levels ranging from 0.89–1.44 mM. It is most commonly observed in hospital patients, occurring in 0.24–3.1% of all hospitalization cases.[23,26] Hypophosphatemia does not necessarily mean phosphate depletion; it is a disease that can occur in the presence of low, normal or high total body phosphate. In the case of normal or high total body phosphate there is a shift from the extracellular pool to the intracellular compartment, resulting in hypophosphatemia. The term phosphate depletion thus refers to a reduction of the total body phosphate. Moderate and severe cases of hypophosphatemia are characterized by plasma phosphate concentrations of 0.32–0.65 mM and < 0.32 mM, respectively.[26] There are three mechanisms by which hypophosphatemia can occur: internal redistribution, loss of phosphate from the body through increased urinary excretion and decreased intestinal absorption.[6,23,26] The three causes are discussed below, and summarized in Table 1.1.

Decreased intestinal absorption is rarely caused by malnutrition, as phosphates are ubiquitously found in foods. It is most likely to occur because of vitamin D deficiency, prolonged use of phosphate binders, or alcoholism.[6,27] Decreased calcitriol (see Chapter 1.1.3) synthesis results in an increase in PTH (see Chapter 1.1.1) production which causes a decrease in intestinal absorption of phosphorus, resulting in hypophosphatemia. Familial

disorders of vitamin D metabolism such as vitamin D-resistance rickets and x-linked vitamin D-resistant rickets are associated with hypophosphatemia.[23,28]

Increased redistribution is the cause of the majority of cases of hypophosphatemia. An acute shift in phosphate from the extracellular to the intracellular compartment is primarily responsible for the lowering of the serum phosphate levels. Any treatment that stimulates glycolysis leads to the formation of phosphorylated glucose compounds, resulting in an intracellular shift of phosphorus.[23] This can include intravenous glucose intake, causing the release of insulin, increasing the cellular uptake of glucose and phosphate. This stimulates glycolysis, leading to accelerated production of phosphorylated metabolites and a rapid shift of phosphate ions into the cells.[26,27]

Hypophosphatemia caused by increased urinary excretion of phosphorus is commonly seen in patients suffering from hyperparathyroidism. This is because there is an increased loss of phosphate due to the inhibition of the cotransporter by PTH. Patients usually present with hypercalcemia (see Chapter 1.1.7), moderate hypophosphatemia and decreased renal tubular reabsorption. Fanconi syndrome causes an impairment of the proximal tubule leading to a urinary loss of compounds normally reabsorbed by the proximal tube; this can cause hypophosphatemia amongst other electrolyte disorders.[23] Patients using diuretics will often manifest with hypophosphatemia.[26,27]

The major mechanisms responsible for symptoms of hypophosphatemia are a decrease in intracellular ATP and 2,3-DPG (diphosphoglycerate). Under certain clinical situations, such as diabetic acidosis, and in patients with prolonged hyperventilation, symptoms are non-existent because phosphate depletion is not prolonged. Clinical manifestations are usually not observed unless plasma phosphorus levels fall below 0.32 mM.[23] In skeletal muscle and bone, phosphate deficiency may result in myopathy, weakness and bone pain caused by mobilization of the bone mineral in an attempt to maintain a normal serum phosphate concentration; this can result in osteopenia and osteomalacia (see Chapter 1.2.1). Usually, these symptoms only occur in conjunction with vitamin D deficiency.[26] Cardiovascular,

neurological and hematological effects are generally only observed in severe cases of phosphate depletion, and can lead to respiratory failure, coma, seizures, hemolysis, leukocyte and platelet dysfunction.[6,26]

In order to treat hypophosphatemia, one must determine the cause of the phosphate depletion. In most cases increasing dietary intake of phosphate-rich foods (such as milk) is often enough;[6] however, in extreme cases, oral or intravenous phosphate repletion must be used, however, this can lead to hypocalcemia (see Chapter 1.1.7), metastatic calcification, hyperkalemia, hypernatremia, metabolic acidosis and hyperphosphatemia.[6,23]

Hypophosphatasia

Hypophosphatasia is a rare, but sometimes fatal hereditary form of rickets or osteomalacia (see Chapter 1.2.1) characterized by defective bone mineralization and a deficiency of the tissue-nonspecific form of alkaline phosphatase (TNSALP).[29] The disease is characterized by a below normal circulating alkaline phosphatase activity, increased urinary excretion of phosphoethanolamine and inorganic pyrophosphates.[30] Pyrophosphates are necessary to inhibit the formation of calcium–phosphate crystals, leading to the defect in bone mineralization seen in patients suffering from hypophosphatasia.[31]

Hypophosphatasia can manifest itself at various ages, and is currently recognized in five different clinical forms: perinatal (which is usually lethal), infantile, childhood, adult and odontohypophosphatasia.[29] While perinatal and infantile forms are considered to be autosomal recessive traits, childhood and adult forms of hypophosphatasia are usually found to be autosomal recessive, but can occasionally be dominant.[30] The TNSALP enzyme is vital for proper skeletal mineralization; hypophosphatasia is the result of a mutation in the TNSALP gene which lowers the serum activity of the enzyme. The diseased manifests as rickets in children and osteomalacia in adults.[29,31] Symptoms including anything from stillbirths to loss of teeth at an adult age. Shorter limbs and deformity, along with hypomineralization are all results of the mutation in the TNSALP gene.[29]

Hyperphosphatemia

Hyperphosphatemia is a disease of high serum phosphate concentration which can occur because of increased intake or increased absorption in the GI tract, increased production of phosphates or decreased loss such as a decrease in urinary excretion.[23] An increase in dietary phosphate intake which overwhelms the renal excretory capacity through the urinary tract results in hyperphosphatemia. It can be a result of administration of too much phosphate or by overdose of vitamin D.[23]

An increase in plasma phosphate concentration from endogenous sources is observed in tumor-lysis syndrome (TLS), rhabdomyolysis, bowel infarction, malignant hyperthermia and severe hemolysis. TLS is a group of metabolic complications usually caused by chemotherapy treatments for lymphomas and leukemias. They are characterized by electrolyte abnormalities such as hyperkalemia (see Chapter 1.1.5), hyperphosphatemia and hypercalcemia (see Chapter 1.1.7) leading to acute renal failure; hyperphosphatemia is the most common of the aforementioned electrolytic disturbances caused by TLS.[32] Rhabdomyolysis is a disease that, due to injury to muscle tissue, causes the rapid breakdown of skeletal muscle. This damage can be caused by physical injury, chemical or biological factors, resulting in hyperkalemia, hyperphosphatemia, and hypermagnesemia.[33] Phosphorus, and other electrolytes, are released from damaged muscle and accumulate, causing hyperphosphatemia.[34] Malignant hyperthermia can be a fatal genetic metabolic disorder of skeletal muscle, which can trigger rhabdomyolysis because of sustained muscle rigidity, leading to hyperphosphatemia.[35] Metabolic acidosis or other acid-base disorders (such as lactic acidosis, diabetic ketoacidosis and respiratory acidosis) release phosphorus from endogenous stores, resulting in hyperphosphatemia.[23]

Reduced loss of phosphates can be a result of renal failure, hypoparathyroidism (see Chapter 1.1.2), acromegaly, tumoral calcinosis, bisphosphonate therapy, magnesium deficiency or multiple myeloma.[23] Renal failure results in phosphate retention, which leads to the development of hyperphosphatemia, hypocalcemia, and increased PTH levels.[36]

Hypoparathyroidism is caused by decreased activity of the parathyroid hormone, which leads to hypocalcemia and hyperphosphatemia due to increased levels of serum phosphorus. Tumoral calcinosis is a rare condition that results in abnormal calcifications around joints and hyperphosphatemia, but normal PTH levels. It is thought that hyperphosphatemia in tumoral calcinosis is the result of increased tubular reabsorption of phosphate, despite normal PTH levels. The elevated serum calcium-phosphate solubility product can lead to the deposition of calcium-phosphate salts at the joints.[37] Bisphosphonates (see Chapter 1.6), in high dosages, can cause hyperphosphatemia by enhancing renal tubular reabsorption of phosphorus.[38]

Untreated hyperphosphatemia can lead to secondary hyperparathyroidism, renal osteodystrophy, increased deposition of calcium-phosphate complexes in soft tissues, inhibition of calcitriol production and mortality.[33,39] Treatment is usually carried out by decreased protein intake or, especially in the case of kidney disease, by phosphate binders such as aluminum, magnesium or calcium.[39,40] More recently the salt lanthanum carbonate has been used to bind excess serum phosphate, with decreased side effects.[39]

1.1.6   Bone Structure, Function and Remodeling

Primarily composed of osseous tissue, bone is responsible for structural support, protection of organs and storage of minerals in the body. Bone is a dynamic tissue that constantly undergoes resorption and desorption by a tightly regulated cycle in which bone is destroyed by osteoclast cells and regenerated by osteoblast cells, as seen in Figure 1.5a.[41] This remodeling is necessary not only to maintain the structural integrity of the skeleton, but for calcium and phosphorus homeostasis.[42]

The principal cells found in bone are osteoclasts, osteoblasts and osteocytes. Osteoblasts, derived from mesenchymal cells are responsible directly for bone formation. Bone resorption occurs by osteoclasts, which are derived from hematopoietic stem cells, while osteocytes are

derived from osteoblasts that are trapped in the osteiod.[43] The exact function of osteocytes has not been elucidated; it appears they are responsible for enhancing bone remodeling by recruiting osteoclasts to sites where bone remodeling is required, such as where microdamage has occured.[44]

There are two distinctively different types of bone in the body: (a) cortical bone and (b) trabecular bone. The skeleton is comprised of 80% cortical bone and 20% trabecular bone. The main differences between the two types of bone are that cortical bone is more dense than trabecular bone, while trabecular bone is remodeled between 3 to 10 times more often than cortical bone.[43]
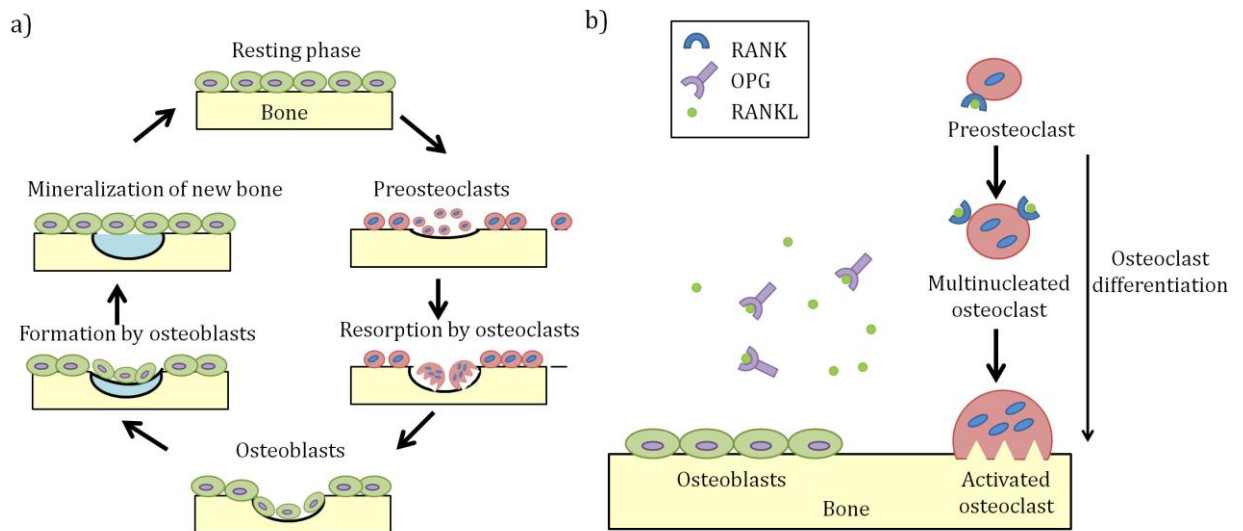
Figure 1.5. Bone turnover cycle.[43,44]

The integrity of the skeleton is maintained by the bone remodeling cycle, seen in Figure 1.5. In the cycle, bone resorption is initiated by osteoclast precursors which become active

osteoclasts, creating a resorptive pit (lacuna). Osteoblasts come in and fill the lacuna with unmineralized bone matrix (osteoid). This then undergoes a mineralization process ultimately replacing old bone with new bone.[43] In this manner, 2–5% of cortical bone is remodeled yearly, while trabecular bone is remodeled more actively because of its higher surface area to volume ratio.[44]

Osteoclasts are regulated by the nuclear factor-κB NFκB-RANKL (RANK ligand), a 317 amino acid peptide member of the tumor necrosis factor (TNF) superfamily.[44] RANKL has two known receptors—RANK and osteoprotegerin (OPG).[43] Osteoclasts express RANK, while RANKL is mainly produced by osteoblasts and stromal cells. When RANKL interacts with RANK, osteoclast differentiation is promoted. This RANKL/RANK interaction results in activation, differentiation and fusion of hematopoietic cells of osteoclasts, which initiates the resorption process. OPG is a receptor antagonist that blocks the RANKL/RANK interaction, resulting in apoptosis of osteoclast cells.[43,44]

The metabolic functions of the skeleton are controlled by two calcium-regulating hormones: PTH and vitamin D. Calcitonin also plays a role in inhibiting bone formation, but plays little role in homeostasis of calcium. Estrogen is another important hormone that can influence bone remodeling.[42]

1.1.7   Calcium

Calcium is vital to many biological functions, and is a key structural component in skeleton and teeth. It plays a vital role in skeletal and myocardial muscle function, and in neurotransmission. Approximately 90% of calcium is found in the bone mineral, hydroxyapatite, located in bones and teeth. The remaining 10% is found in the extracellular

fluid and the cytoplasm, where 50% of it is free, ionized calcium, 40% is bound to albumin and globulin, and the other 10% is bound to bicarbonate, phosphate and citrate.[45]

In order to fully understand calcium disorders, it is important to understand both the role of the PTH (see Chapter 1.1.1) and vitamin D (see 1.1.3). Calcium homeostasis is maintained by the parathyroid hormone, vitamin D and calcitonin. PTH is responsible for increasing serum calcium, renal calcium reabsorption, skeletal turnover and renal production of the metabolite of vitamin D, calcitriol. In the following sections disorders of calcium metabolism, hypocalcemia, hypercalcemia, disorders of parathyroid hormone, calcifications, osteomalacia, osteoporosis, Paget's disease and milk-alkali syndrome are explored.

Hypocalcemia

Hypocalcemia is a metabolic disorder occurring when plasma calcium concentration < 2.1 mM. It can be a result of a multitude of diseases, summarized in Table 1.1. It is almost always caused by an impairment of parathyroid hormone or impairment of vitamin D action or synthesis; however, it can be caused by an increase in tissue sequestration of calcium, which is observed in pancreatitis, burns or toxic shock. Osteomalacia or rickets, discussed in Chapter 1.2 may also result in hypocalcemia.

Hypocalcemia is characterized by tetany, asphyxia, cramps, altered mental status, seizures, muscle spasms, hypotension, alopecia and coarse dry skin. Factitious hypocalcemia is usually caused by blood sample contamination with ethylenediaminetetraacetic acid (EDTA). Decreased parathyroid activity (see Chapter 1.1.2) resulting in hypoparathyroidism and pseudohypoparathyroidism are discussed earlier in this chapter. Malabsorption of vitamin D or impairment of vitamin D synthesis are discussed in Chapter 1.1.3.[46]

Hypercalcemia

Hypercalcemia is defined as a total plasma calcium level > 2.55 mM.[4] Usually, high levels of serum calcium indicate primary hyperparathyroidism or malignancy. Other causes of

hypercalcemia which account for less than 10% of all cases of hypercalcemia include: vitamin D intoxication, tuberculosis, some fungal infections, Addison's disease, milk-alkali syndrome, vitamin A intoxication, thiazide diuretics, familial hypocalciuric hypercalcemia, prolonged immobilization in patients with high skeletal turnover, and recovery from acute renal failure (especially associated with rhabdomyolysis).[47]

Factitious (pseudohypercalcemia) hypercalcemia and hypocalcemia (pseudohypocalcemia) are also quite common. Calcium in serum is either bound to proteins, principally albumin, or is free (ionized) calcium. When measuring the total plasma or serum concentration of calcium, it is the ionized calcium levels that are important. With patients suffering from chronic illness or malnutrition, serum albumin may be low (hypoalbuminemia), causing a reduction in the total, but not in the ionized serum calcium; this is referred to as factitious hypocalcemia. On the other hand hyperalbuminemia, caused by volume depletion or multiple myeloma, leads to increased protein binding of calcium, which results in an elevated serum total calcium concentration without any rise in the serum ionized calcium concentration; this is referred to as factitious hypercalcemia.[4]

Symptoms of hypercalcemia are usually not observed until > 3 mM plasma concentration. Symptoms include nausea, vomiting, constipation, muscular weakness, lethargy, myalgia and ectopic calcification. Mental disturbances such as psychosis, apathy, confusion, depression and (rarely) coma are also observed. Hypercalcemia may also predispose the patient to the occurrence of peptic ulcers and pancreatitis.[4]

1.2 Bone Density Disorders

1.2.1 Osteomalacia

Osteomalacia is a clinical syndrome of vitamin D deficiency (see Chapter 1.1.3), or a problem with the body's ability to break down vitamin D, characterized by major deficits in bone mineralization and by relatively minor changes in calcium and phosphate homeostasis in the blood, resulting in proximal muscle weakness. In children this is called rickets, in which structural changes related to defective bone mineralization are added to the features of osteomalacia that are seen in the adult manifestation of this disease.[48]

Osteomalacia due to vitamin D deficiency is rare in North America because of the routine fortification of milk and other dairy products with vitamin D. The characteristic histological feature of the disease is defective mineralization of the osteoid, leading to its accumulation on bone surfaces. Clinically, osteomalacia manifests as progressive generalized bone pain, muscle weakness, hypercalcemia, pseudofractures, and, in its late stages, by a waddling gait. Patients with various GI disorders are at risk.[49] Treatment involves the administration of calcium and vitamin D supplements.

1.2.2 Paget's Disease

Paget's disease is a chronic disorder of the adult skeleton which causes increased resorption of bone resulting in a softened bone and increased bone deposition, leading to enlarged bone. The disease is characterized by focal abnormalities of increased bone turnover, usually isolated to the pelvis, femur, skull, tibia, vertebrae, clavicle and humerus.[50,51] The pathophysiology of Paget's disease is believed to occur by an increase in osteoclastic bone resorption due to an increase in both the size and the number of osteoclasts. These osteoclasts

possess a higher than normal number of nuclei and contain characteristic nuclear inclusion bodies, which are microcylindrical structures that resemble virus particles.[50]

The occurrence of Paget's disease increases with age, affecting 1–2% of Caucasian adults over the age of 55, as well as 8% of men and 5% of women over the age of 80. The disease also more commonly presents in men, affecting twice as many men as women.[50,51] These abnormalities can give rise to bone which appears mosaic in appearance, caused by a mixture of woven and lamellar bone. Most patients are asymptomatic until diagnosis by X-ray of the bones, some present with bone pain, fracture and nerve impingement as a result of poorly formed, enlarged bones.[51] Most patients suffering from the disease also present with an increase in serum alkaline phosphatase.

The increase in osteoclastic bone turnover leads to bone mineral that is disorganized; the bone has reduced mechanical strength and generally leads to an increase in deformities and fractures at affected sites. It is believed that a defect in apoptosis of these enlarged Pagetic osteoclasts maybe the cause of this increased bone turnover.[50] While the cause of Paget's disease is incompletely understood, genetic factors clearly play an important role. Roughly 15% of patients have a positive family history, and the risk of developing Paget's disease has been estimated to be 7–10 times greater in first-degree relatives than in the general population. Environmental factors such as low dietary calcium intake or vitamin D deficiency during childhood may also play a role in the onset of Paget's disease.[50]

Treatment involves the use of antiresorptive medications such as calcitonin and bisphosphonates (see Chapter 1.6) which inhibit osteoclastic bone resorption. This, along with anti-inflammatory drugs, can help alleviate bone pain. Bisphosphonates can help reduce bone turnover rates, improve bone pain, promote healing of osteolytic lesions, and help restore normal bone histology in Paget's disease, replacing woven bone by lamellar bone.[50] Dietary calcium and vitamin D deficiency is common in older patients, as it is important that this deficiency is corrected before starting bisphosphonate therapy.[50,51] Heel lifts are often used to help normalize gait when one lower extremity develops bowing (becomes bent).

Surgery is often necessary to remove pressure from compressed nerves or to replace an osteoarthritic joint.[51]

1.2.3 Osteoporosis

Osteoporosis, the most prevalent bone density disorder, is a skeletal disease that is characterized by low bone mineral mass and a deterioration of bone tissue. Caused by an imbalance between bone forming osteoblasts and bone resorbing osteoclasts, it leads to an increase in bone fragility and susceptibility of fracture. Often known as a "silent" disease because it is asymptomatic until fracture occurs, it affects 3.4 million Canadians a year, putting an escalating pressure on our health care system.[52] At the cellular level, bone loss occurs because of a perturbation between the activity of osteoclasts and osteoblasts. Estrogen deficiency following menopause results in a remodeling imbalance, with a substantial increase in bone turnover. Remodeling rates nearly double in the first year after menopause; however, though formation rates increase, it is not sufficient to keep up with resorption rates.[42,43] Osteoporosis has been divided into type 1, or postmenopausal osteoporosis, and type 2, or senile osteoporosis, based on differences in etiology. Recent studies indicate that estrogen deficiency plays an important role in the pathogenesis of both type 1 and type 2 osteoporosis.[42]

Osteoporosis is defined as a loss of bone mass and strength, leading to an increased likelihood of fracture. This can occur because of a failure to reach optimal peak bone mass as a young adult, excessive resorption after peak bone mass has been reached or an impaired formation during remodeling.

1.2.4   Milk-alkali Syndrome

First identified in 1923, this is a disease that historically was caused by the use of dairy products and alkaline powders, such as milk and bicarbonate used to treat peptic ulcers.[53] In 1985, with the introduction of proton pump inhibitors and antibiotic therapies of *H. pylori*, for the treatment of these ulcers, milk-alkali syndrome has become rare. There has been an increase in incidence of milk-alkali syndrome as a result of malignancy, primary hyperparathyroidism and over-the-counter calcium supplements used to combat osteoporosis.[54] Milk-alkali syndrome is caused by a triad of hypercalcemia (see Chapter 1.1.7), metabolic alkalosis and renal insufficiency.

1.2.5   Calcifying Disorders

Calcification

As discussed in Chapters 1.1.1 and 1.1.3, serum calcium is tightly regulated by PTH and calcitriol. Despite this careful regulation, calcification and ossification of cutaneous and subcutaneous tissues may occur. Cutaneous calcification can be divided into four major categories: dystrophic, metastatic, idiopathic and iatrogenic. Dystrophic calcification is the result of local tissue injuries and abnormalities. Metastatic calcification is caused by abnormal calcium and phosphate metabolism. Calcification generally results in secondary ossification of tissues, but primary ossification is rare. Idiopathic calcification occurs without identifiable underlying tissue abnormalities or abnormal calcium or phosphate metabolism. Iatrogenic calcification occurs as a result of intravenous infusion of calcium chloride or calcium gluconate.[45,55]

Calcinosis

Calcinosis causes vascular calcification and skin necrosis that occurs as a result of end stage renal disease (ENRD). It also presents itself in individuals with chronic renal failure, hypercalcemia, hyperphosphatemia and secondary hyperparathyroidism and it is associated with poor phosphate and calcium control.[56]

1.3   The Lanthanides

Rare earth elements were first discovered in 1787 when Carl Axel Arrhenius identified a grayish-black and very heavy mineral which he subsequently named "ytterbite". The first subgroups isolated were called "ceria", "terbia", "yttria" and "ytterbia" corresponding to mixtures of the light, middle, heavy and very heavy rare earths, respectively. It was thought that these mixtures were pure elements because of their similar chemical behaviour. In 1803, cerium was the first of the lanthanides to be isolated with high purity.[57]

Lanthanide or lanthanoid (Ln) is the International Union of Pure and Applied Chemistry (IUPAC) name of the "d-element" lanthanum (La, atomic number: 57) and the following 14 "f-elements" from cerium to lutetium, seen in Table 1.3.[58] Rare earth, meanwhile, is the historical term still utilized for the lanthanides (La–Lu) plus yttrium (Y) and scandium (Sc). This is a reflection of the fact that these two elements are associated with the lanthanides in their natural occurrence, usually found as mixed ores of the rare earths.[59]

In physiological solutions, with the exception of Ce(IV) and Eu(II), the lanthanides are only stable as trivalent ions. The preferred coordination number of all lanthanides is 8–9, but complexes of 6–12 coordination are quite stable. In aqueous solution, the hydration shell of lanthanides is between 9–12 water molecules; this number has not been unequivocally determined.[57] The ionic character of complexes of trivalent lanthanide ions is very high, with a typical order in strength of bonding of O > N > S.

Table 1.3. The lanthanides, their electronic configuration and size.

Lanthanide (Ln)	La	Ce	Pr	Nd	Pm	Sm	Eu	Gd
Atomic number	57	58	59	60	61	62	63	64
Atomic electronic configuration	$[Xe]4f^05d^16s^2$	$[Xe]4f^15d^16s^2$	$[Xe]4f^36s^2$	$[Xe]4f^46s^2$	$[Xe]4f^56s^2$	$[Xe]4f^66s^2$	$[Xe]4f^76s^2$	$[Xe]4f^75d^16s^2$
Ln^{3+} electronic configuration	$[Xe]4f^0$	$[Xe]4f^1$	$[Xe]4f^2$	$[Xe]4f^3$	$[Xe]4f^4$	$[Xe]4f^5$	$[Xe]4f^6$	$[Xe]4f^7$
Ln^{3+} radius (pm);[60] CN=6	103.2	101	99	98.3	97	95.8	94.7	93.8

Lanthanide (Ln)		Tb	Dy	Ho	Er	Tm	Yb	Lu
Atomic number		65	66	67	68	69	70	71
Atomic electronic configuration		$[Xe]4f^96s^2$	$[Xe]4f^{10}6s^2$	$[Xe]4f^{11}6s^2$	$[Xe]4f^{12}6s^2$	$[Xe]4f^{13}6s^2$	$[Xe]4f^{14}6s^2$	$[Xe]4f^{14}5d^16s^2$
Ln^{3+} electronic configuration		$[Xe]4f^8$	$[Xe]4f^9$	$[Xe]4f^{10}$	$[Xe]4f^{11}$	$[Xe]4f^{12}$	$[Xe]4f^{13}$	$[Xe]4f^{14}$
Ln^{3+} radius (pm);[60] CN=6		92.3	91.2	90.1	89.0	88.8	86.8	86.1

Where the electronic configuration for xenon is, $[Xe] = 1s^22s^22p^63s^23p^64s^23d^{10}4p^65s^24d^{10}5p^6$
and CN = coordination number.

29

1.4   *Lanthanides in Medicine*

Found only in trace amounts in the body, the lanthanides play no known essential biochemical role.[61] The earliest therapeutic application of lanthanides was the use of cerium oxalate ($Ce_2(C_2O_4)_3$) as an antiemetic (Figure 1.6).[57] Although its mechanism has never been elucidated, it was used from the mid-nineteenth century to the mid-twentieth century.[57] Eventually cerium oxalate was replaced by antihistamines for the treatment of emesis.[57] Cerium nitrate ($Ce(NO_3)_3$) is used, along with silver sulfadiazine (Figure 1.6), under the trade name Flammacerium™ for the topical treatment of extensive burns.[57]

Lanthanides are known to interfere with the calcium-dependent reactions involved in the blood clotting cascade; this behaviour accounts for the long-known anticoagulant effects of lanthanides, most notably $Ce(NO_3)_3$. However, severe side effects, coupled with the availability of heparin, have hampered the development of lanthanides as antithrombotic drugs.[57,62]

Magnetic resonance imaging (MRI) contrast agents are used to improve the visibility of internal body structures in MRI. They work by altering the relaxation times of water in tissues and body cavities where they are present. Gadolinium is the metal of choice for MRI imaging because of its high magnetic moment and long intrinsic relaxation time of the electron-spin state, which has to be long enough for efficient transfer of magnetic information from the coordinated bulk water. Thus with seven unpaired f-electrons, Gd(III) possesses not only a high magnetic moment (7.9 B.M.), but also a totally symmetric electronic state ($^8S_{7/2}$ ground state), which makes the electronic relaxation time much longer than that for other Ln(III) ions.[63]

The main setback of Gd(III) in the use of contrast agents is that it exhibits significant toxicity in its "free" aqua-ion form.[63] Likewise, it is well known that excess "free" gadolinium can incorporate into the bone.[64] As a result of the toxicity and the possible transmetallation/transchelation by calcium proteins and bone, it is essential that the metal

ions are bound in a complex of high stability. As a result, most Gd(III) contrast agents involve octadentate macrocyclic and acyclic chelators.[63,64]

The radioisotope [153]Sm is used in bone palliative care in metastatic cancer patients. It is used because Sm^{3+} is known to "target" and bind to bone. It is chelated to the tetra-phosphonate derivative of EDTA, ethylenediaminetetra(methylene phosphonate) (**EDTMP**), known as samarium lexidronam or Quadramet™, seen in Figure 1.6. Both the phosphonates along with [153]Sm^{3+} help direct the molecule towards bone. Once in bone, the radioisotope emits beta particles (electrons) which kill the nearby cancer cell, alleviating pain.[65,66].

Cerium oxalate

Silver sulfadiazine   Samarium lexidronam
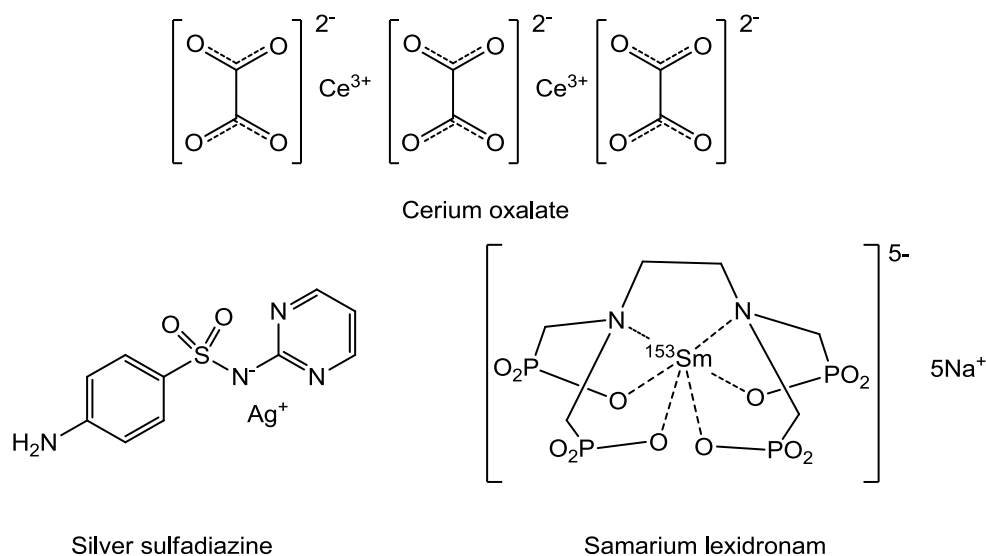
Figure 1.6. Lanthanides in medicine: cerium oxalate and silver sulfadiazine, used in the treatment of burns and the proposed structure of samarium lexidronam, used for the treatment of bone cancer.

Recently, lanthanum carbonate, sold under the trade name Fosrenol™, has been used in the treatment of hyperphosphatemia. Hyperphosphatemia is a disease of high serum phosphate concentration that can occur because of a multitude of kidney and electrolytic disorders. Generally, however, Fosrenol™ is used in the treatment of ENRD (end stage renal disease). Lanthanum(III) binds the excess phosphates and helps with their excretion. Lanthanum

carbonate is an ideal phosphate binder because it has a high affinity for phosphates and can bind them rapidly. It is also scarcely soluble and thus has very little systemic absorption through the GI tract. [62,67]

Lanthanum carbonate has replaced aluminum-based binders which were used in the 1970s and 1980s. Aluminum hydroxide is absorbed from the gut and is quite toxic. Both calcium carbonate and calcium acetate are effective phosphate binders in dialysis patients; however, calcium-based agents can result in hypercalcemia (excess serum Ca^{2+}). *In vitro* phosphate binding studies comparing a number of lanthanide salts and complexes identified lanthanum carbonate as having favourable phosphate binding properties.[62] Further studies demonstrated that improved phosphate binding was obtained for the tetrahydrate $La_2(CO_3)_3 \cdot 4H_2O$, with binding activity retained across the full pH range 1–7.[62,67]

1.5   *Lanthanides in the Body*

The lanthanides are isomorphic replacements for calcium;[61] Birnbaum[68] and Williams[69] were the first to report the biochemical similarity of Ca(II) and Ln(III). Ln(III) is able to replace Ca(II) in calcium proteins because they have similar chemical properties. Both Ln(III) and Ca(II) are hard acids, and thus favour ligands that are hard bases, binding preferentially with ligands that donate oxygen atoms.[61,68,69] Both have variable coordination numbers (CN) with flexible coordination geometries. While ionic radius depends on CN, it has been observed that regardless of the CN, the ionic radius of calcium always falls in the range of the radii of the lanthanide series.[61]

Lanthanides can thus be used to probe the structure and function of calcium-binding proteins, macromolecules and cells. Since the lanthanides possess unique magnetic properties due to their electronic configurations, they have some of the highest magnetic susceptibilities of any metal cations and can be used to alter the nuclear magnetic resonance (NMR) and electron paramagnetic resonance (EPR) signals causing chemical shift perturbations. Likewise,

terbium possesses luminescent properties and can be used to spectroscopically probe calcium binding sites.[61,70]

Due to their similar ionic radii, lanthanide ions are able to replace calcium ions in many biomolecules without necessarily substituting for them functionally, as seen in Table 1.4.[57] Substitution of lanthanide ions for calcium ions in enzymes generally results in an inhibition of the enzyme process, with the exception of the activation of trypsin, acetylcholinesterase and α-amylase in which cases Ln^{3+} substitution has been observed to have a stimulatory effect on the processes for which these enzymes are responsible.[57,61] However, it should be noted that lanthanide ions cannot easily penetrate the cellular membranes of living cells. Thus, despite being similar in size to calcium ions, this restricts the scope of their biological effects.[61]

Lanthanide ions, the second from the bottom row of the Periodic Table, abbreviated herein as Ln(III), are known functional mimics of Ca(II) ions and have been shown to affect the bone remodeling cycle[71] and to distribute preferentially in bone.[72-74] Lanthanides can be divided into three groups: the light lanthanides (lanthanum to samarium), the transition group lanthanides (europium, gadolinium, terbium), and the heavy lanthanides (dysprosium to lutetium).[72] Biodistribution studies in rats have shown that the heavier Ln(III) ions preferentially accumulate in bone rather than the liver or kidney, with 50–70% depositing in bone, compared to less than 25% for the lighter Ln.[72,73] The elimination of Ln^{3+} from the bone is also slow, with a half life of 2.5 years; elimination from soft tissues such as the liver has a half life of about 15 days.[72,73]

Table 1.4. The role of calcium enzymes, and the effect of lanthanide ions (Ln^{3+}) binding to them.[61]

Enzyme/Activity	Role of Ca^{2+} in the enzyme	Effect of Ln^{3+}
Activation of trypsinogen by trypsin	Substrate binding; stabilizes against autolysis	Stimulation
Acetylcholinesterase	Changes conformation	Stimulation (1 µM Tb^{3+}) Inhibition (500 µM Tb^{3+})
α-amylase	Stabilizes conformation	Replacement of Ca^{2+} giving 14-101% activity
Staphylococcal nuclease	Substrate binding	Inhibition
Factor X activation	Substrate binding: catalysis	Inhibition
Clostridiopeptidase A	Substrate binding: thermostabilizer	Inhibition
Phospholipase A_z	?	Inhibition
Calcium ATPase	Formation of intermediate phosphorylated enzyme	Inhibition
Activation of prothrombin by activated Factor X	Binding of the cofactors factor V and phospholipids	Inhibition

1.6   *Current Treatments for Osteoporosis*

The few therapies that exist to prevent the progressive degradation of bone caused by osteoporosis (discussed earlier in Chapter 1.2.3) each have shortfalls. Simple nonpharmacological therapies include increased dietary calcium and vitamin D intake or supplementation, weight-bearing exercise and fall prevention, but are not always sufficient on their own for the treatment of osteoporosis.[75]
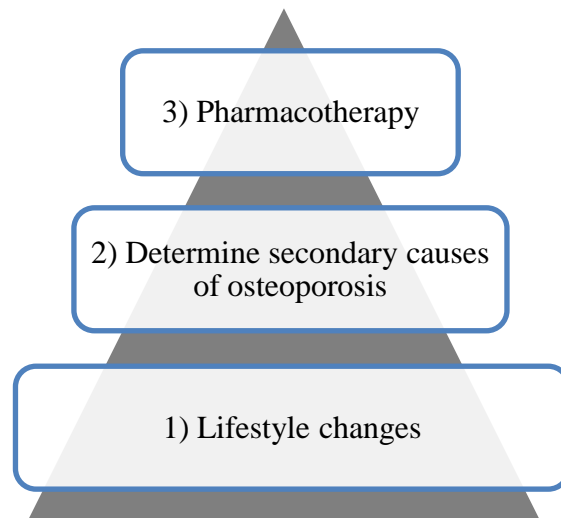
Figure 1.7. Pyramidal approach for the treatment of osteoporosis according to the U.S. Surgeon General.[76]

According to the U.S. Surgeon General, the recommendations for the treatment of osteoporosis include a pyramidal, bottom-up, approach, as seen in Figure 1.7.[76] The first level and point of attack in the treatment of osteoporosis includes increasing physical activity, nutritional supplementation and fall prevention. Physical activity is necessary for bone formation and maintenance throughout life. Weight-bearing exercise has been shown to increase bone mineral density (BMD) at some skeletal sites. Lower impact exercises have not demonstrated to increase BMD, but may play an important role in fall prevention, and

thus reducing risks of fractures. Improvements in mobility, muscle function and balance by exercise can also help in fall prevention. Smoking and alcohol consumption can result in a reduced bone mass, and thus an increase in fractures; these habits must be curtailed to help prevent fractures. Nutritional supplementation with calcium is essential for attaining and maintaining bone mass. Vitamin D (see Chapter 1.1.3) is essential for the absorption of calcium; serum vitamin D concentration decreases with increasing age, so supplementation is necessary for maintenance of bone mass.[77]

Once lifestyle changes have been addressed, secondary causes of osteoporosis must be addressed. Rickets, kidney disease, Paget's disease (see Chapter 1.2) and endocrine disorders all lead to osteoporosis. Medications for the treatment of thyroid and arthritis as well as immunosuppressants can affect bone density.[76]

If all of these factors have been addressed, pharmacological intervention is necessary. Pharmacological interventions include antiresorptive treatments such as bisphosphonates, SERMs (selective estrogen receptor modulators), calcitonin, hormone replacement therapy and anabolic treatments such as teriparatide. Antiresorptive treatments reduce bone resorption more than promoting bone formation, thereby suppressing bone turnover and loss, whereas anabolic agents stimulate bone formation more than bone resorption.[75,76] The only SERM approved for the treatment of osteoporosis is raloxifene (Figure 1.8) and it acts as an estrogen agonist on bone and lipid metabolism and as an estrogen antagonist in the breast and endometrium. Raloxifene, unlike estrogen, does not result in an increased risk of breast cancer; however, the drug increases the risk of stroke and venous thromboembolism.[78,79]

Estrogen replacement therapy has some merit in the prevention and treatment of postmenopausal-osteoporosis. Estrogen acts directly on bone cells through high-affinity estrogen receptors, and if begun soon enough, estrogen therapy prevents the early phase of bone loss associated with the onset of osteoporosis and decreases the incidence of osteoporosis related fractures.[80] There is evidence however that estrogen therapy can increase the risk of certain cancers[80] and cardiovascular disease.[78]

Calcitonin, a hormone produced in the thyroid gland, has been found to be an inhibitor of osteoclastic bone resorption.[81,82] Miacalcin[TM] (calcitonin-salmon), marketed by Novartis, a synthetic 32 amino acid polypeptide of the same sequence as found in calcitonin of salmon origin,[83] has been approved for the treatment of osteoporosis.[81,82] However, it suffers from poor oral absorption, and thus, must be administered either by subcutaneous injection or by nasal spray.[81,82] It has demonstrated efficacy in decreasing vertebral fractures, but not for improvement to the occurrence of nonvertebral or hip fractures.[81,82] It has not been found to be as effective as other antiresorptive, and thus is generally prescriped in conjuction with bisphosphonate therapy.[78,81,82]
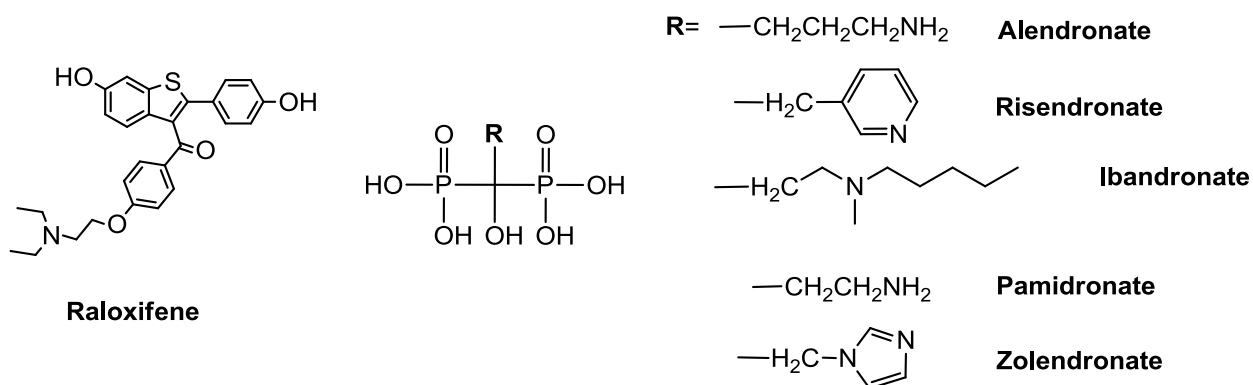
Figure 1.8. Drugs for the treatment of osteoporosis: raloxifene a selective estrogen receptor modulator (right), and structures of some of the bisphosphonates in clinical use (left).

The most widely used class of drugs, bisphosphonates, are stable analogues of pyrophosphates that have a strong affinity for bone apatite; these agents inhibit bone resorption by reducing the recruitment and activity of osteoclasts and increasing apoptosis. It is well known that bisphosphonates help increase bone mineral density (BMD) by preventing degradation of bone (Figure 1.8).[84,85]

The only anabolic drug approved for the treatment is osteoporosis is teriparatide (recombinant human PTH(1–34).[82] PTH or teriparatide stimulates osteoblasts, markedly

increases bone formation, reduces the risk of fractures, and can help increase the microarchitecture of bone; however, it is administered by daily injection, making it quite costly as a treatment option.[81,86,87]

1.6.1 Shortfalls of Bisphosphonates

Bisphosphonates are a class of drugs characterized by a P-C-P backbone, which mimics the P-O-P pyrophosphate backbone, but are stable to enzymatic hydrolysis, irreversibly binding to bone.[84,85] They are used to treat metabolic bone disorders such as hypercalcemia (see Chapter 1.1.7) and Paget's disease (see Chapter 1.2.2), and an oral form, typically alendronate or risendronate, is used for the treatment of postmenopausal osteoporosis (Figure 1.8). Due to their poor lipophilicity and polarity they possess very low oral bioavailability, typically $< 1\%$. As a result, bisphosphonates must be administered in a very high dosage to compensate for low bioavailability, resulting in GI upset.[85,88] Additionally, there is mounting evidence indicating that bisphosphonates cause osteonecrosis of the jaw, with 5% of all cases associated with oral bisphosphonates used to treat osteoporosis.[89] Bone strength is measured not only by the amount of bone tissue and the microarchitectural arrangement of bone, but also by the degree of mineralization.[90] Bisphosphonates work by inhibiting bone resorption and decreasing bone turnover, which then increases the age of bone tissue.[91,92] Studies in dogs indicate that mineralization of bone due to bisphosphonates leads to an inability to repair microcracks and microdamage, resulting in more fragile bone.[91,93] Studies in dogs indicate that impaired bone turnover of approximately 50% from bisphosphonates is associated with a five- to sevenfold increase in microdamage, leading to a reduction in bone's capacity to absorb energy.[93] Increasing mineralization improves the structural rigidity of bone, while at the same time making the tissue more brittle.[94]

Furthermore, taking a bisphosphonate is not simple as there are special dosing requirements such as fasting overnight, taking on an empty stomach and remaining standing for 30 minutes after taking a dose. Medication is expensive and weekly dosages are often not

covered by private insurance. As a result, patient compliance with bisphosphonates is low.[95,96] Many studies have been carried out to examine patient compliance on daily and weekly dosages of bisphosphonates; on average only 58–76% of patients on a weekly dosage were compliant, whereas 46–64% on a daily dosage were compliant after one year.[96]

The adverse effects of oral bisphosphonate treatment may be overcome with intravenous (IV) administration either monthly or yearly; however, this is not the ideal regimen for strong patient compliance. Zoledronate, pamidronate and ibandronate are the most commonly intravenously administered bisphosphonates because they allow shorter infusion times and can be administered at lower dosages, since they are more potent against osteoporosis (Figure 1.8). Pamidronate and ibandronate both require administration over 1–4 h, whereas zoledronate requires administration over 15 min, and is thus now the treatment of choice for infusion treatments with bisphosphonates. However, patients who are administered bisphosphonates through IV infusion suffer from adverse side effects ranging from flu-like symptoms to bone pain, nausea, vomiting, anemia, serum electrolyte imbalances and decreased renal function.[97-99] No studies on health care costs or patient compliance with intravenous bisphosphonate therapy have been carried out, as IV treatment is still relatively new. It is evident that though effective, due to their adverse side effects, cost and low patient compliance, more effective medications are necessary for the treatment of postmenopausal osteoporosis.

1.6.2 Alternatives to Anabolic and Antiresorptive Treatments for Osteoporosis

A new potential class of osteoporosis drugs, based on bone strengthening by strontium or lanthanide compounds, affects the bone remodeling cycle.[71] Lanthanide ions (Ln(III)) are functional mimics of Ca(II) ions,[62] sharing similar ionic radii, donor atom preferences, and almost identical coordination numbers in protein binding sites; therefore, Ln(III) can potentially replace Ca(II) in hydroxyapatite, thus affecting the bone remodeling cycle. Strontium (Sr^{2+}) is a bone-seeking ion that at low doses stimulates bone density in

osteoporotic patients. It has been shown to increase the volume of bone and the number of bone forming sites.[100] Oral Sr^{2+} ranelate (marketed as Protelos) stimulates osteoblast proliferation and inhibits osteoclast activity;[101,102] however, the potential toxicity of chronic strontium accumulation in bone may limit the chronic utility of this product. Low doses of Ln(III) have been shown to act similarly to strontium ranelate.[62]

A lanthanum carbonate preparation, Fosrenol ($La_2(CO_3)_3$), as discussed earlier in Chapter 1.4, is a commercial agent for treatment of hyperphosphatemia, and also inhibits osteoclast activity while stimulating osteoblast proliferation.[103] Fosrenol is approved for use in Europe, Canada and the United States. In 2009 the European Union widened the use of Fosrenol, approving it for the use of chronic kidney disease for patients not on dialysis treatments.[104] In 2007, the U.S. Food and Drug Administration (FDA) voted 8–4 that phosphate binders, such as Fosrenol, be studied to see if their use could be extended; currently no phosphate binders have been approved in the U.S. for pre-dialysis treatment.[105,106] The tolerability and efficacy of lanthanum carbonate were found to be similar to a variety of approved therapeutic calcium binders, with no hypercalcemia and with improved parathyroid hormone levels. The major adverse effect is gastrointestinal discomfort and upset. Pharmacokinetic studies in animals have shown that 94–99% of the administered lanthanum carbonate passed completely through the GI tract.[107] This strong elimination requires that high levels of the compound be administered, an undesirable protocol for chronic use, and suggests that judicious ligand choice ought to positively influence biodistribution towards a modest uptake.

1.7   *Thesis Overview*

In this thesis I explore the development of an alternative treatment of bone density disorders, involving the study of a potentially orally active lanthanide complex. In Chapter 2 the synthesis of a series of ligands that are small, bidentate, and monoprotic is explored, followed by the coordination to Ln(III) to form neutral, *tris*-ligand complexes. The protonation constants of the free ligands and formation constants with La^{3+} and Gd^{3+} are also

determined. In Chapter 3, the lipophilicity of the ligands, the toxicity of the ligands and complexes in MG-63 cells and Caco-2 cells are explored, along with the cell uptake and bifunctional transport in Caco-2 cells. The interaction of the metal complexes, free ligands and free metal ions with hydroxyapatite (HAP) are discussed in Chapter 4. In Chapter 5, the potential use of curcuminoids in the treatment of osteoporosis is explored. Final conclusions, ongoing work and future work are discussed in Chapter 6.

Chapter 2. Synthesis, Characterization and Physical Properties of Lanthanide Complexes

2.1   Introduction

3-Hydroxy-4-pyrones, and their close analogues 3-hydroxy-4-pyridinones have been extensively studied because of their potential use in medicine. They can form metal complexes with a variety of metal ions[108] and these ligands are of interest because of their ability to effectively bind metals in their di- and tri-valent oxidation states.[108,109] Hydroxypyrones and -pyridinones possess hydroxylic and ketonic oxygens ortho to one another (Figure 2.1), and in their anionic form readily form complexes with metal ions.[109] The hydroxypyrones and pyridinones are intermediate in structure between diketones and catechols (1,2-dihydroxybenzenes).[109]

Figure 2.1. Common nomenclature for the 3-hydroxy-4-pyrones: pyromeconic acid (3-hydroxy-4-pyrone), kojic acid (5-hydroxy-2-(hydroxymethyl)-4-pyrone), maltol (3-hydroxy-2-methyl-4-pyrone) and ethyl maltol (3-hydroxy-2-ethyl-4-pyrone) and one 3-hydroxy-4-pyridinone, **HL1** (3-hydroxy-1,2-dimethyl-4-pyridinone).

A number of hydroxypyrones, such as kojic acid, maltol and ethyl maltol (Figure 2.1) occur naturally in the plant kingdom.[109] Kojic acid (5-hydroxy-2-(hydroxymethyl)-4-pyrone) is a

fungal metabolite produced by many species of *Aspergillus*, *Actobacter* and *Penicillium*.[109,110] Maltol (3-hydroxy-2-methyl-4-pyrone) was first extracted from larch bark and has since been obtained from other plants, including pine needles.[109,110] Maltol and its close congener ethyl maltol are approved food additives, because of their flavour properties, and are used in perfumes, because of a strong odour component.[109,110]

Hydroxypyrones have been extensively studied because they form complexes with various metal ions that are potentially useful in medical therapy.[110] The most famous are the antidiabetic vanadium complexes; the oxovanadium(IV) complex with ethyl maltol (bis(ethylmaltolato)oxovanadium(IV)), has been in phase II clinical trials as an insulin-mimetic agent.[111] Aluminium(III) complexes with pyromeconic acid, kojic acid and maltol have been investigated because of their neurological properties,[110] while *tris*(maltolato)iron (III) is a potent compound for the treatment of iron deficiency anaemia.[110] Biological activity is also observed in complexes of these ligands with gallium, zinc, indium and molybdenum.[110]

Previous work has demonstrated that 3-hydroxy-4-pyridinones can form neutral stable complexes with a variety of transition metals. Group 13 (Al^{3+}, Ga^{3+} and In^{3+}) and iron complexes have been the most extensively studied. Al^{3+} 3-hydroxy-4-pyridinone complexes have been considered for the treatment of aluminium toxicity, particularly in Alzheimer's disease[112], while gallium and indium complexes have been studied for their imaging potential using single photon emission computed tomography (SPECT) and positron emission tomography (PET).[113] 3-Hydroxy-4-pyridinone complexes of iron have been studied for the treatment of iron overload disorders;[114] 3-hydroxy-1,2-dimethyl-4-pyridinone (H**L1**, deferiprone, Figure 2.1) is an approved oral drug for the treatment of iron overload disorders sold under the tradename Ferriprox[TM].[115] There are also more recent developments in using multi-dentate 3-hydroxy-4-pyridinone derivatives for Gd^{3+} and Eu^{3+} MRI contrast agents.[116,117] Tetra-, hexa-, and octadentate analogues of pyridinones can be prepared by the incorporation of two, three or four of the chelating units. Hexadentate hydroxypyridinones have been of particular interest in recent years in view of the high stability and substitution-

inertness of their metal complexes.[109] 3-Hydroxy-4-pyridinones have also been coordinated to actinides[118] and form stable *tris*-ligand complexes with lanthanide ions.[71]

2.1.1   Hydroxypyridinones

3-Hydroxy-4-pyridinones are heterocyclic compounds that include a nitrogen atom in the ring and hydroxylic and ketonic oxygen atoms in positions 3 and 4, respectively, which confer the strong chelating properties exhibited by the ligands towards M^{II}/M^{III} metal ions.[108] This family of ligands can be prepared from the naturally occurring 3-hydroxy-4-pyrones.[108] 3-Hydroxy-4-pyrones can be converted into 3-hydroxy-4-pyridinones by reaction with ammonia or with primary amines. In this reaction the pyrone ring oxygen is replaced by

$\diagdown$
$\diagup N$-R, providing a general route for many potential ligands (Figure 2.2).[109] In principle these conversions should be straightforward one-pot syntheses; however, for many amines, reaction with hydroxypyrones is a long, tedious, and low yielding process.[109] It is often necessary to protect the hydroxyl group as a methoxy or benzyloxy group, followed by the amine insertion reaction, extraction, deprotection (usually by hydrogenation) and purification (Figure 2.2).[108] Sometimes the use of dipolar aprotic solvents such as dimethylsulfoxide (DMSO) or acetonitrile can encourage the amine to react, but this approach can fail in that a solvent of this type may encourage Schiff base formation at the expense of the desired Michael reaction.[109]

Almost any amine can be reacted with a 3-hydroxy-4-pyrone, given the right conditions; this means that a variety of derivatized 3-hydroxy-4-pyridinones are accessible. The hydrophilic-lipophilic balance of ligands, and indeed of complexes, is crucial to transport across biological membranes. This is usually assessed through determination of partition or distribution coefficients. The hydrophilicity-lipophilicity can be tailored, with small or negligible changes in their chelating properties, to optimize this property for delivery to the sites where the ligand is required.[109,113] This can be achieved simply by introducing appropriate substituents on the endocyclic nitrogen atom. 3-Hydroxy-4-pyridinones with

different lipid solubilities but similar binding constants for iron can be produced by modifying the functionality on the ring nitrogen atom.[119]
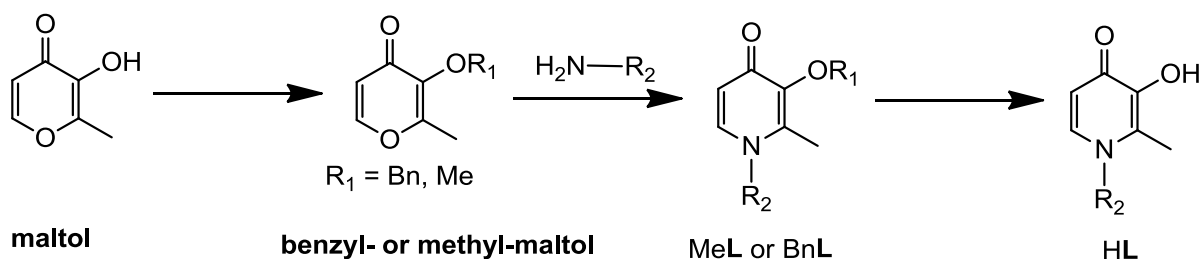
Figure 2.2. General route for the synthesis of a 3-hydroxy-4-pyridinone. The reaction starts with the naturally occurring maltol, followed by protection of the 3-oxy group with either a benzyl (Bn) or methyl (Me) group. The pyrone then undergoes an amine insertion reaction to afford either Bn**L** or Me**L** (the benzyl- or methyl-protected pyridinone); finally the methyl or benzyl groups are deprotected, affording H**L** (the free 3-hydroxy-4-pyridinone).

2.1.2   Design of the Ligand System

As discussed in Chapter 1, there is a lot of potential for the treatment of bone density disorders with the delivery of lanthanides to bone. Previous work in the Orvig group has been focused on adjusting the ligand structure around Ln^{3+} (Ln = La, Eu, Tb, Yb) ions in order to increase the oral bioavailability of lanthanides, so as to decrease unwanted side effects.[71] 3-Hydroxy-4-pyrones and 3-hydroxy-4-pyridinones were investigated because they are small, monoprotic, bidentate proligands that have low toxicity profiles and have been investigated for numerous biological applications. The ligand and lanthanide complexes investigated in the preliminary investigation are shown in Figure 2.3.

45

The suitability of these compounds for bone resorption disorders was investigated in cellular uptake studies and bidirectional transport assays in Caco-2 cells, a model of the gastrointestinal (GI) lining. From these preliminary investigations it was found that the ligand, H**L1** (3-hydroxy-1,2-dimethyl-4-pyridinone), increased the lanthanide uptake into cells. The complexed form, La(**L1**)$_3$ (*tris*(1,2-dimethyl-3-oxy-4-pyridinonato)lanthanum(III)), was found to have low toxicity *in vitro*, and to have improved GI uptake compared to other compounds investigated, including lanthanum carbonate.[71] One of the shortfalls of La(**L1**)$_3$ is its limited solubility in aqueous media, making it difficult to administer in *in vitro* and *in vivo* assays.
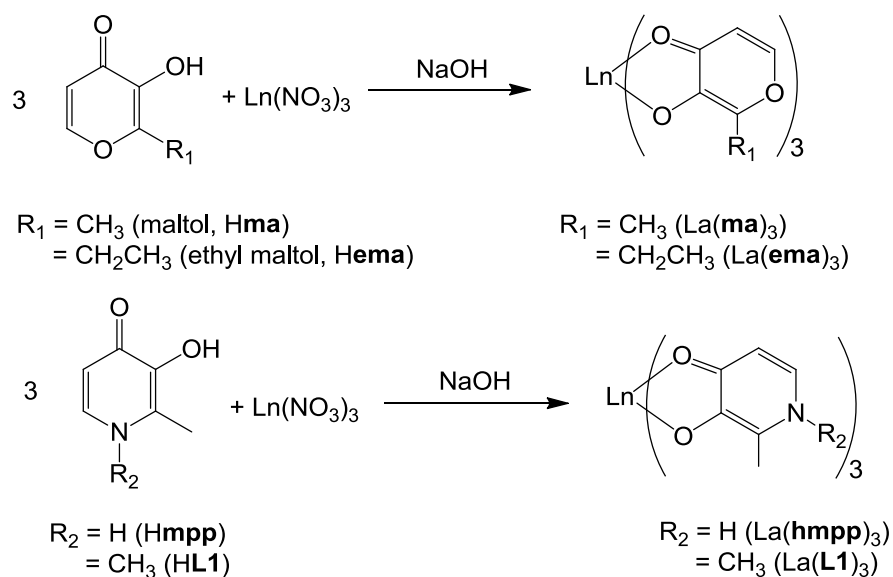
Figure 2.3. First generation lanthanide pyrone and pyridinone ligands, and their complexes for the potential treatment of bone density disorders.

Optimizing the lipophilic/hydrophilic balance of the 3-hydroxy-4-pyridinones by varying the R$_2$-group (Figure 2.3) has the potential to lead to further improvements in the GI uptake of the lanthanides. In this way the potency of the compound can be increased by incorporating

carefully selected targeting moieties into the ligand system in order to increase the selectivity *in vivo*. As discussed earlier, the binding affinity of the ligand varies minimally with changes to the R group. This is of significant importance as this allows one to tune the lipophilicity in favour of liposomes or biological membranes, without affecting the binding affinity to the metal.[108,119]

As can be seen in Figure 2.4 hydroxyl, carboxyl, phosphate and bisphosphonate functional groups have been chosen for the current work and incorporation into the 3-hydroxy-4-pyridinone ligand system. These functional groups were carefully selected in order to tune the lipophilicity of the ligands, help direct the lanthanides towards bone, and to increase the water solubility of the complexes. Hydroxyl groups were selected because of their tendency to form hydrogen bonds and thus increase the water solubility of the ligands and their complexes; hydroxyl groups have also been shown to increase the affinity of complexes to bone.[120] Likewise, carboxylates were chosen because they participate in hydrogen bonding as well, and are thus quite water soluble. The alkyl chain length was varied to tune the lipophilicity of the ligands.[113] Phosphate and diphosphonic acid (bisphosphonate) groups were incorporated so as to direct the complexes towards bone. Literature precedent[121] demonstrates that molecules containing phosphate arms tend to localize on the surface of hydroxyapatite and are retained in bone; specifically, bisphosphonates that contain a P-C-P backbone where the two phosphonic acid groups are bonded to the same carbon are known to be osteoclast mediating bone resorption inhibitors.[121] Moreover, a variety of alkyl chain lengths were used in order to tune the lipophilicity of the ligands.
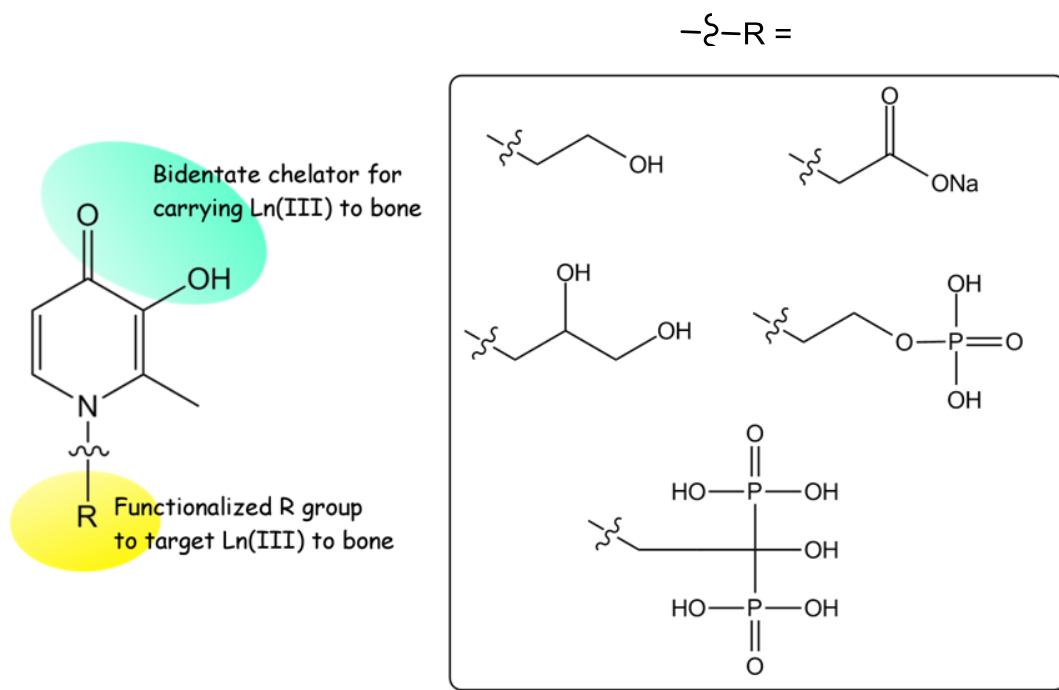
Figure 2.4. Second generation ligand design.

2.1.3   Experimental Overview

Herein, the synthesis and characterization of a library of sixteen 3-hydroxy-4-pyridinone ligands containing hydroxyl, carboxyl, diol, diphosphonic acid and phosphate functional groups are described. Eight of these proligands were then deprotonated and coordinated to Ln^{3+} (Ln = La, Eu, Gd or Lu) with moderate to high yields. Characterization of the metal complexes ^{1}H nuclear magnetic resonance (NMR) spectroscopy (for La and Lu complexes only), Fourier transform infrared (FTIR) spectroscopy and electron spray ionization mass spectrometry (ESI-MS) confirmed their formation. The protonation constants of three of ligands were studied, along with the stability constants of H**L1** with La^{3+} and Gd^{3+}, confirming the formation of stable 3:1 *tris*-ligand complexes with pyridinones.

48

2.1.4 Nomenclature for the Synthesized 3-Hydroxy-4-pyridinones

The different forms of the ligands, protected, free, and coordinated to a lanthanide ion, are named differently. The sixteen ligands synthesized for this study are reported in Figure 2.5.
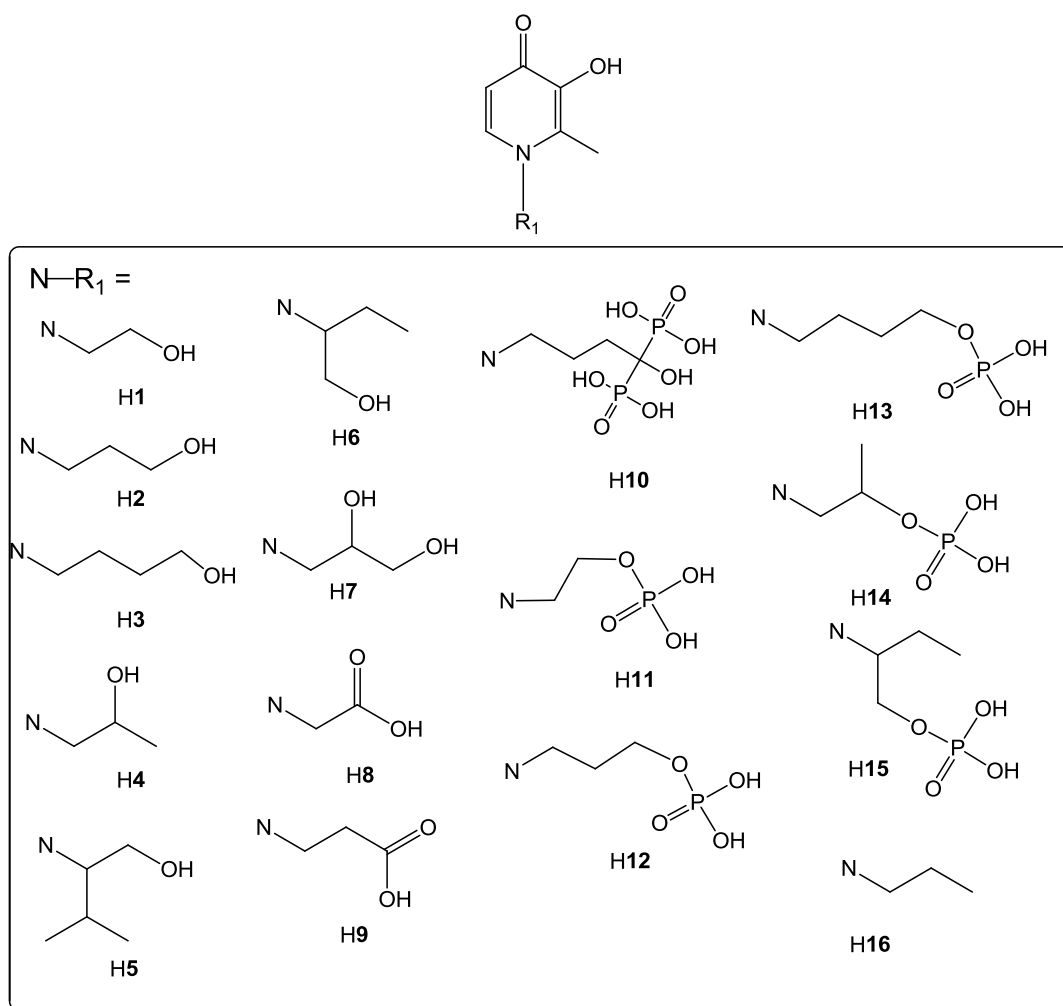
Figure 2.5. A summary of the ligands synthesized in this study.

The pyridinones are named according to their state (free ligand, benzyl-protected ligand and complexed ligand); the number correlates to particular *N*-substituent. For example, as seen in

Figure 2.6, the number corresponds to the ligand anion (**L⁻**), H denotes a hydroxy group at the 3 position (**HL**) while Bn denotes a benzyl group at the 3-oxy position (**BnL**). When the pyridinone is coordinated to a metal, the hydroxyl at the 3-oxy position of the free ligand is deprotonated, and is thus named by the metal and the number of ligands that are coordinated to that metal (Ln(**L**)$_3$).
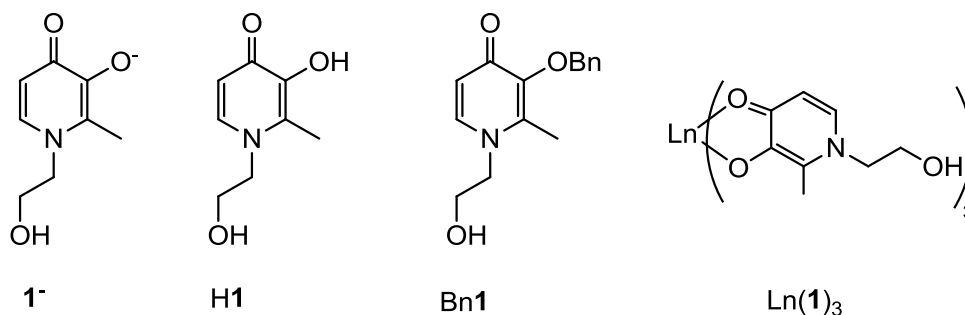
Figure 2.6. Naming convention used for the ligand 3-oxy-2-methyl-1-(2-hydroxyethyl)-4-pyridinone (**1⁻**).

The numbering scheme used for characterization by ^{1}H and ^{13}C NMR spectroscopy is shown in Figure 2.7.

R$_1$ = alkyl, alkyl-OH, alkyl-diol, alkyl-COOH, alkyl-OPO$_3$H$_2$
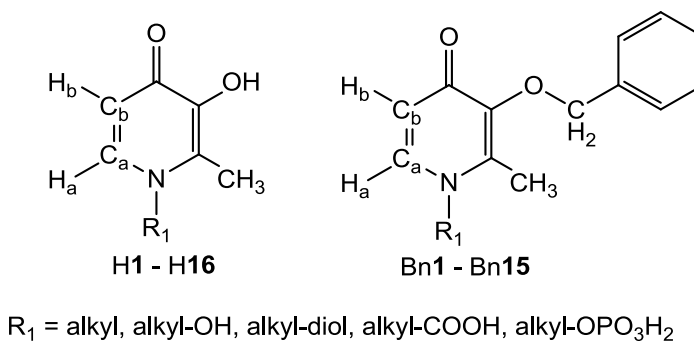
Figure 2.7. The general chemical structure of the 3-hydroxy- and 3-benzyloxy-4-pyridinones and the numbering system used for ^{1}H and ^{13}C{^{1}H} NMR spectroscopic characterization.

2.2   *Experimental*

2.2.1   Materials

All solvents used for the synthesis of the ligands and metal complexes were HPLC grade and purchased from Fisher Scientific, as were anhydrous sodium sulphate, hydrochloric acid, potassium hydroxide, sodium hydroxide and formaldehyde (aqueous solution 37% w/w). Water was purified using an Elgastat Maxima HPLC reverse osmosis and deionization system or a PureLab Ultra system (Elga, Bucks, England). All water used was type 1, 18.2 MΩ-cm, treated with a full spectrum UV to control bacterial levels. Maltol, iminodiacetic acid and hypophosphorous acid (50% w/w aqueous solution) were purchased from Sigma-Aldrich, and the primary amines were purchased either from Sigma-Aldrich or Acros Organics, with the exception of 4-amino-1-hydroxybutane-1,1-diphosphonic acid (alendronate) which was purchased from TCI America. Lanthanum nitrate, europium nitrate, gadolinium nitrate and lutetium nitrate were purchased from Sigma-Aldrich and Alfa Aesar as their hexahydrates and used without further purification. Analytical thin layer chromatography (TLC) plates (which were alumina backed ultra pure silica gel 60 Å, 250 μm), and flash column silica gel (standard grade, 60 Å, 32-63 mm) were purchased from Silicycle. Hydrobromic acid (33% w/v in glacial acetic acid) was obtained from Acros Organics. Reverse phase C18 (Waters, Sep-Pak, 1 g) columns were purchased from Waters Limited (Mississauga, ON, Canada) and CombiFlash RediSepPak columns were purchased from Teledyne Isco Inc. (Lincoln, NE, U.S.).

For the potentiometric titrations, 3-hydroxy-1,2-dimethyl-4-pyridinone was purchased from Sigma-Aldrich, along with La^{3+} and Gd^{3+} atomic absorption (AA) standards. An aqueous 50% sodium hydroxide solution was purchased from Acros Organics.

2.2.2 Instrumentation

Elemental analyses for C, H, and N (Fisons EA 1108 instrumentation) were completed by David Wong or by Derek Smith at the UBC Chemistry Mass Spectrometry/Microanalysis Services. High resolution mass spectrometry electrospray ionization (Micromass LCT instrumentation) was performed by Derek Smith at the UBC Chemistry Mass Spectrometry/Microanalysis Services. Low resolution mass spectra were obtained on a Bruker Esquire Ion Trap ESI-MS spectrometer. ^{1}H, ^{13}C$\{^1$H$\}$ and ^{31}P$\{^1$H$\}$ nuclear magnetic resonance (NMR) spectra were recorded at room temperature using a Bruker AV-300 or AV-400 spectrometer; all phosphorus NMR spectra were referenced externally to H_3PO_4 (85% w/w). Fourier transform infrared (FTIR) spectra were obtained on a Nicolet 6700 FTIR equipped with a Smart Orbit diamond attenuated total reflectance attachment. A Biotage Initiator Microwave Synthesizer was used in the synthesis of **H10** and purification of some of the ligand precursors was accomplished on a CombiFlash automated column system fitted with a UV-detector.

2.2.3 Synthesis of 3-Hydroxy-4-pyridinones by Direct Insertion
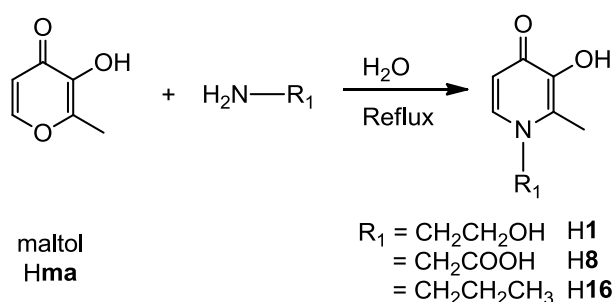
Figure 2.8. Synthesis of 3-hydroxy-2-methyl-pyridinone from 3-hydroxy-2-methyl-4-pyrone by the direct insertion of a primary amine.

The syntheses of H**1**, H**8** and H**16** were achieved by the direct insertion of the appropriate primary amine into 3-hydroxy-2-methyl-4-pyrone (maltol) as shown in Figure 2.8.

3-Hydroxy-2-methyl-1-(2-hydroxyethyl)-4-pyridinone (H1)
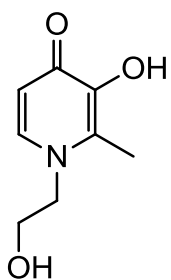
Based on a modification of a literature procedure,[122] maltol (9.30 g, 73.4 mmol, 1.0 equiv) was dissolved in hot water (50 mL); 2-aminoethanol (14.0 g, 0.229 mol, 3.1 equiv) was added and the mixture was stirred and refluxed for 70 h. The reaction mixture was cooled to room temperature and the water was removed under reduced pressure affording a dark brown oil. The crude oil was triturated with 2-propanol (30 mL) and maintained at 4 °C for 5 h, after which time a dark brown solid formed. The solid was collected by filtration, recrystallized from hot water (15 mL) and stored at 4 °C overnight. The resulting solid was subsequently filtered and dried *in vacuo*, affording light brown crystals, H**1** (5.09 g, 41%). ^{1}H NMR (400 MHz, D_2O) δ = 7.62 (d, J = 7.2 Hz, 1 H, H_a), 6.49 (d, J = 7.2 Hz, 1 H, H_b), 4.20 (t, J = 5.1 Hz, 2 H, CH_2-OH), 3.85 (t, J = 5.3 Hz, 2 H, N-CH_2), 2.40 (s, 3 H, ring CH_3). ^{13}C{^{1}H} NMR (101 MHz, D_2O) δ = 169.1 (ring C=O), 144.8 (C_a), 139.2 (ring C-OH), 135.1 (ring C-CH$_3$), 112.3 (C_b), 60.3 (CH$_2$-OH), 56.0 (N-CH$_2$), 11.8 (ring CH$_3$). MS (-ESI) *m/z* =168.3 [M - H]$^-$. Anal. Calc. (found): $C_8H_{11}NO_3$: C, 56.80 (56.42); H, 6.55 (6.56); N, 8.28 (8.30).

1-Carboxymethyl-3-hydroxy-2-methyl-4-pyridinone (H8)
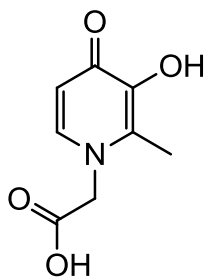
Based on a modification from a procedure reported previously in the Orvig group,[123] maltol (4.98 g, 39.5 mmol, 1.0 equiv) was added to hot water (100 mL) in the presence of glycine (5.97 g, 79.5 mmol, 2.0 equiv). The mixture was stirred and heated to 80 °C; the pH was increased to 9 by the dropwise addition of 6 M NaOH and monitored by pH paper. The reaction was brought to reflux and maintained for 24 h. The reaction mixture was cooled to room temperature and half of the water was removed

by rotary evaporation. The pH of the crude product was brought to ~3 with the addition of 6 M HCl, at which time a light brown solid precipitated. The precipitate was isolated by filtration and was subsequently recrystallized from hot water and stored at 4 °C overnight. The resulting solid was filtered and dried *in vacuo* to yield light brown crystals, H**8** (2.90 g, 40%). ^{1}H NMR (400 MHz, 0.1 M NaOD) δ = 7.18 (d, *J* = 6.8 Hz, 1 H, H_a), 6.31 (d, *J* = 7.2 Hz, 1 H, H_b), 4.52 (s, 2 H, N-CH_2), 2.18 (s, 3 H, ring CH_3). ^{13}C{^{1}H} NMR (101 MHz, 0.1 M NaOD) δ = 175.2 (CH$_2$-*C*OOH), 173.0 (ring *C*=O), 155.3 (C_a), 135.7 (ring *C*-OH), 133.8 (ring *C*-CH$_3$), 111.6 (C_b), 58.6 (N-*C*H$_2$), 12.3 (ring *C*H$_3$). MS (-ESI) *m/z* =182.3 [M - H]$^-$. Anal. Calc. (found): C$_8$H$_9$NO$_4$: C, 52.46 (52.64); H, 4.85 (4.92); N, 7.65 (7.66).

3-Hydroxy-2-methyl-1-propyl-4-pyridinone (H**16**)
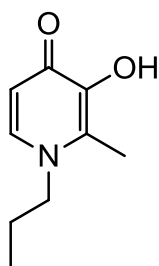
In a manner similar to that previously published,[124] maltol (5.11 g, 40.5 mmol, 1.0 equiv) and propylamine (10.0 mL, 0.122 mol, 3.0 equiv) were dissolved in hot water (100 mL). The mixture was mechanically stirred, and brought to and maintained at reflux for 24 h. The reaction mixture was cooled to room temperature and the water was removed under reduced pressure, affording a dark brown solid. The solid was then recrystallized from hot acetone and maintained at 4 °C overnight. The resulting solid was isolated by filtration, rinsed with cold acetone (4 °C) and dried *in vacuo* giving light brown crystals, H**16** (1.76 g, 26%). ^{1}H NMR (400 MHz, CD$_3$OD) δ = 7.60 (d, *J* = 7.0 Hz, 1 H, H_a), 6.37 (d, *J* = 7.0 Hz, 1 H, H_b), 4.00 (t, *J* = 7.5 Hz, 2 H, N-CH_2), 2.42 (s, 3 H, ring CH_3), 1.66 - 1.85 (m, 2 H, CH_2-CH$_3$), 0.96 (t, J = 7.5 Hz, 3 H, CH$_2$-CH_3). ^{13}C{^{1}H} NMR (101 MHz, CDCl$_3$) δ = 170.6 (ring *C*=O), 147.4 (C_a), 139.1 (ring *C*-OH), 132.9 (ring *C*-CH$_3$), 112.7 (C_b), 56.8 (N-*C*H$_2$), 25.2 (*C*H$_2$-CH$_3$), 12.0 CH$_2$-*C*H$_3$), 11.1 (ring *C*H$_3$). MS (+ESI) *m/z* =190.4 [M + H]$^+$. Anal. Calc. (found): C$_9$H$_{13}$NO$_2$: C, 64.65 (64.40); H, 7.84 (7.87); N, 8.38 (8.28).

2.2.4 Synthesis of 3-Benzyloxy-4-pyridinones

The syntheses of the 3-benzyloxy-2-methyl-4-pyridinones were achieved by the ammonolysis of 3-benzyloxy-2-methyl-4-pyrone (Bn**ma**) with the appropriate primary amine, as shown in Figure 2.9.

$$R_1 = \begin{array}{ll}
(CH_2)_2OH & Bn\mathbf{1}\\
(CH_2)_3OH & Bn\mathbf{2}\\
(CH_2)_4OH & Bn\mathbf{3}\\
CH_2C(OH)CH_3 & Bn\mathbf{4}\\
CH(CH_2OH)CH(CH_3)_2 & Bn\mathbf{5}\\
CH(CH_2OH)CH_2CH_3 & Bn\mathbf{6}\\
CH_2CH(OH)CH_2OH & Bn\mathbf{7}\\
(CH_2)_2COOH & Bn\mathbf{9}
\end{array}$$
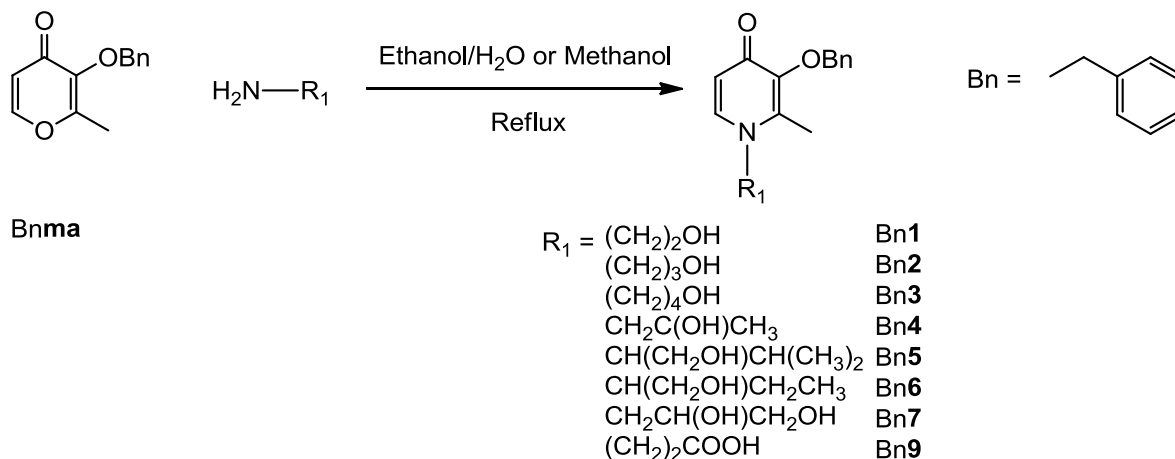
Figure 2.9. Synthesis of 3-benzyloxy-2-methyl-4-pyridinones from 3-benzyloxy-2-methyl-4-pyrone by the direct insertion of primary amines.

3-Benzyloxy-2-methyl-4-pyrone (Bnma)
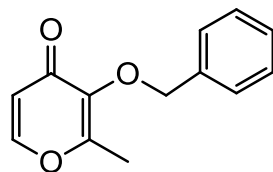
The synthesis of Bn**ma** was achieved by a modified literature procedure.[125] To a mixture of 3-hydroxy-2-methyl-4-pyrone (maltol; 7.00 g, 55.5 mmol, 1 equiv) dissolved in methanol (50 mL) a solution of NaOH (2.47 g in 10 mL water, 61.7 mmol, 1.2 equiv) was added dropwise. Benzyl chloride (9.30 mL, 66.8 mmol, 1.2 equiv) was added to the stirred mixture, which was then refluxed for 40 h. The mixture was cooled to room temperature and the solvent was removed by rotary evaporation to afford an orange oil and a white precipitate (NaCl). The oil was partitioned in water (40 mL) and dichloromethane (30 mL), separated

55

and the organic layer was dried over anhydrous Na_2SO_4. The organic layer was then filtered and concentrated, affording a yellow oil. The crude oil was recrystallized from ethanol and stored at 4 °C overnight. A white precipitate formed which was filtered through a coarse frit, rinsed with cold diethyl ether (4 °C), and dried *in vacuo*, to yield a white solid, Bn**ma** (9.484 g, 79%). ^{1}H NMR (400 MHz, CDCl$_3$) δ = 7.60 (d, J = 5.5 Hz, 1 H, H_a), 7.30 - 7.43 (m, 5 H, Bn C$_6$H$_5$), 6.37 (d, J = 5.8 Hz, 1 H, H_b), 5.17 (s, 2 H, Bn-CH_2), 2.09 (s, 3 H, ring CH_3). MS (+ESI) *m/z* =217.2 [M + H]$^+$.

3-Benzyloxy-2-methyl-1-(2-hydroxyethyl)-4-pyridinone (Bn1)
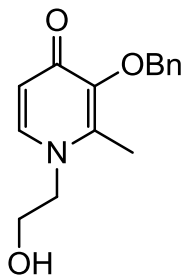
Based on a modification of a literature procedure,[126] Bn**ma** (12.55 g, 57.9 mmol, 1.0 equiv) and 2-aminoethanol (5.40 mL, 89.5 mmol, 1.5 equiv) were dissolved in a mixture of ethanol (50 mL) and deionized water (50mL). 6 M NaOH (1.70 mL, 10.2 mmol, 0.18 equiv) was added to adjust the pH > 11; the mixture was heated to reflux and maintained for 48 h. Upon cooling the mixture to room temperature, the solvent was concentrated by rotary evaporation affording a brown oil, which was then dissolved in water. The pH of the crude mixture was decreased to 1–2 using 6 M HCl and washed with diethyl ether. The pH of the aqueous layer was then adjusted to 7–8 with 6 M NaOH and the product was extracted with dichloromethane (3 × 100 mL). The combined organic layers were dried over anhydrous Na_2SO_4 and the drying agent was removed by filtration. The filtrate was collected and the solvent was removed by rotary evaporation, yielding a dark brown solid. The solid was recrystallized from ethanol and diethyl ether; upon precipitation, the product was isolated by filtration and dried *in vacuo* affording a light brown solid, Bn**1** (5.57 g, 37%). ^{1}H NMR (400 MHz, D$_2$O) δ = 7.71 (d, J = 7.4 Hz, 1 H, H_a), 7.40 (s, 5 H, Bn C$_6$H$_5$), 6.57 (d, J = 7.4 Hz, 1 H, H_b), 5.02 (s, 2 H, Bn-CH_2), 4.10 (t, J = 5.3 Hz, 2 H, CH_2-OH), 3.76 (t, J = 5.1 Hz, 2 H, CH_2-OH), 2.06 (s, 3 H, ring CH_3). MS (+ESI) *m/z* =260.4 [M + H]$^+$.

56

3-Benzyloxy-2-methyl-1-(3-hydroxypropyl)-4-pyridinone hydrochloride (Bn**2**•HCl) [126]
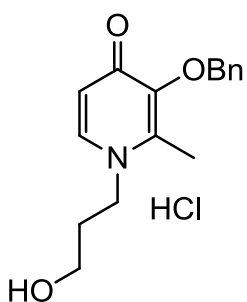
Based on a modification of a literature procedure,[126] Bn**ma** (5.09 g, 23.6 mmol, 1.0 equiv) and 3-aminopropanol (2.70 mL, 35.5 mmol, 1.5 equiv) were dissolved in a mixture of ethanol (40 mL) and deionized water (40 mL). 1 M NaOH (4.00 mL, 4.00 mmol, 0.17 equiv) was added to adjust the pH > 11; the mixture was heated to reflux and maintained for 18 h. Upon cooling the mixture to room temperature, the solvent was concentrated by rotary evaporation affording a brown oil, which was then dissolved in water. The pH of the crude mixture was decreased to 1–2 using 6 M HCl and washed with diethyl ether. The pH of the aqueous layer was then adjusted to 7–8 with 6M NaOH and the product was extracted with dichloromethane (3 × 50 mL). The combined organic layers were dried over anhydrous Na_2SO_4 and the drying agent was removed by filtration. The filtrate was collected and the solvent was removed by rotary evaporation, yielding a yellow oil. The oil was dissolved in ethanol and 6.0 M HCl was then used to lower the pH to ~0.5. The solvent was removed by rotary evaporation affording a pale yellow solid, which was recrystallized from ethanol and diethyl ether. Upon precipitation the product was collected by filtration and dried *in vacuo*, affording an off-white solid, Bn**2**•HCl (4.31 g, 59%). ^{1}H NMR (300 MHz, D_2O) δ = 8.04 (d, J = 7.1 Hz, 1 H, H_a), 7.41 (s, 5 H, Bn C_6H_5), 6.98 (d, J = 7.1 Hz, 1 H, H_b), 5.12 (s, 2 H, Bn-CH_2), 4.25 (t, J = 7.3 Hz, 2 H, N-CH_2), 3.53 (t, J = 5.9 Hz, 2 H, CH_2-OH), 2.28 (s, 3 H, ring CH_3), 1.81 - 1.99 (m, 2 H, N-CH$_2$-CH_2-CH$_2$-OH). MS (-ESI) m/z = 308.3, 310.3 [M + Cl]$^-$.

3-Benzyloxy-2-methyl-1-(4-hydroxybutyl)-4-pyridinone hydrochloride (Bn**3**•HCl)[126]
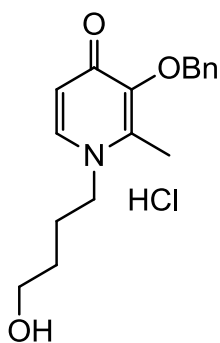
Based on a modification of a literature procedure,[126] Bn**ma** (4.01 g, 18.5 mmol, 1.0 equiv) and 4-amino-1-butanol (2.56 mL, 2.78 mmol, 1.5 equiv) were dissolved in a mixture of ethanol (32 mL) and deionized water (32 mL). NaOH (0.126 g, 3.15 mmol, 0.17 equiv) was added to adjust the pH > 11; the mixture was heated to reflux and maintained for 15 h. Upon cooling the mixture to room temperature, the solvent was concentrated by rotary evaporation, affording a brown oil, which was then dissolved in water. The pH of the crude mixture was decreased to 1–2 using 6 M HCl and washed with diethyl ether. The pH of the aqueous layer was then adjusted to 7–8 with 6 M NaOH and the product was extracted with dichloromethane (3 × 40 mL). The combined organic layers were dried over anhydrous Na_2SO_4 and the drying agent was removed by filtration. The filtrate was collected and the solvent was removed by rotary evaporation, yielding a brown oil. The oil was dissolved in ethanol and 6.0 M HCl was then used to lower the pH to ~0.5. The solvent was removed by rotary evaporation affording a pale yellow solid, which was recrystallized from ethanol and diethyl ether. Upon precipitation, the product was collected by filtration and dried *in vacuo*, affording a light brown solid, Bn**3**•HCl (3.23 g, 54%). ^{1}H NMR (300 MHz, CDCl₃) δ = 8.69 (d, J = 7.1 Hz, 1 H, H_a), 8.03 (d, J = 7.1 Hz, 1 H, H_b), 7.36 (s, 5 H, Bn C_6H_5), 5.23 (s, 2 H, Bn-CH_2), 4.41 (t, J = 7.8 Hz, 2 H, N-CH_2), 3.75 (t, J = 5.6 Hz, 2 H, CH_2-OH), 2.41 (s, 3 H, ring CH_3), 1.96 (q, J = 7.5 Hz, 2 H, CH_2-CH₂-OH), 1.66 (q, J = 5.5 Hz, 2 H N-CH₂-CH_2). MS (+ESI) m/z = 288.2 [M + H]$^+$.

3-Benzyloxy-2-methyl-1-(2-hydroxypropyl)-4-pyridinone (Bn**4**)
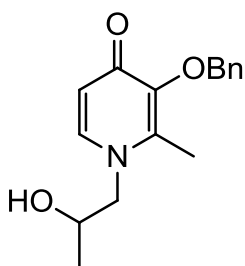
Bn**ma** (5.01 g, 23.2 mmol, 1.0 equiv) and (±)-1-aminopropan-2-ol (3.58 mL, 46.4 mmol, 2.0 equiv) were dissolved in a mixture of ethanol (40 mL) and deionized water (40 mL). NaOH (0.157 g, 3.94 mmol, 0.17 equiv) was added to adjust the pH > 11; the mixture was heated to reflux and maintained at reflux for 92 h. Upon cooling the

mixture to room temperature, the solvent was concentrated by rotary evaporation, affording a brown oil, which was then dissolved in water. The pH of the crude mixture was decreased to 1–2 using 6 M HCl and washed with diethyl ether. The pH of the aqueous layer was then adjusted to 7–8 with 6M NaOH and the product was extracted with dichloromethane (3×50 mL). The combined organic layers were dried over anhydrous Na_2SO_4 and the drying agent was removed by filtration. The filtrate was collected and the solvent was removed by rotary evaporation, yielding a brownish-orange solid. The solid was recrystallized from ethanol and diethyl ether; upon precipitation, the product was isolated by filtration and dried *in vacuo* affording a light orange-brown solid, Bn**4** (3.71 g, 59%). ^{1}H NMR (400 MHz , CDCl$_3$) $\delta =$ 7.22 - 7.45 (m, 6 H, H_a, Bn C$_6$$H_5$), 6.16 (d, 7.3 Hz, 1 H, H_b), 5.07 (dd, $J = 1.7, 11.2$ Hz, 1 H, Bn-CH_2), 4.93 (dd, $J = 3.4, 11.3$ Hz, 1 H, Bn-CH_2), 4.02 - 4.16 (m, 1 H, CH-OH), 3.76 (dd, $J = 2.1, 14.3$ Hz, 1 H, N-CH_2), 3.51 (dd, $J = 9.6, 14.3$ Hz, 1 H, N-CH_2), 2.11 (s, 3 H ring CH_3), 1.20 (d, $J = 6.5$ Hz, 3 H, CH(OH)CH_3). MS (+ESI) *m/z* = 569.3 [M$_2$ + Na]$^+$.

3-Benzyloxy-2-methyl-1-(1-hydroxy-3-methylbutan-2-yl)-4-pyridinone (Bn**5**)

Bn**ma** (5.06 g, 23.4 mmol, 1.0 equiv) and ($\pm$)-2-amino-3-methyl-1-butanol (4.00 mL, 36.3 mmol, 1.6 equiv) were dissolved in a mixture of ethanol (25 mL) and deionized water (25 mL). NaOH (0.172 g, 4.31 mmol, 0.18 equiv) was added to adjust the pH > 11; the mixture was heated to reflux and maintained at reflux for 90 h. Upon cooling the mixture to room temperature, the solvent was concentrated by rotary evaporation, affording a brown oil, which was then dissolved in water. The pH of the crude mixture was decreased to 1–2 using 6 M HCl and washed with diethyl ether. The pH of the aqueous layer was then adjusted to 7–8 with 6M NaOH and the product was extracted with dichloromethane (3×50 mL). The combined organic layers were dried over anhydrous Na_2SO_4 and the drying agent was removed by filtration. The filtrate was collected and the solvent was removed by rotary evaporation, yielding an orange oil. The orange oil was loaded onto a silica column (95:5 CHCl$_3$: CH$_3$OH), and the product was eluted in 95:5 CHCl$_3$: CH$_3$OH. The appropriate fractions were collected and concentrated by rotary

evaporation, which yielded an orange solid, which was subsequently recrystallized from ethanol and diethyl ether. The resulting solid was recovered by filtration to afford a light brown solid, Bn**5** (0.429 g, 6%). [^1]H NMR (300 MHz, CD$_3$OD) δ = 7.85 (d, J = 7.8 Hz, 1 H, H_a), 7.25 - 7.42 (m, 5 H, Bn C$_6$*H*$_5$), 6.57 (d, J = 7.5 Hz, 1 H, H_b), 5.15 (d, J = 11.2 Hz, 1 H, Bn-C*H*$_2$), 5.05 (d, J = 11.2, 1 H, Bn-C*H*$_2$), 3.73 - 4.05 (m, 3 H, C*H*-CH$_2$-OH), 2.07-2.20 (m, 1 H, C*H*(CH$_3$)$_2$), 2.15 (s, 3H, ring C*H*$_3$), 1.08 (d, J = 6.6 Hz, 3 H, CH-C*H*$_3$), 0.65 (d, J = 6.9 Hz, 3 H, CH-C*H*$_3$). MS (+ESI) m/z = 625.8 [M$_2$ + Na]$^+$.

3-Benzyloxy-2-methyl-1-(1-hydroxybutan-2-yl)-4-pyridinone (Bn**6**)

Bn**ma** (5.02 g, 23.2 mmol, 1.0 equiv) and (±)-2-amino-1-butanol (4.37 mL, 4.13 mmol, 2.0 equiv) were dissolved in a 1:1 mixture of ethanol (40 mL) and deionized water (40 mL). NaOH (0.160 g, 4.00 mmol, 0.17 equiv) was added to adjust the pH > 11; the mixture was heated to reflux and maintained there for 88 h. Upon cooling the mixture to room temperature, the solvent was concentrated by rotary evaporation, affording a brown oil, which was then dissolved in water. The pH of the crude mixture was decreased to 1–2 using 6 M HCl and washed with diethyl ether. The pH of the aqueous layer was then adjusted to 7–8 with 6M NaOH and the product was extracted with dichloromethane (3 × 50 mL). The combined organic layers were dried over anhydrous Na$_2$SO$_4$ and the drying agent was removed by filtration. The filtrate was collected and the solvent was removed by rotary evaporation, yielding an orange oil. The solid was recrystallized from ethanol and diethyl ether; upon precipitation, the product was isolated by filtration and dried *in vacuo* affording a light brown solid, Bn**6** (6.66 g, 30%). [^1]H NMR (300 MHz, D$_2$O) δ = 7.78 (d, J = 7.8 Hz, 1 H, H_a), 7.21 - 7.49 (m, 5 H, Bn C$_6$*H*$_5$), 6.64 (d, J = 7.5 Hz, 1 H, H_b), 5.01 (s, 2 H, Bn-C*H*$_2$), 4.22 - 4.40 (m, 1 H, N-C*H*), 3.59 - 3.84 (m, 2 H, C*H*$_2$-OH), 1.98 (s, 3 H, ring C*H*$_3$), 1.53 - 1.88 (m, 2 H, C*H*$_2$CH$_3$), 0.64 (t, J = 7.3 Hz, 3 H, CH$_2$C*H*$_3$). MS (+ESI) m/z = 597.7 [M$_2$ + Na]$^+$.

3-Benzyloxy-2-methyl-1-(2,3-dihydroxypropyl)-4-pyridinone (Bn7)

Bn**ma** (2.12 g, 9.80 mmol, 1.0 equiv) and (±)-3-aminopropane-1,2-diol (1.37 g, 15.0 mmol, 1.5 equiv) were dissolved in methanol (20 mL); the stirred mixture was heated to and maintained at reflux for 72 h. The reaction was cooled at to 4 °C overnight, during which time a pale yellow solid precipitated, that was subsequently filtered and rinsed with cold methanol (4 °C, 20 mL) and diethyl ether (20 mL). The solid was recrystallized from ethanol and diethyl ether; upon precipitation, the solid was recovered by filtration, dried *in vacuo*, affording a pale yellow solid, Bn**7** (1.74 g, 61%). ^{1}H NMR (400 MHz, D$_2$O): δ = 7.68 (d, J = 7.3 Hz, 1 H, H_a), 7.38 (s, 5 H, Bn C$_6$$H_5$), 6.55 (d, J = 7.3 Hz, 1 H, H_b), 5.01 (s, 2 H, Bn-CH_2), 4.07 - 4.21 (m, 1 H, CH_2-OH), 3.87 (d, J = 14.6 Hz, 1 H, CH_2-OH), 3.76 - 3.84 (m, 1 H, CH-OH), 3.54 (dd, J = 13.2, 5.0 Hz, 2 H, N-CH_2), 2.05 (s, 3 H, ring CH_3). ^{13}C NMR (75 MHz, D$_2$O): δ = 175.1 (ring C=O), 147.1 (ring C-O-Bn), 145.8 (C_a), 142.4 - 129.5 (4 peaks, Bn C_6H$_5$), 129.4 (ring C-CH$_3$), 116.9 (C_b), 74.7 (CH$_2$-Bn), 72.3 (CH-OH), 64.7 (CH$_2$-OH), 57.8 (N-CH$_2$), 13.3 (ring CH$_3$). MS (+ESI) m/z = 290.4 [M + H]$^+$.
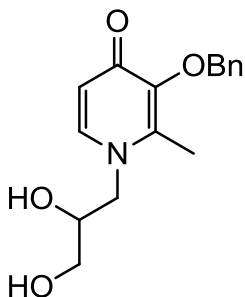
## 1-Carboxyethyl-3-benzyloxy-2-methyl-4-pyridinone (Bn9)[126]
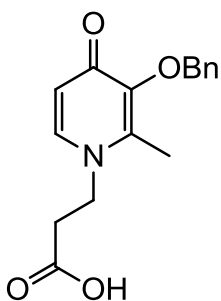
Based on a modification of a literature procedure,[126] Bn**ma** (5.09 g, 23.5 mmol, 1.0 equiv) and β-alanine (3.22 g, 3.61 mmol, 1.5 equiv) were dissolved in a mixture of ethanol (40 mL) and deionized water (40 mL). The pH was increased from 7 to 13 using 6M NaOH; the mixture was heated to reflux and maintained for 18 h. Upon cooling the mixture to room temperature, the solvent was concentrated by rotary evaporation to afford a brown oil, which was then dissolved in water. The pH of the crude mixture was decreased to 1–2 using 6 M HCl and washed with diethyl ether. The pH of the aqueous layer was then adjusted to 7–8 with 6M NaOH and the product was extracted with dichloromethane (3 × 50 mL). The combined organic layers were dried over anhydrous Na$_2$SO$_4$ and the drying agent was removed by filtration. The filtrate was collected and the

solvent was removed by rotary evaporation, yielding a yellow oil. The oil was dissolved in ethanol and 6.0 M HCl was then used to lower the pH to ~0.5. The solvent was removed by rotary evaporation to afford a pale yellow solid, which was recrystallized from ethanol and diethyl ether. Upon precipitation the product was collected by filtration and dried *in vacuo*, affording a pale yellow solid, Bn**9** (3.05 g, 45%). ^{1}H NMR (300 MHz, D$_2$O) δ = 7.86 (d, J = 7.3 Hz, 1 H, H_a), 7.28 - 7.48 (m, 5 H, Bn C$_6$H$_5$), 6.68 (d, J = 7.3 Hz, 1 H, H_b), 5.03 (s, 2 H, Bn-CH_2), 4.28 (t, J = 6.9 Hz, 2 H, N-CH_2), 2.68 (t, J = 7.0 Hz, 2 H, CH_2-COOH), 2.13 (s, 3 H, ring CH_3). MS (-ESI) *m/z* = 286.3 [M - H]$^-$.

2.2.5   Synthesis of 3-Hydroxy-4-pyridinones from 3-Benzyloxy-4-pyridinones: Debenzylation

The syntheses of the 3-hydroxy-2-methyl-4-pyridinones, H**2**, H**3**, H**4**, H**5**, H**6**, H**7** and H**9**, were achieved by the debenzylation of the appropriate 3-benzyloxy-2-methyl-4-pyridinones (Bn**2**, Bn**3**, Bn**4**, Bn**5**, Bn**6**, Bn**7** and Bn**9**) as shown in Figure 2.10.

R$_1$ = (CH$_2$)$_3$OH	Bn**2**
(CH$_2$)$_4$OH	Bn**3**
CH$_2$C(OH)CH$_3$	Bn**4**
CH(CH$_2$OH)CH(CH$_3$)$_2$	Bn**5**
CH(CH$_2$OH)CH$_2$CH$_3$	Bn**6**
CH$_2$CH(OH)CH$_2$OH	Bn**7**
(CH$_2$)$_2$COOH	Bn**9**

R$_1$ = (CH$_2$)$_3$OH	H**2**
(CH$_2$)$_4$OH	H**3**
CH$_2$C(OH)CH$_3$	H**4**
CH(CH$_2$OH)CH(CH$_3$)$_2$	H**5**
CH(CH$_2$OH)CH$_2$CH$_3$	H**6**
CH$_2$CH(OH)CH$_2$OH	H**7**
(CH$_2$)$_2$COOH	H**9**
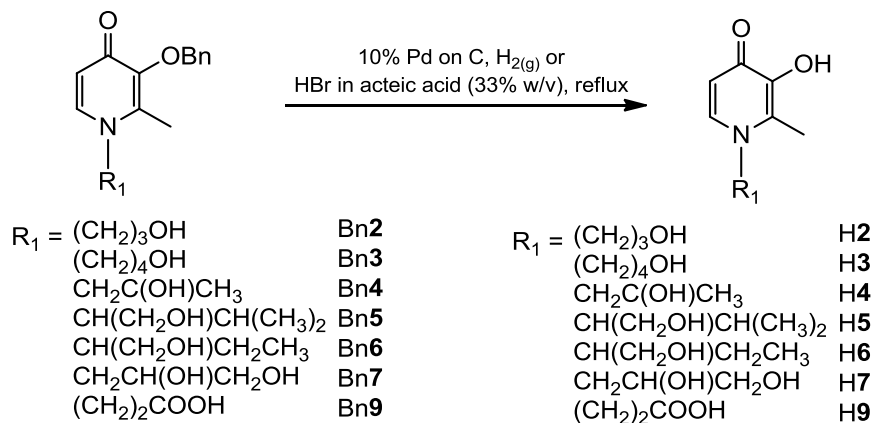
Figure 2.10. Synthesis of 3-hydroxy-2-methyl-4-pyridinone from 3-benzyloxy-2-methyl-4-pyridinones, by the removal of the benzyl protecting group.

3-Hydroxy-2-methyl-1-(3-hydroxypropyl)-4-pyridinone hydrochloride (H2•HCl)[126]
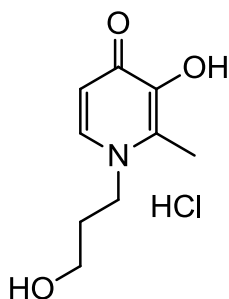
Based on a modification of a literature procedure,[126] 3-benzyloxy-2-methyl-1-(3-hydroxypropyl)-4-pyridinone hydrochloride (Bn2•HCl; 1.00 g, 3.23 mmol, 1.0 equiv) was suspended in a mixture of ethanol (9 mL) and deionized water (1 mL) and the pH was lowered to 1 with 6 M HCl. The hydrogenation catalyst (10% w/w of Pd on C; 0.406 g) was added and the flask was flushed once with a balloon filled with $H_{2(g)}$. The reaction was stirred under the $H_{2(g)}$-filled balloon for 6 h at room temperature. The dark suspension was filtered to remove the catalyst, which was rinsed with ethanol, methanol and water. The solvent was removed by rotary evaporation to afford the crude product as an oil. The oil was dissolved in ethanol and 6.0 M HCl was then used to lower the pH to ~0.5. The solvent was removed by rotary evaporation affording a pale yellow solid, which was recrystallized from ethanol and diethyl ether. Upon precipitation the product was collected by filtration and dried *in vacuo*, affording a white solid, H2•HCl (0.519 g, 73%). ^{1}H NMR (300 MHz, D$_2$O) δ = 8.02 (d, J = 7.1 Hz, 1 H, H_a), 7.07 (d, J = 6.9 Hz, 1 H, H_b), 4.40 (t, J = 7.4 Hz, 2 H, N-CH_2), 3.63 (t, J = 5.8 Hz, 2 H, CH_2-OH), 2.58 (s, 3 H, ring CH_3), 2.05 (quin, J = 6.7 Hz, 2 H, N-CH$_2$-CH_2-CH$_2$-OH). ^{13}C{^{1}H} NMR (101 MHz, D$_2$O) δ = 158.5 (ring C=O), 142.7 (C_a), 142.6 (ring C-OH), 138.7 (ring C-CH$_3$), 111.1 (C_b), 57.9 (CH$_2$-OH), 53.9 (N-CH$_2$), 31.8 (N-CH$_2$-CH$_2$-CH$_2$-OH), 12.3 (ring CH$_3$). MS (+ ESI) m/z = 184.3 [M +H]$^+$. Anal. Calc. (found): C$_9$H$_{13}$NO$_3$•HCl: C, 49.21 (48.91); H, 6.42 (6.35); N, 6.38 (6.32).

3-Hydroxy-2-methyl-1-(4-hydroxybutyl)-4-pyridinone hydrochloride (H3•HCl)[126]
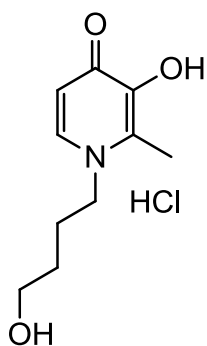
Based on a modification of a literature procedure,[126] 3-benzyloxy-2-methyl-1-(4-hydroxybutyl)-4-pyridinone hydrochloride (Bn3•HCl; 0.501 g, 1.55 mmol, 1.0 equiv) was dissolved in a mixture of ethanol (8 mL) and deionized water (1 mL). The hydrogenation catalyst (10% w/w of Pd on C; 93.0 mg) was added and the flask was flushed once with a balloon filled with $H_{2(g)}$. The reaction was stirred under the $H_{2(g)}$-filled balloon for

6 h at room temperature. The dark suspension was filtered to remove the catalyst, which was rinsed with ethanol, methanol and water. The solvent was removed by rotary evaporation to afford the crude product as an oil. The oil was dissolved in ethanol and 6.0 M HCl was then used to lower the pH to ~0.5. The solvent was removed by rotary evaporation affording a pale yellow solid, which was recrystallized from ethanol and diethyl ether. Upon precipitation the product was collected by filtration and dried *in vacuo*, affording an off-white solid, H**3**•HCl (0.261 g, 72%). ^{1}H NMR (400 MHz, D$_2$O) δ = 8.00 (d, *J* = 7.2 Hz, 1 H, *H*$_a$), 7.05 (d, *J* = 7.2 Hz, 1 H, *H*$_b$), 4.31 (t, *J* = 7.7 Hz, 2 H, N-C*H*$_2$), 3.57 (t, *J* = 6.3 Hz, 2 H, C*H*$_2$-OH), 2.55 (s, 3 H, ring C*H*$_3$), 1.76 - 1.91 (m, 2 H, C*H*$_2$-CH$_2$-OH), 1.48 - 1.62 (m, 2 H, N-CH$_2$-C*H*$_2$). ^{13}C{^{1}H} NMR (101 MHz, D$_2$O) δ = 158.6 (ring *C*=O), 142.7(*C*$_a$), 142.3 (ring *C*-OH), 138.5 (ring *C*-CH$_3$), 111.3 (*C*$_b$), 60.9 (*C*H$_2$-OH), 56.5 (N-*C*H$_2$), 28.2 (N-CH$_2$-*C*H$_2$), 26.0 (*C*H$_2$-CH$_2$-OH), 12.2 (ring *C*H$_3$). MS (+ESI) *m/z* = 198.2 [M + H]$^+$. Anal. Calc. (found): C$_{10}$H$_{15}$NO$_3$•HCl: C, 51.40 (51.49); H, 6.90 (6.95); N, 5.99 (5.95).

3-Hydroxy-2-methyl-1-(2-hydroxypropyl)-4-pyridinone (H4)
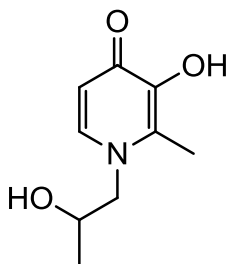
To afford the free pyridinone, 3-benzyloxy-2-methyl-1-(2-hydroxypropyl)-4-pyridinone (Bn**4**; 0.508 g, 1.86 mmol, 1.0 equiv) was dissolved in a mixture of ethanol (8 mL) and deionized water (2 mL). The hydrogenation catalyst (10% w/w of Pd on C; 89.2 mg) was added and the flask was flushed once with a balloon filled with H$_{2(g)}$. The reaction was stirred under the H$_{2(g)}$-filled balloon for 6 h at room temperature. The dark suspension was filtered to remove the catalyst, which was rinsed with ethanol, methanol and water. The solvent was removed by rotary evaporation to afford the crude product as brown solid, which was recrystallized from ethanol and diethyl ether. The precipitate that formed was collected by filtration and dried *in vacuo*, affording a pale brown solid, H**4** (0.170 g, 50%). ^{1}H NMR (400 MHz, CD$_3$OD) δ = 7.59 (d, *J* = 7.2 Hz, 1 H, *H*$_a$), 6.39 (d, *J* = 7.2 Hz, 1 H, *H*$_b$), 4.10 (dd, *J* = 14.1, 3.2 Hz, 1 H, C*H*-OH), 3.96 - 4.05 (m, 1 H, N-C*H*$_2$), 3.83 - 3.91 (m, 1 H, N-C*H*$_2$), 2.45 (s, 3 H, ring C*H*$_3$), 1.24 (d, *J* = 6.5 Hz, 3 H, CH(OH)C*H*$_3$). ^{13}C{^{1}H} NMR (101 MHz, CD$_3$OD) δ = 170.8 (ring *C*=O), 147.1 (*C*$_a$), 140.2

(ring C-OH), 133.4 (ring C-CH$_3$), 112.3 (C_b), 67.8 (CH-OH), 61.5 (N-CH_2), 21.0 (CH(OH)CH_3), 12.56 (ring CH_3). MS (+ESI) m/z = 184.3 [M + H]$^+$. Anal. Calc. (found): C$_9$H$_{13}$NO$_3$: C, 59.00 (59.03); H, 7.15 (7.15); N, 7.65 (7.38).

3-Hydroxy-2-methyl-1-(1-hydroxy-3-methylbutan-2-yl)-4-pyridinone (H5)
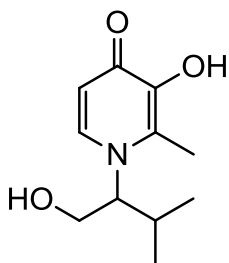
To afford the free pyridinone, 3-benzyloxy-2-methyl-1-(1-hydroxy-3-methylbutan-2-yl)-4-pyridinone (Bn**5;** 1.30 g, 4.32 mmol, 1.0 equiv) was dissolved in a mixture of ethanol (18 mL) and deionized water (3 mL). The hydrogenation catalyst (10% w/w of Pd on C; 0.104 g) was added and the flask was flushed once with a balloon filled with H$_{2(g)}$. The reaction was stirred under the H$_{2(g)}$-filled balloon for 6 h at room temperature. The dark suspension was filtered to remove the catalyst, which was rinsed with ethanol, methanol, dichloromethane, 2-propanol and water. The solvent was removed by rotary evaporation to afford the crude product as an orange solid, which was recrystallized from ethanol and diethyl ether. The precipitate that formed was collected by filtration and dried *in vacuo*, affording an off-white solid, H**5** (0.253 g, 28%). ^{1}H NMR (300 MHz, CD$_3$OD) δ = 7.78 (d, J = 7.3 Hz, 1 H, H_a), 6.49 (d, J = 7.3 Hz, 1 H, H_b), 4.03 - 4.19 (m, 1 H, CH-CH$_2$-OH), 3.78 - 4.03 (m, 2 H, CH-CH_2-OH), 2.46 (s, 3 H, ring CH_3), 2.11 - 2.30 (m, 1 H, CH(CH$_3$)$_2$), 1.06 - 1.19 (m, 3 H, CH-CH_3), 0.76 (d, J = 6.6 Hz, 3 H, CH-CH_3). ^{13}C{^{1}H} NMR (101 MHz, CD$_3$OD) δ = 170.2 (C=O), 135.5 (ring C-CH$_3$), 112.9 (C_b), 69.9 (CH-OH), 63.2 (CH-CH$_2$-OH), 31.4 (CH_2-OH), 20.0 (CH(CH$_3$)$_2$), 19.6 (CH(CH_3)$_2$), 12.6 (ring CH_3). Anal. Calc. (found): C$_{11}$H$_{17}$NO$_3$: C, 62.54 (62.29); H, 8.11 (8.15); N, 6.63 (6.71). MS (+ESI) m/z = 212.3 [M + H]$^+$.

3-Hydroxy-2-methyl-1-(1-hydroxybutan-2-yl)-4-pyridinone (H**6**)
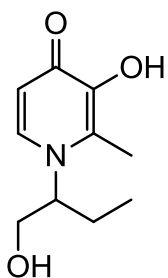
To afford the free pyridinone, 3-benzyloxy-2-methyl-1-(1-hydroxybutan-2-yl)-4-pyridinone (Bn**6**; 0.465 g, 1.62 mmol, 1.0 equiv) was dissolved in a mixture of ethanol (8 mL) and deionized water (2 mL). The hydrogenation catalyst (10% w/w of Pd on C; 88.2 mg) was added and the flask was flushed once with a balloon filled with $H_{2(g)}$. The reaction was stirred under the $H_{2(g)}$-filled balloon for 6 h at room temperature. The dark suspension was filtered to remove the catalyst, which was rinsed with ethanol, methanol and water. The solvent was removed by rotary evaporation to afford the crude product as pink solid, which was recrystallized from ethanol and diethyl ether. The precipitate that formed was collected by filtration and dried *in vacuo*, affording a pale pink solid, H**6** (0.262 g, 82%). ^{1}H NMR (400 MHz, CD$_3$OD) δ = 7.73 (d, J = 7.5 Hz, 1 H, H_a), 6.49 (d, J = 7.2 Hz, 1 H, H_b), 4.36 - 4.48 (m, 1 H, N-CH), 3.70 - 3.87 (m, 2 H, CH_2-OH), 2.48 (s, 3 H, ring CH_3), 1.71 - 1.99 (m, 2 H, CH_2CH$_3$), 0.86 (t, J = 7.3 Hz, 3 H, CH$_2$-CH_3). ^{13}C{^{1}H} NMR (100 MHz, CD$_3$OD) δ = 170.5 (ring C=O), 146.8 (C_a), 135.0 (ring C-OH), 134.5 (ring C-CH$_3$), 113.2 (C_b), 65.5 (N-CH), 65.3 (CH$_2$-OH), 25.4 (CH$_2$-CH$_3$), 12.6 (CH$_2$$CH_3$), 10.5 (ring CH$_3$). MS (+ESI) m/z = 198.2 [M + H]$^+$. Anal. Calc. (found): C$_{10}$H$_{15}$NO$_3$: C, 60.90 (60.80); H, 7.67 (7.68); N, 7.10 (7.19).

3-Hydroxy-2-methyl-1-(2,3-dihydroxypropyl)-4-pyridinone (H**7**)
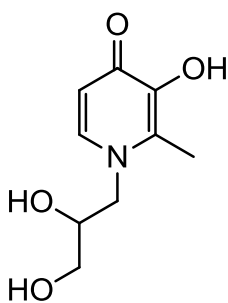
To afford the free pyridinone, 3-benzyloxy-1-(2,3-dihydroxypropyl)-2-methyl-4-pyridinone (Bn**7**; 0.284 g, 0.98 mmol, 1.0 equiv) was dissolved in deionized water (10 mL). The hydrogenation catalyst (10% w/w of Pd on C; 58.0 mg) was added and the flask was flushed once with a balloon filled with $H_{2(g)}$. The reaction was stirred under the $H_{2(g)}$-filled balloon for 6 h at room temperature. The dark suspension was filtered to remove the catalyst, which was rinsed with ethanol, methanol and water. The solvent was removed by rotary evaporation to afford the crude product as brown solid, which

was recrystallized from ethanol and diethyl ether. The precipitate that formed was collected by filtration and dried *in vacuo*, affording a light pink solid, H**7** (66.9 mg, 34%). ^{1}H NMR (300 MHz, CD$_3$OD): δ = 7.61 (d, J = 7.1 Hz, 1 H, H_a), 6.39 (d, J = 7.1 Hz, 1 H, H_b), 4.24 - 4.37 (m, 1 H, CH_2-OH), 3.88 - 3.98 (m, 1 H, CH_2-OH), 3.77 - 3.88 (m, 1 H, CH-OH), 3.55 (dd, J = 10.2, 5.4 Hz, 2 H, N-CH_2), 2.46 (s, 3 H, ring CH_3). ^{13}C{^{1}H} NMR (75 MHz, CD$_3$OD): δ = 170.8 (ring C=O), 147.2 (C_a), 140.2 (ring C-OH), 133.5 (ring C-CH$_3$), 112.4 (C_b), 72.4 (*C*H-OH), 64.8 (*C*H$_2$-OH), 57.8 (N-*C*H$_2$), 12.4 (ring *C*H$_3$). MS (+ESI) *m/z* = 200.4 [M + H]$^+$. Anal. Calc. (found): C$_{10}$H$_{15}$NO$_3$: C, 54.26 (53.47); H, 6.58 (6.68); N, 7.03 (7.02).

1-Carboxyethyl-3-hydroxy-2-methyl-4-pyridinone (H**9**)[126]
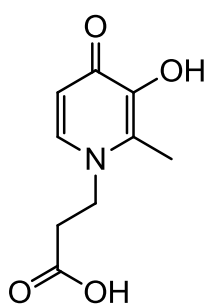
To afford the free pyridinone, 1-carboxyethyl-3-benzyloxy-2-methyl-4-pyridinone (Bn**9**; 0.447 g, 1.56 mmol, 1.0 equiv) was refluxed in a solution of 33% w/v hydrobromic acid in glacial acetic acid (4.00 mL) for 1 h. The solvent was removed under reduced pressure affording a light peach coloured solid. The precipitate was dissolved in water (10 mL), and the acid was neutralized by the additon of 6M NaOH. After the removal of water by rotary evaporation, the ensuing solid was redissolved in water and acidified in the presence of 6 M HCl to a pH of 2.5. The water was removed under reduced pressure resulting in a solid, which was recrystallized in ethanol and diethyl ether. The product precipitated, was recovered by filtration, and dried *in vacuo*, affording a light pink solid, H**9** (0.150 g, 58%). ^{1}H NMR (400 MHz, 0.1 M NaOD) δ = 7.27 (d, J = 6.8 Hz, 1 H, H_a), 6.30 (d, J = 6.8 Hz, 1 H, H_b), 4.20 (t, J = 7.3 Hz, 2 H, N-CH_2), 2.56 (t, J = 7.2 Hz, 2 H, CH_2-COOH), 2.32 (s, 3 H, ring CH_3). ^{13}C{^{1}H} NMR (101 MHz, 0.1 M NaOD) δ = 179.0 (CH$_2$-*C*OOH), 172.6 (ring C=O), 155.6 (C_a), 135.0 (ring C-OH), 132.7 (ring C-CH$_3$), 111.7 (C_b), 52.2 (N-CH$_2$), 38.6 (*C*H$_2$-COOH), 12.1 (ring *C*H$_3$). MS (+ESI) *m/z* = 198.2 [M + H]$^+$. Anal. Calc. (found): C$_9$H$_{11}$NO$_4$: C, 54.82 (54.93); H, 5.62 (5.72); N, 7.10 (6.98).

2.2.6 Synthesis of a Pyridinone Functionalized with a Diphosphonic Acid

(4-(3-(Benzyloxy)-2-methyl-4-oxopyridin-1-yl)-1-hydroxybutane-1,1-diyl)diphosphonic acid (Bn**10**)
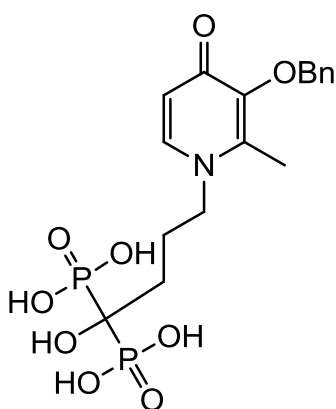
Bn**ma** (0.616 g, 2.84 mmol, 1.0 equiv) and 4-amino-1-hydroxybutane-1,1-diphosphonic acid (0.968 g, 3.89 mmol, 1.4 equiv) were suspended in water (13 mL) and methanol (7 mL) in a microwave vial (10–20 mL vial, Biotage). The pH of the reaction was increased by the addition of 6 M NaOH (0.492 g, 12.3 mmol, 4.3 equiv), and heated to 100 °C for 16 h in a microwave reactor (Biotage Initiator Microwave Synthesizer). The solvent was removed under reduced pressure, dissolved in water and washed with dichloromethane. The aqueous solution was then loaded onto a C18 (Waters, Sep-Pak, 1 g) reverse phase column and eluted with water. The appropriate fractions were collected and the pH was lowered to 1 with the addition of 6 M HCl. The solvent was removed by rotary evaporation. The resulting solid was then recrystallized from water; the resulting precipitate was recovered by filtration and dried *in* vacuo, affording a white solid, Bn**10** (0.668 g, 52%). ^{1}H NMR (400 MHz, 0.1 M NaOD): δ = 7.80 (d, J = 7.3 Hz, 1 H, H_a), 7.36 - 7.45 (m, 5 H, Bn C$_6$H$_5$), 6.55 (d, J=7.3 Hz, 1 H, H_b), 4.98 (s, 2 H, Bn-CH_2), 3.98 (t, J = 7.6 Hz, 2 H, N-CH_2), 2.18 (s, 3 H, ring CH_3), 1.92 (m, 4 H, N-CH$_2$-CH_2-CH_2). ^{13}C{^{1}H} NMR (75 MHz, 0.1 M NaOD) δ = 172.9 (ring C=O), 146.1 (ring C-O-Bn), 144.9 (C_a), 141.0 – 129.0 (4 peaks, Bn C_6H$_5$), 128.8 (ring C-CH$_3$), 116.2 (C_b), 74.4 (CH_2-Bn), 73.8 (t, $J_{C,P}$ = 126.8 Hz, P-C-P), 55.3 (N-CH_2), 30.8 (N-CH$_2$-CH_2), 25.5 (t, ^{2}J = 6.9 Hz, CH_2-C(PO_3H$_2$)$_2$), 12.4 (ring CH_3). ^{31}P{^{1}H} (400 MHz, D$_2$O): δ = 19.60 (C(PO_3H$_2$)$_2$). MS (-ESI) m/z = 446.2 [M - H]$^{-}$.

(4-(3-(Hydroxy)-2-methyl-4-oxopyridin-1-yl)-1-hydroxybutane-1,1-diyl)diphosphonic acid (H10)
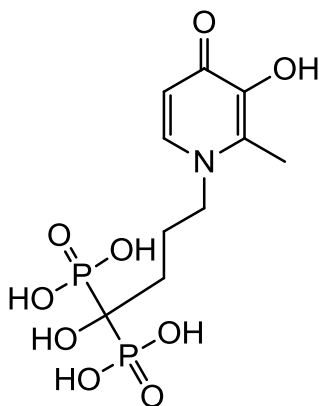
(4-(3-(Benzyloxy)-2-methyl-4-oxopyridin-1(4H)-yl)-1-hydroxybutane-1,1-diyl)diphosphonic acid (Bn**10**; 0.468 g, 1.05 mmol, 1.0 equiv) was suspended in deionized water (25 mL), the pH was increased to 7 with the addition of 6M NaOH, followed by the addition of the hydrogenation catalyst (10% w/w of Pd on C; 200 mg), wetted in water (0.5 mL). The reaction flask was flushed once using a balloon filled with $H_{2(g)}$. The reaction was stirred under the $H_{2(g)}$-filled balloon overnight at room temperature. The dark suspension was filtered to remove the catalyst, and the filtrate was concentrated under reduced pressure affording a white solid that was dissolved in water. The solution pH was adjusted to 1.5 with the addition of 6.0 M HCl, resulting in precipitation. The compound was recovered by filtration and recrystallized from water; the resulting precipitate was isolated by filtration and dried *in vacuo*, affording a white solid, H**10** (0.123 mg, 33%). ^{1}H NMR (400 MHz, 0.1 M NaOD) δ = 7.40 (d, *J* = 6.8 Hz, 1 H, H_a), 6.34 (d, *J* = 6.8 Hz, 1 H, H_b), 3.96 (t, *J* = 7.5 Hz, 2 H, N-CH_2), 2.37 (s, 3 H, ring CH_3), 2.05 (br. s., 2 H, N-CH$_2$-CH_2-CH$_2$), 1.92 (br. s., 2 H, N-CH$_2$-CH$_2$-CH_2 ^{13}C{^{1}H} NMR (101 MHz, 0.1 NaOD) δ = 172.1 (ring *C*=O), 155.4 (ring *C*-O-Bn), 135.6 (C_a), 132.8 (ring *C*-CH$_3$), 111.5 (C_b), 76.0 (t, J_{PCP} = 133.8 Hz, P-*C*-P), 56.2 (N-*C*H$_2$), 32.7 (N-CH$_2$-*C*H$_2$), 26.1, (t, ^2J = 6.1 Hz, N-CH$_2$-CH$_2$-*C*H$_2$), 12.4 (ring *C*H$_3$).). ^{31}P{^{1}H} NMR (162MHz, 0.1 M NaOD) δ = 19.15 (C-(*P*O$_3$H$_2$)$_2$). MS (-ESI) *m/z* = 356.1 [M - H]$^-$.

2.2.7 Synthesis of Dihydrogen Phosphate Functionalized 3-Benzyloxy-4-pyridinones

The syntheses of the dihydrogen phosphate functionalized 3-benzyloxy-2-methyl-4-pyridinones, Bn**11**, Bn**12**, Bn**13**, Bn**14**, and Bn**15**, were achieved by the phosphorylation of

the appropriate hydroxy functionalized 3-benzyloxy-2-methyl-4-pyridinone, B**n1**, B**n2**, B**n3**, B**n4** and B**n6**, as shown in Figure 2.11.

$R_1 = (CH_2)_2OH$ B**n1**
$(CH_2)_3OH$ B**n2**
$(CH_2)_4OH$ B**n3**
$CH_2C(OH)CH_3$ B**n4**
$CH(CH_2OH)CH_2CH_3$ B**n6**

$R_2 = (CH_2)_2OPO_3H_2$ B**n11**
$(CH_2)_3OPO_3H_2$ B**n12**
$(CH_2)_4OPO_3H_2$ B**n13**
$CH_2C(OPO_3H_2)CH_3$ B**n14**
$CH(CH_2OPO_3H_2)CH_2CH_3$ B**n15**
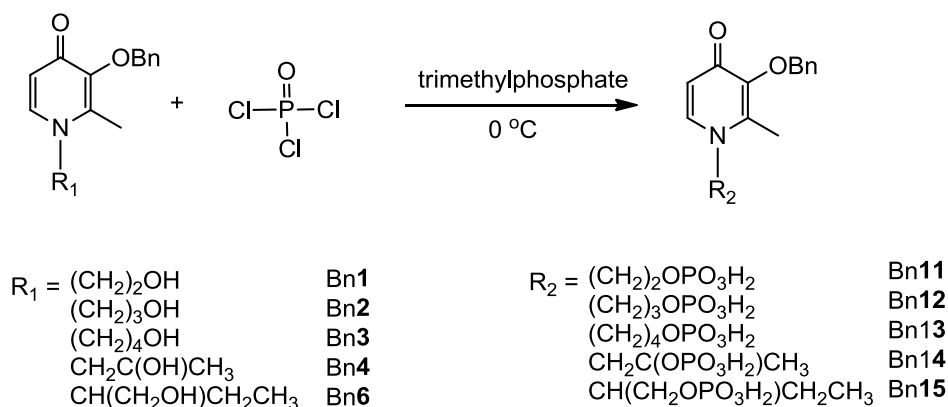
Figure 2.11. Synthesis of dihydrogen phosphate functionalized 3-benzyloxy-2-methyl-4-pyridinones.

2-(3-(Benzyloxy)-2-methyl-4-oxopyridin-1-yl)ethyl dihydrogen phosphate (B**n11**)
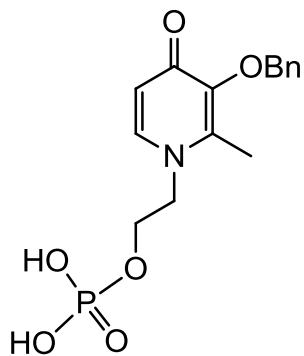
Trimethyl phosphate (31.0 mL, 0.265 mol) was added to a Schlenk flask charged with 3-benzyloxy-2-methyl-1-(2-hydroxyethyl)-4-pyridinone (B**n1**; 2.05 g, 7.91 mmol, 1.0 equiv) under an inert atmosphere ($N_{2(g)}$) and stirred at 0 °C. Phosphorus oxychloride (2.40 mL, 25.7 mmol, 3.2 equiv) was added and the reaction was maintained at 0 °C for 4 h. The reaction was then quenched by the addition of ice and stirred for an additional 10 min. The pH of the mixture was adjusted to 1.5 with the addition of 6 M NaOH; concentration by rotary evaporation yielded a pale yellow oil with a white precipitate (NaCl). The oil was dissolved in a minimum volume of methanol and the salt was removed by filtration. The methanol was removed from the filtrate under reduced pressure, resulting in a yellow oil, which was suspended and stirred in dichloromethane (200 mL) overnight. A white precipitate formed which was isolated by filtration and subsequently recrystallized from deionized water. The

70

resulting white precipitate was collected by filtration and dried *in vacuo*, affording white powder, Bn**11** (1.10g, 41%). ^{1}H{^{31}P} NMR (300 MHz, D$_2$O) δ = 8.12 (d, *J* = 6.4 Hz, 1 H, *H*$_a$), 7.45 (br. s., 5 H, Bn C$_6$*H*$_5$), 7.07 (d, *J* = 6.9 Hz, 1 H, *H*$_b$), 5.12 (s, 2 H, Bn-C*H*$_2$), 4.41 - 4.54 (m, 2 H, C*H*$_2$-OPO$_3$H$_2$), 4.13 (t, *J* = 4.3 Hz, 1 H, N-C*H*$_2$), 2.39 (s, 3 H, ring C*H*$_3$). ^{31}P{^{1}H} NMR (121 MHz, D$_2$O) δ = 0.61 (CH$_2$-O*P*O$_3$H$_2$). MS (-ESI) *m/z* =338.3 [M - H]$^-$.

3-(3-(Benzyloxy)-2-methyl-4-oxopyridin-1-yl)propyl dihydrogen phosphate (Bn**12**)
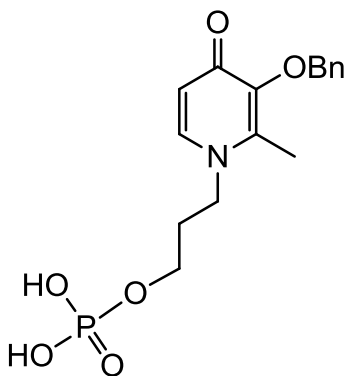
Trimethyl phosphate (16.0 mL, 0.128 mol) was added to a Schlenk flask charged with 3-benzyloxy-2-methyl-1-(3-hydroxypropyl)-4-pyridinone hydrochloride (Bn**2**•HCl; 0.974 g, 3.14 mmol, 1.0 equiv) under an inert atmosphere (N$_{2(g)}$) and stirred at 0 °C. Phosphorus oxychloride (1.12 mL, 12.0 mmol, 3.8 equiv) was added and the reaction was maintained at 0 °C for 4 h. The reaction was then quenched by the addition of ice and stirred for an additional 10 min. The mixture was made basic with the addition of 6M NaOH to a pH of ~12, and washed with dichloromethane (3 × 20 mL). The aqueous layer was subsequently acidified to 1.5 with 6 M HCl and the mixture was concentrated by the removal of solvent under reduced pressure, yielding a yellow oil with a white precipitate (NaCl). The oil was dissolved in a minimal volume of methanol and the salt was removed by filtration. The methanol was removed from the filtrate by rotary evaporation, affording a yellow oil. A CombiFlash automated column system was used to isolate Bn**12** from the crude mixture. The yellow oil was dissolved in 95:5 H$_2$O:CH$_3$OH. A reverse phase C18 column (CombiFlash, RediSepR$_f$ Gold, 5.5 g) was primed with 95:5 H$_2$O:CH$_3$OH and the crude mixture was loaded onto the column. The compound was eluted with a gradient of 95:5 H$_2$O:CH$_3$OH to 50:50 H$_2$O:CH$_3$OH. The fractions from the second peak that eluted were collected and the solvent was removed under reduced pressure and dried *in vacuo*, affording a white solid, Bn**12** (0.183 g, 17%). ^{1}H{^{31}P} NMR (400 MHz, D$_2$O) δ = 8.15 (d, *J* = 6.8 Hz, 1 H, *H*$_a$), 7.43 (br. s., 5 H, Bn C$_6$*H*$_5$), 7.10 (d, *J* = 6.5 Hz, 1 H, *H*$_b$), 5.13 (s, 2 H, Bn-C*H*$_2$), 4.34 (d, *J* = 6.1 Hz, 2 H, C*H*$_2$-OPO$_3$H$_2$), 3.83 (d, *J* = 5.1 Hz, 2 H,

N-CH_2), 2.36 (br. s., 3 H, ring CH_3), 1.96 - 2.08 (m, 2 H, N-CH$_2$-CH_2-CH$_2$-OPO$_3$H$_2$). ^{31}P{^{1}H} NMR (162 MHz, D$_2$O) δ = 0.87 (CH$_2$-OPO$_3$H$_2$). MS (-ESI) m/z = 352.3 [M - H]$^-$. HRMS (-ESI); Calc. (found): C$_{16}$H$_{20}$NO$_6$P: 352.0950 (352.0948) [M - H]$^-$.

4-(3-(Benzyloxy)-2-methyl-4-oxopyridin-1-yl)butyl dihydrogen phosphate (Bn13)
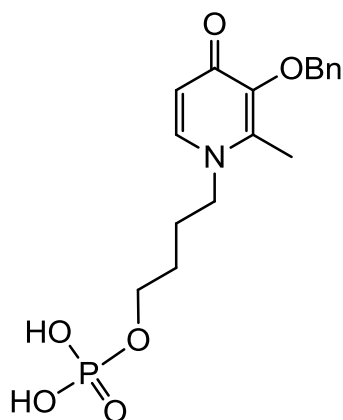
Trimethyl phosphate (16.0 mL, 0.128 mol) was added to a Schlenk flask charged with 3-benzyloxy-2-methyl-1-(4-hydroxybutyl)-pyridinone hydrochloride (Bn**3**•HCl; 1.09 g, 3.38 mmol, 1.0 equiv) under an inert atmosphere (N$_{2(g)}$) and stirred at 0 °C. Phosphorus oxychloride (1.12 mL, 12.0 mmol, 3.6 equiv) was added and the reaction was maintained at 0 °C for 4 h. The reaction was then quenched by the addition of ice and stirred for an additional 10 min. The mixture was made basic with the addition of 6M NaOH to a pH of ~12, and washed with dichloromethane (3 × 20 mL). The aqueous layer was subsequently acidified to 1.5 with 6 M HCl and the mixture was concentrated by the removal of solvent under reduced pressure, yielding a yellow oil with a white precipitate (NaCl). The oil was dissolved in a minimal volume of methanol and the salt was removed by filtration. The methanol was removed from the filtrate by rotary evaporation, affording a yellow oil. A CombiFlash automated column system was used to isolate Bn**13** from the crude mixture. The yellow oil was redissolved in 95:5 H$_2$O:CH$_3$OH. A reverse phase C18 column (CombiFlash, RediSepR$_f$ Gold, 5.5 g) was primed with 95:5 H$_2$O:CH$_3$OH and the crude mixture was loaded onto the column. The compound was eluted with a gradient of 95:5 H$_2$O:CH$_3$OH to 50:50 H$_2$O:CH$_3$OH. The fractions from the second peak that eluted were collected and the solvent was removed under reduced pressure and dried *in vacuo*, affording a white solid, Bn**13** (0.308 g, 25%). ^{1}H{^{31}P} NMR (400 MHz, CH$_3$OH) δ = 8.27 (d, J = 7.3 Hz, 1 H, H_a), 7.43 - 7.56 (m, 5 H, Bn C$_6H_5$), 7.24 (d, J = 7.3 Hz, 1 H, H_b), 5.21 (s, 2 H, Bn-CH_2), 4.35 (t, J = 7.8 Hz, 2 H, CH_2-OPO$_3$H$_2$), 3.96 (d, J = 6.4 Hz, 2 H, N-CH_2), 2.44 (s, 3 H, ring CH_3), 1.90 (d, J = 7.3 Hz, 2 H, CH_2-CH$_2$-OPO$_3$H$_2$), 1.69 (d, J = 7.6 Hz, 2 H, N-CH$_2$-CH_2). ^{31}P{^{1}H} NMR (162 MHz, CH$_3$OH) δ = 1.74 (CH$_2$-OPO$_3$H$_2$).

MS (-ESI) m/z = 368.3 [M + H]$^+$. HRMS (-ESI); Calc. (found): $C_{17}H_{22}NO_6P$: 366.1107 (366.1101) [M - H]$^-$.

1-(3-(Benzyloxy)-2-methyl-4-oxopyridin-1-yl)propan-2-yl dihydrogen phosphate (Bn14)
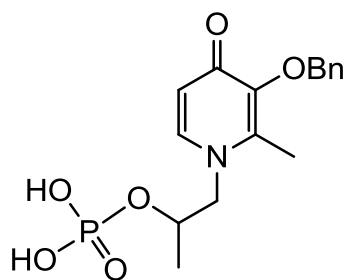
Trimethyl phosphate (16.0 mL, 0.128 mol) was added to a Schlenk flask charged with 3-benzyloxy-2-methyl-1-(2-hydroxypropyl)-4-pyridinone (Bn**4**; 1.09 g, 4.00 mmol, 1.0 equiv) under an inert atmosphere ($N_{2(g)}$) and stirred at 0 °C. Phosphorus oxychloride (1.12 mL, 12.0 mmol, 3.0 equiv) was added and the reaction was maintained at 0 °C for 4 h. The reaction was then quenched by the addition of ice and stirred for an additional 10 min. The pH was made basic with the addition of 6M NaOH to a pH of ~12, and washed with dichloromethane (3 × 25 mL). The aqueous layer was subsequently acidified to 1.5 with 6 M HCl and the mixture was concentrated by the removal of solvent under reduced pressure, yielding a yellow oil with a white precipitate (NaCl). The oil was dissolved in a minimal volume of methanol, and the salt was removed by filtration. The methanol was removed from the filtrate by rotary evaporation, affording a yellow oil. A normal phase silica column was used for the isolation of Bn**14**. The crude oil was loaded onto a silica column and was separated using the eluent 9:1 2-propanol:ammonia. The eluent polarity was then increased by the addition of water to 9:2:1 2-propanol:water:ammonia. The appropriate fractions were collected and the solvent was removed by rotary evaporation. The solid was then dissolved in water and the pH was adjusted to 1.5 with the addition of 6 M HCl and loaded onto a C18 (Waters, Sep-Pak, 1 g) reverse phase column. The column was rinsed with water (3 mL), the eluent was then switched to methanol and the compound was collected. The solvent was removed under reduced pressure and dried *in vacuo* to give a white solid, Bn**14** (0.338 g, 24%). ^{1}H{^{31}P} NMR (400 MHz, D_2O) δ = 7.64 (d, J = 7.3 Hz, 1 H, H_a), 7.32 (s, 5 H, Bn C$_6$H$_5$), 6.49 (d, J = 7.3 Hz, 1 H, H_b), 4.82 - 4.96 (m, 2 H, Bn-CH_2), 4.29 (br. s., 1 H, CH-OPO$_3$H$_2$), 3.82 - 4.06 (m, 2 H, N-CH_2), 2.06 (s, 3 H, ring CH_3), 1.14 (d, J = 6.1 Hz, 3 H,

CH(OPO$_3$H$_2$)CH_3). ^{31}P{^{1}H} NMR (162 MHz, D$_2$O) δ = 0.86 (CH-OPO$_3$H$_2$). MS (-ESI) m/z = 352.3 [M - H]$^-$. HRMS (-ESI); Calc. (found): C$_{16}$H$_{20}$NO$_6$P: 352.0950 (352.0642) [M - H]$^-$.

2-(3-(Benzyloxy)-2-methyl-4-oxopyridin-1-yl)butyl dihydrogen phosphate (Bn**15**)
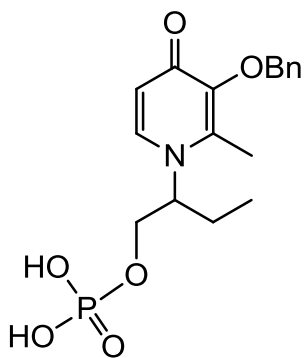
Trimethyl phosphate (16.0 mL, 0.128 mol) was added to a Schlenk flask charged with 3-benzyloxy-2-methyl-1-(1-hydroxybutan-2-yl)-4-pyridinone (Bn**6**; 1.20 g, 4.18 mmol, 1.0 equiv) under an inert atmosphere (N$_{2(g)}$) and stirred at 0 °C. Phosphorus oxychloride (1.12 mL, 12.0 mmol, 2.9 equiv) was added and the reaction was maintained at 0 °C for 4 h. The reaction was then quenched by the addition of ice and stirred for an additional 10 min. The pH of the mixture was made basic with the addition of 6M NaOH to a pH of ~12, and washed with dichloromethane (3 × 25 mL). The aqueous layer was subsequently acidified to 1.5 with 6 M HCl and the mixture was concentrated by the removal of solvent under reduced pressure, yielding a yellow oil with a white precipitate (NaCl). The oil was dissolved in a minimal volume of methanol and the salt was removed by filtration. The methanol was removed from the filtrate by rotary evaporation, affording a yellow oil. A CombiFlash automated column system was used to isolate Bn**15** from the crude mixture. The yellow oil was redissolved in 95:5 H$_2$O:CH$_3$OH. A reverse phase C18 column (CombiFlash, RediSepR$_f$ Gold, 5.5 g) was primed with 95:5 H$_2$O:CH$_3$OH and the crude mixture was loaded onto the column. The compound was eluted with a gradient of 95:5 H$_2$O:CH$_3$OH to 50:50 H$_2$O:CH$_3$OH. The fractions from the second peak that eluted were collected and the solvent was removed under reduced pressure and dried *in vacuo*, affording a white solid, Bn**15** (0.529 g, 34%). ^{1}H{^{31}P} NMR (400 MHz, D$_2$O) δ = 7.85 (d, J = 7.5 Hz, 6 H, H_a), 7.37 (s, 5 H, *Bn*-CH$_2$), 6.64 (d, J = 7.5 Hz, 1 H, H_b), 4.97 - 5.05 (m, 2 H, Bn-CH_2), 4.37 - 4.47 (m, 1 H, CH), 3.90 - 3.96 (m, 1 H, CH_2-OPO$_3$H$_2$), 3.83 - 3.89 (m, 1 H, CH_2-OPO$_3$H$_2$), 2.11 (s, 3 H, ring CH_3), 1.82-1.92 (m, 1 H, CH_2-CH$_3$), 1.62 - 1.78 (m, 1 H, CH_2-CH$_3$), 0.63 (t, J = 7.3 Hz, 2 H, CH$_2$-CH_3). ^{31}P{^{1}H} NMR (162 MHz, D$_2$O) δ = 0.98 (CH$_2$-OPO$_3$H$_2$). MS (+ESI) m/z = 368.3 [M + H]$^+$. HRMS (+ESI); Calc. (found): C$_{17}$H$_{22}$NO$_6$P: 368.1263 (368.1269) [M + H]$^+$.

### 2.2.8 Synthesis of Dihydrogen Phosphate Functionalized 3-Hydroxy-4-pyridinones

The syntheses of the dihydrogen phosphate functionalized 3-hydroxy-2-methyl-4-pyridinones, **H11**, **H12**, **H13**, **H14**, and **H15**, were achieved by the debenzylation of the appropriate 3-benzyloxy-2-methyl-4-pyridinone, Bn**11**, Bn**12**, Bn**13**, Bn**14** and Bn**15**, as shown in Figure 2.12.

$R_1=$ $(CH_2)_2OPO_3H_2$ Bn**11**
  $(CH_2)_3OPO_3H_2$ Bn**12**
  $(CH_2)_4OPO_3H_2$ Bn**13**
  $CH_2C(OPO_3H_2)CH_3$ Bn**14**
  $CH(CH_2OPO_3H_2)CH_2CH_3$ Bn**15**

$R_2 =$ $(CH_2)_2OPO_3H_2$ **H11**
  $(CH_2)_3OPO_3H_2$ **H12**
  $(CH_2)_4OPO_3H_2$ **H13**
  $CH_2C(OPO_3H_2)CH_3$ **H14**
  $CH(CH_2OPO_3H_2)CH_2CH_3$ **H15**
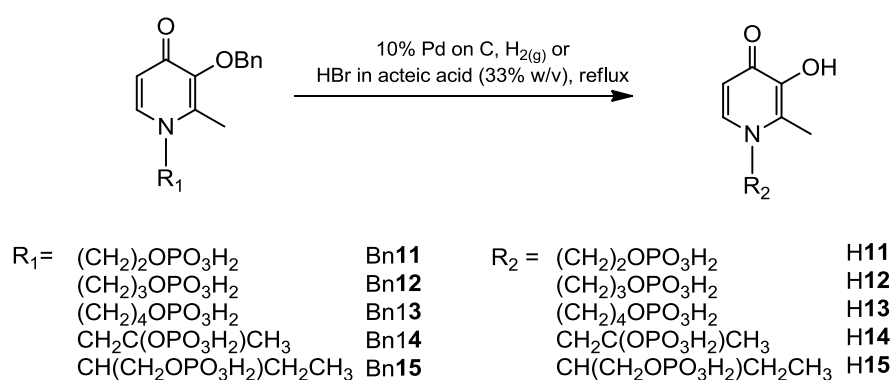
Figure 2.12. Synthesis of dihydrogen phosphate functionalized 3-hydroxy-2-methyl-4-pyridinones.

2-(3-Hydroxy-2-methyl-4-oxopyridin-1-yl)ethyl dihydrogen phosphate (H11)
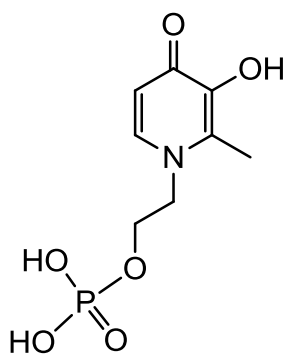
2-(3-(Benzyloxy)-2-methyl-4-oxopyridin-1-yl)ethyl   dihydrogen phosphate (Bn**11**; 2.50 g, 7.38 mmol, 1.0 equiv) was refluxed in a 33% w/v hydrobromic acid-acetic acid solution (40.0 mL) for 1 h. Excess solvent was removed by rotary evaporation affording a light peach coloured solid. The precipitate was dissolved in water (10 mL), neutralized with the addition of 6M NaOH and the solvent was removed under reduced pressure. The resulting solid was

75

redissolved in water, acidified to pH 1.5 with 6 M HCl, affording a white solid which was collected by filtration. The solid was recrystallized in hot water, isolated by filtration and dried *in vacuo*, affording a white solid, **H11** (0.590 g, 32%). ^{1}H$\{^{31}$P$\}$ NMR (400 MHz, 0.1 M NaOD) δ = 7.41 (d, J = 6.5 Hz, 1 H, H_a), 6.36 (d, J = 6.1 Hz, 1 H, H_b), 4.22 (d, J = 5.5 Hz, 2 H, CH_2-OPO$_3$H$_2$), 3.98 (d, J = 5.1 Hz, 2 H, N-CH_2), 2.37 (br. s., 3 H, ring CH_3). ^{13}C$\{^1$H$\}$ NMR (101 MHz , 0.1 M NaOD) δ = 172.8 (ring C=O), 155.5 (C_a), 135.4 (ring C-OH), 133.8 (ring C-CH$_3$), 111.4 (C_b), 62.8 (CH$_2$-OPO$_3$H$_2$), 55.3 (N-CH$_2$), 12.4 (ring CH$_3$). ^{31}P$\{^1$H$\}$ NMR (162 MHz, 0.1 M NaOD) δ = 4.68 (CH$_2$-OPO$_3$H$_2$). MS (+ESI) m/z = 294.2 [M - H + 2Na$^+$]$^+$. Anal. Calc. (found): C$_8$H$_{12}$NO$_6$P•H$_2$O: C, 35.96 (35.46); H, 5.28 (5.21); N, 5.24 (5.13).

3-(3-Hydroxy-2-methyl-4-oxopyridin-1-yl)propyl dihydrogen phosphate (H12)
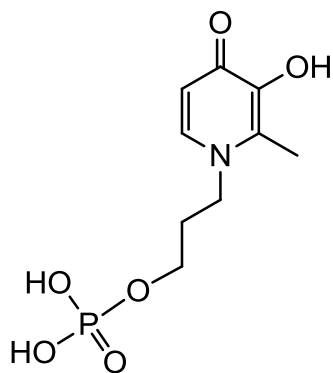
3-(3-(Benzyloxy)-2-methyl-4-oxo-4-pyridin-1-yl)propyl dihydrogen phosphate (Bn**12**; 0.183 g, 0.518 mmol, 1.0 equiv) was suspended in deionized water (25 mL), the pH was increased to 3 with the addition of 6M NaOH, followed by the addition of the hydrogenation catalyst (10% w/w of Pd on C; 20.0 mg), wetted in water (0.5 mL). The reaction flask was flushed once using a balloon filled with H$_{2(g)}$. The reaction was stirred under the H$_{2(g)}$-filled balloon for 6 hours at room temperature. The dark suspension was filtered to remove the catalyst, and the filtrate was concentrated under reduced pressure, affording a pale pink solid, which was dissolved in water, adjusted to pH 1.5 with 6 M HCl and recrystallized in water. The resulting solid was isolated by filtration and dried *in vacuo*, affording a white solid, H**12** (64.9 mg, 48%). ^{1}H$\{^{31}$P$\}$ NMR (400 MHz, 0.1 M NaOD) δ = 7.40 (d, J = 6.8 Hz, 1 H, H_a), 6.37 (d, J = 6.8 Hz, 1 H, H_b), 4.09 - 4.19 (m, 2 H, CH_2-OPO$_3$H$_2$), 3.73 - 3.80 (m, 2 H, N-CH_2), 2.38 (s, 3 H, ring CH_3), 2.00 (d, J = 6.1 Hz, 2 H, N-CH$_2$-CH_2-CH$_2$-OPO$_3$H$_2$). ^{13}C$\{^1$H$\}$ NMR (101 MHz, 0.1 M NaOD) δ = 172.4 (ring C=O), 155.7 (C_a), 135.4 (ring C-OH), 133.1 (ring C-CH$_3$), 111.6 (C_b), 60.8 (CH$_2$-OPO$_3$H$_2$), 52.3 (N-CH$_2$), 31.6 (N-CH$_2$-CH$_2$-CH$_2$-OPO$_3$H$_2$), 12.2 (ring CH$_3$). ^{31}P$\{^1$H$\}$ NMR (162 MHz,

0.1 M NaOD) δ = 4.65 (CH$_2$-OPO$_3$H$_2$). MS (+ESI) m/z = 264.4 [M + H]$^+$. HRMS (+ESI); Calc. (Found): C$_9$H$_{14}$NO$_6$P: 264.0641 (264.0637) [M + H]$^+$.

4-(3-Hydroxy-2-methyl-4-oxopyridin-1-yl)butyl dihydrogen phosphate (H13)
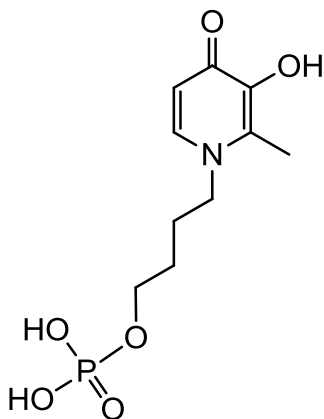
4-(3-(Benzyloxy)-2-methyl-4-oxopyridin-1-yl)butyl dihydrogen phosphate (Bn**13**; 0.308 g, 0.838 mmol, 1.0 equiv) was suspended in deionized water (25 mL), the pH was increased to 3 with the addition of 6M NaOH, followed by the addition of the hydrogenation catalyst (10% w/w of Pd on C; 20.0 mg), wetted in water (0.5 mL). The reaction flask was flushed once using a balloon filled with H$_{2(g)}$. The reaction was stirred under the H$_{2(g)}$-filled balloon for 6 hours at room temperature. The dark suspension was filtered to remove the catalyst, and the filtrate was concentrated under reduced pressure, affording an off-white solid, which was dissolved in water, adjusted to pH 1.5 with 6 M HCl and recrystallized in methanol. The resulting solid was isolated by filtration and dried, affording a white solid, H**13** (24.9 mg, 11%). ^{1}H{^{31}P} NMR (300 MHz, D$_2$O) δ = 7.68 (d, J = 7.3 Hz, 1 H, H_a), 6.40 (d, J = 7.3 Hz 1 H, H_b), 4.07 - 4.18 (m, 2 H, CH_2-OPO$_3$H$_2$), 3.92 (t, J = 5.9 Hz, 2 H, N-CH_2), 2.46 (s, 3 H, ring CH_3), 1.79 - 1.99 (m, 2 H, CH_2-CH$_2$- OPO$_3$H$_2$), 1.58 - 1.77 (m, 3 H, N-CH$_2$-CH_2). ^{13}C{^{1}H} NMR (101 MHz, D$_2$O) δ = 158.6 (ring C=O), 142.7 (C_a), 142.5 (ring C-OH), 138.6 (ring C-CH$_3$), 111.1 (ring C-CH$_3$), 65.1(CH$_2$- OPO$_3$H$_2$), 56.4 (N-CH$_2$), 49.0 (N-CH$_2$-CH$_2$), 26.5 (CH$_2$-CH$_2$-OPO$_3$H$_2$), 12.3 (ring CH$_3$). ^{31}P{^{1}H} NMR (122 MHz, D$_2$O) δ = 1.02 (CH$_2$-OPO$_3$H$_2$). MS (-ESI) m/z = 276.5 [M - H]$^-$. HRMS (-ESI); Calc. (Found): C$_{10}$H$_{16}$NO$_6$P: 276.0640 (276.0637) [M - H]$^-$.

1-(3-Hydroxy-2-methyl-4-oxopyridin-1-yl)propan-2-yl dihydrogen phosphate (H14)
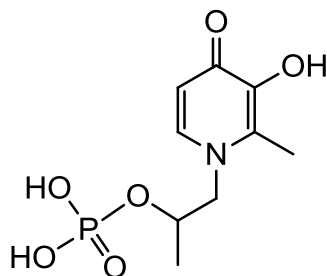
1-(3-(Benzyloxy)-2-methyl-4-oxopyridin-1-yl)propan-2-yl dihydrogen phosphate (Bn**14**; 0.338 g, 0.956 mmol, 1.0 equiv) was suspended in deionized water (20 mL), the pH was increased to 7 with the addition of 6M NaOH, followed by the addition of the hydrogenation catalyst (10% w/w of Pd on C; 20.0 mg), wetted in water (0.5 mL). The reaction flask was flushed once using a balloon filled with $H_{2(g)}$. The reaction was stirred under the $H_{2(g)}$-filled balloon for 6 hours at room temperature. The dark suspension was filtered to remove the catalyst, and the filtrate was concentrated under reduced pressure and dried *in vacuo*, affording an off white solid, H**14** (0.250 mg, 99%). $^1H\{^{31}P\}$ NMR (300 MHz, D_2O) δ = 8.13 (br. s., 1 H, H_a), 7.24 (br. s., 1 H, H_b), 4.60 (br. s., 1 H, C*H*-OPO$_3$H$_2$), 4.46 (br. s., 2 H, N-C*H*$_2$), 2.70 (s, 3 H, ring C*H*$_3$), 1.46 (d, J = 5.5 Hz, 3 H, CH(OPO$_3$H$_2$)C*H*$_3$). $^{31}P\{^1H\}$ NMR (162 MHz, D_2O) δ = 1.17 (CH-O*P*O$_3$H$_2$). MS (-ESI) *m/z* = 262.2 [M - H]$^-$. HRMS (-ESI); Calc. (Found): $C_9H_{14}NO_6P$: 262.0481 (262.0481) [M - H]$^-$.

2-(3-Hydroxy-2-methyl-4-oxopyridin-1-yl)butyl dihydrogen phosphate (H15)
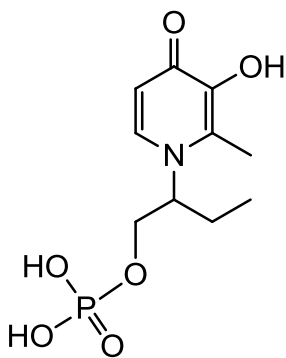
2-(3-(Benzyloxy)-2-methyl-4-oxopyridin-1-yl)butyl dihydrogen phosphate (Bn**15**; 0.394 g, 1.072 mmol, 1.0 equiv) was suspended in deionized water (20 mL), the pH was increased to 7 with the addition of 6M NaOH, followed by the addition of the hydrogenation catalyst (10% w/w of Pd on C; 20.0 mg), wetted in water (0.5 mL). The reaction flask was flushed once using a balloon filled with $H_{2(g)}$. The reaction was stirred under the $H_{2(g)}$-filled balloon for 6 hours at room temperature. The dark suspension was filtered to remove the catalyst, and the filtrate was concentrated under reduced pressure and dried *in vacuo*, affording an off-white solid, H**15** (30.0 mg, 10%). $^1H\{^{31}P\}$ NMR (400 MHz, D_2O) δ = 7.76 (d, J = 7.3 Hz, 1 H, H_a), 6.59 (d, J = 7.3 Hz, 1 H, H_b), 4.52 - 4.70 (m, 1 H, N-C*H*), 3.99 (m, 1

H, CH_2-OPO$_3$H$_2$), 3.87 - 3.96 (m, 1 H, CH_2-OPO$_3$H$_2$), 2.48 (s, 3 H, ring CH_3), 1.88 - 2.00 (m, 1 H, CH_2CH$_3$), 1.73 - 1.86 (m, 1 H, CH_2CH$_3$), 0.78 (t, J = 7.3 Hz, 3 H, CH$_2$CH_3). ^{13}C{^{1}H} NMR (101 MHz, D$_2$O) δ = 169.2 (ring C=O), 136.7 (C_a), 134.3 (ring C-OH), 134.2 (ring C-CH$_3$), 112.9 (C_b), 65.8 (N-CH), 63.3, (CH$_2$-OPO$_3$H$_2$) 24.2 (CH$_2$-CH$_3$), 12.4 (CH$_2$-CH$_3$), 9.3 (ring CH$_3$). ^{31}P{^{1}H} NMR (162 MHz, D$_2$O) δ =0.64 (CH$_2$-OPO$_3$H$_2$). MS (-ESI) m/z = 276.2 [M - H]$^-$. HRMS (-ESI); Calc. (Found): C$_{10}$H$_{16}$NO$_6$P: 276.0637 (276.0638) [M - H]$^-$.

2.2.9 Synthesis of 3-Hydroxy-4-pyridinones Lanthanide Complexes

All lanthanide complexes were synthesized by the deprotonation of the pyridinone with sodium hydroxide in the presence of the desired lanthanide (III) nitrate hexahydrate salt, as summarized in Figure 2.13.

R$_1$ = (CH$_2$)$_2$OH	H**1**		R$_1$ = (CH$_2$)$_2$OH	Ln(**1**)$_3$
(CH$_2$)$_3$OH	H**2**		(CH$_2$)$_3$OH	Ln(**2**)$_3$
(CH$_2$)$_4$OH	H**3**		(CH$_2$)$_4$OH	Ln(**3**)$_3$
CH$_2$C(OH)CH$_3$	H**4**		CH$_2$C(OH)CH$_3$	Ln(**4**)$_3$
CH(CH$_2$OH)CH(CH$_3$)$_2$	H**5**		CH(CH$_2$OH)CH(CH$_3$)$_2$	Ln(**5**)$_3$
CH(CH$_2$OH)CH$_2$CH$_3$	H**6**		CH(CH$_2$OH)CH$_2$CH$_3$	Ln(**6**)$_3$
CH$_2$COOH	H**8**		CH$_2$COOH	Na$_3$[Ln(**8**)$_3$]
(CH$_2$)$_2$COOH	H**9**		(CH$_2$)$_2$COOH	Na$_3$[Ln(**9**)$_3$]
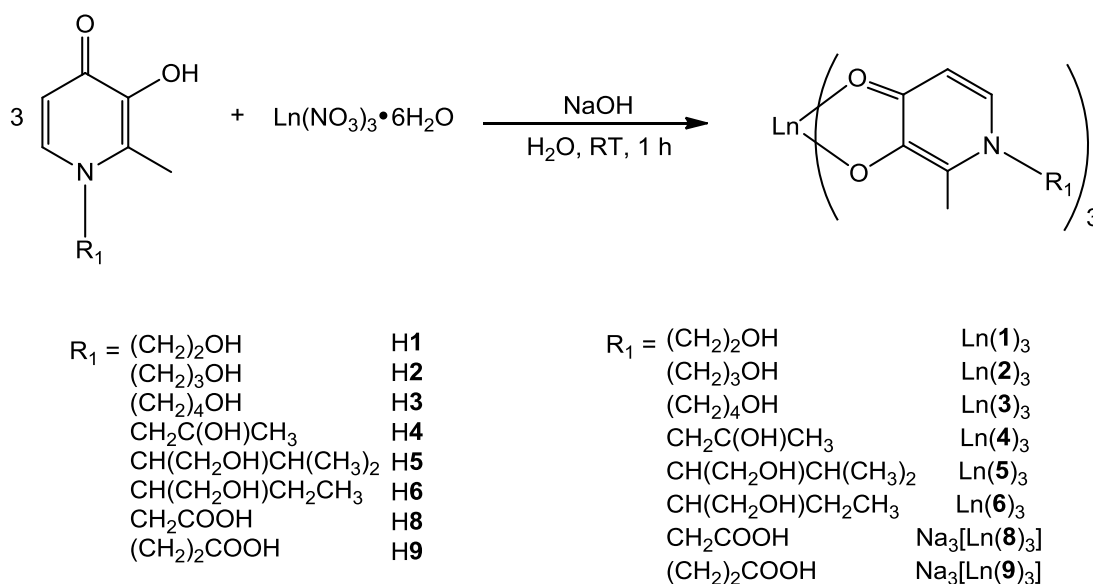
Figure 2.13. The general synthetic route for the production of Ln(**L**)$_3$, where Ln = La, Eu, Gd or Lu .

***Tris*(1-(2-hydroxyethyl)-2-methyl-3-oxy-4-pyridinonato)lanthanide(III),** Ln(**1**)$_3$

Ln = La, Eu, Lu
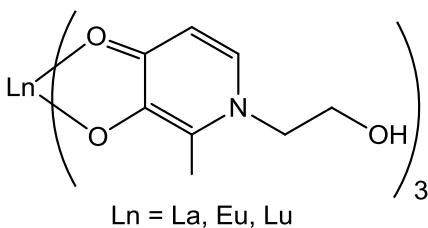
H1 (0.100 g, 0.60 mmol, 3.0 equiv) was suspended in water (10 mL); the pH of the ligand solution was increased to 3.17–3.44 with the addition of 1 M NaOH in order to solubilize the ligand. Ln(NO$_3$)$_3$•6H$_2$O (86.0–99.2 mg, 0.20 mmol, 1.0 equiv) was added to the ligand solution and the pH of the mixture was raised slowly over 10–15 min with the dropwise addition of 1 M NaOH (Ln^{3+} = La, pH 10.9; Eu, pH 10.9; Lu, pH 10.2) and the resulting mixture was continuously stirred for 1 h. The solution was concentrated under reduced pressure, redissolved in 1 − 2 mL of water and precipitated out with the addition of acetone (50 mL). The metal complex was collected by centrifugation (4000 RPM); the supernatant was discarded. All the complexes were dried *in vacuo* to yield 41−89% of Ln(**1**)$_3$.

***Tris*(1-(2-hydroxyethyl)-2-methyl-3-oxy-4-pyridinonato)lanthanum(III),** La(**1**)$_3$
^{1}H NMR (400 MHz, D$_2$O) d = 7.29 (br. s., 3 H, *H*$_a$), 6.32 (br. s., 3 H, *H*$_b$), 4.11 (br. s., 6 H, C*H*$_2$-OH), 3.79 (br. s., 6 H, N-C*H*$_2$), 2.21 (br. s., 9 H, ring C*H*$_3$). ^{13}C{^{1}H} NMR (101 MHz, D$_2$O) δ = 172.4 (ring *C*=O), 136.0 (ring *C*-OH, *C*$_a$), 134.8 (ring *C*-CH$_3$), 110.5 (*C*$_b$), 60.4 (*C*H$_2$-OH), 56.5 (N-*C*H$_2$), 12.0 (ring *C*H$_3$). MS (+ESI) *m/z* = 644.1, 645.1, 646.2 [M + H]$^+$. HRMS (+ESI); Calc. (found): C$_{24}$H$_{31}$^{139}LaN$_3$O$_9$: 644.1124 (644.1119) [M + H]$^+$.

***Tris*(1-(2-hydroxyethyl)-2-methyl-3-oxy-4-pyridinonato)europium(III),** Eu(**1**)$_3$
MS (+ESI) *m/z* = 656.3, 657.2, 658.2, 659.2, 660.2 [M + H]$^+$. HRMS (+ESI); Calc. (found): C$_{24}$H$_{31}$^{151}EuN$_3$O$_9$: 656.1259 (656.1275) [M + H]$^+$.

***Tris*(1-(2-hydroxyethyl)-2-methyl-3-oxy-4-pyridinonato)lutetium(III)Lu(1)₃**

^{1}H NMR (400 MHz, D$_2$O) δ = 7.31 (br. s., 3 H, H_a), 6.32 (br. s., 3 H, H_b), 4.08 (br. s., 6 H, CH_2-OH), 3.74 (br. s., 6 H, N-CH_2), 2.17 (br. s., 9 H, ring CH_3). MS (+ESI) m/z = 680.1, 681.2, 682.1 [M + H]$^+$. HRMS (+ESI); Calc. (found): C$_{24}$H$_{31}$^{175}LuN$_3$O$_9$: 680.1468 (680.1473) [M + H]$^+$.

***Tris*(1-(3-hydroxypropyl)-2-methyl-3-oxy-4-pyridinonato)lanthanide(III), Ln(2)₃**

Ln = La, Eu, Gd, Lu
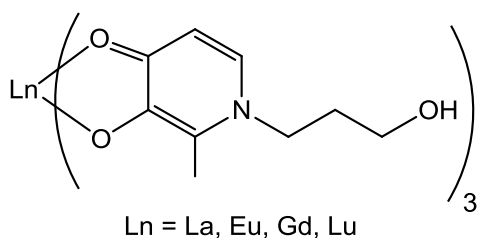
H**2**•HCl (0.100 g, 0.46 mmol, 3.0 equiv) was suspended in water (10 mL); Ln(NO$_3$)$_3$•6H$_2$O (79.2– 85.9 mg, 0.18 mmol, 1.0 equiv) was added to the ligand solution. The pH of the mixture was raised slowly over 10–15 min with the dropwise addition of 1 M NaOH (Ln^{3+} = La, pH 9.7; Eu, pH 10.1; Gd, pH 10.0; Lu, pH 9.6) and the resulting mixture was continuously stirred for 1 h. The solution was concentrated under reduced pressure, redissolved in 1–2 mL of water and precipitated out with the addition of acetone (50 mL). The metal complex was collected by centrifugation (4000 RPM); the supernatant was discarded. All the complexes were dried *in vacuo* to yield 34–91% of Ln(**2**)₃.

***Tris*(1-(3-hydroxypropyl)-2-methyl-3-oxy-4-pyridinonato)lanthanum(III), La(2)₃**

^{1}H NMR (400 MHz, D$_2$O) δ = 7.31 (br. s., 3 H, H_a), 6.31 (br. s., 3 H, H_b), 4.06 (br. s., 6 H, N-CH_2), 3.55 (br. s., 6 H, CH_2-OH), 2.24 (br. s., 9 H, ring CH_3), 1.74 - 2.04 (m, 6 H, N-CH$_2$-CH_2-CH$_2$-OH). ^{13}C{^{1}H} NMR (101 MHz, D$_2$O) δ = 162.2 (ring C=O), 135.4 (C_a), 134.3 (ring C-OH) 133.8 (ring C-CH$_3$) 109.6 (C_b), 58.2 (CH$_2$-OH), 52.0 (N-CH$_2$), 32.4, (N-CH$_2$-CH$_2$-CH$_2$-OH) 7.5 (ring CH$_3$). MS (+ESI) m/z = 686.2, 687.2, 688.3 [M + H]$^+$.HRMS (+ESI); Calc. (found): C$_{27}$H$_{37}$^{139}LaN$_3$O$_9$: 686.1593 (686.1591) [M + H]$^+$.

***Tris*(1-(3-hydroxypropyl)-2-methyl-3-oxy-4-pyridinonato)europium(III), Eu(2)₃**

MS (+ESI) m/z = 698.3, 699.3, 700.3, 701.2, 702.3 [M + H]$^+$. HRMS (+ESI); Calc. (found): C$_{27}$H$_{37}$^{151}EuN$_3$O$_9$: 698.1728 (698.1723) [M + H]$^+$.

***Tris*(1-(3-hydroxypropyl)-2-methyl-3-oxy-4-pyridinonato)gadolinium(III),** Gd(**2**)$_3$

MS (+ESI) *m/z* = 723.0, 724.2, 725.2, 726.2, 727.2, 728.2, 729.2, 730.1 [M + Na]$^+$.HRMS (+ESI); Calc. (found): C$_{27}$H$_{36}$^{155}GdN$_3$NaO$_9$: 724.1576 (724.1563) [M + Na]$^+$.

***Tris*(1-(3-hydroxypropyl)-2-methyl-3-oxy-4-pyridinonato)lutetium(III),** Lu(**2**)$_3$

^{1}H NMR (300 MHz, CD$_3$OD) δ = 7.40 (br. s., 3 H, *H*$_a$), 6.28 (br. s., 3 H, *H*$_b$), 4.13 (br. s., 6 H, N-C*H*$_2$), 3.54 (br. s., 6 H, C*H*$_2$-OH), 2.52 (br. s., 3 H, ring C*H*$_3$), 2.38 (br. s., 6 H, N-CH$_2$-CH$_2$-CH$_2$-OH). MS (+ESI) *m/z* = 722.3, 723.2, 724.3 [M + H]$^+$. HRMS (+ESI); Calc. (Found): C$_{27}$H$_{37}$^{175}LuN$_3$O$_9$: 722.1938 (722.1937) [M + H]$^+$.

***Tris*(1-(4-hydroxybutyl)-2-methyl-3-oxy-4-pyridinonato)lanthanide(III),** Ln(**3**)$_3$

Ln = La, Eu, Lu
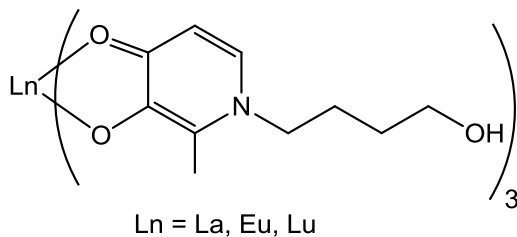
H**3**•HCl (0.100 g, 0.43 mmol, 3.0 equiv) was dissolved in water (10 mL); Ln(NO$_3$)$_3$•6H$_2$O (62.7–66.8 mg, 0.14 mmol, 1.0 equiv) was added to the ligand solution. The pH of the mixture was raised slowly over 10–15 min with the dropwise addition of 1 M NaOH (Ln^{3+} = La, pH 10.2; Eu, pH 9.4; Lu, pH 9.4) and the resulting mixture was continuously stirred for 1 h. The solution was concentrated under reduced pressure, redissolved in 1–2 mL of water and precipitated out with the addition of acetone (50 mL). The metal complex was collected by centrifugation (4000 RPM); the supernatant was discarded. All of the complexes were dried *in vacuo* to yield 63–95% of Ln(**3**)$_3$.

***Tris*(1-(4-hydroxybutyl)-2-methyl-3-oxy-4-pyridinonato)lanthanum(III),** La(**3**)$_3$

^{1}H NMR (400 MHz, D$_2$O) δ = 7.25 (br. s., 3 H, *H*$_a$), 6.28 (br. s., 3 H, *H*$_b$), 3.96 (br. s., 6 H, N-C*H*$_2$), 3.53 (br. s., 6 H, C*H*$_2$-OH), 2.18 (br. s., 9 H, ring C*H*$_3$), 1.69 (br. s., 6 H, C*H*$_2$-CH$_2$-OH), 1.49 (br. s., 6 H, N-CH$_2$-C*H*$_2$). ^{13}C{^{1}H} NMR (101 MHz, D$_2$O) δ = 172.6 (ring *C*=O), 157.4 (*C*$_a$, ring *C*-OH), 134.4 (ring *C*-CH$_3$), 112.3 (*C*$_b$), 61.1 (*C*H$_2$-OH), 54.8 (N-*C*H$_2$), 28.3

(N-CH$_2$-CH$_2$), 26.8 (CH$_2$-CH$_2$-OH), 11.8 (ring CH$_3$). MS (+ESI) m/z = 728.2, 729.2, 730.2 [M + H]$^+$. HRMS (+ESI); Calc. (found): C$_{30}$H$_{43}$^{139}LaN$_3$O$_9$: 728.2063 (728.2065) [M + H]$^+$.

Tris(1-(4-hydroxybutyl)-2-methyl-3-oxy-4-pyridinonato)europium(III), Eu(**3**)$_3$

MS (+ESI) m/z = 740.4, 741.3, 742.3, 743.3, 744.3 [M + H]$^+$. HRMS (+ESI); Calc. (Found): C$_{30}$H$_{43}$^{151}EuN$_3$O$_9$: 740.2198 (740.2202) [M + H]$^+$.

Tris(1-(4-hydroxybutyl)-2-methyl-3-oxy-4-pyridinonato)lutetium(III), Lu(**3**)$_3$

^{1}H NMR (300 MHz, CD$_3$OD) δ = 7.36 (br. s., 3 H, H_a), 6.26 (br. s., 3 H, H_b), 4.03 (br. s., 6 H, N-CH_2), 3.55 (br. s., 6 H, CH_2-OH), 2.51 (br. s., 9 H, ring CH_3), 2.37 (br. s., 6 H, CH_2-CH$_2$-OH), 1.54 (br. s., 6 H, N-CH$_2$-CH_2). MS (+ESI) m/z = 764.4, 765.3, 766.4 [M + H]$^+$. HRMS (+ESI); Calc. (found): C$_{30}$H$_{43}$^{175}LuN$_3$O$_9$: 764.2407 (764.2402) [M + H]$^+$.

Tris(1-(2-hydroxypropyl)-2-methyl-3-oxy-4-pyridinonato)lanthanide(III), Ln(**4**)$_3$

Ln = La, Eu, Gd, Lu
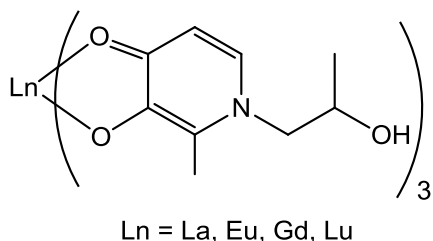
H**4** (0.106 g, 0.58 mmol, 3.0 equiv) was dissolved in water (10 mL); Ln(NO$_3$)$_3$•6H$_2$O (82.0–87.3 mg, 0.19 mmol, 1.0 equiv) was added to the ligand solution. The pH of the mixture was raised slowly over 10–15 min with the dropwise addition of 1 M NaOH (Ln^{3+} = La, pH 10.3; Eu, pH 11.7; Gd, pH 10.7 Lu, pH 9.4) and the resulting

mixture was continuously stirred for 1 h. The solution was concentrated under reduced pressure, redissolved in 1–2 mL of water and precipitated out with the addition of acetone (50 mL). The metal complex was collected by centrifugation (4000 RPM), the supernatant was discarded. All of the complexes were dried *in vacuo* to yield 54–96% of Ln(**4**)$_3$.

Tris(1-(2-hydroxypropyl)-2-methyl-3-oxy-4-pyridinonato)lanthanum(III), La(**4**)$_3$

^{1}H NMR (300 MHz, CD$_3$OD) δ = 7.18 (br. s., 3 H, H_a), 6.35 (br. s., 3 H, H_b), 3.96 (br. s., 6 H, N-CH_2), 3.80 (d, J = 6.8 Hz, 3 H, CH-OH), 2.30 (s, 9 H, ring CH_3), 1.16 (d, J = 5.0 Hz, 9

H, CH(OH)CH_3). MS (+ESI) m/z = 686.2, 687.2, 688.3 [M + H]$^+$. HRMS (+ESI); Calc. (found): C$_{27}$H$_{37}$^{139}LaN$_3$O$_9$: 686.1593 (686.1594) [M + H]$^+$.

$Tris$(1-(2-hydroxypropyl)-2-methyl-3-oxy-4-pyridinonato)europium(III), Eu(**4**)$_3$

MS (+ESI) m/z = 698.3, 699.3, 700.3, 701.2, 702.3, 703.4 [M + H]$^+$. HRMS (+ESI); Calc. (Found): C$_{27}$H$_{37}$^{151}EuN$_3$O$_9$: 698.1728 (698.1727) [M + H]$^+$.

$Tris$(1-(2-hydroxypropyl)-2-methyl-3-oxy-4-pyridinonato)gadolinium(III), Gd(**4**)$_3$

MS (+ESI) m/z = 701.4, 702.4, 703.4, 704.4, 705.4, 706.3, 707.3, 708.3, 709.3 [M + H]$^+$. HRMS (+ESI); Calc. (Found): C$_{27}$H$_{37}$^{155}GdN$_3$O$_9$: 702.1756 (702.1758) [M + H]$^+$.

$Tris$(1-(2-hydroxypropyl)-2-methyl-3-oxy-4-pyridinonato)lutetium(III), Lu(**4**)$_3$

^{1}H NMR (400 MHz, D$_2$O) δ = 7.37 (br. s., 3 H, H_a), 6.38 (d, J = 6.7 Hz, 3 H, H_b), 4.16 (br. s., 3 H, N-CH_2), 4.06 (br. s., 3 H, N-CH_2), 3.87 (m, 3 H, CH-OH), 2.28 (br. s., 3 H, ring CH_3), 1.20 (d, J = 6.1 Hz, 9 H, CH(OH)CH$_3$) MS (+ESI) m/z = 722.4, 723.2, 724.3, 725.4 [M + H]$^+$. HRMS (+ESI); Calc. (Found): C$_{27}$H$_{37}$^{175}LuN$_3$O$_9$: 722.1938 (722.1932) [M + H]$^+$.

$Tris$(1-(1-hydroxy-3-methylbutan-2-yl)-2-methyl-3-oxy-4-pyridinonato) lanthanum(III), La(5)$_3$
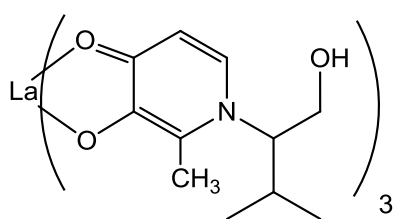
H**5** (95.8 mg, 0.45 mmol, 3.0 equiv) was dissolved in methanol (10 mL); La(NO$_3$)$_3$•6H$_2$O (73.0 mg, 0.15 mmol, 1.0 equiv) was added to the ligand solution. The pH of the mixture was raised slowly over 10–15 min with the dropwise addition of 1 M NaOH to pH 9.5, and the resulting mixture was continuously stirred for 1 h. The solution was concentrated under reduced pressure, redissolved in 1–2 mL of water and precipitated out with the addition of acetone (50 mL). The metal complex was collected by centrifugation (4000 RPM) and the supernatant was discarded. The lanthanum complex was dried $in\ vacuo$ to yield 53% of

product. ^{1}H NMR (400 MHz, CD$_3$OD) δ = 7.49 (br. s., 3 H, H_a), 6.64 (br. s., 3 H, H_b), 4.08 (br. s., 3 H, CH-CH$_2$-OH), 3.86 (br. s., 6 H, CH-CH_2-OH), 2.41 (br. s., 9 H, ring CH_3), 2.16 (s, 3 H, CH(CH$_3$)$_2$), 1.08 (br. s., 9 H, CH-CH_3), 0.66 (br. s., 9 H, CH-CH_3). ^{13}C{^{1}H} NMR (101 MHz, CD$_3$OD) δ = 158.4 (C=O), 140.7 (C_a), 134.6 (ring C-CH$_3$), 129.8 (ring C-OH), 121.3 (C_b), 62.2 (N-CH), 45.1 (CH$_2$-OH), 30.4 (C(CH$_3$)$_2$), 18.8 (C(CH$_3$)$_2$), 18.6 (C(CH$_3$)$_2$) 11.3 (ring CH$_3$). MS (+ESI) m/z = 792.2, 793.2, 794.2 [M + Na]$^+$. HRMS (+ESI); Calc. (found): C$_{33}$H$_{48}$^{139}LaN$_3$O$_9$Na: 792.2352 (792.2355) [M + Na]$^+$.

Tris(1-(1-hydroxybutan-2-yl)-2-methyl-3-oxy-4-pyridinonato)lanthanide(III), Ln(**6**)$_3$

Ln = La, Eu, Gd, Lu
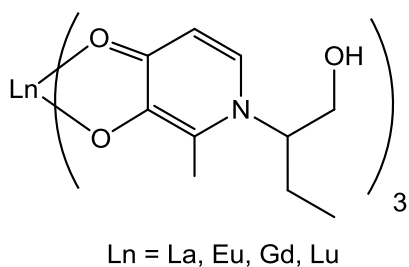
H**6** (0.100 g, 0.51 mmol, 3.0 equiv) was suspended in water (10 mL); the pH was decreased to 3.5–3.7 with the addition of 1 M NaOH in order to solubilize the ligand. Ln(NO$_3$)$_3$•6H$_2$O (73.0–81.4 mg, 0.17 mmol, 1.0 equiv) was added to the ligand solution. The pH of the mixture was raised slowly over 10–15 min with the dropwise addition of 1 M NaOH (Ln^{3+} = La, pH 9.5; Eu, pH 10.9; Gd, pH 9.45 Lu, pH 10.2) and the resulting mixture was continuously stirred for 1 h. The solution was concentrated under reduced pressure, redissolved in 1–2 mL of water and precipitated out with the addition of acetone (50 mL). The metal complex was collected by centrifugation (4000 RPM), the supernatant was discarded. All of the complexes were dried *in vacuo* to yield 65–73% of Ln(**6**)$_3$.

Tris(1-(1-hydroxybutan-2-yl)-2-methyl-3-oxy-4-pyridinonato)lanthanum(III), La(**6**)$_3$

^{1}H NMR (400 MHz, CD$_3$OD) δ = 7.34 (br. s., 3 H, H_a), 6.46 (d, J = 2.0 Hz, 3 H, H_b), 4.37 (br. s., 3 H, N-CH), 3.73 (br. s., 6 H, CH_2-OH), 2.37 (br. s., 9 H, ring CH_3), 1.58 - 1.97 (m, 6 H, CH_2CH$_3$), 0.79 (br. s., 9 H, CH$_2$CH_3). ^{13}C{^{1}H} NMR (101 MHz, CD$_3$OD) δ = 159.5 (ring C=O, C_a), 129.4 (ring C-OH, ring C-CH$_3$), 111.9 (C_b), 69.0 (N-CH), 65.5 (CH$_2$-OH), 25.8 (CH$_2$CH$_3$), 13.2 (CH$_2$$CH_3$), 10.7 (ring CH$_3$). MS (+ESI) m/z = 728.3, 729.2, 730.2 [M + H]$^+$. HRMS (+ESI); Calc. (found): C$_{30}$H$_{43}$^{139}LaN$_3$O$_9$: 728.2063 (728.2072) [M + H]$^+$.

Tris(1-(1-hydroxybutan-2-yl)-2-methyl-3-oxy-4-pyridinonato)europium(III), Eu(**6**)$_3$

MS (+ESI) m/z = 740.5, 741.4, 742.4, 743.3, 744.4, 745.4, 746.3 [M + H]$^+$. HRMS (+ESI); Calc. (found): C$_{30}$H$_{43}$^{151}EuN$_3$O$_9$: 740.2198 (740.2202) [M + H]$^+$.

Tris(1-(1-hydroxybutan-2-yl)-2-methyl-3-oxy-4-pyridinonato)gadolinium(III), Gd(**6**)$_3$

MS (+ESI) m/z = 743.2, 744.4, 745.4, 746.4, 747.3, 748.3, 749.3, 750.3, 751.3 [M + H]$^+$. HRMS (+ESI); Calc. (found): C$_{30}$H$_{43}$^{153}GdN$_3$O$_9$: 744.2226 (744.2232) [M + H]$^+$.

Tris(1-(1-hydroxybutan-2-yl)-2-methyl-3-oxy-4-pyridinonato)lutetium(III), Lu(**6**)$_3$

^{1}H NMR (400 MHz, D$_2$O) δ = 7.47 (br. s., 3 H, H_a), 6.49 (br. s., 3 H, H_b), 4.46 (br. s., 3 H, N-CH), 3.79 (br. s., 6 H, CH_2-OH), 2.29 (br. s., 9 H ring CH_3), 1.80 (br. s., 3 H, CH_2CH$_3$), 1.66 (br. s., 3 H, CH_2CH$_3$), 0.72 (br. s., 9 H, CH$_2$CH_3). MS (+ESI) m/z = 764.4, 765.4, 766.3, 767.3 [M + H]$^+$. HRMS (+ESI); Calc. (found): C$_{30}$H$_{43}$^{175}LuN$_3$O$_9$: 764.2407 (764.2407) [M + H]$^+$.

Sodium _tris_(1-carboxymethyl-2-methyl-3-oxy-4-pyridinonato)lanthanide(III), Na$_3$[Ln(**8**)$_3$]
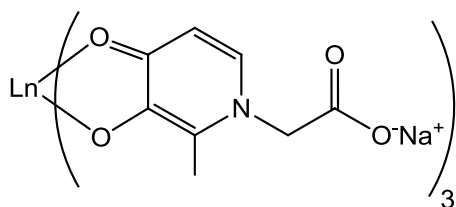
Ln = La, Eu, Gd, Lu

H**8** (0.101 g, 0.55 mmol, 3.0 equiv) was suspended in water (10 mL); the pH was increased to 3.9 with the addition of 1 M NaOH in order to solubilize the ligand. Ln(NO$_3$)$_3$•6H$_2$O (78.6–85.6 mg, 0.18 mmol, 1.0 equiv) was added to the ligand solution. The pH of the mixture was raised slowly over 10–15 min with the dropwise addition of 1 M NaOH (Ln^{3+} = La, pH 9.5; Eu, pH 10.9; Gd, pH 9.45 Lu, pH 10.2) and the resulting mixture was continuously stirred for 1 h. The solution was concentrated under reduced pressure, redissolved in 1–2 mL of water and precipitated out with the addition of acetone (50 mL). The metal complex was collected by centrifugation (4000 RPM), the supernatant was discarded. All complexes were dried _in vacuo_ to yield 81–95% of Na$_3$Ln(**8**)$_3$.

Sodium *tris*(1-carboxymethyl-2-methyl-3-oxy-4-pyridinonato)lanthanum(III), Na$_3$[La(**8**)$_3$]

^{1}H NMR (400 MHz, D$_2$O) δ = 7.24 (d, *J* = 6.1 Hz, 3 H, *H*$_a$), 6.36 (br. s., 3 H, *H*$_b$), 4.53 (br. s., 6 H, C*H*$_2$-COOH), 2.12 (br. s., 9 H, ring C*H*$_3$). ^{13}C{^{1}H} NMR (101 MHz, D$_2$O) δ = 174.6 (CH$_2$-*C*OO$^-$), 172.6 (ring *C*=O), 156.1 (*C*$_a$), 134.8 (ring *C*-CH$_3$, ring *C*-OH), 110.5 (*C*$_b$), 58.4 (N-*C*H$_2$), 12.0 (ring *C*H$_3$). MS (-ESI) *m/z* = 706.0, 707.0, 708.0 [M - 2Na + H]$^-$. HRMS (-ESI); Calc. (found): C$_{24}$H$_{22}$^{139}LaN$_3$NaO$_{12}$: 706.0165 (706.0167) [M - 2Na + H]$^-$. Anal. Calc. (found): C$_{24}$H$_{21}$LaN$_3$Na$_3$O$_{12}$•H$_2$O: C, 37.47 (37.81); H, 3.01 (3.14); N, 5.46 (5.46).

Sodium *tris*(1-carboxymethyl-2-methyl-3-oxy-4-pyridinonato)europium(III), Na$_3$[Eu(**8**)$_3$]

MS (-ESI) *m/z* = 718.0, 719.0, 720.0, 721.0, 722.7 [M - 2Na + H]$^-$. HRMS (-ESI); Calc. (found): C$_{24}$H$_{22}$^{151}EuN$_3$NaO$_{12}$: 718.0300 (718.0292) [M - 2Na + H]$^-$. Anal. Calc. (found): C$_{24}$H$_{21}$EuN$_3$Na$_3$O$_{12}$•H$_2$O: C, 36.84 (37.84); H, 2.96 (3.33); N, 5.37 (5.12).

Sodium *tris*(1-carboxymethyl-2-methyl-3-oxy-4-pyridinonato)gadolinium(III), Na$_3$[Gd(**8**)$_3$]

MS (-ESI) *m/z* = 721.0, 722.0, 723.0, 724.0, 725.0, 726.0, 727.1, 728.0, 729.0 [M - 2Na + H]$^-$. HRMS (-ESI); Calc. (found): C$_{24}$H$_{22}$^{154}GdN$_3$NaO$_{12}$: 721.0310 (721.0330) [M - 2Na + H]$^-$. Anal. Calc. (found): C$_{24}$H$_{21}$GdN$_3$Na$_3$O$_{12}$•2H$_2$O: C, 35.78 (35.98); H, 3.13 (3.22); N, 5.22 (5.36).

Sodium *tris*(1-carboxymethyl-2-methyl-3-oxy-4-pyridinonato)lutetium(III), Na$_3$[Lu(**8**)$_3$]

^{1}H NMR (300 MHz, D$_2$O) δ = 7.34 (br. s., 3 H, *H*$_a$), 6.43 (br. s., 3 H, *H*$_b$), 4.60 (br. s., 6 H, C*H*$_2$-COOH), 2.17 (br. s., 9 H, ring C*H*$_3$). MS (-ESI) *m/z* = 720.1, 721.1, 722.1, 723.1 [M - 3Na + 2H]$^-$. HRMS (-ESI); Calc. (found): C$_{24}$H$_{23}$^{175}LuN$_3$O$_{12}$: 720.0690 (720.0675) [M - 3Na + 2H]$^-$.

Sodium *tris*(1-carboxyethyl-2-methyl-3-oxy-4-pyridinonato)lanthanide(III), Na₃[Ln(9)₃]
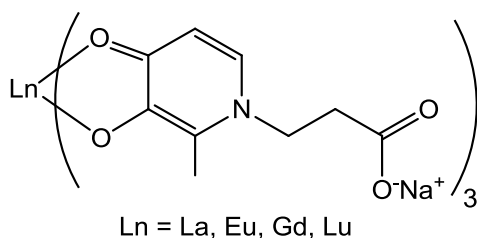
H**9** (0.102 g, 0.52 mmol, 3.0 equiv) was suspended in water (10 mL); $Ln(NO_3)_3 \cdot 6H_2O$ (74.6–81.9 mg, 0.18 mmol, 1.0 equiv) was added to the ligand solution. The pH of the mixture was raised slowly over 10–15 min with the dropwise addition of 1 M NaOH (Ln^{3+} = La, pH 10.6; Eu, pH 10.3; Gd, pH 10.8 Lu, pH 11.1) and the resulting mixture was continuously stirred for 1 h. The solution was concentrated under reduced pressure, redissolved in 1–2 mL of water and precipitated out with the addition of acetone (50 mL). The metal complex was collected by centrifugation (4000 RPM), the supernatant was discarded. All compounds were dried *in vacuo* to yield 45–99% of $Na_3Ln(9)_3$.

Ln = La, Eu, Gd, Lu

Sodium *tris*(1-carboxyethyl-2-methyl-3-oxy-4-pyridinonato)lanthanum(III), Na₃[La(9)₃]

^{1}H NMR (400 MHz, D_2O) δ = 7.31 (br. s., 3 H, H_a), 6.29 (br. s., 3 H, H_b), 4.18 (br. s., 6 H, N-CH_2), 2.53 (br. s., 6 H, CH_2-COOH), 2.22 (br. s., 9 H, ring CH_3). ^{13}C{^{1}H} NMR (101 MHz, D_2O) δ = 178.7 (CH₂-COO⁻), 172.4 (ring C=O), 156.4 (C_a), 134.1 (ring C-OH), 133.5 (ring C-CH₃), 110.6 (C_b), 52.1 (N-CH₂), 38.4 (CH₂-COOH), 11.8 (ring CH₃). MS (-ESI) m/z = 748.1, 749.1, 749.2, 750.1 [M - 2Na + H]⁻. HRMS (-ESI); Calc. (found): $C_{27}H_{28}{}^{139}LaN_3NaO_{12}$: 748.0634 (748.0632) [M - 2Na + H]⁻. Anal. Calc. (found): $C_{27}H_{27}LaN_3Na_3O_{12} \cdot 2H_2O$: C, 39.87 (39.28); H, 3.84 (3.60); N, 5.17 (5.08).

Sodium *tris*(1-carboxyethyl-2-methyl-3-oxy-4-pyridinonato)europium(III), Na₃[Eu(9)₃]

MS (-ESI) m/z = 738.1, 739.1, 740.1, 741.1, 742.1 [M - 3Na + 2H]⁻. HRMS (-ESI); Calc. (found): $C_{27}H_{29}{}^{151}EuN_3O_{12}$: 738.0950 (738.0938) [M - 3Na + 2H]⁻.

Sodium *tris*(1-carboxyethyl-2-methyl-3-oxy-4-pyridinonato)gadolinium(III) Na₃[Gd(9)₃]

MS (-ESI) m/z = 741.1, 742.1, 743.1, 744.1, 745.1, 746.1, 747.1, 748.1, 749.1 [M - 3Na + 2H]$^+$. HRMS (-ESI); Calc. (found): $C_{27}H_{29}{}^{155}GdN_3O_{12}$: 742.0978 (742.0972) [M - 3Na + 2H]$^-$.

Sodium *tris*(1-carboxyethyl-2-methyl-3-oxy-4-pyridinonato)lutetium(III), Na$_3$[Lu(**9**)$_3$]

^{1}H NMR (300 MHz, D$_2$O) δ = 7.41 (d, J = 5.7 Hz, 3 H, H_a), 6.36 (d, J = 6.2 Hz, 3 H, H_b), 4.23 (br. s., 6 H, N-CH_2), 2.57 (br. s., 6 H, CH_2-COOH), 2.26 (br. s., 9 H, ring CH_3). MS (-ESI) m/z = 784.1, 785.1, 786.1, 787.1 [M - 2Na + H]$^-$. HRMS (-ESI); Calc. (found): $C_{27}H_{28}{}^{175}LuNaN_3O_{12}$: 784.0979 (784.0980) [M - 2Na + H] $^-$.

2.2.10 Synthesis of Hexadentate Phosphinate-EDTA Complexes of Lanthanides

The chelation of H$_5$**XT** to lanthanides was accomplished by the deprotonation of the ligand with the addition of potassium hydroxide in the presence of the appropriate lanthanide nitrate hexahydrate salt, affording K$_2$[Ln(**XT**)] as shown in Figure 2.14.
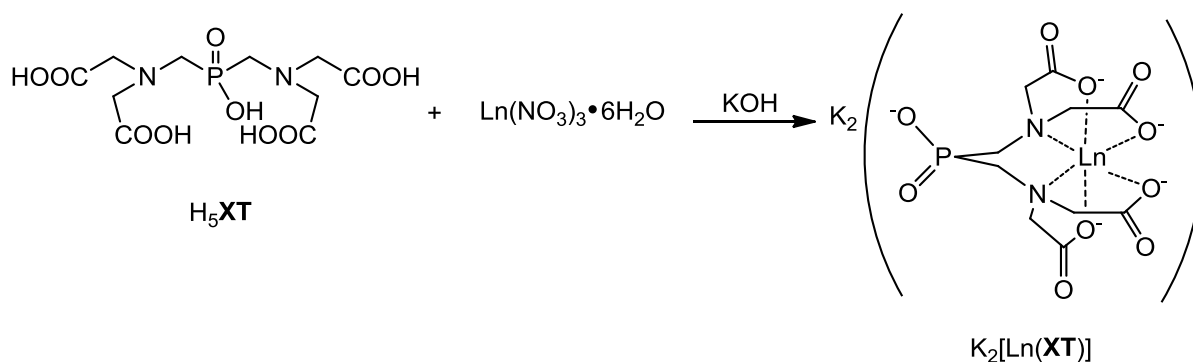
Figure 2.14. Synthesis of K$_2$[Ln(XT)] from H$_5$XT.

Bis[[bis(carboxymethyl)amino]methyl]phosphinate (H₅XT•HCl) This was prepared as previously published by our laboratory.[127] Iminodiacetic acid (2.7 g, 20 mmol) was dissolved in a 50% aq. solution of H_3PO_2 (1.3 g, 10 mmol). To this mixture, hydrochloric acid (6 M, 4.0 mL, 24.0 mmol) was added and the solution was heated to reflux. An aqueous solution of formaldehyde (37%; 3.2 g, 40 mmol) was added dropwise to the reaction mixture and the reflux was continued for an additional 12 h. Upon cooling to room temperature a white precipitate formed and was collected by filtration, rinsed with methanol and dried *in vacuo*, affording a white solid, H₅**XT**•HCl, (0.502 g, 13%) ^{1}H{^{31}P} NMR (300 MHz, D₂O) δ = 4.20 (s, 8 H, N-CH_2-COOH), 3.58 (d, J = 9.6 Hz, 4 H, N-CH_2-PO). ^{31}P{^{1}H} NMR (121 MHz, D₂O) δ = 18.75. MS (+ESI) m/z = 357.1 [M + H]$^+$. Anal. Calc. (found): $C_{10}H_{17}N_2O_{10}P$•HCl: C, 30.59 (30.93); H, 4.62 (4.68); N, 7.13 (7.05).

General Synthesis of K₂[Ln(**XT**)]

The synthesis of K₂[Ln(**XT**)] was achieved by a method published from our group.[127] H₅**XT**•HCl (40 mg, 0.10 mmol) and Ln(NO₃)₃•6H₂O (Ln = La, Eu, Lu) were dissolved in a minimum amount of water (2 mL). The pH was increased slowly by the dropwise addition of 0.1 M NaOH until the solution reached a pH of 7 − 8. The solution was then concentrated by rotary evaporation. The residue was redissolved in methanol (3 mL) and water (0.5 mL), precipitated with acetone and centrifuged (4000 ppm) to collect the white or yellow precipitate. The supernatant was decanted and remaining white pellet was dissolved in methanol, precipitated with acetone and the product was isolated by centrifugation and dried, affording a white or yellow solid. All complexes were dried *in vacuo* to yield 72 − 89% of K₂[Ln(**XT**)].

K₂[La(**XT**)]

HRMS (-ESI); Calc. (found): $C_{10}H_{12}K^{139}La\ N_2O_{10}P$: 528.8930 (528.8933) [M - K]$^-$.

K$_2$[Eu(**XT**)]

HRMS (-ESI); Calc. (found): C$_{10}$H$_{12}$^{151}EuKN$_2$O$_{10}$P: 540.9065 (540.9062) [M - K]$^-$.

K$_2$[Lu(**XT**)]

HRMS (-ESI); Calc. (found): C$_{10}$H$_{12}$K^{175}LuN$_2$O$_{10}$P: 564.9275 (564.9279) [M - K]$^-$.

2.2.11 Determination of Stability Constants of 3-Hydroxy-4-pyridinones with Lanthanide Ions

Potentiometric equilibrium measurements of the 3-hydroxy-4-pyridinones H**L1**, H**4** and H**9** and stability constant determinations of H**L1** with La^{3+} and Gd^{3+} were performed on a Metrohm Titrando 809 equipped with a Ross combination pH electrode and a Metrohm Dosino 800 automatic burette. The titration apparatus consisted of a 10 mL water-jacketed glass vessel maintained at 25.0 ± 0.1 °C (Julabo water bath). Nitrogen, purified through a 10% NaOH solution to exclude any CO$_2$, was passed through the solution prior and during the titrations. The electrode was calibrated using a standard HCl solution before each potentiometric equilibrium study. Data was collected in triplicate using PC Control (Version 6.0.91, Metrohm), and was analyzed by a standard computer treatment program (MacCalib) to obtain the calibration parameter E$_0$.

A NaOH solution (0.15 M) was prepared from the dilution of 50% NaOH (Acros Organics) with freshly boiled 18.2 MΩ-cm water under a stream of purified N$_2$(g), producing carbonate-free solution. The solution was standardized against freshly recrystallized potassium hydrogen phthalate. Titration of the NaOH solution with a standard HCl solution was performed regularly to determine the extent of carbonate accumulation in the base solution and determined by plotting (V$_o$ + V$_t$) x 10^{-pH} versus V$_t$ (a Gran plot).[128]

Determination of the acid dissociation constants was achieved by the titration of base into the ligand in acid. Ligand solutions (0.0010 M) were prepared by dissolving the ligands in a known amount of acid with an ionic strength of 0.16 M NaCl. Potentiometric titrations were performed by the automatic addition of base (CO_2 free NaOH) into the ligand solutions. While the equilibrium was rapidly established in less that 10 min, up to 15 min was permitted for stabilization between each addition of base.

The metal-ligand stability constants were obtained by the titration of base into variable ratio metal-ligand solutions, where the ligand concentration was kept constant and the concentration of either the La(III) or Gd(III) was varied. Metal ion solutions were prepared from the appropriate atomic absorption (AA) standard (Fluka, a subsidiary of Sigma-Aldrich). The exact amount of acid present in the metal standard was determined by titration of an equimolar solution of metal and Na_2H_2EDTA (disodium ethylenediaminetetraacetic acid), and determined from the corresponding Gran plot.[128] Metal ion solutions of La (0.00100–0.00029 M) and Gd (0.00100–0.00025 M) were prepared by dilution of the appropriate AA standard with H**L1** (0.001 M) in a solution of 0.16 M NaCl. The ligand-to-metal ratios for the titrations were 1:1, 2:1, 3:1 and 4:1 for both H**L1**-La and H**L1**-Gd.

The hydrolysis constants for La(III)[129] and Gd(III)[130] were taken from Baes and Mesmer,[130] and Barnum[129] and were included in the calculations. The protonation constants of the ligands H**L1**, H**4** and H**9**, and the metal-ligand stability constants with H**L1** were calculated from the titration data using Hyperquad 2008.[131] All values and errors represent an average of at least three independent titration experiments.

2.3   Results and Discussion

2.3.1   Synthesis of 3-Hydroxy-4-pyridinones Containing Hydroxyl, Carboxyl, 1,2-Diol and Alkyl Substituents

Route I:
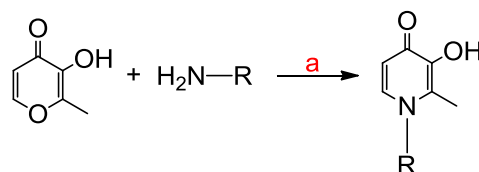
Route II:
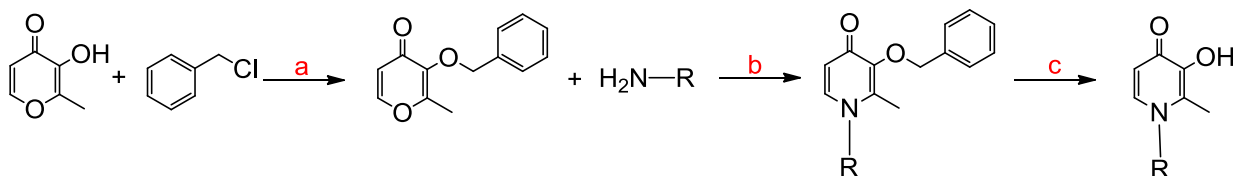
Scheme 2.1. General synthesis of a 3-hydroxy-4-pyridinone. Route I: a) NaOH, H_2O, reflux 24–70 h. Route II: a) benzyl chloride, NaOH, methanol, reflux 40 h; b) NaOH, ethanol/water or methanol, reflux 15–92 h; c) HBr in acetic acid 33% w/v or $H_{2(g)}$, 10% P/C.

The syntheses of 3-hydroxy-2-methyl-4-pyridinones functionalized with hydroxy, carboxy, alkyl and 1,2-diol substituents were achieved by one of two routes – the direct ammonolysis of maltol, or the ammonolysis of benzyl-protected maltol, as seen in Scheme 2.1. The syntheses of **H1**, **H8** and **H16** proceeded by the former route, while the syntheses of **H1**, **H2**, **H3**, **H4**, **H5**, **H6**, **H7**, **H8** and **H9** were accomplished by the later route, via the syntheses of **Bn1**, **Bn2**, **Bn3**, **Bn4**, **Bn5**, **Bn6**, **Bn7**, **Bn8** and **Bn9**, followed by debenzylation.

2.3.2   Synthesis of 3-Hydroxy-4-pyridinones by Direct Ammonolysis

The syntheses of H**1**, H**8** and H**6** were accessed by the direct ammonolysis of the pyrone, maltol, with the appropriate primary amine (Scheme 2.1, Route I). Generally, only the synthesis with small alkylamines can be achieved by the direct insertion method.[108] It is known that the insertion of the unprotected 3-hydroxy-4-pyrones leads to longer reaction times and difficulty isolating the product. As can be seen from Table 2.1, higher equivalents of the amine in the direct insertion syntheses were required to obtain yields comparable to the benzyl protected route.

Conventional organic separation techniques cannot be employed without the protection of the 3-hydroxy group. The product (H**1**, H**8** or H**16**) and both starting materials (primary amine and maltol) are soluble in aqueous solvents, but only sparsely soluble in organic solvents, such as dichloromethane, chloroform or diethyl ether, commonly used in organic separations. Thus, the ideal recrystallizing solvent must be found, which is often an arduous task.

For example, Epstein *et al.*[122] reported in the synthesis of H**1** that triturating the crude mixture with 2-propanol results in the precipitation of the ligand, which could then be recrystallized from water; however, in the absence of trituration, the ligand could not be isolated. Likewise Kontoghiorghes *et al.*[124] discovered that acetone was a recrystallization solvent for the isolation of H**16** recrystallization. H**1**, H**8** and H**16** were fully characterized by ^{1}H and ^{13}C NMR spectroscopy, ESI-MS and elemental analysis (EA).

Table 2.1. Equivalents of amine used to synthesize each ligand, and the respective yields.

Compound	Nucleophile (amine)		Equivalent of amine	Yield (%)
H1	2-aminoethanol		3.1	41
H8	glycine		2.0	40
H16	propylamine		3.0	26
Bn1	2-aminoethanol		1.5	37
Bn2•HCl	3-aminopropanol		1.5	59
Bn3•HCl	4-amino-1-butanol		1.5	54
Bn4	(±)-1-aminopropan-2-ol		2.0	59
Bn5	(±)-2-amino-3-methyl-1-butanol		1.6	6
Bn6	(±)-2-amino-1-butanol		2.0	30
Bn7	(±)-3-aminopropane-1,2-diol		1.5	61
Bn9	β-alanine		1.5	45
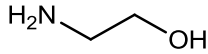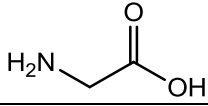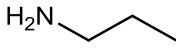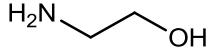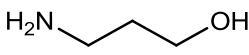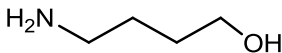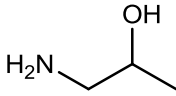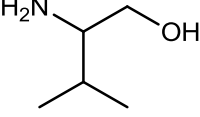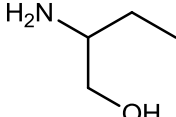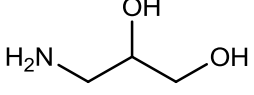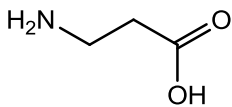
2.3.3   Synthesis of 3-Hydroxy-4-pyridinones by the Benzyl-Protected Route

The syntheses of the remaining 3-hydroxy-4-pyridinones were attempted by the direct insertion method (Scheme 2.1, Route I); while the desired products formed, the reactions resulted in oils that could not easily be separated from the starting materials. As a result, the remaining pyridinone ligands were prepared by a three step process (Scheme 2.1, Route II): first the 3-hydroxy functional group of the pyrone is protected with a benzyl-ether generating 3-benzyl-2-methyl-4-pyrone; the benzyl-protected pyrone was then reacted with the appropriate primary amine and finally the protecting group was removed to yield the free 3-hydroxy-2-methyl-4-pyridinone.

The starting material **Bnma** was synthesized according to our literature.[125] Using commercially available maltol, the 3-hydroxy group of the pyrone was protected via a Williamson ether synthesis, as seen in Figure 2.15. A reasonable yield (79%) was obtained after recrystallization from ethanol.
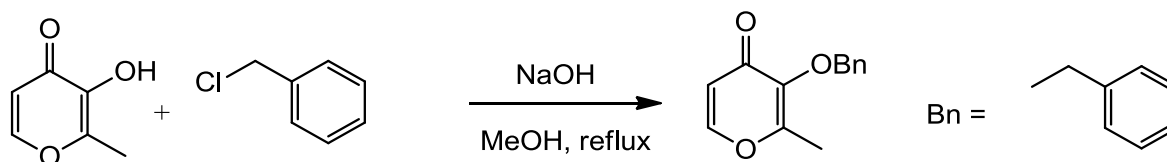
Figure 2.15. Synthesis of 3-benzyl-2-methyl-4-pyrone (Bnma).

The syntheses of the 3-benzyloxy pyridinone ligand precursors, Bn**1**, Bn**2**, Bn**3**, Bn**4**, Bn**5**, Bn**6**, Bn**7,** and Bn**9**, were carried out using Bn**ma**. Bn**1**, Bn**2**, Bn**3** and Bn**9** have been previously synthesized by Dobbin *et al.*,[126] while Bn**4**, Bn**5**, Bn**6** and Bn**7** were based on but are variations of previously published methods (Figure 2.9).[71,126]

Bn**ma** was reacted with the appropriate primary amine using a catalytic amount of base. In this way, Bn**ma** undergoes a base-catalyzed ammonolysis reaction where the amine

nucleophile attacks the pyrone ring at either the 2 or 6 position, as seen in Figure 2.16.[132] Due to steric hindrance at the 2 position, it is expected that the nucleophilic attack occurs at the 6 position. The pyrone **I** to pyridinone **VI** reaction involves a Michael-type nucleophilic addition of the primary amine to the ring (**II**) producing an ammonium ion at the 6 position (**III**) which tautomerizes (**IV**) resulting in the oxygen of the pyrone ring being protonated. The amine is deprotonated in the presence of base (**V**) followed by dehydration, to form the 3-hydroxy-2-methyl-4-pyridinone (**VI**).
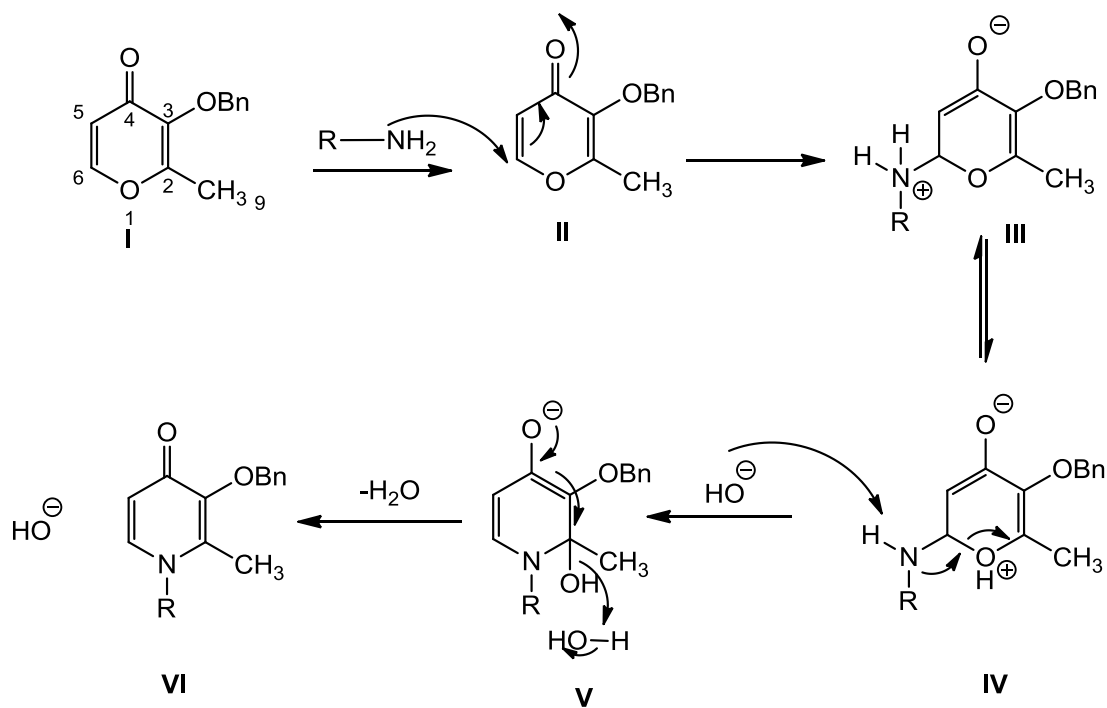
Figure 2.16. Generally agreed on mechanism of the base catalyzed amine insertion to produce 3-benzyloxy-4-pyridinone from 3-beznyloxy-4-pyrone.[132]

Upon ammonolysis, of the benzyl-protected pyrone, the crude reaction mixture was concentrated and suspended in water. The pH was adjusted to approximately 1 and washed with diethyl ether. The Bn**ma** went into the organic phase, while the pyridinone remained in the aqueous phase; this is likely because under acidic conditions the nitrogen of the pyridinone ring was protonated which increased the aqueous solubility of the pyridinone salt.

97

The pH was then adjusted to 7–8; at this pH the nitrogen was no longer protonated which decreased its aqueous solubility and increased its organic solubility. The product was then partitioned in dichloromethane and extracted in the organic layer. By protecting the 3-hydroxy group, the solubility of the ligand precursors in organic solvents such as dichloromethane increases significantly; adjusting the pH allows control of the solubility of the benzyl-protected pyridinones in aqueous or organic solvents, simplifying the purification of the ligands.

The syntheses of Bn**1**, Bn**2**, B-**3** and Bn**9** have been previously reported by Dobbin *et al.*[126] and were obtained in yields comparable to literature reports; Bn**4**, Bn**6**, and Bn**7** were all obtained in moderate yields. Bn**6** required a higher equivalent of amine than did the other syntheses—this is mainly due to the steric hindrance of the nucleophile compared to the other amines, Table 2.1. For the syntheses of Bn**2** and Bn**3** the products had to be crystallized as their HCl salts as previously reported because attempts to isolate the product at a neutral pH as with the other ligands did not work.[126]

Due to poor conversion rates from the pyrone to the pyridinone, the excess primary amine made separation of Bn**5** from the starting materials difficult. The isolation of Bn**5** required the use of normal phase silica gel column chromatography to remove the excess amine. Attempts at increasing the molar ratio of the amine to increase the yield resulted in greater difficulty separating the amine from the product.

Due to the high aqueous solubility of Bn**7**, the pyridinone could not be isolated by extraction into organic solvents. The crude mixture dissolved in methanol was left at 4 °C overnight and a pale yellow precipitate formed, obviating the need for separation. The solid was collected and recrystallized from ethanol and diethyl ether.

Four literature 3-benzyloxy-4-pyridinone ligands were synthesized (Bn**1**, Bn**2**•HCl, Bn**3**•HCl and Bn**9**) along with four novel 3-benzyloxy-4-pyridinone ligands (Bn**4**, Bn**5**, Bn**6** and Bn**7**). All of the products were characterized by ^{1}H NMR spectroscopy and ESI-MS.

2.3.4 Deprotection of the 3-Benzyloxy-4-pyridinone Derivatives to Yield 3-Hydroxy-4-pyridinones

Once the key desired functional group was inserted into the pyridinone ring, the 3-benzyloxy pyridinones could be deprotected to afford the free 3-hydroxy pyridinones, as shown in Scheme 2.1 Route II. The final step in the ligand synthesis involved the deprotection of the benzyl group by the use of either hydrobromic acid in glacial acetic acid or hydrogenation catalyzed by palladium on carbon.

Ligands H**2**, H**3**, H**4**, H**5**, H**6** and H**7** were accessed by the hydrogenation of Bn**2**, Bn**3**, Bn**4**, Bn**5**, Bn**6** and Bn**7**, respectively. To catalyze the hydrogenation process, a small amount of palladium on carbon was used in the presence of an atmospheric pressure of $H_2(g)$. For some of the ligands, in order to increase the aqueous solubility, a small amount of hydrochloric acid was added. Due to limited solubility of Bn**9** in water, methanol or ethanol under neutral or acidic conditions, Bn**9** was deprotected using HBr in acetic acid.

The ligands H**1**, H**2**, H**3**, H**4**, H**5**, H**6,** H**7** and H**9** were obtained in moderate to good yields, with the exception of H**5**. This is likely due its poor solubility in water and organic solvents. In the final step of the hydrogenation, the crude mixture must be filtered in order to remove the hydrogenation catalyst. Due to the limited solubility of H**5**, a significant amount of the ligand likely remained in the Pd/C mixture.

The ligands were characterized by ^{1}H and ^{13}C NMR spectroscopy, ESI-MS, IR and elemental analysis. Three literature 3-hydroxy-4-pyridinones were synthesized (H**2**•HCl, H**3**•HCl and H**9**), along with four novel 3-benzyloxy-4-pyridinone ligands (H**4**, H**5**, H**6** and H**7**). Figure 2.17 shows a comparison of the ^{1}H NMR spectroscopic shifts observed for the four novel pyridinones. The pyridinone ^{1}H and ^{13}C{^{1}H} NMR spectra were easily assigned by comparison to previous work done on similar compounds,[71] as well as comparison of the spectra of starting materials or simpler structural analogues. The resonances for both H_a and

H_b were found in the range of 7.6–7.8 ppm and 6.3–6.5 ppm, respectively, while the alkyl resonances were observed between 0.7–4.5 ppm.
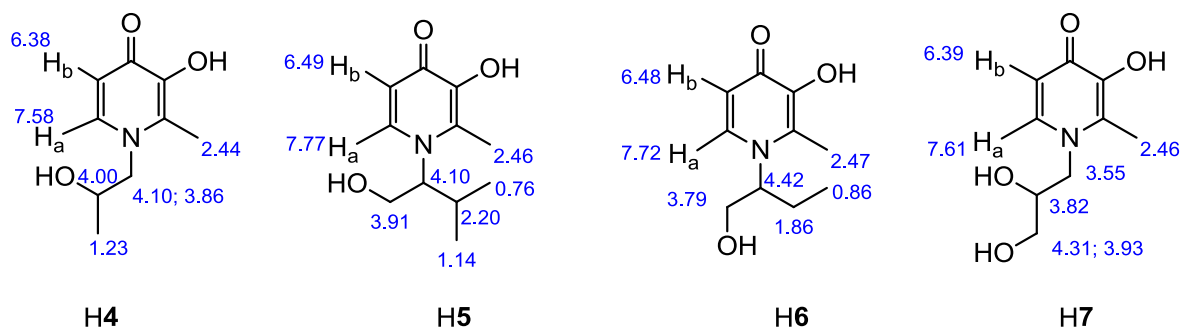
Figure 2.17. ^{1}H NMR (300 MHz, CD$_3$OD, RT) spectroscopic shifts reported in ppm for the novel hydroxy functionalized 3-hydroxy-4-pyridinones.

2.3.5   Synthesis of a Bisphosphonate 3-Hydroxy-4-pyridinone

Bisphosphonates or diphosphonic acids are potent antiosteoporotic agents that are known to bind irreversibly to bone.[85] Incorporation of a bisphosphonate (BP) functional group into a hydroxypyridinone that could be subsequently coordinated to a lanthanide ion could help the molecule target bone. Thus the synthesis of a pyridinone functionalized with a diphosphonic functional group was successfully attempted.

Figure 2.18 shows a schematic of a bisphosphonate functional group; the X substituent alters the binding efficacy of the BP to bone and thus the potency.[133] Efficacy studies with BPs demonstrated that the a hydroxy (OH) at the X position is 10–20 fold more potent than the other substituents at the X position.[133]

X = H, NH$_2$, OH
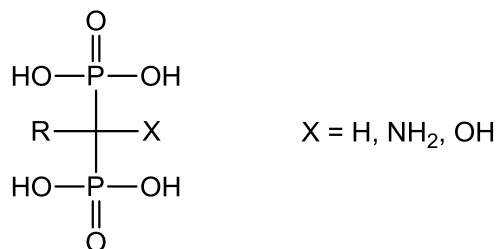
Figure 2.18. Bisphosphonate functional group, where R is generally an alkyl or aryl substituent; the X group has been shown to significantly alter the binding strength of the bisphosphonate to bone.[133]

From an exhaustive search of the literature, there appear to be two general routes for the synthesis of a hydroxyl-BP (BP-OH). Figure 2.19 shows that the general synthesis of BP-OHs involves a carboxylic acid, which is activated, usually by the formation of an acid chloride and then reacted with either a phosphite ester (P(OSiMe$_3$)$_3$) or phosphorous acid to form the BP-OH.[85,134,135] In the presence of POCl$_3$ or PCl$_3$ the reaction generally results in a two phase melt which is difficult to stir.[134] The second general method usually involves the synthesis of an acid chloride from the carboxylic acid using either POCl$_3$, PCl$_3$ or oxalyl chloride (ClC(O)C(O)Cl).[136,137,138] Alternatively, a catecholborane has been used to activate the carboxylic acid in the presence of dry tetrahydrofuran (THF).[135] Once activated, the carboxylate can be reacted with trimethylsilylphosphite (P(OSiMe$_3$)$_3$) to produce the methyl ester diphosphonic acid, followed by the hydrolysis of the methyl ester in the presence of methanol to produce the BP-OH.

In order to synthesize a 3-hydroxy-4-pyridinone with a BP-OH functional group, 1-carboxymethyl-3-benzyloxy-2-methyl-4-pyridinone (Figure 2.20) was synthesized according to a literature preparation[126] from the base-catalyzed reaction of B**nma** with glycine. The protected pyridinone was necessary as PCl$_3$ is known to convert hydroxyl groups into halides and POCl$_3$ is known to phosphorylate free hydroxyl groups.[139]

Method 1: a) POCl$_3$ or PCl$_3$, PO$_3$H$_3$
b) H$_2$O

Method 2: a) Activation of the carboxylic acid
b) P(OSiMe$_3$)$_3$
c) MeOH
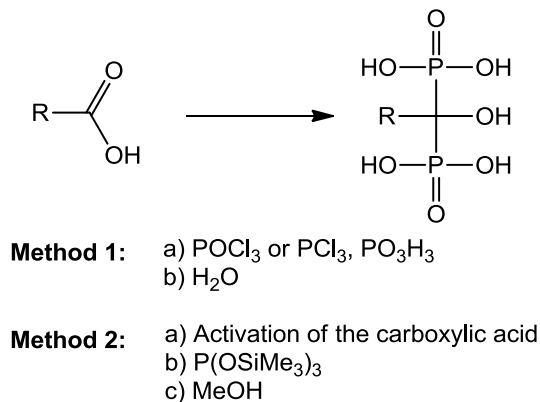
Figure 2.19. The synthesis of hydroxyl-bisphosphonates from a carboxylic acid occurs by the activation of the carboxylic acid, followed by phosphorylation with either phosphorus acid or trimethylsilylphosphite.

Various synthetic methods were attempted in the synthesis of a BP-OH functionalized 3-hydroxy-4-pyridinone from a carboxylic acid, as seen in Figure 2.20; however solubility issues were the greatest limiting factor. In the attempted synthesis of the acid chloride described in Figure 2.20 Method 1[85,136] the 1-carboxyl-3-benxyloxy-4-pyridinone starting material would not dissolve in dichloromethane; thus the formation of the acid chloride did not occur.

Figure 2.20 Method 2[137,138] involved dissolving the starting material in dry toluene – again the product would not dissolve, and no product formation was observed. Lastly, in an attempt to activate the carboxylic acid using catecholborane as seen in Figure 2.20 Method 3,[135] the starting material would not dissolve in anhydrous THF, again leading to no evidence of product formation. Due to the limited solubility of the carboxy-pyridinone starting material, a different approach was sought.

Alendronate (4-amino-1-hydroxybutane-1,1-diphosphonic acid) is an approved BP-OH sold under the trademark Fosamax[TM] by Merck for the treatment of osteoporosis.[140] The patent on this particular BP-OH expired in 2008 allowing for generic versions to be sold, making this BP-OH available at an affordable cost.[141]

102
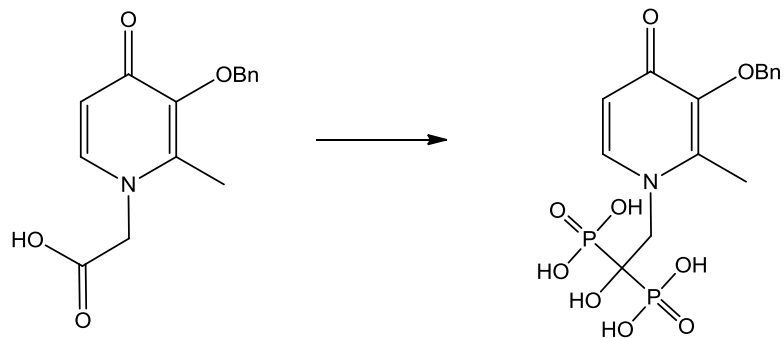
Method 1: a) ClOCOCCl, DCM, pyridine

Method 2: a) POCl$_3$, PO$_3$H$_3$ in toluene
b) H$_2$O

Method 3: a) Catecholborane in THF
b) P(OSiMe$_3$)$_3$
c) MeOH

Figure 2.20. Methods attempted in order to synthesize a BP-OH from a 3-hydroxy-4-pyridinone.

Using a BP-OH with a primary amine, the direct amine insertion into Bn**ma** was possible as seen in Figure 2.21. The isolation of Bn**10** was achieved by washing the crude mixture with dichloromethane in order to remove the Bn**ma** starting material, followed by purification by reverse phase chromatography. Lastly, the BP-OH, Bn**10**, was recrystallized in hot water to remove any residual alendronate. The bisphosphonate was then deprotected by a simple hydrogenation reaction catalyzed by Pd on C.

In the ^{31}P NMR spectrum of Bn**11**, the characteristic BP resonance at ~20 ppm helped confirm product formation of the bisphopshonate. Furthermore, coupling observed between the P-C-P functional groups in the ^{13}C NMR spectrum of Bn**11** further corroborates the synthesis of the BP-OH functionalized pyridinone. Thus, the first bisphosphonate functionalized 3-hydroxy-4-pyridinone is reported, characterized by HRMS ESI (high resolution mass spectrometry electrospray ionization) and ^{1}H, ^{13}C and ^{31}P NMR spectroscopy.
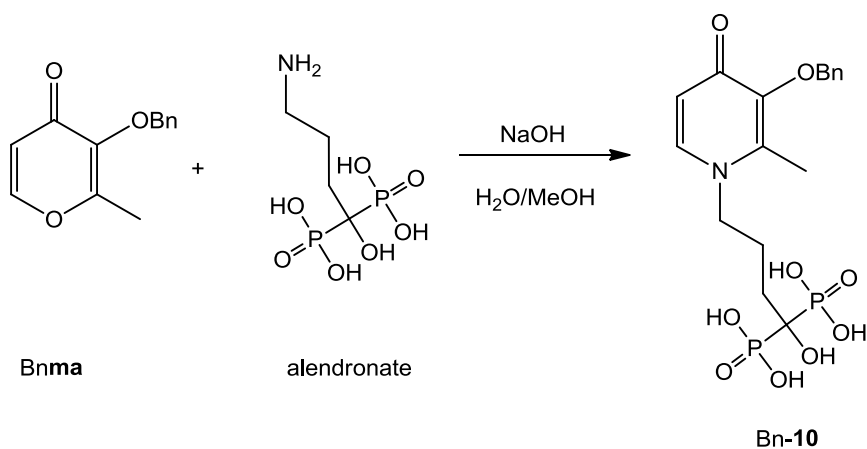
Figure 2.21. Synthesis of a 3-benzyloxy-4-pyridinone with a hydroxy-bisphosphonate functional group from the base-catalyzed ammonolysis of an amino hydroxy-bisphosphonate with benzyl protected maltol.

2.3.6 Synthesis of Phosphorylated 3-Hydroxy-4-pyridinones

The syntheses of phosphorylated 3-hydroxy-4-pyridinones were accessed by phosphorylation of the benzyl-protected hydroxyl pyridinones (Bn**1**, Bn**2**, Bn**3**, Bn**4** and Bn**6**). The general procedure (Scheme 2.2) involved phosphorylation of the hydroxyl group with POCl$_3$ which produced a phosphorodichloridate intermediate in the presence of trimethylphosphate (Scheme 2.2a). The unreacted POCl$_3$, along with the phosphorodichloridate were then hydrolyzed with the addition of ice to produce the dihydrogen phosphate (Scheme 2.2b). The reaction was worked up by washing the reaction with dichloromethane to remove the trimethylphosphate.

For Bn**11**, the removal of trimethylphosphate was achieved by simply stirring the crude product in dichloromethane after which the product precipitated and was recovered by filtration and subsequent recrystallization from water. Thus, the first example of a phosphate produced by the phosphorylation of a primary hydroxyl group purified simply by recrystallization of the ligand has been reported.

104

Unfortunately, separation of **Bn12**, **Bn13**, **Bn14** and **Bn15** was not as trivial; the trimethylphosphate was removed by increasing the pH of the solution to approximately 12, and then washing with dichloromethane. The high pH ensured that the phosphate was ionized, which increased its aqueous solubility resulting in a better partition of the product in the aqueous layer and the trimethylphosphate in the organic layer. However, under basic conditions trimethylphosphate is known to be a methylating agent for nitrogen-containing heterocyclic compounds;[142] thus, this workup was performed in a timely manner to prevent the methylation of the product.
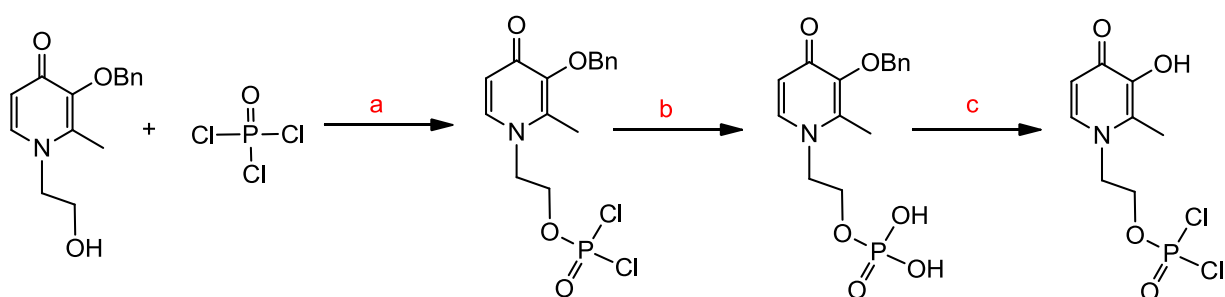
Scheme 2.2. Synthesis of the dihydrogenphosphate functionalized 3-hydroxy-4-pyridinone, H**11**; a) trimethylphosphate, 0 °C, 4 h; b) H$_2$O, 0 °C, 10 min; c) HBr in acetic acid 33% w/v or H$_{2(g)}$, 10% P/C.

After washing with dichloromethane, the crude mixture was immediately neutralized with the addition of HCl. Trace amounts of trimethylphosphate, along with other side products, were still found to remain in the crude mixture as monitored by ^{1}H{^{31}P} and ^{31}P{^{1}H} NMR spectroscopy, as well as TLC (7:2:1 2-propanol:water:ammonia).[143] As a result, separation of **Bn12**, **Bn13**, **Bn14** and **Bn15** was achieved either by normal-phase silica gel chromatography or by reverse-phase C18 chromatography. As trimethylphosphate was notoriously difficult to remove, the reaction was attempted in anhydrous pyridine[139] and acetonitrile;[144] however, limited solubility of both the product and the starting material prevented the use of either solvent.

Finally, the benzyl ether (Scheme 2.2c) was removed either by the use of hydrobromic acid in glacial acetic acid or the hydrogenation of the benzyl group in the presence of $H_2(g)$ with a catalytic amount of Pd on C.

^{31}P and ^1H NMR spectra helped confirm product formation. In the $^{31}P\{^1H\}$ NMR spectrum the appearance of a single resonance between 0–3 ppm confirmed the phosphorylation of the pyridinone. The inclusion of a phosphate on the pyridinone did not, however, result in any new peaks in $^1H\{^{31}P\}$ NMR spectra, as seen in Figure 2.22 or in the $^{13}C\{^1H\}$NMR spectrum. It did, however, result in downfield shifts of the resonances, especially with the hydrogens closest to the hydroxyl or phosphate peaks (Figure 2.22). The largest downfield shift is assigned to the multiplet found in the 3.7–3.9 ppm region, attributed to the CH_2-O-hydrogens. A summary of the ^1H NMR spectroscopic shifts, compared to those of the free hydroxy functionalized ligand are reported in the Appendix (Table A.1). The five novel 3-hydroxy-pyridinones with a phosphate were characterized by ^1H, $^{13}C\{^1H\}$ and $^{31}P\{^1H\}$ NMR spectroscopy and HRMS ESI, with the exception of **H11** which was characterized by elemental analysis (EA).
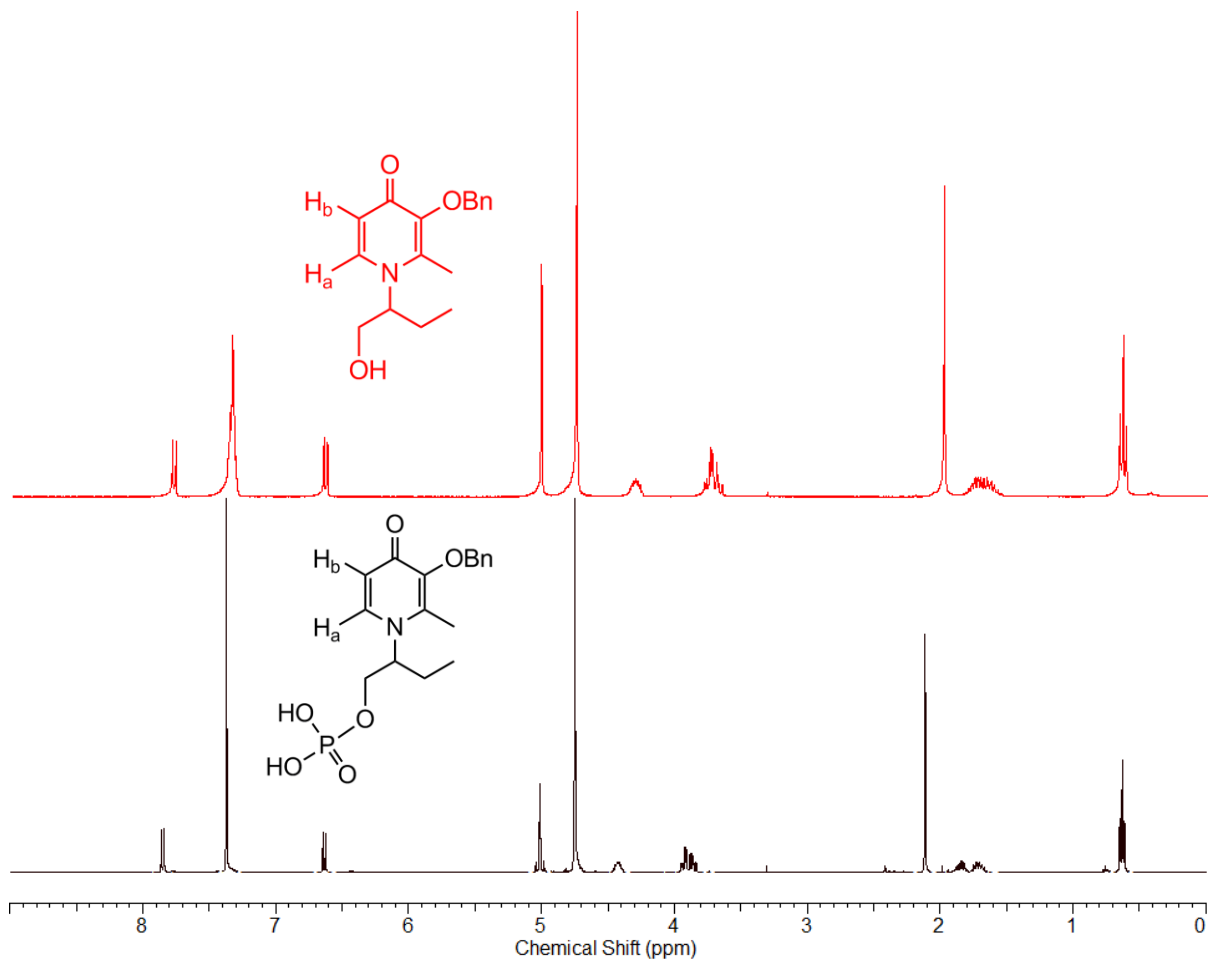
Figure 2.22. ^{1}H NMR (300 MHz, D$_2$O, RT) spectra of Bn**6** (top) and Bn**15** (bottom).

2.3.7   Synthesis and Characterization of *Tris*(pyridinonato)lanthanide(III) Complexes

All lanthanide pyridinone complexes were synthesized by the deprotonation of the 3-hydroxy of the pyridinone with sodium hydroxide in the presence a lanthanide (III) nitrate hexahydrate salt. All the complexes were synthesized in water, with the exception of La(**5**)$_3$; due to the limited solubility of H**5** in water, La(**5**)$_3$ was synthesized in methanol. The ligands, H**1** and H**8**, were not soluble in water at room temperature, thus they were dissolved by the

addition of NaOH; the pH was monitored to it was not above 4 to prevent hydrolysis of the metal ion. Once the ligand was dissolved, the desired lanthanide salt was added to the solution, and the pH was carefully adjusted to 9.5–10.5. The resulting complexes were soluble in water; the complexes were isolated by precipitation with the addition of acetone and were recovered by centrifugation.

The ligands H**1**, H**2**, H**3**, H**4**, H**5**, H**6**, H**8** and H**9** were all successfully coordinated to a lanthanide ion. Complexation of the ligands were attempted with La^{3+}, Eu^{3+}, and Lu^{3+} and in most cases Gd^{3+}, with the exception of H**5** in which only the lanthanum complex was synthesized. The attempted syntheses of La(**10**)$_3$ and La(**11**)$_3$ failed; upon complexation with either the phosphonate or phosphate containing ligand to the lanthanum ion, a highly insoluble product formed. It is well known that phosphates and phosphonates can bind metal ions, such as lanthanides.[145] Likely, a polymeric mixture of lanthanide-bound phosphate or phosphonate and lanthanide-bound 3-oxy-4-pyridinone was synthesized, making separation impossible.

The ^{1}H NMR spectra of the lanthanum and lutetium complexes were useful in elucidating the structure of the metal complexes. A summary of the ^{1}H NMR spectra for the lanthanum complexes compared to the free ligands can be seen in Table 2.2, while sample ^{1}H NMR spectra of H**1**, La(**1**)$_3$ and Lu(**1**)$_3$ can be seen in Figure 2.23.

Table 2.2. A comparison of ^{1}H NMR spectral shifts for HL and La(L)$_3$.
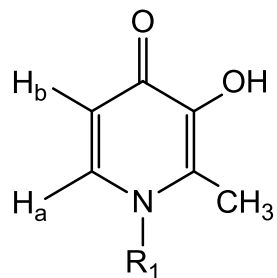
Compound	Solvent	H_a	H_b	Ring CH$_3$	N-CH_2 or N-CH	N-CH$_2$-CH_2	CH_2-CH$_2$-OH	CH_2-OH or CH-OH	alkyl-CH_3	CH-CH$_2$ or CH-CH
H1	D$_2$O	7.62	6.49	2.40	3.85	-	-	4.20		
La(**1**)$_3$	D$_2$O	7.29	6.32	2.21	3.79			4.11		
H2·HCl	D$_2$O	8.02	7.07	2.58	4.40	2.05	-	3.63		
La(**2**)$_3$	D$_2$O	7.31	6.31	2.24	4.06	1.74 - 2.04		3.55		
H3·HCl	D$_2$O	8.00	7.05	2.55	4.31	1.48 - 1.62	1.76 - 1.91	3.57		
La(**3**)$_3$	D$_2$O	7.25	6.28	2.18	3.96	1.49	1.69	3.53		
H4	CD$_3$OD	7.59	6.39	2.45	3.96 - 4.05; 3.83 - 3.91			4.10	1.24	
La(**4**)$_3$	CD$_3$OD	7.18	6.35	2.30	3.96			3.80	1.16	
H5	CD$_3$OD	7.78	6.49	2.46	4.03 - 4.19			3.78 - 4.03	1.06 - 1.19; 0.76	2.11 - 2.30
La(**5**)$_3$	CD$_3$OD	7.49	6.64	2.41	4.08			3.86	1.08; 0.66	2.16

Compound	Solvent	H_a	H_b	Ring CH_3	N-CH_2 or N-CH	N-CH$_2$-CH_2	CH_2-CH$_2$-OH	CH_2-OH or CH-OH	alkyl-CH_3	CH-CH$_2$ or CH-CH
H6	CD$_3$OD	7.73	6.49	2.48	4.36 - 4.48			3.70 - 3.87	0.86	1.71 - 1.99
La(6)$_3$	CD$_3$OD	7.34	6.46	2.37	*4.37*			3.73	0.79	1.58 – 1.97
H8	D$_2$O	7.89	7.00	2.43	4.87	-	-	-		
Na$_3$[La(8)$_3$]	D$_2$O	7.24	6.36	2.12	4.53					
H9	0.1M NaOD	7.27	6.30	2.32	4.20	2.56				
Na$_3$[La(9)$_3$]	D$_2$O	7.31	6.29	2.22	4.18	2.53				
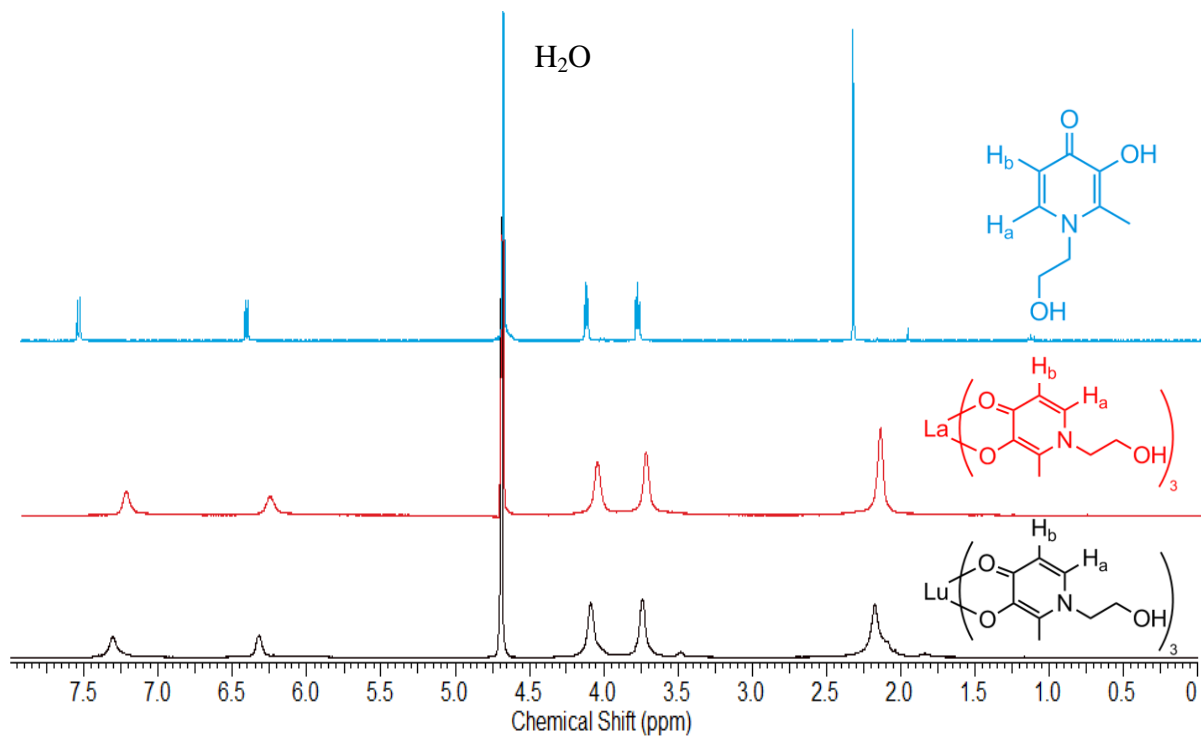
Figure 2.23. ^{1}H NMR (400 MHz, D$_2$O, RT) spectra of H**1** (top), La(**1**)$_3$ (middle) and Lu(**1**)$_3$ (bottom).

As seen in both Figure 2.23 and Table 2.2 the resonances for the ring hydrogens, H_a and H_b in the pyridinone metal complexes are shifted upfield compared to those of the free ligands. Similar upfield shifts have been previously reported in our lab.[71] Generally, larger upfield shifts were observed for H_a over H_b as can be seen in Figure 2.23. While for the alkyl hydrogens, as they are further away from the metal ion, only slight upfield shifts were observed. In the ^{1}H NMR spectra of the metal complexes, broad peaks were observed – this is attributed to the coordination of water in the coordination sphere, and to rapidly interconverting Δ and Λ stereoisomers and geometric *fac* and *mer* isomers at RT.[146] The ^{1}H NMR spectra of La(**4**)$_3$, La(**5**)$_3$ and Ln(**6**)$_3$ displayed broader spectral peaks than observed for the other Ln^{3+} complexes; this is attributed to the racemic mixture of *R* and *S* isomers of the ligands. As a result, a mixture of *R,R,R*-Ln(**L**)$_3$, *S,S,S*-Ln(**L**)$_3$, *R,R,S*-Ln(**L**)$_3$, *R,S,S*-Ln(**L**)$_3$ as

111

well as both the Δ and Λ stereoisomers and geometric *fac* and *mer* orientations can be produced, leading to broadening and averaging of the ^{1}H NMR environments.
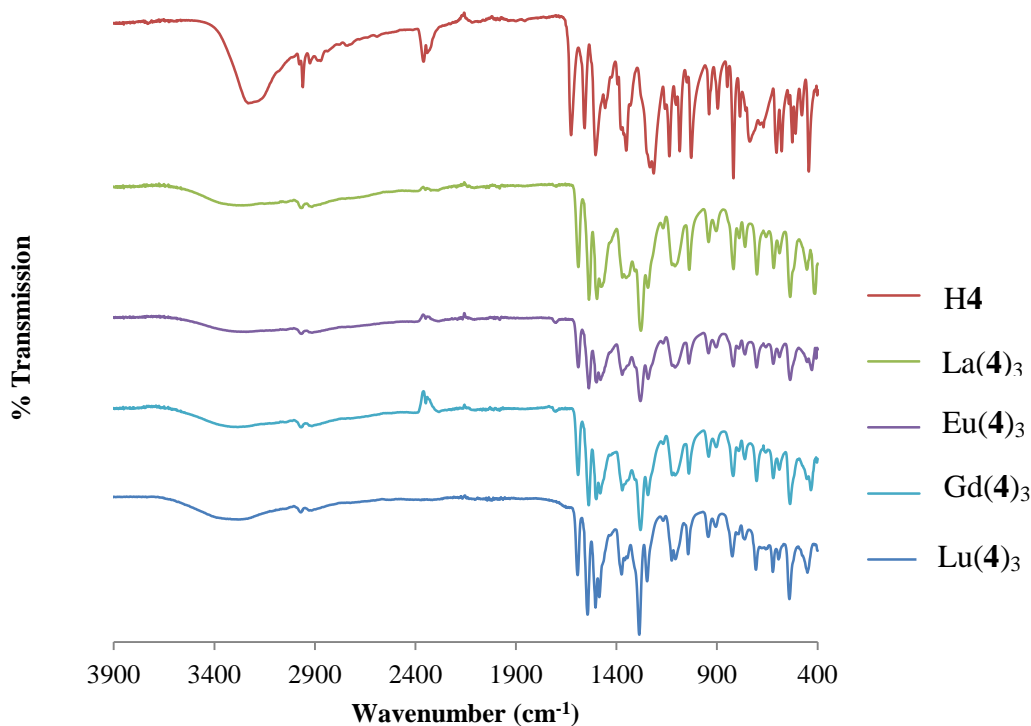
Figure 2.24. Solid state IR spectra for, top to bottom: H**4**, La(**4**)$_3$, Eu(**4**)$_3$, Gd(**4**)$_3$ and Lu(**4**)$_3$; the spectra are offset for clarity.

The IR spectra of all of the complexes were also helpful in confirming the formation of the complexes. Table 2.3 gives a summary of the IR stretching frequencies of both the free ligands and the metal complexes, while IR spectra for H**4** and the Ln(**4**)$_3$ complexes can be seen in Figure 2.24. A characteristic four-band IR spectral pattern is observable at 1650-1460 cm^{-1} in the free ligands that can be attributed to the pyridinone ring and C=O stretching frequencies.[147,148] Due to strong coupling, the ν_{ring} and $\nu_{C=O}$ stretching modes are indistinguishable from one another; thus the bands are collectively assigned to ν_{ring} and $\nu_{C=O}$ in Table 2.3.

Table 2.3. Selected IR stretching frequencies of the free ligands and their lanthanide complexes.

Compound	ν_{OH}	ν_{C-H} (CH$_3$ or CH$_2$)		$\nu_{C=O}$ or ν_{ring}				ν_{C-O}	ν_{C-N}	ν_{M-O}		
H1	3292	2938	2923	1620	1562	1558	1495	1336	1223			
La(1)$_3$	~3200	2916	2874	1593	1538	1498	1478	1341	1282	526	460	424
Eu(1)$_3$	~3200	2916	2873	1590	1537	1497	1477	1341	1279	523	457	430
Lu(1)$_3$	~3200	2929	2879	1594	1543	1504	1486	1341	1283	533	458	-
H2	3247	2956	2931	1640	1583w	1529	1506	1329	1235			
La(2)$_3$	~3200	2915	2877	1588	1537	1496	1463	1339	1279	522	460	424
Eu(2)$_3$	~3200	2929	2874	1592	1539	1497	1464	1337	1279	531	458	434
Lu(2)$_3$	~3200	2929	2879	1594	1543	1530	1470	1339	1283	534	459	-
H3	3301	2964	2933	1637	1586w	1531	1509	1333	1235			
La(3)$_3$	~3200	2929	2854	1590	1537	1497	1464	1338	1277	528	471	422
Eu(3)$_3$	~3200	2930	2868	1592	1538	1497	1467	1338	1278	525	478	428
Lu(3)$_3$	~3200	2930	2866	1593	1538	1502	1470	1339	1285	532	471	452
H4	3232	2960	2925	1625	1558	1504	1456	1351	1233			
La(4)$_3$	~3200	2968	2916	1590	1537	1497	1476	1352	1279	536	453	413
Eu(4)$_3$	~3200	2968	2914	1590	1538	1499	1480	1372	1281	536	452	428
Gd(4)$_3$	~3200	2969	2916	1592	1540	1501	-	1339	1281	538	452	433
Lu(4)$_3$	~3200	2970	2917	1593	1544	1504	1486	1374	1287	540	450	-

Compound	ν_{OH}	ν_{C-H} (CH$_3$ or CH$_2$)			$\nu_{C=O}$ or ν_{ring}				ν_{C-O}	ν_{C-N}	ν_{M-O}		
H**5**	3117	2966	2948		1624	1570	1527w	1504	1339	1234			
La(**5**)$_3$	3306	2963	2874		1591	1538	1495	1463	1337	1274	528	464	423
H**6**	3085	2964	2930	2875	1625	1570	1527w	1504	1358	1274			
La(**6**)$_3$	~3200	2965	2931	2876	1590	1537	1495	1463	1358	1274	524	495	417
Eu(**6**)$_3$	~3200	2964	2930	2876	1592	1540	1496	1464	1340	1258	528	496	438
Gd(**6**)$_3$	~3200	2964	2930	2876	1592	1541	1496	1464	1340	1258	529	497	438
Lu(**6**)$_3$	~3200	2966	2932	2877	1595	1546	1501	1475	1342	1279	537	497	446
H**8**	~3200	3067	2950		1657	1634	1553	1464	1385	1256			
La(**8**)$_3$	~3200		-		1597	1538	1498	1476	1359	1281	540	437	419
Eu(**8**)$_3$	~3200		-		1598	1539	1499	1480	1361	1283	539	435	421
Gd(**8**)$_3$	~3200		-		1597	1540	1499	1480	1361	1283	538	439	427
Lu(**8**)$_3$	~3200		-		1600	1546	1504	1482	1363	1286	540	456	428
H**9**	~3200	3091	3041		1681	1634	1567	1519	1354	1238			
La(**9**)$_3$	~3200		-		1583	1537	1497		1341	1278	512	479	422
Eu(**9**)$_3$	~3200		-		1587	1539	1497		1344	1280	524	480	429
Gd(**9**)$_3$	~3200		-		1584	1538	1498		1346	1280	524	480	430
Lu(**9**)$_3$	~3200		-		1591	1544	1504		1348	1285	529	485	450

w = weak

114

The metal complex spectra were dominated by peaks corresponding to the ligand (Figure 2.24 and Table 2.3). Upon complexation, the characteristic four-band IR spectral pattern is preserved with a bathochromic shift around 30–50 cm^{-1} and a possible reordering upon formation of the *tris*(3-oxy-4-pyridinonato)lanthanide complexes. When coordinated to a lanthanide ion the v_{O-H} stretch at around 3300–3000 cm^{-1} observed in the free ligand, is replaced by a broad peak due to the coordination of waters in the lattice of the metal complex. The most distinctive characteristic upon complexation of a lanthanide ion is the appearance of new peaks between 400–550 cm^{-1} assigned to the formation of metal-oxygen (v_{M-O}) stretching frequencies.[149]

In the infrared spectra of **H8** and **H9**, very broad bands are observed around 3200 cm^{-1}, attributed to the strong intermolecular hydrogen bonding of the carboxyl groups.[123] There is also an obstruction of the characteristic four-band pattern of v_{ring} and $v_{C=O}$ stretching frequencies observed in 3-hydrody-4-pyridinones due to delocalization of the double bond character as a consequence of the zwitterionic nature of the ligands. As a result two wide bands were observed, and both assigned to a mixture of the pyridinone ring stretching frequencies as well as to the carboxylate anion.

Lastly, the IR spectra for the La^{3+}, Eu^{3+}, Gd^{3+} and Lu^{3+} complexes were all nearly superimposable within each ligand set, indicating that the metal complexes are isostructural. The <10 cm^{-1} variation observed between the different metals is attributed to the size difference between the lanthanide ions. The greatest difference is observed between the lanthanum and lutetium complexes, while the smallest differences are observed between europium and gadolinium.

Product formation of the lanthanide ion complexes was confirmed by low resolution and high resolution mass spectrometry, ^{1}H NMR (for La and Lu only) and ^{13}C{^{1}H} NMR (for La only) with the exception of La(**4**)$_3$, the sample was not concentrated enough for analysis by ^{13}C NMR) spectroscopy. Samples were also analyzed by FTIR, and representative complexes

were characterized by elemental analysis (EA). A summary of the isotopic distributions observed in the ESI-MS spectra can be found in the Appendix (Table A.2).

2.3.8 Synthesis of a Hexadentate Phosphinate-EDTA Derivative Coordinated to Lanthanides

Lanthanide ions were coordinated to H$_5$**XT** as previously reported by our laboratory.[127] K$_2$[Ln(**XT**)] was synthesized as the phosphinate functionality of the ligand could potentially help the complex localize towards bone, much like ^{153}Sm^{3+}-**EDTMP**,[65,66] discussed in Chapter 1.4. Likewise, it was also synthesized so as to compare one hexadentate ligand to that of the bidentate 3-hydroxy-4-pyridinones coordinated to the lanthanide ions.

2.3.9 Determination of Stability Constants of 3-Hydroxy-4-pyridinones with Lanthanide Ions

The determination of the stability constants allows for the prediction of the thermodynamic stability of complexes *in vitro* and *in vivo* at physiologically relevant pHs. The two stepwise acid dissociation constants (pK$_{an}$) for H**L1** and H**4** (pK$_{a1}$ and pK$_{a2}$) and the three stepwise acid dissociation constants for H**9** (pK$_{a1}$, pK$_{a2}$ and pK$_{a3}$), shown in Figure 2.25, were determined for the amphoteric 3-hydroxy-4-pyridinones and are reported in Table 2.4.

The acid dissociation constants calculated for H**L1** agree quite well with those reported previously in the literature.[150-152] Likewise, the pK$_{a2}$ of H**L1** and H**4** and the pK$_{a3}$ of H**9** are similar as seen in Table 2.4, indicating that the R group does not significantly alter the ionizability of the 3-hydroxyl group.[119] It also indicates that the deprotonated carboxyethyl group of H**9** does not significantly affect the electron density of the pyridinone ring.

In Table 2.5, the stability constants (log K_n) of H**L1** with La^{3+} and Gd^{3+} are reported. Not surprisingly, the binding constant of the ligand with Gd^{3+} is higher than that of La^{3+}. This can easily be explained by the larger ionic radius of La^{3+} (103.2 pm, CN = 6)[60] versus that of Gd^{3+} (93.8 pm, CN = 6).[60] While the 3-hydroxy-4-pyridinones are known to form stable *tris*-ligand complexes with other trivalent cations such as Ga^{3+},[150] In^{3+} [150] and Fe^{3+},[151,152] the larger coordination sphere of the lanthanides, and their preferred coordination geometry of 8 or 9,[57] suggests the possibility of the formation of 4:1 complexes for H**L1** with Ln^{3+} ions. As a result, excess of ligand was titrated in the presence of the lanthanides to achieve a 4:1 ligand to metal ratio but no evidence of a 4:1 complex was observed with either La^{3+} or Gd^{3+} ions. The binding constants of *tris*-ligand complexes with H**L1** were quite high with a log β_3 = 17.46 and 20.07 for La(**L1**)$_3$ and Gd(**L1**)$_3$ respectively.

Table 2.4. Acid dissociation constants (pK$_{a1}$, pK$_{a2}$, pK$_{a3}$) for the 3-hydroxy-4-pyridinone ligands H**L1**, H**4** and H**9** at 25 °C and 0.16 M NaCl. Numbers in parentheses represent SD between replicates.

Constant	HL1	H4	H9
pK$_{a1}$	3.63(1)	3.11(3)	2.86(5)
pK$_{a2}$	9.71(1)	9.58(2)	3.99(4)
pK$_{a3}$			9.64(3)

where pK$_{an}$ = -log[K$_{an}$] n = 1,2,3

$$R = CH_3, \; H\textbf{L1}; \quad R = CH_2CH(OH)CH_3, \; H\textbf{4}$$

$$H_2\textbf{L}^+ \rightleftharpoons H^+ + H\textbf{L} \qquad K_{a1} = \frac{[H^+][H\textbf{L}]}{[H_2\textbf{L}^+]} \tag{2.1}$$

$$H\textbf{L} \rightleftharpoons H^+ + \textbf{L}^- \qquad K_{a2} = \frac{[H^+][\textbf{L}^-]}{[H\textbf{L}]} \tag{2.2}$$

$$H_3\textbf{L}^+ \rightleftharpoons H^+ + H_2\textbf{L} \qquad K_{a1} = \frac{[H^+][H_2\textbf{L}]}{[H_3\textbf{L}^+]} \tag{2.3}$$

$$H_2\textbf{L} \rightleftharpoons H^+ + H\textbf{L}^- \qquad K_{a2} = \frac{[H^+][H\textbf{L}^-]}{[H_2\textbf{L}]} \tag{2.4}$$

$$H\textbf{L}^- \rightleftharpoons H^+ + \textbf{L}^{2-} \qquad K_{a3} = \frac{[H^+][\textbf{L}^{2-}]}{[H\textbf{L}^-]} \tag{2.5}$$
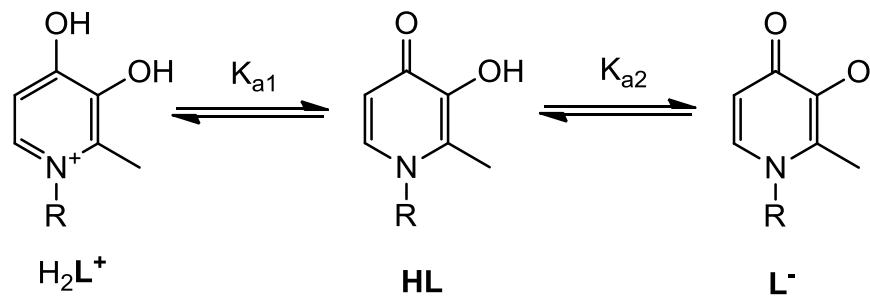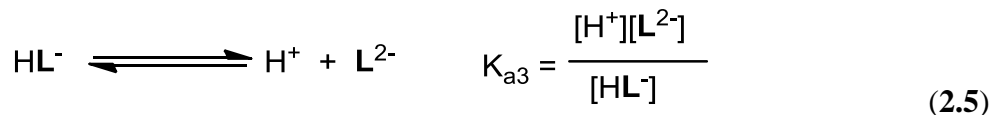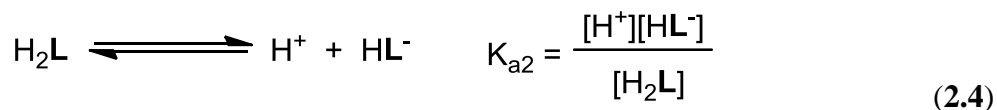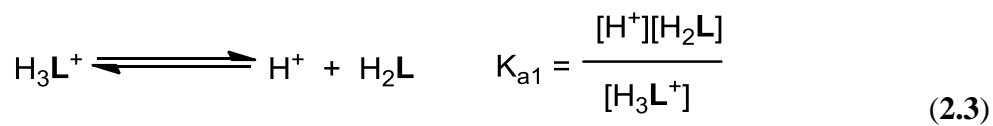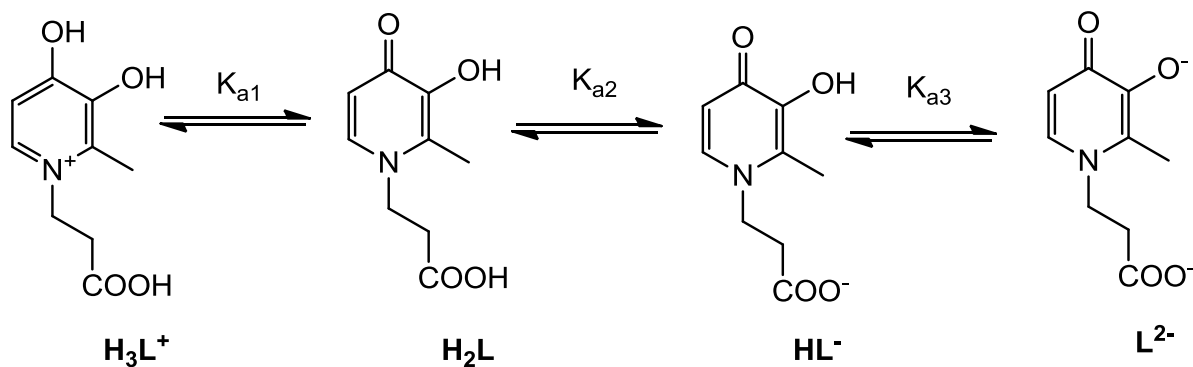
Figure 2.25. The stepwise acid dissociation equilibria of the 3-hydroxy-4-pyridinones.

It is well known that lanthanide ions can exchange for calcium in proteins.[61] One such protein, trypsin, is found to bind lanthanides quite effectively.[153] The log K_n values calculated for porcine trypsin with La^{3+} and Gd^{3+} were determined to be 2.25 and 2.53, respectively.[153] As seen in Table 2.5, log β_1 for the 1:1 ligand to metal is significantly higher with H**L1** than trypsin. Thus, there is not a significant worry of potential transchelation of Gd^{3+} or La^{3+} with trypsin *in vivo*.

$$\beta_n = \frac{[\mathbf{ML}_n^{(3-n)+}]}{[M^{3+}][\mathbf{L}^-]^n} \tag{2.6}$$

$$K_4 = \frac{[\mathbf{ML}_3(OH)^-]}{[\mathbf{ML}_3][OH^-]} \tag{2.7}$$

Table 2.5. Log metal-ligand stability constants (β_n) and the $\mathbf{ML}_3OH$ stability constant (log K_4) at 25 °C and 0.16 M NaCl. Numbers in parentheses represent SD between replicates.

Constant	Equation	La^{3+}	Gd^{3+}
log β_1	$M^{3+} + L^- \rightleftharpoons ML^{2+}$	7.06(5)	8.15(4)
log β_2	$M^{3+} + 2L^- \rightleftharpoons ML_2^+$	12.6(1)	14.60(6)
log β_3	$M^{3+} + 3L^- \rightleftharpoons ML_3$	17.5(1)	20.07(9)
log K_4	$ML_3 + OH^- \rightleftharpoons ML_3(OH)^-$	7.94(6)	9.1(1)

Determination of the stability constants of Lu^{3+} with H**L1** was attempted; however, near pH 4 precipitation occurred in the presence of the ligand. Potentiometric UV studies with lower concentrations of metal and ligand may circumvent this problem and may be a solution to determine the binding constants for H**L1** with Lu^{3+}. As Lu^{3+} (86.1 pm, CN = 6)[60] has a smaller ionic radius that Gd^{3+} or La^{3+} it would be expected that the binding constants are larger for Lu^{3+}. Speciation plots for Gd^{3+} and La^{3+} can be found in the Appendix (Figure A.1), reported for concentrations of 1 mM of Ln^{3+} and 3 mM of H**L1**.

2.4   *Conclusions*

A library of ten novel 3-hydroxy-4-pyridinones was successfully synthesized, with varying functional groups and lipophilicities. The straightforward ammonolysis reaction allows for easy access to a variety of pyridinones from the pyrone with the desired functionalized primary amine. Using this synthetic route the first bisphosphonate functionalized 3-hydroxy-4-pyridinone was synthesized; likewise, phosphorylation of a primary alcohol-containing 3-hydroxy-4-pyridinone allowed for the first reported phosphate functionalized 3-hydroxy-4-pyridinones. The carboxylate and alkyl hydroxyl containing pyridinones were then coordinated to La^{3+}, Eu^{3+}, Gd^{3+} or Lu^{3+} ions, producing stable *tris*-ligand complexes.

Lastly, the acid dissociation constants and metal-ligand stability constants with La^{3+} and Gd^{3+} were determined by potentiometric titrations of the 3-hydroxy-4-pyridinones. It was concluded that varying the R group does not significantly alter the pK_a of the 3-hydroxy proton, and the stability constants of 3-hydrody-4-pyridinones, which are larger for Gd^{3+} than for La^{3+}, are likely due to size differences in their ionic radii.

Chapter 3. *In Vitro* Studies of Uncompolexed Ligands and Their Lanthanide Complexes

3.1   Introduction

For decades it has been known that lanthanide ions have a high affinity for bone,[72] and it has been demonstrated that they can have an inhibitory effect on osteoclasts[154] (the cells responsible for bone resorption) and a proliferative effect on osteoblasts[155] (the cells responsible for bone formation). Consequently, they may be of use in the treatment of bone density disorders; however, in order for these ions to have efficacy in the treatment of such disorders, they must be delivered to bone. A library of 3-hydroxy-4-pyridinones and one phosphinate-EDTA ligand have been synthesized (see Chapter 2) and complexed to lanthanide ions (Ln = La, Eu, Gd, Lu) under the principle of producing an orally active anti-osteoporotic agent that can pass through the gastrointestinal (GI) tract and effectively deliver lanthanides to bone.

The next step is to establish, *in vitro*, their efficacy in crossing the gastrointestinal tract as well as their cytotoxicity profiles. The toxicity of these compounds is evaluated in two different cell lines, Caco-2 and MG-63 cells. The ability of these complexes to cross the GI tract is analyzed by determining the octanol-water partition coefficients ($P_{o/w}$) of the free ligands, as well as the cellular uptake and apparent permeability of the lanthanide complexes in Caco-2 cells.

Toxicities of the ligands and metal complexes are analyzed by a MTT (3-(4,5-dimethylthiazol-2-yl)-2,5-diphenyltetrazolium bromide)[156] or MTS (3-(4,5-dimethylthiazol-2-yl)-5-(3-carboxymethoxyphenyl)-2-(4-sulfophenyl)-2H-tetrazolium)[157] assay, where the mitochondrial activity of living cells is used to analyze their viability. MG-63 cells are an osteosarcoma cell line that mimic osteoblasts;[158] toxicities are evaluated in these cells to

ensure that these compounds do not have detrimental effects on bone formation. The toxicities of the metal complexes are also evaluated in Caco-2 cells.

The ability of orally administered drugs to be absorbed is principally determined by their capacity to cross the GI tract.[159] It is widely accepted that the absorption, distribution, metabolism and excretion of a drug candidate relies heavily on the lipophilicity of the compound, amongst other properties such as molecular weight and hydrogen bond donor and acceptor capabilities.[160,161] The partition coefficient (P) is often used as a measure of lipophilicity and describes the differentiation of a neutral compound in two immiscible solvents; 1-octanol and water are typically used.[162]

Paired with the partition coefficient studies are uptake studies in Caco-2 Cells; Caco-2 cell monolayers morphologically resemble small-intestine absorptive cells, expressing many of the properties of this organ.[163] These cells are often used to evaluate the *in vitro* oral absorption of drug candidates across the GI tract; the absorption of compounds across this cell line correlates well with *in vivo* absorption in mammals.[164]

3.2   *Experimental*

3.2.1   Materials

Water was purified using an Elgastat Maxima HPLC reverse osmosis and deionization system or a PureLab Ultra system (Elga, Bucks, England). All water used was type 1, 18.2 MΩ-cm, purified by a full spectrum UV to control bacterial levels. All ligands and metal complexes discussed in this chapter were synthesized according to the procedures outlined in Chapter 2 of this thesis.

For the inductively coupled mass spectrometry (ICP-MS) studies the lanthanum standard (1000 µg/mL in 2% HNO_3) was purchased from High Purity Standards (North Charleston, SC, U.S.). Optima nitric acid (a high purity acid containing the least metal content of any commercially available acid, typically used for trace metal analysis), centrifuge tubes (15 mL) and test tubes (16 × 150 mm) were purchased from Fisher Scientific.

For the MG-63 studies, cells were obtained from American Type Culture Collection (ATCC, Rockville, MD, U.S.). Media for the cells, minimum essential media alpha (MEM-α), fetal bovine serum (FBS), 0.25% trypsin-EDTA, penicillin-streptomycin-neomycin 100X (Pen-Strep) and phosphate buffer saline solution (PBS) were purchased from Life Technologies (Burlington, Ontario, Canada). T-75 culture flasks and 96-well plates were purchased from Corning-Costar (Cambridge, MA, U.S.A). Sterile 15 mL and 50 mL centrifuge tubes were purchased from Fisher Scientific. Barrier pipette tips were purchased from Diamed (Mississauga, Ontario, Canada). 3-(4,5-Dimethylthiazol-2-yl)-2,5-diphenyltetrazolium bromide (MTT) was purchased from Alfa Aesar and *cis*-diamminedichloroplatinum(II) (cisplatin) was obtained from Acros Organics. For the octanol-water partition coefficient studies 4-(2-hydroxyethyl)-1-piperazineethanesulfonic acid (HEPES) and 1-octanol were purchased from Sigma-Aldrich; sodium chloride was purchased from Fisher Scientific.

Caco-2 cells were also obtained from ATCC, and the cells were cultured in Dulbecco's modified Eagle's medium (DMEM), fetal bovine serum (FBS), bovine serum albumin (BSA) and Hank's balanced salt solution (HBSS) were purchased from Life Technologies (Burlington, Ontario, Canada). Culture flasks, transwell (12 well) and polycarbonate (12, 24 and 96 well) plates were purchased from Corning (Corning, NY, U.S.). MTS Cell Titer 96® Aqueous One Solution Cell Proliferation Assay and CytoTox96® Non-radioactive Cytotoxicity Assay were from Promega (Madison, WI, U.S.). Bicinchoninic acid assay (BCA) protein analysis kit was provided by Pierce (Rockford, IL, U.S.), while the lysis buffer, radioimmunoprecipitation assay (RIPA) was purchased from Sigma-Aldrich.

3.2.2 Instrumentation

Lanthanide concentration was analyzed on a Perkin Elmer Sciex Elan 6000 inductively coupled plasma mass spectrometer (ICP-MS). Ultraviolet-visible (UV-vis) spectrum measurements were taken on a Varian Vary 100 Bio UV-vis. A Savant vacuum concentrator Speedvac Plus, model SC110A, was used at the highest temperature setting of 60 °C to concentrate the samples prior to acid digestion for ICP-analysis.

The absorbances of the plates for the MTT studies were measured at room temperature at 595 nm using a Beckman Coulter DTX 800 Multimode Detector. For the BCA and MTS assays the absorbances were measured at room temperature on a Multiskan Ascent Multi-plate reader from Labsystems at wavelengths of 492 nm and 540 nm, respectively. The transepithelial electrical resistance (TEER) values were monitored using a Millipore Millicell-ERS (Bedford, MA, U.S.).

3.2.3 Cytotoxicity of Ligands and Metal Complexes in MG-63 Cells

MG-63 cells were obtained from Dr. Rizhi Wang, Materials Engineering, UBC, after their first passage. The cytotoxicity studies were performed in the UBC Chemistry Biological Services Facility. The medium used to culture the cells was minimum essential medium (MEM-α) supplemented with 10% fetal bovine serum (FBS) and 1% penicillin-streptomycin-neomycin 100X (Pen-Strep). The cells were incubated at 37 °C in a humidified atmosphere of 5% CO_2 and 95% O_2. Cells were cultured in T-75 cm^3 Corning tissue culture flasks.

Cells were revived from a frozen suspension containing 500,000 cells in 5% DMSO in medium (1 mL). Upon revival, the cell mixture was thawed to room temperature with 20 mL of medium and incubated at 37 °C in a humidified atmosphere of 5% CO_2 and 95% O_2 overnight. After 24 h, the medium was exchanged for 12 mL of fresh medium. After 96 h,

medium was exchanged for treatment with 5 mL of 0.5% trypsin-EDTA in order to lift up the cells. The cells were counted using a haemocytometer, and 1 million cells were divided and passaged into two different culture flasks and incubated with 12 mL of fresh medium. Medium was changed every third day and every 5-6 days the cells were subcultured by trypsination to either new culture flasks or flat bottom 96-well plates. Cells were either passaged to new culture flasks, where 500,000 cells were cultured in each flask and incubated with 12 mL of medium, or to 96-well plates, where 10,000 cells were plated per well in 100 µL of medium.

Toxicity of the ligand and metal complexes was determined using a modified MTT (2-(4,5-dimethylthiazol-2-yl)-2,5-diphenyltetrazolium bromide) assay.[156] MG-63 cells were seeded into 96-well plates at a density of 10,000 cells/well in 100 µL of medium. After 24 h of incubation, the medium was exchanged for solutions of either the free ligands or the lanthanide complexes, affording concentrations of 0.01, 0.1, 10, 50, 100, 200, 500 and 1000 µg/mL of compound dissolved in medium. To determine the toxicity of La($L1$)$_3$, due to its limited aqueous solubility, a 0.25% DMSO/medium solution was used to test the complex; also as a result of limited solution, the highest concentration of La($L1$)$_3$ tested was 600 µg/mL. As a positive control cisplatin (*cis*-diamminedichloroplatinum(II)) was incubated at concentrations of 1, 5, 10, 25, 50, 100, 250, 500 and 1000 µM in 0.25% DMSO/medium. As negative controls, 100% medium and 0.25% DMSO/medium were incubated with the cells. For each compound concentration, the assay was performed in triplicate.

After 48 h of treatment a 50 µL aliquot of MTT (2.5 mg/mL in PBS) was added to each well of the plate. The cells were incubated for 3 h with the MTT solution, allowing for the formation of formazan crystals at the bottom of the wells. The MTT/media/compound treatment was aspirated, leaving the formazan crystals, which were subsequently dissolved in 100 µL of DMSO. The absorbance of each well was measured at 595 nm using a Beckman Coulter DTX 800 Multimode Detector.

Cell viability was calculated relative to the negative control (representative of 100% cell viability). EC_{50}, fifty-percent inhibitory concentration, was calculated using Graphpad Prism^{TM} software. Absorbance readings were background corrected for DMSO absorbance and cell viability was calculated by normalizing the absorbance readings relative to the negative control (100% medium or 0.25% DMSO/media) to 100%. A plot of % cell viability versus the log of drug concentration in µM was plotted and fitted using non-linear regression analysis (sigmoidal dose-response with a variable slope). The EC_{50} value was determined by finding the concentration at which 50% of the cells were viable, relative to the negative control.

3.2.4 Determination of the Octanol-water Partition Coefficient ($P_{o/w}$)

The shake-flask method[165] was used to determine the octanol-water partition coefficients of the free ligands. Solutions of ligands (1 mM; H**1**, H**2**, H**3**, H**4**, H**6**, H**7**, H**8**, H**9**, H**10**, H**11** and H**16**) were dissolved in HEPES buffer (25 mM HEPES, pH 7.4, 0.16 M NaCl). Exactly 0.6 mL of the ligand solutions were placed in a 2 mL Eppendorf tube containing exactly 0.6 mL of 1-octanol. The samples were mixed using a vortex (VWR vortex mixer, speed 10) for 1 min, and inverted for 6 min. Phase separation was achieved by centrifugation of the samples at 6000 rotations per minute (RPM) for 1–2 minutes. The water layer was removed by partially filling a syringe with a detachable needle with air, gentle expulsion of the air while passing through the 1-octanol layer, and withdrawal of the aqueous layer; the syringe was then quickly removed from the mixture, the needle was removed from the syringe and the water layer was collected in a separate Eppendorf tube. The aqueous layer was diluted appropriately using HEPES buffer, and the organic layer was diluted using ethanol. The UV-vis spectrum of each of the solutions was measured, with λ_{max} between 278–281 nm indicating the absorbances of the free ligands. Utilizing Beer's law, the molar absorptivities ($cm^{-1}M^{-1}$) of the ligands in HEPES were determined. From this the concentration of ligand in each layer was calculated. Log $P_{o/w}$ was then calculated using equation 3.1.

$$\log P_{o/w} = \log \left(\frac{[\text{solute}]_{\text{octanol}}}{[\text{solute}]_{\text{water pH 7.4}}} \right)$$

<div align="right">(3.1)</div>

3.2.5 Caco-2 Cell Culture

Caco-2 cells were obtained from Dr. Kishor Wasan, Faculty of Pharmaceutical Sciences, UBC. MTS, cell uptake, bidirectional transport and BCA protein assays were performed there, ICP-MS sample preparation and digestion was completed in the UBC Chemistry Biological Services Facility, and metal ion analyses were performed in the UBC Chemistry Teaching Facilities.

Cells were cultured in complete Dulbecco's modified Eagle's medium (DMEM), supplemented with 10% fetal bovine solution (FBS), 292 µg/mL L-glutamine, 0.1 mM non-essential amino acids, 100 µg/mL penicillin and 100 µg/mL streptomycin in T-75 flasks, 12-well transwell, 12-well, 24-well or 96-well plates depending on the type of experiment. Cells were incubated at 37 °C in a humidified atmosphere of 5% CO_2 and 95% O_2 and the medium was refreshed every other day. Cells were used for studies once they reached 80% confluency. Protocols for the MTS assay, protein concentration analysis, cell uptake and bidirectional transport assays are described below.

Caco-2 Cell MTS Assay

Toxicities of the ligand and metal complexes were determined using a modified MTS (3-(4,5-dimethylthiazol-2-yl)-5-(3-carboxymethoxyphenyl)-2-(4-sulfophenyl)-2H-tetrazolium) assay.[157] Caco-2 cells were seeded onto 96-well plates at a density of 40,000 cells/cm^2 and the medium was refreshed every 48 h. When the cells reached 80% confluency, they were washed 3 times with Hanks balanced salt solution (HBSS) and the culture medium was

exchanged for treatment solutions up to 1000 µM for La($\mathbf{1}$)$_3$, La($\mathbf{2}$)$_3$, La($\mathbf{3}$)$_3$, La($\mathbf{4}$)$_3$, La($\mathbf{6}$)$_3$, Na$_3$[La($\mathbf{8}$)$_3$], Na$_3$[La($\mathbf{9}$)$_3$], K$_2$[La($\mathbf{XT}$)], 1% Triton X-100 (positive control) and media only (negative control). For each compound concentration, the assay was performed in triplicate. After the cells were incubated for 24 h with the lanthanide complexes, MTS (Cell Titer 96R Aqueous One Solution Cell Proliferation Assay Kit) was added to each well. The plate was wrapped in aluminium foil and incubated for 3–4 h at 37 °C in a humidified atmosphere of 5% CO_2 and 95% O_2, allowing for the formation of soluble formazan crystals. Absorbance was measured at room temperature at 492 nm with a Multiskan Ascent Multi-plate reader from Labsystems. Cell viability was calculated relative to the negative control (representative of 100% cell viability). The EC_{50} value was determined by finding the concentration at which 50% of the cells were viable, relative to the negative control.

Caco-2 Cell Protein Concentration Assay

After performing the cell uptake and bifunctional transport assays, cells were lysed (*vide infra*), and protein concentrations of the cell lysates cells were measured by a bicinchoninic acid protein assay (BCA Protein Assay Kit).[166] A bovine serum albumin (BSA) calibration curve was constructed in the range of 25 µg/mL to 2000 µg/mL; aliquots of exactly 20 or 25 µL of cell lysates were pipetted into a 96-well microtiter plate and 200 µL of reagent (mixture of BCA reagents A and B in a ratio of 50:1) was added to each well. Absorbance was measured after 1 h at room temperature at 540 nm with a Multiskan Ascent Multi-plate reader from Labsystems. Protein concentration of each sample was determined against the standard BCA curve. Each concentration was measured in triplicate, and the averaged value was used in further calculations.

Caco-2 Cell Uptake Studies

Caco-2 cells were seeded at 10,000 cells/cm^2 in 12 or 24-well plates and the medium was refreshed every other day until 80–90% confluency was reached. On the day of the experiment, the cells were washed 3 times with PBS and the culture medium was exchanged

for treatment solutions of La(2)$_3$, La(3)$_3$, La(6)$_3$, Na$_3$[La(8)$_3$], Na$_3$[La(9)$_3$], K$_2$[La(XT)]or medium (negative control) at concentrations up to 1000 µM. The cells were then incubated with the compounds for 24 h. Treatment solutions were aspirated and the cells were washed three times with PBS. After wrapping the plates in aluminium foil, they were stored at -20 °C until analysis. Cells were lysed with 250 µL of lysis buffer (RIPA); the cell lysate solutions from each well were transferred into separate 2 mL Eppendorf tubes. The wells were rinsed with another 250 µL of lysis buffer (RIPA); 60–75 µL from each sample was removed for protein analysis by a Pierce BCA assay to determine protein concentration. The remaining 425–440 µL were reserved later for La^{3+} analysis by ICP-MS. The concentrations are reported as % uptake of La^{3+} ion (µM)/mg of protein/well ± SD.

Caco-2 Cell Permeability Studies

Caco-2 cells were seeded at 5000 cells/cm^2 in polycarbonate membrane 12-well transwell plates. The medium was exchanged every other day and uptake studies were conducted when TEER readings reached 500 Ω/cm^2. Prior to the addition of the lanthanide compounds, the culture medium was removed, washed with PBS and replaced with fresh medium in the basolateral (bottom) chamber and fresh medium (negative control), or medium plus compound (treatment), with concentrations up to 1000 µM in the apical (top) chamber. After 24 h incubation, the integrity of the Caco-2 cell monolayers were monitored by measuring the TEER value; 0.3–0.4 mL of medium from the apical chamber and 1 mL from the basolateral chamber were retained for analysis of lanthanide ion content by ICP-MS. The cells were washed three times with PBS, and the polycarbonate membranes were removed, lysed in 250 µL of lysis buffer (RIPA) and transferred into a 2 mL Eppendorf tubes. The wells were rinsed with another 250 µL of lysis buffer (RIPA) and collected in the same Eppendorf tubes; 60–75 µL from each sample was removed for protein analysis by a Pierce BCA assay to determine the protein concentration. The remaining 425–400 µL were reserved for later La^{3+} analysis by ICP-MS. The concentration of Ln^{3+} accumulated in the cells, and the apical and basolateral chambers were evaluated by ICP-MS.

The apparent permeability (P_{app}, cm s^{-1}) coefficients from the bidirectional transport of the Ln^{3+} complexes were calculated using equation 3.2. $\Delta Q/\Delta t$ (nmol s^{-1}) was the flow rate for mass transport across monolayers, A was the surface area of the insert membrane (1.13 cm^2), and C_o was the initial concentration (μM) of the compound added in the apical chamber. The flow rate was calculated by plotting the rate (nmol) of compound increase as a function of time (s) in the donor (basolateral) chamber.

$$P_{app} = \frac{(\Delta Q/\Delta t)}{(A \bullet C_o)}$$

(3.2)

3.2.6 Lanthanum Ion Analysis by ICP-MS

All materials used for the acid digestion process were soaked in a 5% Extran bath overnight, rinsed with 18.2 MΩ-cm water, and washed in a 1% Opitma nitric acid bath overnight. Materials were then washed with 18.2 MΩ-cm water and left to dry in a dust free environment overnight. A lanthanide calibration curve for ICP-MS analysis was prepared by serial dilutions of the lanthanum standard (1000 μg/mL) in 1% Opitma nitric acid, and analyzed at concentrations ranging from 0.0001–10 ppm, where 1 part per million (ppm) is equivalent to 1 μg/mL. The count number was then plotted versus the concentration of the lanthanum ion in ppm. Concentration of lanthanide in each sample was then determined against the standard calibration curve.

Lanthanide ion concentration was analyzed by ICP-MS in the cell lysates for both the cell uptake and bidirectional transport assays and in the apical and basolateral solutions for the transport assays. Prior to analyses, all samples were vacuum centrifuged to complete dryness. The dried samples were acid digested as follows for ICP-MS analysis. The samples were dissolved in 2 mL of concentrated Optima nitric acid and transferred into test tubes (16 ×

150 mm) with 1–2 teflon boiling chips and placed in a block heater. The temperature was maintained at 105 °C overnight. The solutions were cooled to room temperature and 2 mL of 30% hydrogen peroxide was added to each sample which was reheated to 140 °C overnight. The temperature was increased to 150–160 °C until samples were evaporated to dryness. Samples were then dissolved in 3.00 mL of 10% Optima nitric acid in water (% v/v) and stored in 15 mL centrifuge tubes at 4 °C until analyzed for metal ion content.

3.3   Results and Discussion

3.3.1   Toxicity Assay in MG-63 Cells

MG-63 cells are derived from a human osteosarcoma[167] and were selected for cytotoxicity studies as they are considered to behave like osteoblasts.[158] This osteoblast-like cell line was selected because osteoblasts are often difficult to work with, requiring specialized equipment. For example hFOB 1.19 (ATCC) a cell line derived from human fetal osteoblasts requires an incubation temperature of 33.5 °C for the most rapid cell division.[168,169] Many biological laboratories, including the one where these studies were carried out, do not have incubators set up for this condition.

In order for these compounds to be considered for the treatment of bone density disorders, they must exhibit low toxicity profiles in MG-63 cells. Considering the vital role that osteoblasts play in the bone cycle (Figure 1.5) and in the maintenance of bone mass, it is essential that compounds used for the potential treatment of osteoporosis are not toxic to MG-63 cells.

In order to quantify the toxicity of these compounds, a colourimetric MTT assay was utilized.[156] The assay analyzes the mitochondrial activity of the cells by quantifying the amount of purple formazan crystals formed by the mitochondrial reduction of the yellow

tetrazolium (MTT) salt. The amount of purple reagent (formazan crystals) is directly proportional to the percent viability.[156] Cisplatin was used as a positive control to induce cell death, verifying the assay.
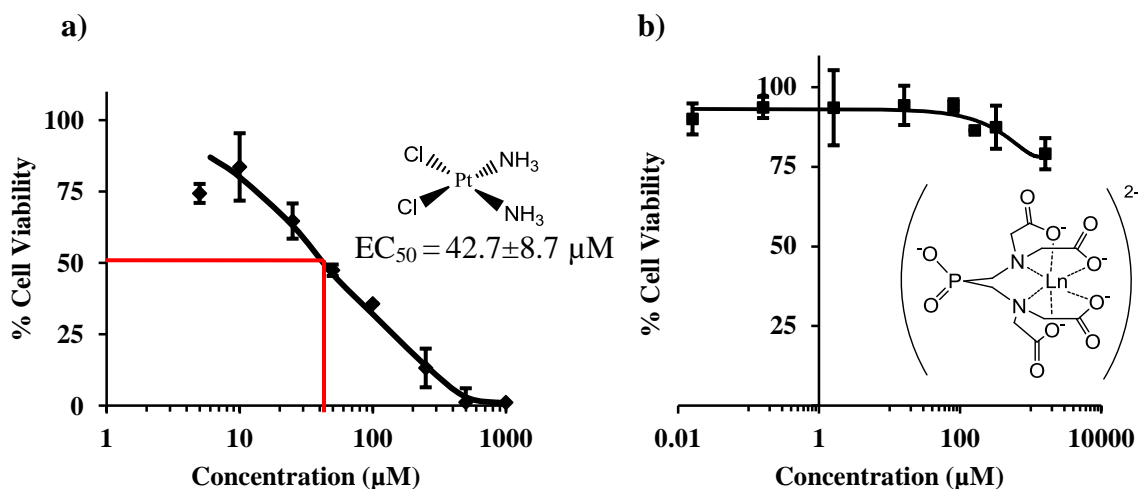
Figure 3.1. Sample survival plots of MG-63 cells exposed to varying concentrations of compound for 48 h, monitored by the MTT assay, n = 3, error bars indicate ± SD of the cell viability. The red line indicates the concentration at which 50% of the cells are no longer viable (EC$_{50}$); a) cisplatin (positive control), b) [La(**XT**)]$^{2-}$.

Cell viability was determined relative to the negative control, 100% cell medium, or 0.25% medium in DMSO. Generally, to compare the effect of drugs on a particular cell line, the half maximal effective concentration (EC$_{50}$) is utilized. While an EC$_{50}$ could be calculated for cisplatin (Figure 3.1a), confirming the assay was effective at determining toxicity, with the exception of La(**2**)$_3$, none of the synthesized ligands or lanthanide ion complexes tested demonstrated any significant toxicity with the cell line at the concentrations tested. Figure 3.1a shows the survival plot for the positive control, cisplatin. The cell viabilities were not low enough, as shown for [La(**XT**)]$^{2-}$ the survival plot for Figure 3.1b; as a result, an EC$_{50}$ could not be calculated for the compounds tested. Table 3.1 and Table 3.2 summarize the toxicities of the tested ligands and metal complexes in MG-63 cells, respectively.

132

The low toxicity profiles of the synthesized compounds makes them of interest for the treatment of osteoporosis. As a comparison, the cytotoxicity of alendronate, marketed under the tradename Fosrenol by Merck^{TM}, an approved bisphosphonate drug for the treatment of osteoporosis,[170] was also tested in MG-63 cells. The data suggests that alendronate, at concentrations $\leq$ 50 µM, is more cytotoxic than H**10**, H$_5$**XT**, [Lu(**XT**)]$^{2-}$, H**9** and [La(**9**)$_3$]$^{2-}$ (Figure 3.2). Additionally, the 3-hydroxy-4-pyridinone functionalized with a bisphosphonate, H**10**, demonstrated a lower toxicity profile than alendronate. Moreover, at lower concentrations ($\leq$ 1 µM) some of the compounds tested, including H**10**, suggest a potential proliferative effect, with cell viabilities > 100% (Figure 3.2). This thriving effect in MG-63 cells is not observed for alendronate. This indicates that H**10**, with its bisphosphonate functionality, known to localize on bone, could be a potential drug candidate for the treatment of osteoporosis on its own. Likewise, [Lu(**XT**)]$^{2-}$ demonstrated extremely low toxicity − even at concentrations as high as 500 µM, cell viability was found to be 93 ± 4%, while at a concentration ~1 µM, the cell viability observed was 113 ± 4%. It should be noted that only 3 replicates have been completed, and further trials need to be completed to assess if these compounds, within error, help proliferate the growth of MG-63 cells.

Table 3.1. Cytotoxicity data (MTT assay) for the free ligands in MG-63 cells, n = 3.

Compound	Functional group	EC_{50} MG-63 Cell (μM)
H**1**	ethyl-OH	> 296
H**2**•HCl	propyl-OH	> 273
H**3**•HCl	butyl-OH	> 1268
H**4**	isopropyl-OH	> 2729
H**6**	secbutyl-OH	> 5070
H**7**	propyl-1,2diol	> 251
H**9**	ethyl-carboxylate	> 5071
H**10**	bisphosphonate	> 1400
H**11**	ethyl-phosphate	> 749
H$_5$**XT**•HCl	phosphinate-EDTA derivative	> 562
H**L1**	methyl	> 360

Table 3.2. Cytotoxicity data (MTT assay) for the Ln^{3+} complexes in MG-63 cells, n = 3.

Compound	Functional group	EC_{50} MG-63 Cell (µM)
La(**1**)$_3$	ethyl-OH	> 147
Eu(**1**)$_3$	ethyl-OH	> 289
Lu(**1**)$_3$	ethyl-OH	> 1400
La(**2**)$_3$	propyl-OH	133 ± 3
Eu(**2**)$_3$	propyl-OH	> 681
La(**3**)$_3$	butyl-OH	> 131
La(**4**)$_3$	isopropyl-OH	> 139
Eu(**4**)$_3$	isopropyl-OH	> 136
Gd(**4**)$_3$	isopropyl-OH	> 676
Na$_3$[La(**8**)$_3$]	methyl-carboxylate	> 1263
Na$_3$[Eu(**8**)$_3$]	methyl-carboxylate	> 625
Na$_3$[Gd(**8**)$_3$]	methyl-carboxylate	> 1241
Na$_3$[Lu(**8**)$_3$]	methyl-carboxylate	> 1209
Na$_3$[La(**9**)$_3$]	ethyl-carboxylate	> 1206
Na$_3$[Eu(**9**)$_3$]	ethyl-carboxylate	> 1187
Na$_3$[Gd(**9**)$_3$]	ethyl-carboxylate	> 590
Na$_3$[Lu(**9**)$_3$]	ethyl-carboxylate	> 1155
K$_2$[La(**XT**)]	phosphinate-EDTA derivative	> 1655
K$_2$[Eu(**XT**)]	phosphinate-EDTA derivative	> 1620
K$_2$[Lu(**XT**)]	phosphinate-EDTA derivative	>1562
La(**L1**)$_3$	methyl	> 102
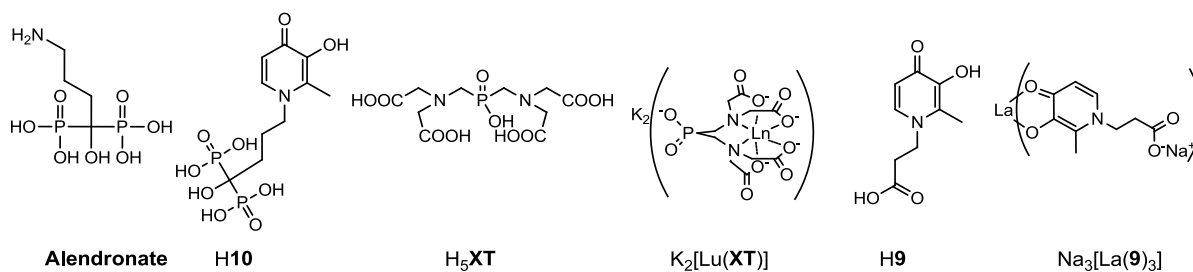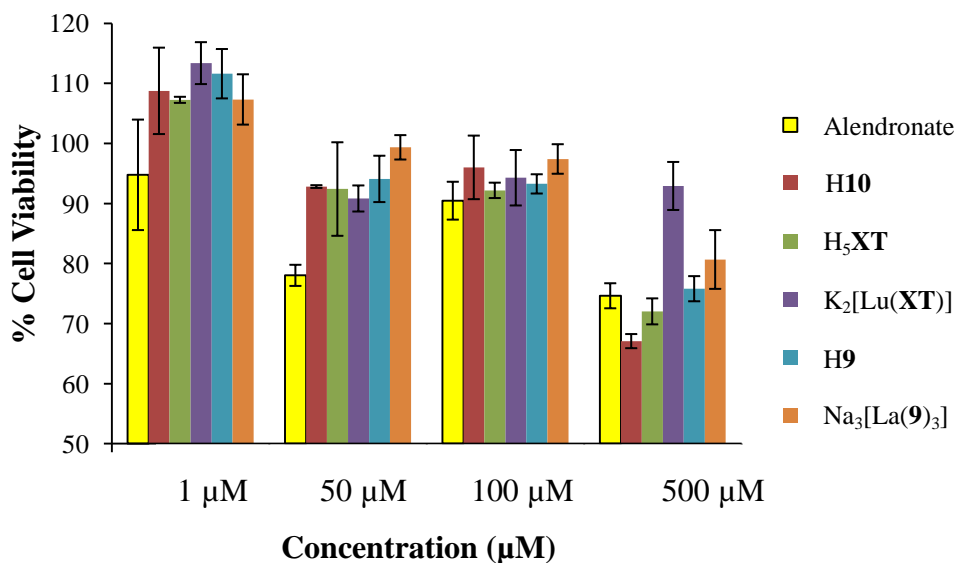
Figure 3.2. A comparison of the toxicity (in MG-63 cells) of alendronate (yellow) to compounds synthesized in this work (top); compounds tested in this study (bottom). Values are reported as % cell viability ± SD.

3.3.2 Partition Coefficients

As the lipophilicity of a compound is such an important factor in drug screening,[161] the partition coefficients of the free ligands were determined by the shake-flask method.[165] It should be noted that the lipophilicity of the free ligand (**HL**) compared to complexed ligand (Ln(**L**)$_3$) would likely be markedly different; however, as only the R$_1$ group of the 3-

136

hydroxy-4-pyridinones (Table 3.3) is varied, a quick screen was accomplished by the experimental determination of log $P_{o/w}$ of just the free ligands.

Log $P_{o/w}$ is conventionally determined in water where the solute is un-ionized; however, due to the ionizable protons of the ligands, a solution buffered to pH 7.4 was used for the aqueous layer in order to give a more accurate description of the lipophilicity of the ligands *in vivo*. The octanol-water coefficient was also calculated for H**L1**, the ligand from the first generation studies that when complexed to La^{3+} was found to have the greatest cell uptake and apparent permeability in Caco-2 cells.[71]

There are three ligands, H**16**, H**6** and H**3** with a log $P_{o/w}$ greater than that of H**L1**; another two ligands, H**4** and H**2** have lipophilicities similar to that of H**L1**. Thus these ligands could potentially have similar or better cell uptake and apparent permeabilities than H**L1**. Not surprisingly, the phosphinate (H**10**) and phosphate (H**11**) functionalized and the carboxylate 3-hydroxy-4-pyridinones (H**8** and H**9**) demonstrated the highest hydrophilicities.

Table 3.3. Log $P_{o/w}$ coefficients of 3-hydroxy-4-pyridinones, in order of decreasing lipophilicities.
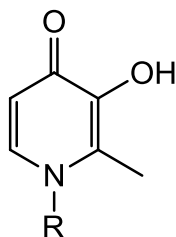
Compound	Functional Group (R)	Log $P_{o/w}$
H**16**		0.85
H**6**		-0.42

Compound	Functional Group (R)	Log $P_{o/w}$
H3		-0.76
HL1		-0.77
H4		-0.82
H2		-0.86
H1		-1.08
H7		-1.37
H11		-1.74
H9		-1.87
H10		-1.89
H8		-1.95
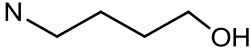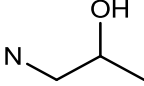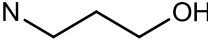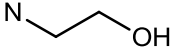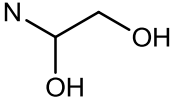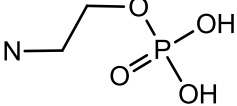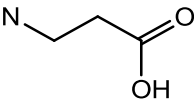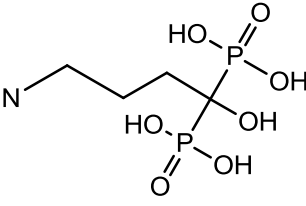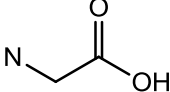
3.3.3 Caco-2 Cell Studies

The GI tract remains the most acceptable route for the administration of drug formulations. It has been demonstrated that Caco-2 cells, derived from a human colon adenocarcinoma,[171] have similar *in vitro* permeability characteristics as human intestinal tissue.[164] Under normal cell culture conditions, these epithelial cells spontaneously differentiate into enterocytes and form polarized monolayers.[171,172] Several characteristics that mimic the small intestine are expressed; the Caco-2 cell monolayers possess well-developed brush border transport systems, enzymes, ion and nutrient channels.[168,173] The cell monolayers have transepithelial electrical resistance (TEER) values of approximately 300 Ω/cm^2, similar to those found in the colon.[172] When cultured in transwell plates (Figure 3.3) that contain a permeable membrane filter, the cells form distinct apical (top) and basolateral (bottom) membranes. It is the apical surface that possesses the brush border and transport systems that are characteristic of the small intestine, discussed above.[171]

The Caco-2 cell model has become an invaluable tool in drug development and predictions of oral absorption in humans.[164] Thus Caco-2 cells, when plated in transwell plates (Figure 3.3), can be used to determine the *in vitro* transepithelial permeability coefficients or apparent permeability (P_{app}) of a drug.

A transwell plate contains an insert that supports a permeable membrane; when Caco-2 cells are plated in the well, they form a monolayer in the apical chamber on top of the porous membrane. In order to calculate the P_{app} of a compound, the compound is added to either the basolateral or apical side (donor chamber) and the drug and the rate of drug absorption over a function of time is measured by monitoring the rate of increase in drug concentration in the opposite side (acceptor chamber). In this way the apical to basolateral flow rate (A➜B) and the basolateral and apical flow rate (B➜A) can be determined.[173] Several studies have demonstrated that the P_{app} (A➜B) across Caco-2 monolayers can be used to estimate the *in vivo* oral absorption of compounds.[164,172,174]
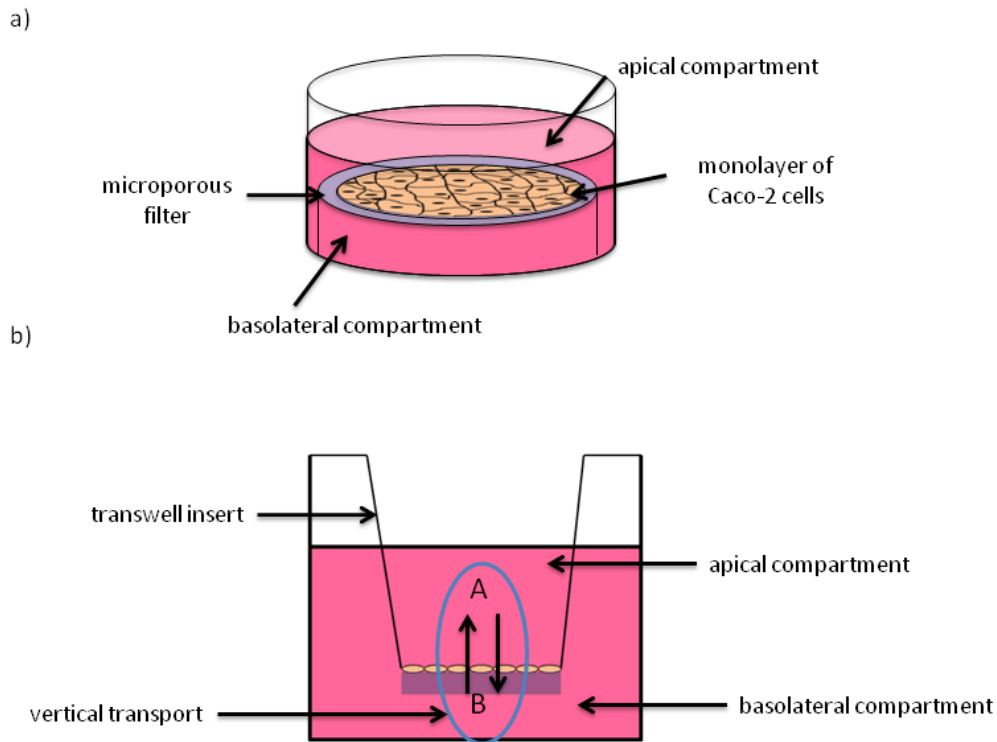
Figure 3.3. Schematic diagram of a transwell plated with a Caco-2 cell monolayer used for the determination of bidirectional transport studies. The cells are cultured on a porous membrane, which yields two accessible sides, basolateral and apical, of the model GI endothelium: a) a schematic of the a single transwell well; b) a cross section of a single transwell well, where A→B represents the apical to basolateral flow rate and B→A represents the basolateral to apical flow rate.

For the purposes of this study, first the toxicities of the compounds in Caco-2 cells were evaluated by an MTS assay. Similar to the MTT assay used for the MG-63 cell toxicity evaluation (see Chapter 3.3.1), the colourimetric assay analyzes the mitochondrial activity of the cells by quantifying the amount of purple formazan formed. The biggest difference between the MTT and MTS assays is that in the MTS assay, the formazan crystals formed are soluble in aqueous media, obviating the need to first aspirate and resolubilize the crystals.[157] Triton-X 100 was used as a positive control to induce cell death.

Much like the low toxicities observed for the metal complexes in the MG-63 cell line (Table 3.1 and Table 3.2), low cytotoxicity profiles were also observed in the Caco-2 cell line. EC_{50} values for La($\mathbf{1}$)$_3$, La($\mathbf{2}$)$_3$, La($\mathbf{3}$)$_3$, La($\mathbf{4}$)$_3$, La($\mathbf{6}$)$_3$, Na$_3$[La($\mathbf{8}$)$_3$], Na$_3$[La($\mathbf{9}$)$_3$] and K$_2$[La($\mathbf{XT}$)] could not be calculated as all the compounds tested had > 80% cell viability at a concentration of 1000 µM.

To evaluate the *in vitro* absorption of the lanthanide complexes, cell uptake and permeability studies in Caco-2 cell monolayers were carried out. In the uptake studies, compounds were introduced to cell monolayers in either 12 well or 24-well plates at concentrations ranging from 100–1000 µM. After a 24 h incubation period, the cells were rinsed, lysed and analyzed for their protein content by a BCA protein assay. The amount of La^{3+} ion in the cell lysate was then analyzed by ICP-MS; the percent of lanthanide taken up by the cells was then calculated and corrected for protein concentration, Figure 3.4.

Inductively coupled plasma mass spectrometry (ICP-MS) is regarded as one of the best analytical tools for the quantitative determination of lanthanides.[175] Unfortunately, this analytical technique only measures the metal content and does not determine the composition of the compound being transported; however, as the lanthanide ion itself is of interest in the treatment of bone density disorders, it is sufficient to determine if the ligands help to increase the bioavailability of the metal ions.

As seen in Figure 3.4, it was observed that one compound, K$_2$[La($\mathbf{XT}$)] was found to have the greatest uptake. The uptake of K$_2$[La($\mathbf{XT}$)] (15.26 ± 0.17%) is comparable to that determined for the lead compound from the first generation complexes, La($\mathbf{L1}$)$_3$ (9.07 ± 2.33 %).[71] Moreover, K$_2$[La($\mathbf{XT}$)] and La($\mathbf{3}$)$_3$ had greater cell uptake than did the benchmark La$_2$(CO$_3$)$_3$ compound, determined in previous studies.[71]
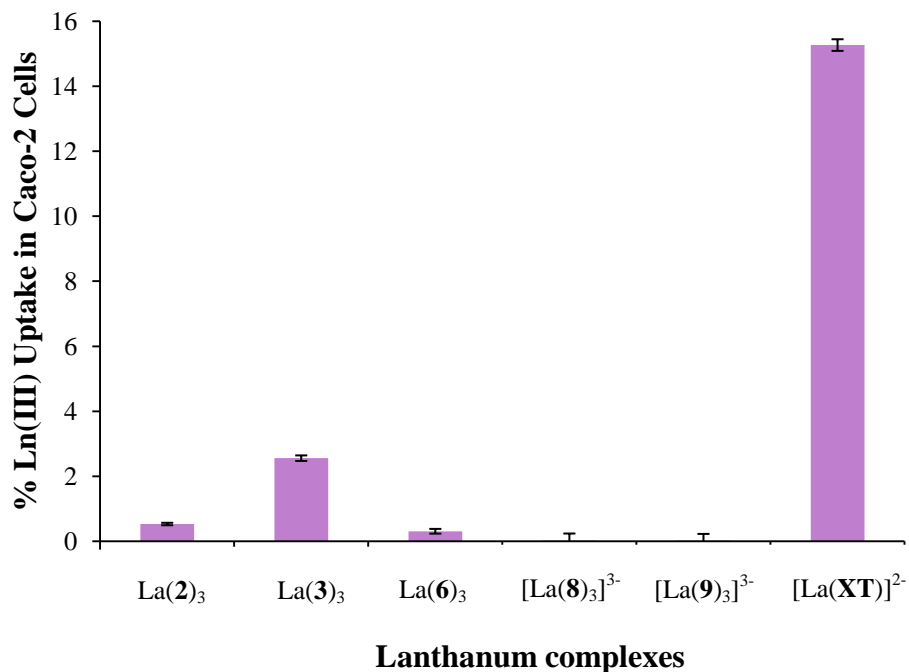
Figure 3.4. Cell uptake of lanthanide complexes, La($\mathbf{2}$)$_3$, La($\mathbf{3}$)$_3$, La($\mathbf{6}$)$_3$, [La($\mathbf{8}$)$_3$]$^{3-}$, [La($\mathbf{9}$)$_3$]$^{3-}$ and [La($\mathbf{XT}$)]$^{2-}$ in Caco-2 cells, after 24 h exposure to compounds. Uptake data are reported as a mean percentage of the concentration of μM of Ln^{3+} taken up by the cells per mg of protein ± SD, n ≥ 3.

The lanthanide complexes, Na$_3$[La($\mathbf{8}$)$_3$] and Na$_3$[La($\mathbf{9}$)$_3$]$_3$ had the poorest cell uptake, which correlated well with the log P$_{o/w}$ values determined for the ligands H$\mathbf{8}$ and H$\mathbf{9}$ (Table 3.3). The partition coefficients for H$\mathbf{6}$ and H$\mathbf{3}$ suggested that La($\mathbf{6}$)$_3$ would have a better cell uptake than La($\mathbf{3}$)$_3$; however, as can be seen in Figure 3.4, the opposite was found to be true.

It should be noted that the conditions of this experiment were different than the conditions under which the uptake of La($\mathbf{L1}$)$_3$ was determined.[71] In this experiment, compounds were incubated in 24-well plates (compounds La($\mathbf{2}$)$_3$, La($\mathbf{3}$)$_3$, La($\mathbf{6}$)$_3$, and K$_2$[La($\mathbf{XT}$)]) or 12-well plates (compounds Na$_3$[La($\mathbf{8}$)$_3$] and Na$_3$[La($\mathbf{8}$)$_3$]) and an incubation time of 24 h. In the study of La($\mathbf{L1}$)$_3$, compounds were incubated for 4 h, but in 6-well plates. As incubation time and surface area can significantly alter the amount of compound that is taken up by the cells, it is

difficult to directly compare these values. That being said, the comparably high uptake of $[La(\mathbf{XT})]^{2-}$ warrants a closer look at this compound in further studies.

It is theorized that the increased uptake of $[La(\mathbf{XT})]^{2-}$, compared to that of the lanthanide pyridinone complexes, has to do with the thermodynamic stability of the complex at physiological pH. A look at the speciation plot of $La(\mathbf{L1})_3$ (Figure A.1), shows that at pH = 7.4 the complex is mainly in its 1:1 $\mathbf{L}:Ln^{3+}$ and 2:1 $\mathbf{L}:Ln^{3+}$ forms, with only a small amount in the 3:1 $\mathbf{L}:Ln^{3+}$ form. Conversely, in the speciation plot[127] of $[La(\mathbf{XT})]^{2-}$ (Figure A.2) it is observed that at a pH of 7.4 the complex is intact. Thus, the increased stability of the $\mathbf{XT}^{5-}$ ligand may result in more of the lanthanide getting taken up by the cell, because the entire complex stays intact.

The A→B (apical to basolateral) transport in Caco-2 cells was also evaluated by introducing the lanthanide complexes in concentrations ranging from 100–1000 µM to the apical side of the cell monolayer in 12-well transwell plates (Figure 3.3). After an incubation time of 24 h, samples from the basolateral and apical side were analyzed for La^{3+} content by ICP-MS. The cell monolayer was lysed and analyzed for protein content (BCA assay) and La^{3+} content by ICP-MS. The cell lysates of $[La(\mathbf{8})_3]^{3-}$ and $[La(\mathbf{9})_3]^{3-}$ have not yet been analyzed for lanthanide content, while the protein concentrations for compounds $La(\mathbf{1})_3$ ad $La(\mathbf{4})_3$ were not analyzed.

The apparent permeability, P_{app}, was calculated by the determining the concentration of lanthanide in the basolateral side by ICP-MS at time point zero and at 24 h. The total lanthanide concentration added in the donor chamber (apical) was calculated by the addition of the amount of lanthanide content found in the apical, basolateral and cell lysate samples. For compounds $Na_3[La(\mathbf{8})_3]$ and $Na_3[La(\mathbf{9})_3]$, as the amounts of lanthanide in the cell lysates were not determined, the total lanthanide concentration added was used to determine the P_{app} value.
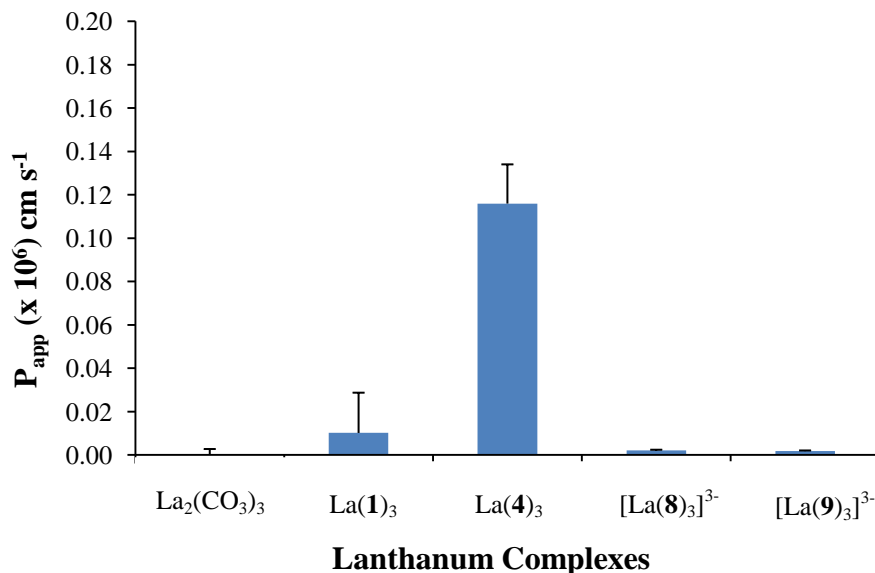
Figure 3.5. Apparent permeability (P_{app}), apical to basolateral transport, of $La_2(CO_3)_3$, $La(\mathbf{1})_3$, $La(\mathbf{4})_3$, $[La(\mathbf{8})_3]^{3-}$ and $[La(\mathbf{9})_3]^{3-}$ in Caco-2 cells after 24 hr of exposure to the lanthanide complexes reported as P_{app} cm s^{-1} ± SD, n ≥ 3.

Apparent permeabilities were calculated for $[La(\mathbf{8})_3]^{3-}$, $[La(\mathbf{9})_3]^{3-}$, $La(\mathbf{1})_3$ and $La(\mathbf{4})_3$, and compared to $La_2(CO_3)_3$. The compound with the highest P_{app} value (Figure 3.5) was found to be $La(\mathbf{4})_3$, which had $P_{app} = (0.12 \pm 0.02) \times 10^{-6}$ cm s^{-1}. The P_{app} of $La(\mathbf{4})_3$ was found to be an order of magnitude lower, compared to P_{app} calculated of the lead compound identified from the first generation complexes, $La(\mathbf{L1})_3$.[71] However, it should be noted, that P_{app} of $La(\mathbf{4})_3$ was still found to be 700 times that of $La_2(CO_3)_3$, so a significant increase in bioavailability was achieved. Likewise, $La(\mathbf{4})_3$ has a apparent permeability three times that of the anti-osteoporotic drug alendronate.[170]

3.4   Conclusions

The library of 3-hydroxy-4-pyridinone ligands has been found to have lipophilicities varying from very hydrophilic (Log $P_{o/w}$ = -1.95, **H8**) to moderately lipophilic (0.85, **H16**), and to

144

have markedly low toxicities in MG-63 cells. The BP-OH functionalized 3-hydroxy-4-pyridinone ligand H10 also demonstrates lower toxicity than alendronate and thus warrants further investigation of the ligand itself.

When coordinated to lanthanide ions, the 3-hydroxy-4-pyridinones have been shown to have low toxicity profiles in both MG-63 and Caco-2 cell lines. H4 and H3 were shown to increase the apparent permeability and cell uptake, respectively, of lanthanum ions *in vitro*. A weak correlation between the calculated octanol-water partition coefficients of the free ligands and the *in vitro* bioavailability of the metal complexes was observed.

Lastly, the phosphinate-EDTA derivative ligand (H_5XT) and its respective lanthanide complexes (Ln^{3+} = La, Eu, Gd) demonstrated extremely low toxicity profiles in MG-63 cells. It was observed that cells had a cell viability > 80%, even in the presence of the highest concentration (1600 μM) of $[La(XT)]^{2-}$ tested. Moreover, $[Lu(XT)]^{2-}$ was found to have a slight proliferative effect in MG-63 cells. The Caco-2 cell uptake of $[La(XT)]^{2-}$ was observed to be higher than the lead compound, $La(L1)_3$, identified from the first generation complexes.[71] Clearly, this series of lanthanide complexes warrants a more thorough investigation for the treatment of bone density disorders.

Chapter 4. Interaction of Lanthanides, 3-Hydroxy-4-pyridinones and Their Metal Complexes with Hydroxyapatite

4.1 Introduction

There are over 200 bones in the adult human skeleton; they are responsible for vital functions such as shelter, support of tissues and vital internal organs, and mechanical rigidity. Bones are the point of attachment for muscles, tendons and ligaments that allow for the movement of body parts. The skeleton is also responsible for storage and homeostasis of minerals, especially calcium and it is our source of red blood cells.[176,177]

These bones constantly undergo a modeling (construction) and remodeling (reconstruction) cycle during life, helping the body to adapt to changing biomechanical forces.[177,178] Bone also undergoes longitudinal and radial growth during childhood and adolescence.[178] Modeling occurs by the independent actions of osteoclasts and osteoblasts – bones can widen or change shape by the addition or removal of bone materials. This takes place in response to physiological influences of mechanical forces, and leads to a gradual adjustment of the skeleton.[177] Remodeling is the process by which old, damaged bone is resorbed by osteoclasts, replaced with newly synthesized bone matrix by osteoblasts followed by mineralization of the matrix to new bone. In this process, old, microdamaged bone is substituted with new, mechanically stronger bone, preserving bone strength.[177,178] This structural restitution occurs only if remodeling is balanced – the volume of new bone equals that of the bone that was removed.[177] Remodeling occurs throughout one's lifetime, beginning at infancy where bone turnover is 100% in one year, to adulthood where bone turnover is 18% per year.[179]

Bone is composed of 50–70% mineral, 20 to 40% organic matrix, 5 to 10% water and < 3% lipids.[177] The mineral content is mostly calcium hydroxyapatite (HAP; $Ca_{10}(PO_4)_6(OH)_2$),

with small amounts of sodium, magnesium, carbonate, fluoride and trace elements. Often, bone mineral is found to have free acid phosphates and absent hydroxyl groups.[177,179] Compared to geological HAP, which has larger crystals and is sparingly soluble, bone apatite has crystal sizes less that 200 Å, and is more soluble, allowing for easier mineralization of human bone. As bone matures, HAP crystals enlarge, and impurities are reduced.[177] While bone mineral is responsible for mechanical rigidity and load-bearing, the organic matrix provides elasticity and flexibility.[177] The principal constituent of the organic matrix is collagen, the most abundant protein in the human body.[180]

Bone mass accounts for 50–70% of bone strength; however, size and shape of bones are not the only factors that affect bone strength. Bone strength is also dependent on the quality, not just the quantity of bone tissue. Bone quality is defined as the influence of factors that affect fracture that are unaccounted for by bone mass or quantity.[177,181,182] These include the micro- and macro-architecture of bone, the material properties of the HAP mineral (its type and crystal alignment), collagen (structure and cross-linking) and the level of microdamage to the bone.[181]

As discussed in Chapter 1, lanthanides are known to accumulate in bone. *In vitro* studies carried out in rats by Durbin and co-workers (see Chapter 1.5) showed that lanthanides preferentially accumulate in bone.[72,73] It has been shown that Gd^{3+}, the main element used in MRI contrast agents (see Chapter 1.4), accumulates in bone if it is not chelated sufficiently.[64] The radioisotope ^{153}Sm (see Chapter 1.4) is used in bone pain palliation in terminal cancer patients because of its 'bone-seeking' properties.[65,66] Likewise it has been shown that lanthanum carbonate (see Chapter 1.4), a drug used to sequester excess phosphate in those suffering from hyperphosphatemia, has been found to accumulate in bone.[39]

As lanthanides accumulate in bone, it is important to understand what effect they have on bone quality. Patients suffering from renal osteodystrophy (ROD), which is characterized by abnormalities in bone turnover, mineralization and bone volume, have higher levels of phosphates in the serum (hyperphosphatemia), are often treated with phosphate binders such

as $La_2(CO_3)_3$.[183] It has been found that lanthanum carbonate-treated ROD patients after one year sustained a reduction in their excessively elevated bone turnover and a reduction in suppressed bone turnover, along with increased normal bone turnover. Severe defective mineralization was no longer observed after one year of treatment with lanthanum carbonate.[183,184] Lanthanum carbonate has also been found to increase osteocalcin and bone-specific alkaline phosphatase, which correlate with factors that increase bone formation; however, the increase was not seen as significant. Histological changes in these same ROD patients showed that changes and improvement in bone turnover were found to be significant in the patients treated for one year with $La_2(CO_3)_3$. After two years of treatment with $La_2(CO_3)_3$, they observed an increase in bone volume that was also found to be significant.[185]

It has also been demonstrated that rare earth metal ions are effective at improving the acid resistance of enamel.[186] Lanthanum was found to improve the rehardening of surface-softened enamel.[187] Cerium has been found to reduce the acid susceptibility of dentine significantly.[188]

As it has been demonstrated, in the previous examples, the positive effect lanthanides can have on bone mineral, it is important to study whether or not the lanthanides from our complexes actually interact with HAP. In this chapter, this intecation along with the degree of this interaction, and the effects this interaction has on the bone mineral quality will be explored. Likewise, the ability of the ligands to direct the complexes towards bone will also be studied. Lastly, as lanthanides clearly have an affinity for bone, calorimetry studies will be sued to determine the strength of this affinity. For compound names, refer to Chapter 2.1.4.

4.2   Experimental

4.2.1   Materials

Hydroxyapatite and 4-(2-hydroxyethyl)-1-piperazineethanesulfonic acid (HEPES) were purchased from Sigma-Aldrich. Sodium chloride and piperazine were purchased from Fisher Scientific. Water was purified using an Elgastat Maxima HPLC reverse osmosis and deionization system or a PureLab Ultra system (Elga, Bucks, England). All water used was type 1, 18.2 MΩ-cm, purified by a full spectrum UV to control bacterial levels. 3-Hydroxy-1,2-dimethyl-4-pyridinone (H**L1**, deferiprone) was purchased form Sigma-Aldrich. All other ligands and metal complexes were synthesized according to procedures outlined in Chapter 2 of this thesis. For studies involving the free metal ions, these were obtained from Alfa Aesar as the perchlorate salts.

Optima nitric acid (a high purity acid containing the least metal content of any commercially available acid, used in trace metal analysis), microcentrifuge tubes (1.5 and 2 mL) and centrifuge tubes (15 mL and 50 mL) were purchased from Fisher Scientific. Inductively-coupled mass spectrometry (ICP-MS) standards were purchased from High-Purity Standards (Charleston, SC, U.S.). Xylenol orange sodium salt was purchased from Riedel-de Haën a subsidiary of Sigma-Aldrich. Hydroxyapatite used in the following experiments was purchased suspended in an aqueous phosphate buffer (0.001 M, pH 6.8) based on the HAP monomer ($Ca_5(PO_4)_3OH$). The hydroxyapatite was filtered to remove the phosphate buffer and rinsed with water. The white slurry was dried at 115 °C overnight, affording a white solid. All concentrations given for HAP are based on the molecular formula of the monomer ($Ca_5(PO_4)_3OH$).

4.2.2 Instrumentation

An Innova 44 incubator shaker (New Brunswick Scientific, Enfield, CT, U.S.) was used at 37 °C and 225 RPM to incubate the HAP samples. Ultraviolet-visible (UV-vis) spectrum measurements were acquired on a Varian Cary 100 Bio UV-Vis. A Fisher Scientific Minicentrifuge was used to separate HAP from supernatant and a Savant vacuum concentrator Speedvac Plus, model SC110A, was used at the highest temperature setting of 60 °C to concentrate HAP and supernatant samples prior to acid digestion for ICP-MS analysis. Lanthanide concentration was analyzed on a Perkin Elmer Sciex Elan 6000 inductively coupled plasma mass spectrometer (ICP-MS).

Surface Area Analysis of Hydroxyapatite by Nitrogen Adsorption

The surface area and porosity were analyzed by nitrogen adsorption/desorption using a Micromeritics Accelerated Surface Area & Porosity 2000 system. Nitrogen multilayer adsorption was determined using Brunauer-Emmett-Teller (BET) surface area analysis.

Analysis by Fourier Transform Infrared Spectroscopy

Infrared spectra were obtained using a Thermo Scientific Nicolet 6700 FT-IR spectrometer, equipped with a Smart Orbit diamond attenuated total reflectance attachment in the mid- and far-infrared regions.

Analysis by Powder X-ray Diffraction

Samples were run on a Bruker AXS D8 Advance powder X-ray diffractometer, wavelength of CuK_{α} (1.54 Å). Hydroxyapatite samples were made into a fine powder using a mortar and pestle. Samples were run from $2\theta = 5.000–80.000°$, at a step point of $0.040°$ and a step time of 1.6 s at 25 °C.

Analysis by Thermogravimetric Analysis

Samples were analyzed on a Perkin Elmer Pyris 6 thermogravimetric analyser. Hydroxyapatite samples were heated from 23.5–900 °C under an inert atmosphere.

4.2.3 Lanthanide Binding Studies with Hydroxyapatite

As samples in this study were analyzed by ICP-MS, all materials used in this study were washed in a 5% Extran bath overnight, then washed with 18.2 MΩ-cm water, and placed in an 1% Optima nitric acid bath overnight. The materials were then washed with 18.2 MΩ-cm water and left to dry in a dust free environment.

A procedure modified from that reported previously by our group was used to study the *in vitro* hydroxyapatite binding of the metal complexes.[71] Samples containing exactly 20.0 mg (39.8 nmol) of dried hydroxyapatite (HAP) were suspended in 0.900 mL of HEPES buffer (25 mM HEPES, pH 7.4, 0.16 M NaCl) in 2 mL microcentrifuge tubes and incubated overnight at 37 °C in a shaker at 225 RPM, allowing for equilibration of samples.

The metal complexes were dissolved at a concentration of 1 mM, and serially diluted to afford a concentration of 20 μM in the same HEPES buffer. Exactly 0.100 mL of the ligand solutions were added to the HAP suspended in HEPES buffer to afford a 2 μM concentration of the metal complex with the HAP. After 5 min, 15 min, 3 h or 24 h incubation of the metal complex at 37 °C in a shaker at 225 RPM, the samples were centrifuged at 6000 RPM for 1–2 minutes with each time point measured in triplicate. Supernatants were carefully removed and placed in 20 mL scintillation vials. Each pellet was washed twice with exactly 1.00 mL of HEPES buffer to remove any unbound metal ion from the HAP. The supernatant was filtered through a 0.22 μm Millipore filter and exactly 1.00 mL was pipetted into 1.5 mL Eppendorf tubes. The HAP pellets and the supernatant were vacuum centrifuged at 60 °C overnight.

The dried HAP pellets and supernatant samples were acid digested as follows for ICP-MS analysis. The samples were dissolved in 2 mL of concentrated Optima nitric acid and transferred into test tubes (16 × 150 mm) with 1–2 teflon boiling chips and placed in a block heater. The temperature was raised to 105 °C and maintained overnight. The solutions were cooled to room temperature and 2 mL of 30% hydrogen peroxide was added to each sample which was then heated to 140 °C overnight. The temperature was increased to 150–160 °C until samples were evaporated to dryness. Samples were then dissolved in exactly 3.00 mL of 10% Optima nitric acid in water (% v/v) and stored in 15 mL centrifuge tubes at 4 °C until analysis for metal ion content.

Samples were analyzed by ICP-MS without further dilution. Using an ICP-MS metal ion standard, a calibration curve of count number versus lanthanide ion concentration was plotted. Concentration of lanthanide ion was determined by using the calibration curve to determine the concentration of lanthanide ion from the count number of the sample. Percent HAP-binding ± SD was determined by dividing the lanthanide ion concentration from the HAP sample by the total concentration found in both the HAP and supernatant samples and multiplying by 100.

4.2.4   Structural Studies of Lanthanum Binding with Hydroxyapatite

For the purposes of the TGA, PXRD, and FTIR studies, samples containing exactly 0.5000 g (0.995 mmol) of hydroxyapatite were incubated overnight in a shaker at 37 °C at 225 revolutions per minute (RPM) with exactly 50.00 mL of HEPES buffer (25 mM HEPES, pH 7.4, 0.16 M NaCl). $Na_3[La(\mathbf{9})_3]$ was dissolved in HEPES buffer (0.202 mmol), and H**9** was dissolved in HEPES buffer (0.606 mmol). Exactly 0.500 mL of the metal complex and ligand solution was added to HAP-HEPES suspensions. Samples were incubated for 24 h in a shaker at 37 °C at 225 RPM. Samples were centrifuged, rinsed twice with HEPES buffer (2 × 50.00 mL), vortexed and dried *in vacuo* overnight. Samples were analyzed by TGA, PXRD and FTIR for their structural and physical properties.

4.2.5   3-Hydroxy-4-pyridinone Binding Studies with Hydroxyapatite

Modified methods, as described by Murphy *et al.*,[189] Diegmueller, *et al.*,[190] and Ogawa, *et al.*,[191] were used to study the *in vitro* binding of the free 3-hydroxy-4-pyridinones. Samples containing exactly 20.0 mg (39.8 nmol) of dried hydroxyapatite (HAP) were suspended in 0.900 mL of HEPES buffer (25 mM HEPES, pH 7.4, 0.16 M NaCl), 2 mL microcentrifuge tubes and incubated overnight at 37 °C in a shaker at 225 RPM, allowing for equilibration of samples. The ligand solutions were dissolved at a concentration of 1 mM in the same HEPES buffer. Exactly 0.100 mL of the ligand solutions was added to the HAP suspended in HEPES buffer to afford a 0.1 mM concentration of ligand with the HAP. After 5 min, 15 min, 3 h or 24 h of incubation with the ligand at 37 °C in a shaker at 225 RPM, samples were centrifuged at 6000 RPM for 1–2 minutes with each time point measured in triplicate. Supernatants were carefully removed and filtered through a 0.22 µm Millipore filter. The UV-vis spectrum of each of the solutions was measured, with λ_{max} between 278–281 nm, indicating the absorbance of the unbound ligand. Utilizing Beer's law, the molar absorbtivity ($cm^{-1}M^{-1}$) of ligand in HEPES was determined. From this the concentration of unbound ligand were calculated. The concentration of bound ligand was calculated by subtracting the concentration of unbound ligand from the concentration of the stock solution, 0.1 mM ligand in HEPES buffer. The percent HAP-binding ± SD was determined by dividing the concentration of bound ligand by the concentration of the stock solution and multiplying by 100.

4.2.6   Analysis by Xylenol Orange Assay

Approximately 10 mg of ligand, HAP, metal complex and $Ln(NO_3)_3$ samples from the Ln(III)-HAP were qualitatively assayed for the presence of free lanthanide. All the samples were dissolved in hexamethylenetetramine buffer (20% v/v in water, pH 5.0). Additionally HAP and Ln(III)-HAP samples were dissolved in a few drops of 6 M HCl, dissolved in

hexamethylenetetramine buffer and adjusted to pH 5.0. Xylenol orange was dissolved in the same buffer. A few drops were added to each of the solutions – presence of free lanthanide was determined by the appearance of a deep red/purple colour upon the addition of the indicator.

4.2.7   Isothermal Titration Calorimetry Studies with Lanthanides and Hydroxyapatite

Isothermal titration calorimetry (ITC) experiments were performed on a Microcal MSC-ITC (Microcal, Piscataway, NJ, U.S.). Hydroxyapatite and lanthanides, as their perchlorate salts $(Ln(ClO_4)_3)$ were dissolved into filtered piperazine buffer (pH 5.0, 100 mM). For La(III), concentrations of the metal ranged from 2.47–3.15 mM into a solution of 0.1 mM of HAP. For Gd(III) concentration of the metal was 4.00 mM into a solution of 0.1 mM of HAP. Lu(III) metal concentrations ranged from 1.38–3.00 mM into solutions of 0.05–0. 1 mM of HAP. All samples and buffers were degassed prior to calorimetry; for all experiments, four independent titration experiments were performed.

The ITC experiments were conducted by sequentially injecting 5.25 μL of Ln^{3+} into the sample cell containing HAP at 37 °C. For all titrations, the heats of dilution were determined just prior to the HAP experiments; they were obtained by the titration of the free metal sample into piperazine buffer using the same ITC parameters. The heats of dilution were then used as a reference and subtracted from the experiment with HAP. The subtraction curves were analyzed by fitting the corrected data to a binding model (single-set of identical sites) using software provided with the instrument.

4.2.8 Ion-Exchange of Lanthanum Ions for Calcium Ions in Hydroxyapatite

In order to determine what effect large amounts of lanthanum would have on the physical and structural properties of HAP, HAP (0.5 g, 0.995 mmol, 19.9 mM) was suspended in 50 mL of piperazine buffer (100 mM, pH 5.0) and incubated overnight at 37 °C in a shaker at 225 RPM. La(ClO$_4$)$_3$ (50 mL in piperazine buffer, 0.995 mmol, 19.9 mM) was titrated slowly into the HAP solution over 90 min, affording molar ratios of 1:1, 2:1, and 3:1 of La:HAP. Suspensions were maintained at a constant temperature of 37 °C and a pH of 5.0. Samples were incubated in the shaker at 37 °C for 24 hours at 225 RPM. The suspensions were subsequently centrifuged, rinsed with 2 × 50.00 mL of H$_2$O, vortexed and centrifuged again. The HAP was then dried overnight on a freeze dryer at -85 °C under a vacuum of ≤ 500 mTorr. Samples were analyzed by TGA, PXRD and FTIR for their structural and physical properties. Xylenol Orange indicator was used to ensure binding of lanthanides to the HAP samples.

4.3   Results and Discussion

4.3.1   Surface Area Analysis of HAP by Nitrogen Adsorption

The HAP used in this study was analyzed by N$_2$ adsorption, and its surface area was calculated by Brunauer-Emmett-Teller (BET) surface area analysis. The Ca-HAP used in the binding experiments follows a type V isotherm, indicating a mesoporous material,[192] as seen in Figure 4.1, with a BET surface area of 48.2 m^{2}g^{-1}, based on two measurements.
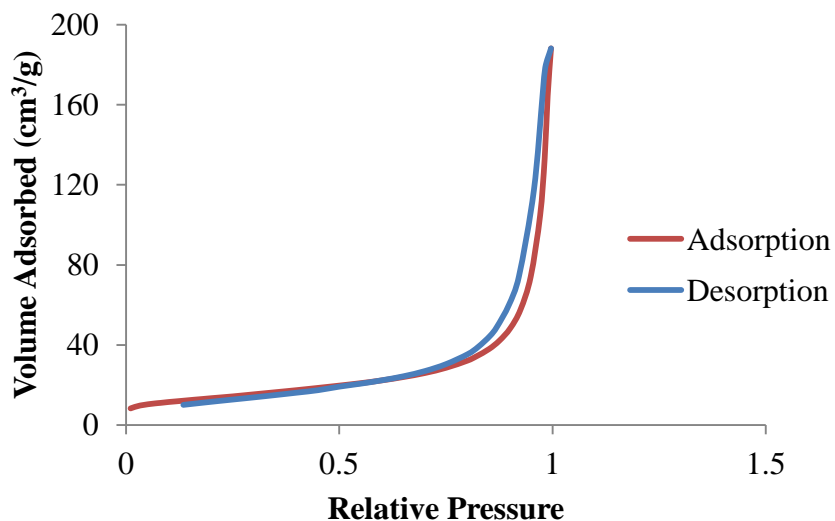
Figure 4.1. Brunauer-Emmett-Teller (BET) isotherm of hydroxyapatite obtained from the surface area analysis using nitrogen adsorption/desorption at STP.

4.3.2 Lanthanide Complex and Ligand Binding Studies with Hydroxyapatite

As can be seen in Figure 4.2, all the metals had near quantitative binding of the lanthanide to hydroxyapatite, with the exception of La($\mathbf{4}$)$_3$, with > 98% to the HAP after 24 h. Minimal variability was observed in the binding between [Eu($\mathbf{8}$)$_3$]$^{3-}$, [La($\mathbf{9}$)$_3$]$^{3-}$, and [La($\mathbf{XT}$)]$^{2-}$. The high percentage of lanthanide bound correlates to our previous work.[71] For the hydroxyl pyridinone complex, La($\mathbf{4}$)$_3$, a larger error was observed due to fluctuations in the plasma the day the experiment was run. This indicates that the binding kinetics are quite fast, with > 90% of the metal or metal-ligand complex bound to HAP after 5 minutes. Numerical values of the amount of Ln(III) bound can be found in the Appendix (Table A.3). Interestingly, [La($\mathbf{XT}$)]$^{2-}$, in which the lanthanum is coordinated to a hexadentate ligand, forming a more thermodynamically stable complex than the bidentate pyridinone complexes had > 97% of the lanthanum bound HAP under physiological conditions.

156

Previous studies performed in the Orvig group used an unbuffered saline solution to incubate HAP with the metal complexes and were thus not performed under physiological conditions.[71] As pH can have a huge affect on the binding affinity, it is important the pH is carefully controlled in a study where binding interactions are being analyzed. Thus, in this study, HEPES buffered to 7.4, 0.16 M NaCl was selected to control both the pH and the ionic strength to physiologically relevant conditions. Careful thought was put into selecting the appropriate buffer; a phosphate buffer, in which the HAP was originally suspended, would compete for metal ions, potentially binding the free lanthanides instead of the HAP.

The lanthanide complexes, La(4)$_3$, Na$_3$Eu(8)$_3$, Na$_3$La(9)$_3$ and K$_2$[La(XT)] were all tested at very low concentration, 2 μM. This concentration was chosen firstly because it is well below the respective EC$_{50}$ values which are reported in Chapter 3.3.1, meaning they are non-toxic at this concentration. Secondly, we wanted to ensure the amount that could interact with the HAP was greater than the amount seen to accumulate in bone in patients who are treated with lanthanum carbonate for 1 year, discussed below.
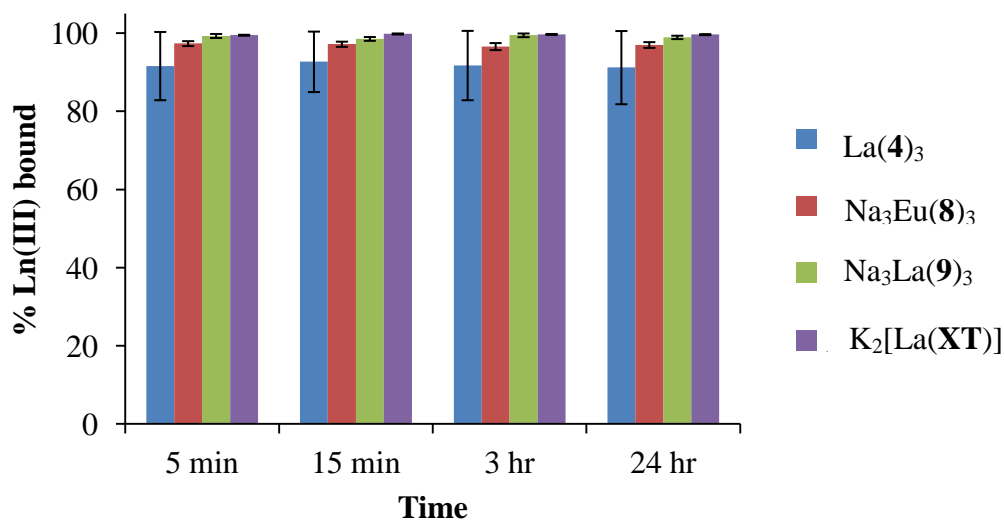
Figure 4.2. Lanthanide metal complexes hydroxyapatite (HAP) binding studies analyzed by ICP-MS. Reported as the mean percentage ± SD of Ln(III) bound to HAP, n = 3.

Studies of patients treated with $La_2(CO_3)_3$ demonstrated that the metal accumulates in bone.[184,193] Patients treated for 1 year with the phosphate binder at a mean dose of 1250 mg/day have a mean accumulation of 1.8 µg/g, and a maximum accumulation of 5.5 µg/g.[184] This correlates with other studies.[193] If we presume that the mechanism of this binding is the ion-exchange of Ca^{2+} for Ln^{3+}, and assume a bone Ca^{2+} concentration of 120 mg/g,[194] the maximum lanthanum dosage concentration observed is 1 in 20,000 (5.5 µg/g divided by 120 mg/g) calcium ions replaced by lanthanum after one year of treatment. Previously, it has been shown that > 98% of the lanthanum in $La_2(CO_3)_3$ is bound to HAP after an incubation time of 24 hours, which correlates well with these studies.[71] In our studies, the concentration of La(III) determined to bind to HAP was between 1–2 mg/g, or 1–2 in 120 calcium ions replaced by lanthanum, which is significantly higher than what has been observed *in vivo* with lanthanum carbonate administration.[184,193]

While it is clear that the lanthanides are interacting with HAP, it is not clear if this is just a surface interaction, or if the Ln(III) is being incorporated into the HAP crystal lattice. Thus xylenol orange was used as an indicator for lanthanide binding. Xylenol orange is a colorimetric indicator of heavy metals,[195] and is well known as an indicator for free lanthanides.[196,197] In hexamethylenetetramine buffer, the ideal pH range for this heavy metal indicator is pH 4.5–6.0.[198]
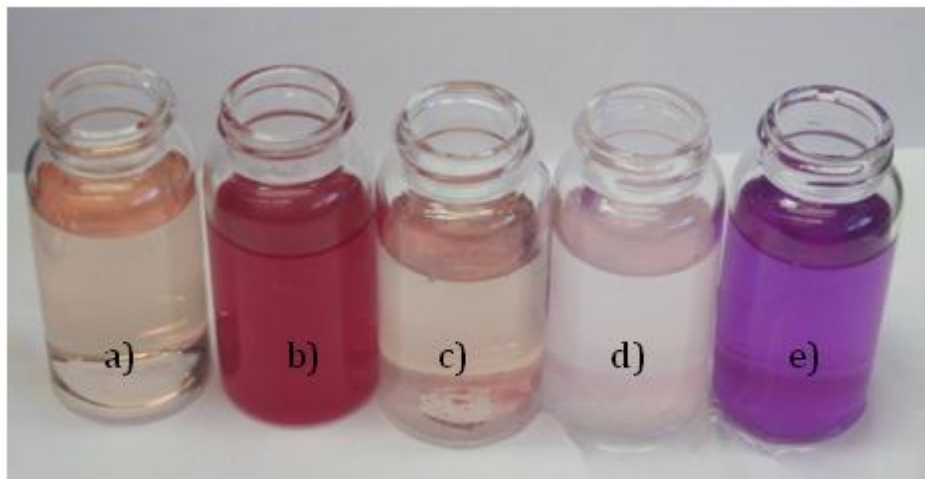
Figure 4.3. Colourimetric xylenol orange assay where: a) Ln-HAP supernatant, b) digested Ln-HAP, c) undigested Ln-HAP d) HAP (control) e) La(NO$_3$)$_3$ (control). The appearance of purple/red indicates the presence of unbound Ln^{3+}.

Under acidic conditions, xylenol orange is a deep red/purple colour when bound to free lanthanides. In contrast, unbound xylenol orange is a yellow-orange colour. Solutions of Ln-HAP supernatant, acid-digested Ln-HAP, undigested Ln-HAP, HAP (negative control), La(NO$_3$)$_3$ (positive control) were buffered to pH 5.0 and a solution of xylenol orange, buffered to pH 5.0 was introduced into each sample. In Figure 4.3 it is evident that (d) the negative control (HAP) is a pale orange colour, indicating no free Ln(III), while (e) the positive control, is a deep red-purple colour, indicating the presence of free Ln(III). Samples (a) and (c)—the supernatants and undigested HAP, respectively, are a light red colour—indicating the presence of trace amounts of free Ln(III), while in (b), the digested HAP, a deep red colour indicates the presence of free lanthanide ions.

From the absence of the deep red/purple colour, this colourimetric assay confirms the ICP-MS results, showing a very small amount of free lanthanide in the supernatant from the undigested HAP sample. Likewise the absence of the deep red/purple colour in the undigested HAP sample, and the appearance of the red/purple upon digestion of the HAP indicates that the lanthanides are being incorporated into the HAP.

As it is clear that the lanthanides bind to HAP, and since these were much higher values ($180 \times$) compared to what was observed with the *in vivo* administration of $La_2(CO_3)_3$, it was important to study if the binding of lanthanides to the HAP caused structural or physical changes to the material. This assay was thus carried out on larger scale (0.5 g HAP vs. 20 mg of HAP) so there was enough to analyze HAP samples by TGA, PXRD, and FTIR.

As can be seen in Figure 4.4a there is not a significant change in the FTIR of HAP with the metal or free ligand. The PXRD spectra shown in Figure 4.4b also have no observable change; the peaks are all the same width and the d-spacing has not been altered by the addition of free ligand or the metal complex. Figure 4.4c shows there is no change in the TGA—the small (~3%) weight loss is likely due to the loss of 1 or 2 equivalents of water. Lastly Figure 4.4d shows there is no change in the FTIR after the TGA when compared to the FTIR spectrum pre-TGA. With no observable change in the FTIR or the PXRD, it is obvious that the crystallinity of the HAP is not affected by the addition of the metal complex or free ligand. The amount of lanthanum ion is low compared to the amount of Ca^{2+} present and thus a large change in any of the spectra would not be expected. However, these results indicate that the lanthanides, bound at a concentration in HAP approximately 180 times that seen physiologically in bone with $La_2(CO_3)_3$, do not significantly alter the structure of the HAP.
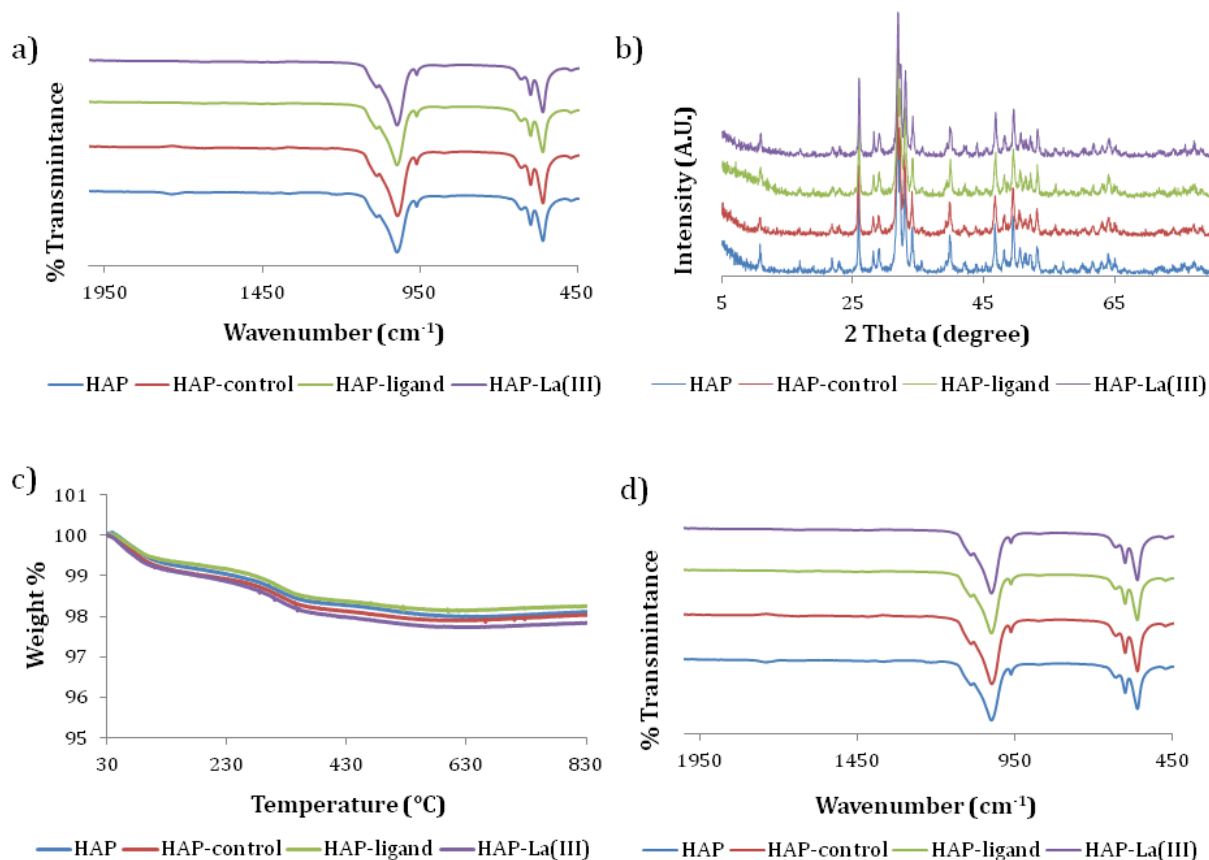
Figure 4.4. Physical spectra of HAP sample (blue), HAP-control (red), HAP-free ligand (green) and HAP-metal (purple). Figure a) FTIR of HAP samples before TGA, b) XRD spectra of samples before TGA, c) TGA of HAP samples and 4d) FTIR of HAP samples after TGA. The FTIR and PXRD spectra are offset for clarity.

4.3.3 3-Hydroxy-4-pyridinone Binding Studies with Hydroxyapatite

As so much care has been taken to functionalize the R-group of the 3-hydroxy-4-pyridinone ligand system, it is important to determine if the functional group increases the binding affinity of the ligands for HAP. One of the shortfalls of the metal complex HAP binding assay is not being able to follow the ligand. While ICP-MS allows for the quantitative

determination of Ln(III) concentration, it does not allow for the quantification of the amount for free ligand and metal-ligand bound to HAP, or unbound in the supernatant.

As a result, a study was carried out in which just the free ligands were monitored. UV-vis spectrophotometry was used as a technique to measure the binding affinity of the ligand for HAP. As H_5XT lacks a chromophore, the hexadentate lanthanide chelator could not be studied for its binding affinity to HAP by UV-vis. Further studies using gas chromatography mass spectrometry (GC-MS) may be worthwhile to monitor the binding of this phosphinate-EDTA derivative to HAP.

The concentration of free ligand, 0.1 mM, is much higher than that used for the lanthanide-complex study. This is mainly because a higher concentration is needed for UV-vis spectrophotometry, compared to the trace amounts of metal needed for ICP-MS analysis. Likewise, it should be noted that the amount of HAP used was still 20 mg, despite the increase in compound concentration. A mole ratio of HAP to compound of 400 was selected; for comparison, in similar studies, the mole ratio of HAP to compound varies from 400–34,000[71,189,191,199]. HEPES buffer was once again used to keep this assay as consistent with the metal complex assay, and buffered to pH 7.4, 0.16 M NaCl, to approximate physiological conditions.

As can be seen in Figure 4.5, the ligand, H**10**, with the bisphosphonate functionality, has a high affinity for HAP with near quantitative binding to HAP, consistent with the literature for similar compounds.[121,200] For H**11**, which contains a phosphate functional group, about 50% of the ligand was bound to HAP after 24 hours. While its affinity is much lower than that of H**11**, it is still quite high. H**7** and H**9**, which possess the 1,2-diol and carboxylate functional groups respectively, have a slightly higher preference for bone than just H**L1** and the hydroxyl group H**1**, especially at lower time points. After 24 hour incubation, all the free ligands seem to have 20–30% of the ligand interacting with the HAP. It is clear that changing the R-group of the 3-hydroxy-4-pyridinone structure can significantly affect the affinity of

the ligand for bone. A complete summary of all the free 3-hydroxy-4-pyridinone ligands tested and their binding affinities is presented in Table 4.1.
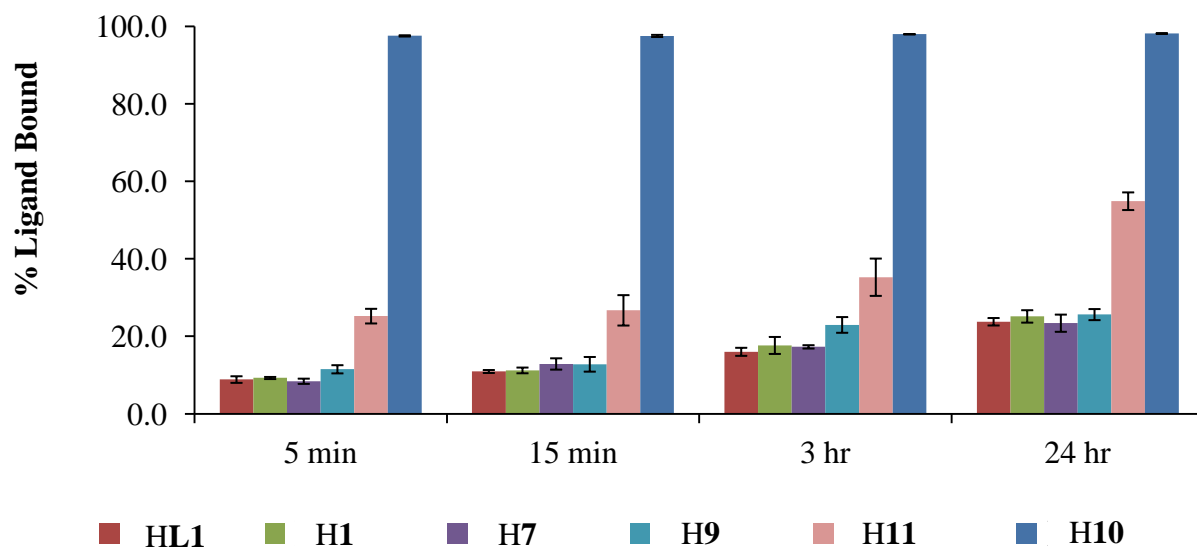
Figure 4.5. 3-Hydroxy-4-pyridinone (ligand) hydroxyapatite (HAP) binding studies analyzed by UV-vis spectrophotometry reported as the mean percentage ± SD of ligand bound to HAP, n = 3.

Table 4.1. 3-Hydroxy-4-pyridinone (ligand) hydroxyapatite (HAP) binding studies analyzed by UV-vis spectrophotometry reported as the mean percentage ± SD of ligand bound to HAP, n = 3.

Time Compound	5 min % Ligand Bound			15 min % Ligand Bound			3 h % Ligand Bound			24 h % Ligand Bound		
HL1	8.9	±	0.9	10.9	±	0.4	16.0	±	1.0	23.8	±	1.0
H1	9.3	±	0.3	11.2	±	0.7	17.7	±	2.2	25.2	±	1.6
H2	7.2	±	0.2	10.1	±	0.1	14.3	±	2.1	22.8	±	0.7
H3	8.8	±	0.4	9.7	±	1.6	17.9	±	2.1	24.4	±	2.1
H4	11.2	±	0.4	14.8	±	0.7	20.6	±	1.0	31.0	±	1.6
H6	7.6	±	0.1	9.5	±	1.1	14.9	±	0.3	22.6	±	2.2
H7	8.4	±	0.7	12.9	±	1.5	17.3	±	0.4	23.4	±	2.2
H8	8.3	±	0.3	11.3	±	1.0	17.2	±	1.1	23.1	±	0.2
H9	11.5	±	1.1	12.8	±	1.9	23.0	±	2.0	25.6	±	1.4
Bn10	98.9	±	0.4	99.5	±	0.2	99.4	±	0.2	99.8	±	0.2
H10	97.6	±	0.2	97.5	±	0.3	98.0	±	0.1	98.2	±	0.1
H11	25.2	±	1.9	26.7	±	3.9	35.3	±	4.8	54.9	±	2.3
H16	3.3	±	1.1	3.7	±	0.7	17.0	±	0.4	17.5	±	0.2

4.3.4 Isothermal Titration Calorimetry Studies with Lanthanides and Hydroxyapatite

As observed from the previous studies with HAP and the metal complexes, large amounts of lanthanides interact with HAP with no significant change in the structure of the bone mineral. It was also observed that most of this interaction happens quickly, with majority of the metal ion bound in < 5 min to HAP. It was clear that this binding interaction warranted

further investigation. Thus isothermal titration calorimetry (ITC) was employed to study the binding affinity and the thermodynamics of the interaction of Ln^{3+} with HAP.

ITC is often used to measure the energy of biochemical reactions, molecular interactions or metal interaction. Examples include ligand-binding interactions, enzyme substrate interactions and interactions among components of multimolecular complexes, at a constant temperature. In ITC, the heat associated with a reaction of the titrant and the sample is the direct thermodynamic observable. Instruments are capable of measuring heat effects arising from reactions involving as little as nanomole amounts of reactants.

ITC is a quantitative technique that can be used to directly measure binding affinity. One experiment yields Gibbs free energy (ΔG), apparent association constant (K_{app}), enthalpy (ΔH) and entropy (ΔS) whose relationship in the standard state is shown in equation 4.1 and under the experimental conditions in equation 4.2.[201,202] ITC also gives the binding stoichiometry (n) of the titrant to substrate. It is important to note that what is actually measured is K_{app} (equation 4.2) not K_{eq}; likewise, ΔH is measured and not ΔH^o.

$$\Delta G^o = -RT\ln K_a = \Delta H^o - T\Delta S^o$$

$$\text{where } K_{eq} = \left(\frac{[\text{Ln-HAP}]}{[\text{HAP}]} \right) \times [\text{Ln}^{3+}]$$

(**4.1**)

$$\Delta G = \Delta G^o + RT\ln K_{app} = \Delta H - T\Delta S$$

$$\text{where } K_{app} = \left(\frac{[\text{Ln-HAP}]}{[\text{HAP}]} \right) \times [\text{Ln}^{3+}] \quad \text{under experimental conditions}$$

(**4.2**)

K_{app}, ΔH and N are determined from the one-site binding model, and are under the stated conditions of temperature (37 °C), buffer (100 mM piperazine buffer) and pH (5.0). A non-

linear regressive fit for a one-site binding model gives the best values for K_{app}, ΔH and n, while ΔS is estimated by the program from the curve fitting.[202] From this, according to equation 4.2, ΔG can be calculated.

In order to obtain the data, typically aliquots of a titrant (protein, peptide or small molecule) are injected into the cell containing protein solution; however, in this experiment aliquots of titrant are metal perchlorate salt which are injected into a cell containing a suspension of hydroxyapatite, as seen in Figure 4.6.
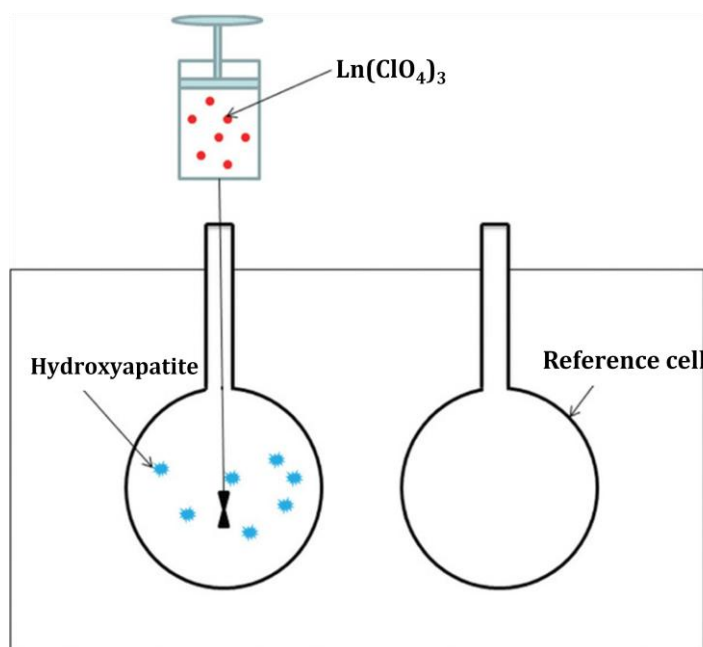
Figure 4.6. Schematic of an isothermal titration calorimetry (ITC) apparatus; aliquots of $Ln(ClO_4)_3$ were titrated into a solution containing hydroxyapatite (HAP).

Isothermal studies were carried out to determine the binding affinity (K_{app}) and stoichiometry (n) of lanthanides to HAP. Attempts to carry out the experiment under physiological conditions failed due to a mixture of free metal ion with metal-hydroxide species that occur for all lanthanides at a pH of 7.4. Thus a pH of 5.0 was chosen to conduct the experiment – at low concentrations only free metal is observed. As can be seen in Figure 4.7 the addition of

the free lanthanide to HAP results in a binding heat. This occurs until a saturation point, where minimal change in the heat is observed as the metal no longer binds to the HAP. The data fit well to a one-site binding model.

In Table 4.2, we see that the stoichiometry for each of La^{3+}, Gd^{3+} and Lu^{3+} is around 3. This means that for every mole of HAP, three moles of lanthanide are binding to the HAP. The association constant (K_{app}) increases with increasing molecular weight of the lanthanides. This is consistent with the lanthanide contraction that is observed across the series of lanthanides, where the atomic radii differ between La^{3+} and Lu^{3+} by approximately 20 pm.[60]
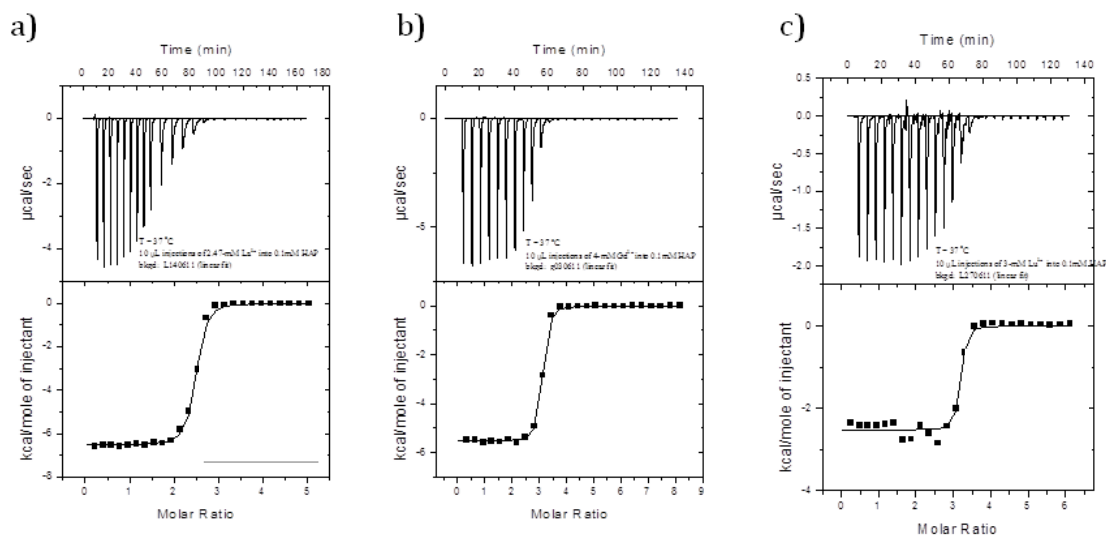
Figure 4.7. Representative isothermal titration calorimetry (ITC) data for Ln(III) with hydroxyapatite (top), and representative fitting curves (bottom): a) La(III), b) Gd(III), c) Lu(III).

The overall Gibbs free energy (ΔG) is negative, indicating the binding is spontaneous. The change in enthalpy (ΔH) is negative, which means this process is exothermic. The process becomes less exothermic with decreasing size of the atomic radius. Lastly, the change in entropy (ΔS) is positive, contributing to the reaction being spontaneous. As temperature is kept constant at 37 °C, the entropy change increases across the series of lanthanides,

167

therefore |ΔH| decreases. However, the Gibbs free energy seems to stay constant across the series of lanthanides. The K_{app} observed is quite high, indicating that HAP has a high affinity for lanthanides.

Table 4.2. Summary of ITC results for titrations of metal into HAP at 37 °C ± SD. N represents the number of metal binding sites per HAP monomer; Gibbs free (ΔG), enthalpy (ΔH), and entropy (TΔS) changes are calculated per mole of binding site.

Metal	n	K_{app} (M^{-1})	ΔG (kcal/mol)	ΔH (kcal/mol)	TΔS (kcal/mol)
La^{3+}	2.4 (±0.1)	2.4 (0.2) x 10^6	-8.71 (0.06)	-6.61 (0.08)	2.09 (0.08)
Gd^{3+}	2.9 (±0.3)	3 (1) x 10^6	-9.9 (0.2)	-5.60 (0.06)	4.3 (0.2)
Lu^{3+}	2.9 (±0.3)	8 (4) x 10^6	-9.3 (0.4)	-2.8 (0.3)	6.5 (0.2)

Bisphosphonates (BPs) are known to have a strong affinity for bone apatite. Oldfield and co-workers[203] studied the thermodynamics of twelve bisphosphonates with human non-demineralized bone powder (60% HAP monomer). ITC experiments were conducted at 37 °C, at a pH of 7.4, to determine the thermodynamics of the interaction BPs and HAP. It was found that half of them bound to HAP in a two-site model, while the other BPs bound to HAP with a one-site model. In site A, one orthophosphate is displaced from the HAP and replaced by one of the phosphonates. In site B, two orthophosphates, or one orthophosphate and one carbonate anion are displaced allowing for a two-site binding from both the phosphonates of the bisphosphonate functional group.[203] They observed, more importantly, that the binding free energy (ΔG) of alendronate and pamidronate to the stronger binding site

was -10.4 kcal/mol and -9.3 kcal/mol which are similar to the free energies observed for the lanthanides with HAP.[203] The study showed that the other 10 bisphosphonates had a Gibbs free energy with HAP that was lower than observed for the lanthanides to HAP.[203] The binding affinity was not reported for the bisphosphonates; however, from equation 4.1 it is seen that the Gibbs free energy of binding is proportional to the natural logarithm of the association constant at the same temperature. This indicates that the energy of the interaction of lanthanides with HAP is similar to or greater than the interaction of bisphosphonates, which are known to bind strongly and irreversibly with bone. The total N (binding to both sites) of the bisphosphonate per mole of HAP is 0.020–0.040, meaning much less bisphosphonate binds to HAP when compared with lanthanide to HAP.[203]

To explain the unusually high number of lanthanides bound per mole of Ca-HAP, one needs to first look at the crystal structure of HAP as seen in Figure 4.8a. As mentioned earlier, the half unit cell molecular formula of hydroxyapatite is $Ca_5(PO_4)_3OH$; however, when Crowley and co-workers crystallized hydroxyapatite, it was observed that the calcium ions are found to be in two different environments.[204] The unit cell of crystalline hydroxyapatite, $(Ca_{10}(PO_4)_6OH_2)$ has 10 cations arranged in two non-equivalent positions. Four are at the M(1) site, which we will refer to as Ca1, which is surrounded by nine oxygen atoms. The second site, M(2), which we will refer to as Ca2, accounts for the other six cations arranged at the apexes of 'staggered' equilateral triangles, surrounded by seven oxygen atoms.[205] Thus, for the ease of discussion, we will redefine the molecular formula of HAP as $(Ca1)_4(Ca2)_6(PO_4)_6OH_2$. Figure 4.8b has the M(2) site removed and Figure 4.8c has the M(1) site removed to make clearer the two different environments of the calcium ions in HAP.
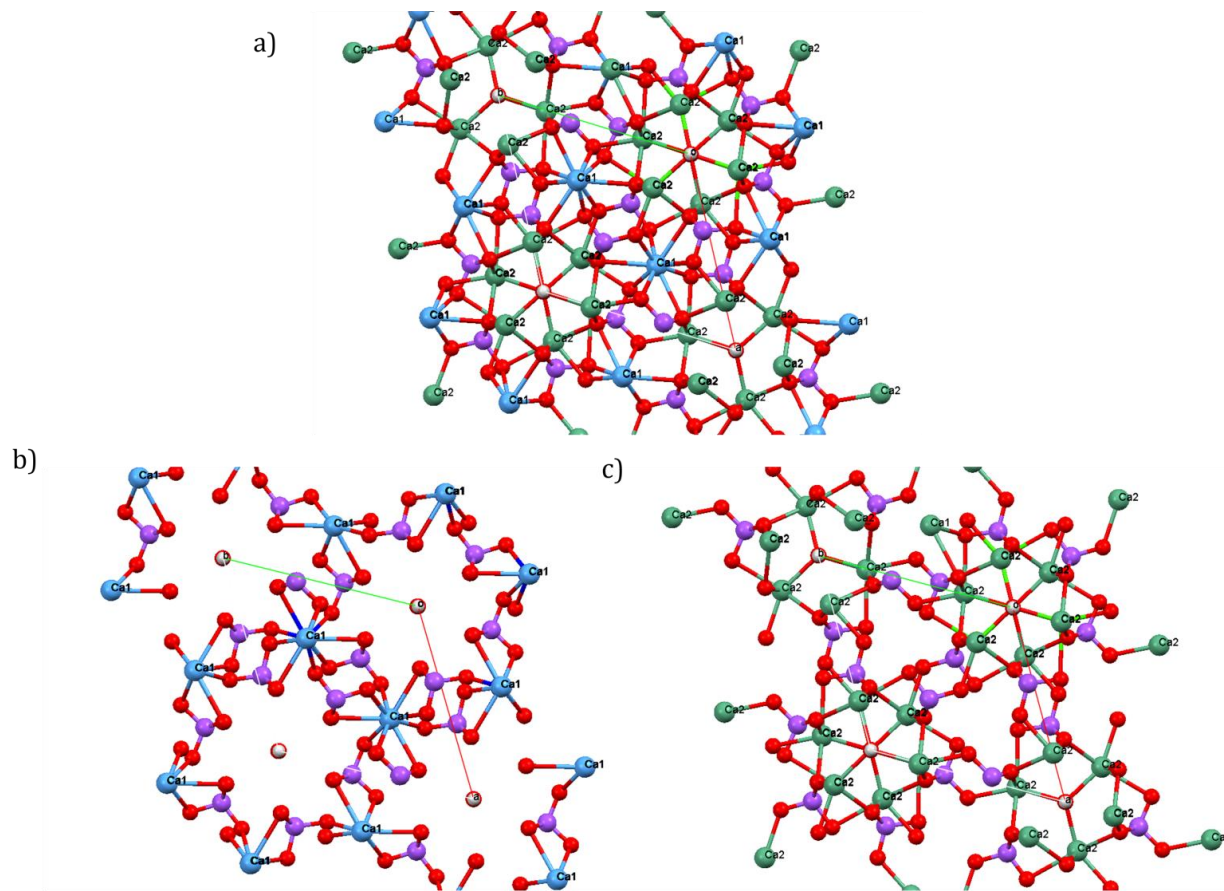
Figure 4.8. Solid state structure of calcium hydroxyapatite[204] where blue (Ca1) is M(1) and green (Ca2) is M(2): a) $(Ca1)_2(Ca2)_3(PO_4)_3OH$; b) $(Ca1)_2(PO_4)_3OH$; c) $(Ca2)_3(PO_4)_3OH$.

HAP can accommodate a large number of different anions or cations in its lattice. The mechanism of the Ln(III) binding to HAP will be explored in this discussion, which will be mainly focused on the ion-exchange of divalent cations for Ca^{2+} ions, as the ion-exchange reactions and mechanisms of trivalent cations with Ca^{2+} in HAP have not been well-investigated. The interaction of metal ions with hydroxyapatite has been studied by two different methods: 1) coprecipitation of metals with hydroxyapatite and 2) ion-exchange of calcium with the metal being analyzed.

These methods should each modify the HAP in a different manner; coprecipitation changes both surface and bulk structures, whilst ion-exchange modifies mainly surface structure.[206] Thus the focus of the discussion on lanthanide ion binding interaction with HAP will mainly be on the substitution of lanthanide ions for divalent calcium ions.[207]

This is consistent with what was observed by Bigi *et al.*[205] in strontium-substituted HAP, where the divalent cation at higher concentrations preferably replaces the Ca^{2+} ions in the M(2) position. Zhu *et al.*[208] studied other divalent metals and found that while Cd^{2+} had a slight preference for the M(2) site, Pb^{2+} preferentially occupied the M(2) sites, especially at higher lead concentrations. Verbeek *et al.*[209] prepared lead-HAP by coprecipitation of Ca-HAP and Pb-HAP, followed by heating at 800 °C at a pressure of 1 atm.

They found that Pb^{2+} had a preference for the M(2) site, while Ca^{2+} has a preference for the M(1) site.[209] Serret *et al.*[207] observed that in the synthesis of lanthanum-substituted calcium hydroxyapatite that the La^{3+} was only observed in the M(2) site, substituting for the Ca^{2+} ions, with no lanthanum in the M(1) position. Get'man *et al.*[210] found that in Nd^{3+} and Dy^{3+} substituted calcium hydroxyapatite, both the ions had a preference for the M(2) position, with most of the lanthanide ions crystallizing in the M(2) position rather than the M(1) position.

Studies involving the ion-exchange of divalent metals for Ca^{2+} yielded the following results. Suzuki and co-workers[211] described the ion-exchange of Ca^{2+} in hydroxyapatite with other

divalent cations, Cd^{2+}, Zn^{2+}, Mg^{2+} and Ni^{2+}. The trend observed in ion-exchangeability of Ca^{2+} was Cd^{2+}, $Zn^{2+} > Ni^{2+} > Ba^{2+}$, Mg^{2+}. In a subsequent paper, they demonstrated that the ion-exchangeability of Ca^{2+} was $Pb^{2+} > Cu^{2+} > Mn^{2+}$, Co^{2+}.[212]

Wakamura *et al.*[206] described the ion exchange of Ni^{2+}, Cu^{2+}, Co^{2+} and Cr^{3+}, concluding that exchangeability of the divalent cations is $Cu^{2+} > Co^{2+}$, Ni^{2+}. They concluded that Cr^{3+} exchangeability with Ca^{2+} was higher than the three aforementioned cations because of the higher chromium content in ion-exchanged HAP. This conclusion was drawn because the mechanism of the trivalent cation was different from that of the divalent cations, as demonstrated by the appearance of a new stretching frequency in the FTIR spectrum of Cr^{3+}-HAP, which the authors assigned as $[Cr(OH)_4]^-$, concluding that while Ni^{2+}, Co^{2+} and Cu^{2+} all ion exchange with the cation Ca^{2+}, Cr^{3+} forms hydrated $Cr(OH)_4^-$ and ion-exchanges with $H_2PO_4^-$. They believed this is the case because Cr^{3+} is more easily hydrolyzed compared to the divalent cations. As there was no mention of pH control in this experiment, it is likely that in the above example, for instance, $[Cr(OH)_4]^-$ coprecipitated with the HAP, and that is why it is observed in the FTIR. As the pH of the solutions in our ITC experiments were maintained at 5.0, it is unlikely that the mechanism by which the authors[206] believe Cr^{3+} is exchanging into HAP is the same for the lanthanides.

Takeuchi *et al.*[213] studied the Ca^{2+}-exchange of the divalent cations, Pb^{2+}, Cu^{2+}, and Cd^{2+}. They observed that Pb^{2+} was exchanged more quickly than the other two cations. Lazić *et al.*[214] also observed that strontium (Sr^{2+}) exchanged by an ion-exchange mechanism at room temperature. Fedoroff and co-workers[215] showed from crystallographic data that Cd^{2+} ion-exchanged in the M(2) site of Ca-Na-HAP.

Lastly, Murata and co-workers theoretically studied the ion exchange ability of various divalent cations in Ca-HAP.[216] They calculated that ion exchange ability depended on the ionic radius. The authors calculated that both Cd^{2+} and Pb^{2+} substituted into the M(2) site of HAP.[216] Sr^{2+}, on the other hand was calculated to substitute into the M(1) site at low concentrations.[216]

172

In 2009 Cheang and co-workers[217] studied the ion-exchange of Nd^{3+} and Gd^{3+} with Ca-HAP. Using the $LnCl_3$ salts at a pH of 7.8, solutions containing 0.2–4 mmol of the metal were added to 10 mmol of HAP. At amounts of up to and including 2 mmol metal ion to 10 mmol HAP, no significant change in the PXRD or FTIR were observed. [217] At the highest amount of 4 mmol: 10 mmol, $Nd(OH)_3$ peaks were observed in both the FTIR and PXRD. No discussion or experimental data were acquired to determine whether the lanthanide ions exchanged for calcium ions in the M(1) or M(2) sites.[217]

From the above studies, it seems reasonable to conclude that the Ln^{3+} ions are likely undergoing an ion-exchange mechanism for the M(2) calcium ions of HAP, explaining the saturation point of Ln^{3+} to HAP ratio of 3:1. This also helps explain why such large amounts of the lanthanide ions are able to bind to HAP. With a ratio of approximately 3:1 Ln(III): HAP, if the lanthanide ions were exchanging for the calcium ions then the cation to phosphorus ratio would remain fixed at [(Ln+Ca)/P] = 1.67, which is often observed for cation-exchanged HAPs.[218]

4.3.5 Non-physiologically Relevant Studies of Lanthanum and Hydroxyapatite: the Facile Synthesis of Rhabdophane from Hydroxyapatite

Lastly, we wanted to see what effect large concentrations of lanthanides had on the structure of Ca-HAP. This experiment was conducted using lanthanum perchlorate at a pH of 5.0, in piperazine buffer. This was chosen because at pH > 5.0 metal hydroxide species form and may not interact in the same way with the bone mineral as the free metal ion.

As seen in Figure 4.9a there is a large change in the FTIR of HAP before TGA analysis. Figure 4.9b shows a significant change in the PXRD with a widening of the peaks, which correlates to an increase in amorphous material in the Ca-HAP, and a complete destruction of the HAP crystal. The TGA shown in Figure 4.9c shows that the destruction of the bone mineral leads to a significant weight-loss on the mineral, especially at a La:HAP ratio of 2:1.

Lastly Figure 4.9d shows that the FTIR post-TGA changes quite significantly as well. This is clear from Figure 4.9 – high concentrations of lanthanum ion introduced to HAP completely destroy the bone mineral at a pH of 5.0.
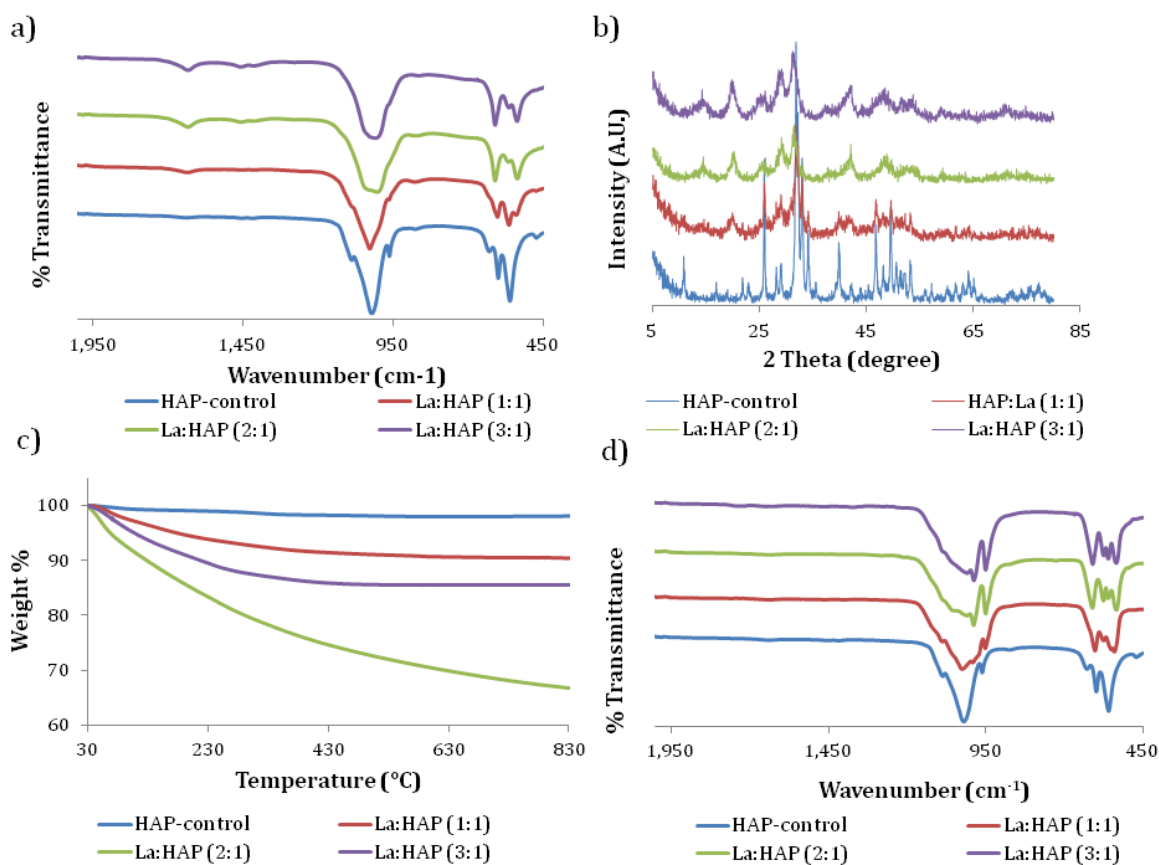
Figure 4.9. Physical spectra of HAP in piperazine buffer (blue), La:HAP (1:1) (red), La:HAP (2:1) (green) La:HAP (3:1) (purple). Figure 4a) FTIR of HAP samples before TGA, b) XRD spectra of samples before TGA, c) TGA of HAP samples and d) FTIR of HAP samples after TGA. The FTIR and PXRD spectra are offset for clarity.

It is important to note that the concentrations of metal ion in piperazine and of HAP differ significantly from those in the ITC experiments. In the ITC experiments the concentration of HAP was 0.1 mM and [La^{3+}] ranged from 2.47-3.15 mM. For these experiments, on the other

174

hand, [HAP] and [La^{3+}] were significantly higher, 19.9 mM and 19.9 mM, respectively. This concentration difference is quite stark, and can cause a huge difference in behaviour.

There are very few studies of the ion exchange of trivalent cations with HAP. In 1990, Tanizawa and co-workers[186] studied the ion-exchange of Ca-HAP with Al^{3+} and La^{3+} in acidic solution. With the addition of Al^{3+} to Ca-HAP, it was observed that HAP became quite amorphous, losing much of its crystallinity as observed by PXRD, and appears to form amorphous $AlPO_4 \cdot nH_2O$. Exchange with La^{3+}, on the other hand, results in crystalline $LaPO_4$. In this study, it should be noted that a fivefold excess of La^{3+} to HAP was used.

Further analysis of the crystal structure obtained of La:HAP at the 3:1 ratio indicates the complete destruction of HAP; however, the material is not amorphous – it has some crystallinity to it. In order to elucidate what new material had been synthesized, a DIFFRACplus TOPAS - XRD was used to fit the PXRD spectrum of La^{3+}:HAP (3:1) with various materials. As shown in Figure 4.10, the PXRD of Ce-rhabdophane fits quite well that of the La^{3+}:HAP (3:1) material. It was clear that HAP was converted to the $LaPO_4$ mineral rhabdophane. This structure is compared to Ce-rhabdophane as the PXRD structure was not of La-rhabdophane was not available in the crystallography database. It is theorized that the exchange of the trivalent cation in exchange for Ca^{2+}, results in perturbation of the HAP crystal structure due to the large size of the La^{3+} ion, eventually leading to the complete destruction of the HAP structure.

Likewise, comparing the FTIR spectra of our "La-HAP" at the 3:1 ratio to that reported of rare earth-rhabdophanes from Assaaoudi et al.[219] further support the synthesis of La-rhabdophane from HAP. In Figure 4.10 are compared the PXRD of La-substituted hydroxyapatite with that of Ce-rhabdophane.

Generally, the synthesis of Ln^{3+}-rhabdophane is a time consuming and energy demanding process. Hikichi et al. have reported the synthesis of rhabdophane by two methods: the first involves mixing $LnCl_3$ and $NaPO_3$ at a temperature range of 200–1000 °C for 5 hours; in the

second method they reported $LnCl_3$ and H_2PO_4 were stirred and the mixture was maintained at 20, 50 and 90 °C for up to 900 days.[220] Patra *et al.*[221] reported a methodology that involved the use of a microwave reactor to convert $NH_4H_2PO_4$ and $Ln(NO_3)_3$ into rhabdophane. Lucas *et al.*[222] have reported the synthesis of rhabdophane by mixing $LnCl_3$ and either H_3PO_4 or $(NH_4)_2HPO_4$; the best yields were obtained by maintaining the reaction for 20 h at a temperature range of 50–80 °C.
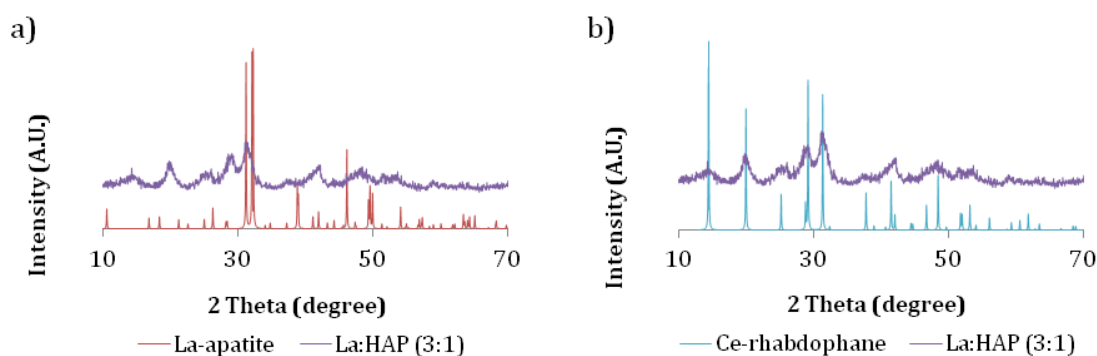
Figure 4.10. Powder X-ray diffraction (PXRD) spectra of La:HAP (3:1) sample (purple) and a) La-apatite,[223] b) cerium-rhabdophane.[224]

4.4   Conclusions

We have demonstrated that the 3-hydroxy-4-pyridinone lanthanide complexes, under physiological temperature and pH, can effectively deliver lanthanides to HAP, used as a model for bone. $K_2[La(\mathbf{XT})]$ also delivers lanthanum to HAP with lanthanum binding in > 95% after 5 minutes to HAP. The lanthanides at a concentration of 1–2 mg/g seem to keep the structural integrity of HAP as shown by no significant changes in the PXRD, TGA and FTIR at these concentrations. The ligand functionalization of the 3-hydroxy-4-pyridinones can also have a big influence of the binding affinity for HAP, with the bisphosphonate and phosphate derivatives possessing the greatest affinity for HAP.

We have also shown that the lanthanides have a high negative Gibbs free energy and association constant with HAP, with binding occurring spontaneously. This binding is equivalent or greater than that of bisphosphonates. The mechanism of binding appears to occur via an ion-exchange of Ca^{2+} by Ln^{3+} with a saturation point of 3 moles of Ln^{3+} to 1 mole of HAP, substituting for the M(2) cation position of the HAP.

Lastly, we have demonstrated that large amounts of lanthanides introduced into HAP causes the destruction of HAP and likely leads to the formation of the mineral La-rhabdophane. This leads to a facile synthesis of rhabdophane, compared to the more time consuming thermal methods.[220-222] Further studies are required to see if this occurs across the series of the lanthanides.

Chapter 5. Curcuminoids and Metal-curcumin Complexes as a Potential Treatment of Bone Density Disorders

5.1   Introduction

5.1.1   Curcumin and its Medicinal Uses

Turmeric, derived from the rhizome of the *Curcuma longa* plant, is a vibrant yellow spice that is not only used to flavour mustards and curries, but also for its medicinal properties in the eastern medicinal practice of Ayurveda.[225] The bright colour is due to the presence of curcuminoids, the active isolate, which make up 3–4% of turmeric powder.[226] The major curcuminoids found in turmeric are curcumin (H**Curc**, 94%), demethoxycurcumin (H**DMC**, 6%) and bisdemethoxycurcumin (H**BDMC**, 0.3%), shown in Figure 5.1.[226,227]

The curcuminoids exist as tautomers of the β-diketone and two interconverting enol-keto forms. NMR studies carried out in DMSO-d_6, D_2O/DMSO-d_6, CD_3OD, CD_3COOD, and $CDCl_3$ all indicate that both curcumin and demethoxycurcumin exist in solution as rapidly interconverting keto-enol tautomers.[228] Curcumin exhibits very low solubility in water although it increases in alkaline conditions, because the deprotonated anion is more soluble.[229] It is highly soluble in DMSO, chloroform and acetone.[225] It has three ionizable protons – the enolic proton has a pK_a of approximately 8.5, and the two phenolic protons that have pK_a values in the range of 10–10.5. Due to its low aqueous solubility, pK_a determination is often carried out in a mixed alcohol/water solvent system. Alternatively, curcumin is often dissolved in basic media for study; however, alkaline decomposition is known to occur over time.[225]

a)

β-diketone tautomer

b)

c)

keto-enol tautomers

$R_1, R_2 = OCH_3$ **Curcumin**   **HCurc**
$R_1 = OCH_3; R_2 = H$ **Demethoxycurcumin**   **HDMC**
$R_1, R_2 = H$ **Bisdemetoxycurcumin**   **HBDMC**
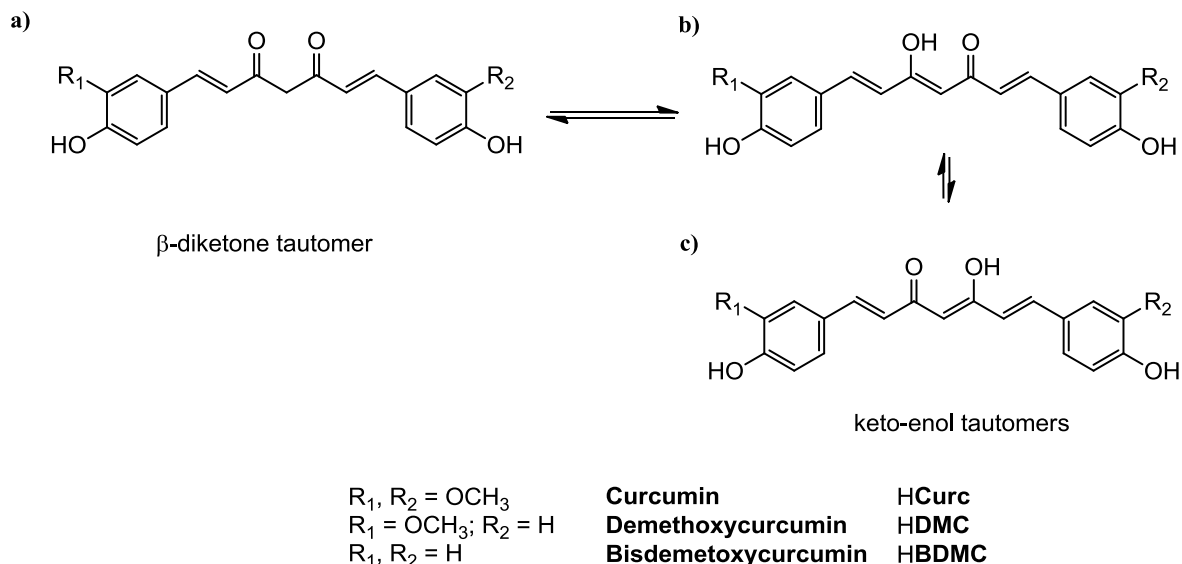
Figure 5.1. The three main curcuminoids isolated from turmeric: curcumin ((1*E*,6*E*)-1,7-bis(4-hydroxy-3-methoxyphenyl)hepta-1,6-diene-3,5-dione), demethoxycurcumin ((1*E*,6*E*)-1-(4-hydroxy-3-methoxyphenyl)-7-(4-hydroxyphenyl)hepta-1,6-diene-3,5-dione), bisdemethoxycurcumin ((1*E*,6*E*)-1,7-bis(4-hydroxyphenyl)hepta-1,6-diene-3,5-dione). The β-diketone (a) and keto-enol tautomers (b and c) are shown.

Curcumin was first isolated by Vogel in 1842, characterized by Lampe and co-workers in 1910 and first synthesized by Lampe and Milobedeska in 1913.[225] Curcumin has a surprising number of medicinal properties, including anti-inflammatory, antioxidant, anticoagulant, anti-fertility, antifungal, antiviral and chemotherapeutic activity, and many other effects.[225-227] Many of these properties stem from the ability of curcumin to acts as a free-radical scavenger and hydrogen donor. It binds metals, particularly iron and copper, and, as a result, has been suggested for the treatment of Alzheimer's disease.[225,230] Previous work in the Orvig group has demonstrated that curcumin can be coordinated to vanadyl (VO^{2+}), gallium (Ga^{3+}) and indium (In^{3+}) by the diketone functionality, forming neutral *bis-* and *tris-*ligand complexes with the respective metal ions.[231]

179

5.1.2 Curcumin and the Treatment of Bone Density Disorders

Amongst the many known and prospective applications of the curcuminoids in medicine is their potential use in the treatment of bone density disorders. Curcumin is a potent inhibitor of the transcription factors NF-κB (nuclear factor-κB) and activator protein-1 (AP-1), which have both been implicated in the survival of osteoclasts, the cells responsible for bone resorption.[232-235] It has been demonstrated that the NF-κB inhibitors pyrrolidine dithiocarbamate, *N*-tosyl-L-phenylalanine chloromethyl ketone and gliotoxin stimulate the apoptosis of rabbit osteoclasts.[232] Ozaki *et al.*[233] established, using mature rabbit osteoclasts, that curcumin stimulates cell apoptosis in osteoclasts. Additionally, using an *in vitro* assay, they also demonstrated that curcumin can dramatically inhibit osteoclastic bone resorption.[233] While the precise mechanism has not been elucidated, it is believed that curcumin inhibits AP-1 and NF-κB transcription. RANKL (RANK-ligand) mediated osteoclastogenesis is not fully understood, but it is known that in the presence of monocytes (RAW 264.7 cells), RANKL induces NF-κB activation, leading to osteoclastogenesis.[233] Bharti *et al.*[235] showed that pre-exposure to curcumin completely suppressed RANKL-induced NF-κB activation. Lastly, French and co-workers[236] demonstrated, using ovariectomized rats (OVX) as a model for postmenopausal osteoporosis, that curcumin both increases bone turnover and bone strength and that at high doses resulted in an increase in femur size.

5.1.3 Separation of the Curcuminoids

Commercial curcumin is sold as a mixture of the three curcuminoids, **HCurc**, **HDMC** and **HBDMC**, shown in Figure 5.1. As a result of their structural similarity, separation of the individual components of curcuminoids is extremely taxing. There are a number of chromatographic techniques that have been reported in the literature for the separation of the three curcuminoids; these include column chromatography,[237,238] preparative thin layer chromatography (prep-TLC),[237] high-performance liquid chromatography (HPLC),[239] high-

performance thin layer liquid chromatography (HPTLC),[240,241] standard countercurrent chromatography (CCC),[242] pH-zone refining countercurrent chromatography (CCC)[242] and microemulsion electrokinetic chromatography (MEEKC).[243]

5.1.4 Curcumin Complexes of Metal Ions

Curcumin has been shown to be a powerful natural chelating agent, due its the β-diketone moiety. As such, it has been coordinated to a variety of metal ions. In our group, curcumin has been previously coordinated to vanadyl, gallium and indium in complexes that were studied for their biological properties.[231]

Due to the abundance of metabolic iron disorders, and the fact that only slight disturbances in iron uptake and loss can lead to deficiency and overload,[2] Fe^{3+}-curcumin binding has been studied. Saladini and co-workers[244] have determined the binding constant for Fe^{3+} coordinated to curcumin using potentiometric techniques, while Bernabé-Pineda *et al.*[245] have studied the formation of **HCurc** complexes with both Fe^{3+} and Fe^{2+} ions, spectrophotometrically and by cyclic voltammetry. Beck and co-workers reported curcumin complexes of Fe^{3+} possessing the formula Fe(**Curc**)$_3$. Likewise, sequestering of Cu^{2+} is important, especially for the treatment of Alzheimer's disease; as a result, natural chelators such as curcumin have been studied extensively. Thus there have been many reports of the synthesis of Cu^{2+} bound to both 1 equivalent and 2 equivalents of **HCurc**.[246-248] Lastly, Beck and co-workers[247] have also successfully synthesized curcumin complexes of Pd(**Curc**)$_2$, and mixed ligand and curcumin complexes of Pd, Rh, Ir, Pt, Co and Ru.

Seltzer *et al.*[249] reported the first example of curcumin coordinated to a lanthanide; they synthesized and studied the near-infrared fluorescent properties of the Nd^{3+} and Yb^{3+} curcumin complexes coordinated to three **HCurc** ligands and one 1,10-phenanthroline-5,6-dione, yielding a neutrally charged complex, as represented in Figure 5.2. Song *et al.*[250] synthesized the Eu^{3+}, Sm^{3+} and Dy^{3+} analogues and studied their antibacterial properties.
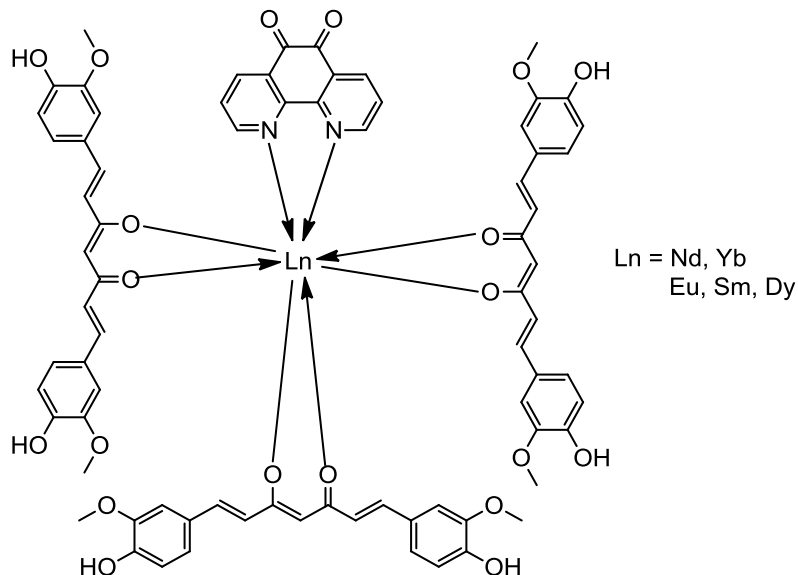
Figure 5.2. Lanthanides coordinated to three curcumin anions (**Curc⁻**) and one 1,10-phenanthroline-5,6-dione.

There are a number of studies that indicate that curcumin may be effective in treating bone density disorders.[232-236] Likewise, as discussed in Chapter 3.1, lanthanides may also be effective for the treatment of bone density disorders. As the curcuminoids possess a β-diketone functionality, and it has been demonstrated that they can be coordinated to the trivalent metal ions, aluminium, gallium and indium,[231] as well as lanthanide ions,[249,250] it may be possible to form a bifunctional anti-osteoporotic agent by coordinating a lanthanide ion with curcumin. Herein, the separation of the three curcuminoids, and the syntheses of Ln(**Curc**)$_3$ (Ln = La^{3+}, Eu^{3+}, Gd^{3+}, Yb^{3+} and Lu^{3+}) are described, along with preliminary toxicity studies in MG-63 cells.

5.2   Experimental

5.2.1   Materials

All solvents were HPLC grade and purchased from Fisher Scientific. Water was purified using an Elgastat Maxima HPLC reverse osmosis and deionization system or a PureLab Ultra system (Elga, Bucks, England). All water used was type 1, 18.2 MΩ-cm, purified by full spectrum UV to control bacterial levels. Curcumin was purchased as a mixture (~70% HCurc) from Sigma-Aldrich, and purified into its three components by chromatography. Lanthanum nitrate, europium nitrate, gadolinium nitrate, lutetium nitrate and gallium nitrate were purchased from Sigma-Aldrich and Alfa Aesar as their hexahydrates and used without further purification. Vanadyl acetylacetonate was purchased from Alfa Aesar without further purification. Analytical thin layer chromatography (TLC) plates (which were alumina backed ultra pure silica gel 60 Å, 250 µm) and flash column silica gel (standard grade, 60 Å, 32–63 mm) were purchased from Silicycle.

For cell studies, MG-63 cells were obtained from American Type Culture Collection (ATCC, Rockville, MD and Manassas, VA, U.S.A.). Media for the cells, minimum essential medium alpha (MEM-α), fetal bovine serum (FBS), 0.25% trypsin-EDTA, Penicillin-Streptomycin-Neomycin 100X (Pen-Strep) and phosphate buffer saline solution (PBS) were purchased from Life Technologies (Burlington, Ontario, Canada). T-75 culture flasks and 96-well plates were purchased from Corning-Costar (Cambridge, MA, U.S.A). Sterile 15 mL and 50 mL centrifuge tubes were purchased from Fisher Scientific. Barrier pipette tips were purchased from Diamed (Mississauga, Ontario, Canada). 3-(4,5-Dimethylthiazol-2-yl)-2,5-diphenyltetrazolium bromide (MTT) was purchased from Alfa Aesar and *cis*-diamminedichloroplatinum(II) (cisplatin) was obtained from Acros Organics.

5.2.2 Instrumentation

Elemental analyses for C, H, and N (Fisons EA 1108 instrumentation) were completed by Mr. David Wong at the UBC Chemistry Mass Spectrometry/Microanalysis Services. ^{1}H NMR spectra were recorded at room temperature using a Bruker AV-300 or AV-400 spectrometer. Low resolution mass spectra were obtained on a Bruker Esquire Ion Trap ESI-MS spectrometer. Fourier transform infrared (FTIR) spectra were obtained on a Nicolet 6700 FTIR equipped with a Smart Orbit diamond attenuated total reflectance attachment. A Labnet Orbit P4 Digital Shaker with platform was used to shake the plates for the MTT assay. A Beckman Coulter DTX 800/880 Series plate reader was used with a filter for 570 nm to read the absorbance values of the plates.

5.2.3 Separation of the Curcuminoids

Curcumin was purchased as a mixture of H**Curc**, H**DMC** and H**BDMC** and thus the three components were isolated from one another. A modified procedure as reported by Vajragupta *et al*.[251] was used to isolate H**Curc**, the major product of the mixture. Crude curcumin (~0.6 g) was dissolved in acetone and adsorbed onto silica (~0.6 g), rotary evaporated and dry loaded onto a silica (170 g) column with 98:5:2 dichloromethane:methanol:acetic acid as the eluent. Fractions 1-6 were collected and rotary evaporated as pure H**Curc**, fractions 7–18 were a mixture of H**Curc** and H**DMC**, while fractions 18–28 were a mixture of H**Curc**, H**DMC** and H**BDMC**.

To isolate H**DMC** and H**BDMC**, preparative TLC plates were impregnated with phosphate ions.[252] The plates were immersed in a solution of NaH_2PO_4 (25 mL H_2O, 1.25 g H_3PO_4 and 0.5 g NaOH) and dried in the oven at 100 °C for 20 minutes. Fractions 7–18 were rotary evaporated, dissolved in a minimal amount of acetone (0.5 mL) and spotted on a phosphate-impregnated TLC plate. Fractions 18–28 were also collected, rotary evaporated, dissolved in

a minimal amount of acetone (0.5 mL) and spotted on a phosphate-impregnated TLC plate; plates were then eluted in a 95:5 dichloromethane:methanol solvent mixture. Fractions 2 and 3 were collected, dissolved in acetone, filtered and rotary evaporated, yielding pure **HDMC** and **HBDMC,** respectively. Figure 5.3 shows the curcuminoids as the keto-enol tautomer, along with the numbering system used for the characterization of the ^{1}H NMR spectra.

$R_1, R_2 = OCH_3$ **Curcumin**   **HCurc**
$R_1 = OCH_3; R_2 = H$ **Demethoxycurcumin**   **HDMC**
$R_1, R_2 = H$ **Bisdemetoxycurcumin**   **HBDMC**
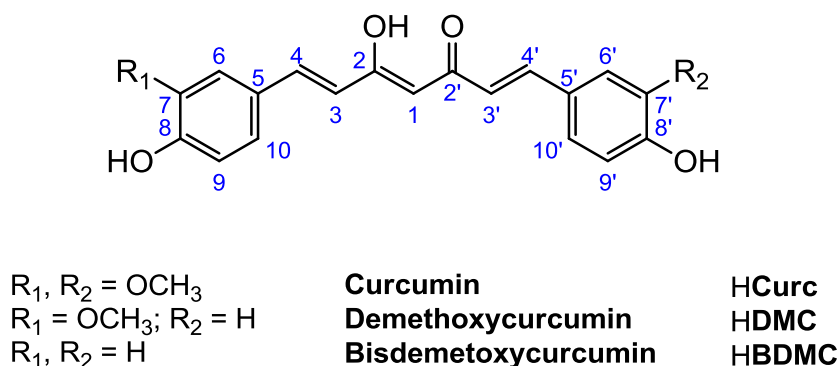
Figure 5.3. The chemical structure of the curcuminoids and the numbering system used for ^{1}H NMR characterization.

HCurc, (1*E*,6*E*)-1,7-bis(4-hydroxy-3-methoxyphenyl)hepta-1,6-diene-3,5-dione

^{1}H NMR (300 MHz, acetone-d_6) δ = 8.19 (br. s, 1 H, 8,8'-OH), 7.60 (d, J = 16.0 Hz, 2H, 4,4'), 7.34 (d, J = 1.8 Hz, 2 H, 6,6'), 7.18 (dd, $J_{6,10}$ = 1.8 Hz $J_{9,10}$ = 8.2 Hz, 2 H, 10,10'), 6.88 (d, J = 8.0 Hz, 2 H, 9,9'), 6.71 (d, J = 15.8 Hz, 2 H, 3,3'), 5.97 (s, 1 H, 1), 3.92 (s, 6 H, 7,7'-O-CH$_3$).

^{1}H NMR (300MHz, DMSO-d_6) δ = 9.64 (s, 2 H, 8,8'-OH), 7.54 (d, J = 15.8 Hz , 2 H, 4,4'), 7.31 (d, J = 1.6 Hz, 2 H, 6,6'), 7.14 (dd, $J_{6,10}$ = 1.8 Hz $J_{9,10}$ = 8.2 Hz, 2 H, 10,10'), 6.81 (d, J = 8.2 Hz, 2 H, 9,9'), 6.75 (d, J = 16.0 Hz, 2 H, 3,3'), 6.05 (s, 1 H, 1), 3.83 (s, 6 H, 7,7'-O-CH$_3$).

MS (-ESI) m/z = 367.3 [L - H]$^-$.

HDMC, (1*E*,6*E*)-1-(4-hydroxy-3-methoxyphenyl)-7-(4-hydroxyphenyl)-hepta-1,6-diene-3,5-dione

^{1}H NMR (400 MHz, acetone-d_6) δ = 7.54 - 7.65 (m, 4 H, 4,4'; 6'; 10'), 7.36 (d, *J* = 1.8 Hz, 1 H, 6), 7.20 (dd, $J_{6,10}$ = 1.7 Hz *J* $_{9,10}$ = 8.5 Hz, 1 H, 10), 6.87 - 6.95 (m, 3 H, 3,3'; 9), 6.64 - 6.76 (m, 2 H, 7'; 9), 5.99 (s, 1 H, 1), 3.90 - 3.95 (m, 3 H, 7-OCH$_3$).

MS (-ESI) *m/z* = 337.3 [L - H]$^-$.

HBDMC, (1*E*,6*E*)-1,7-bis(4-hydroxyphenyl)hepta-1,6-diene-3,5-dione

^{1}H NMR (400 MHz, acetone-d_6) δ = 7.57 (d, *J* = 15.8 Hz, 2 H, 4,4'), 7.53 (d, *J* = 8.5 Hz, 4 H, 6,6'; 10,10'), 6.87 (d, *J* = 8.5 Hz, 4 H, 7,7'; 9,9'), 6.63 (d, *J* = 15.8 Hz, 2 H, 3,3'), 5.95 (s, 1 H, 1).

MS(-ESI) *m/z* = 307.3 [L - H]$^-$.

5.2.4   Metal Complexes of Curcumin Synthesis
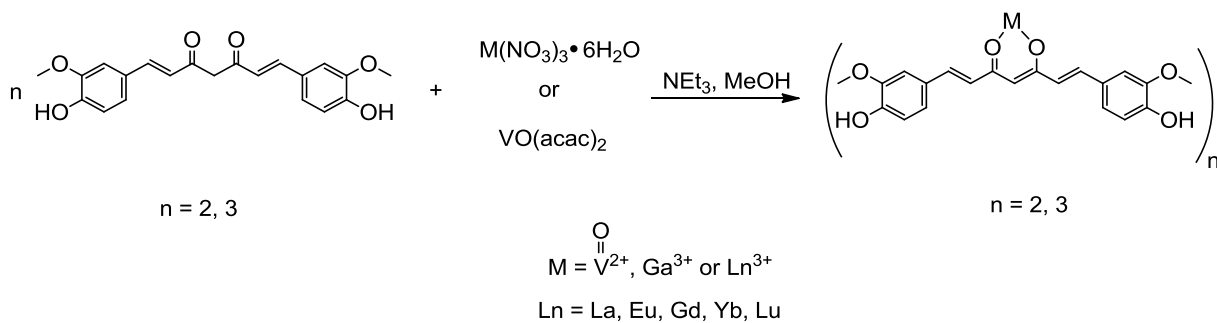
Figure 5.4. Synthesis of metal complexes of HCurc.

186

Synthesis of bis[1,7-bis(4-hydroxy-3-methoxyphenyl)-1,6-heptadiene-3,5-dionato)oxovanadium (IV), (VO(Curc)₂)

 (VO(**Curc**)₂) was synthesized by a method modified from that previously reported in the Orvig group.[231,253] Degassed methanol (7 mL) was added to pure **HCurc** (0.1050 g, 0.2850 mmol) under an inert atmosphere (N_2(g)). The suspension was heated to 80 °C, upon which time the **HCurc** dissolved in the methanol. A degassed solution of VO(acac)₂ (36.5 mg, 0.138 mmol) in methanol (6 mL), under an inert atmosphere was added to the **HCurc** solution dropwise over 15 min. Upon the addition, the reaction solution turned a dark orange-brown colour. After 30 min, a dark orange-brown precipitate formed. The solution was filtered and washed with cold methanol (10 mL), dried *in vacuo*, affording VO(**Curc**)₂ (56.6 mg, 51%). MS(+ESI) m/z = 802.4 [ML₃ + H]⁺. Anal. Calc. (found): $C_{42}H_{38}O_{13}V \cdot H_2O$: C, 61.78 (61.54); H, 4.77 (4.92).

Synthesis of Gallium Curcumin, (Ga(Curc)₃)

(Ga(**Curc**)₃) was synthesized by a method modified from that previously reported in the Orvig group.[231] Methanol (5 mL) was added to pure **HCurc** (0.101 g, 0.274 mmol) and brought to reflux, resulting in a bright orange solution. Ga(NO₃)₃•6H₂O (29.3 mg, 0.081 mmol) was dissolved in hot methanol (2 mL) and added dropwise over 3 min to the **HCurc** solution and the resulting solution was refluxed for 30 min. Triethylamine (38 μL, 0.272 mmol) was diluted with an equal volume of methanol and this solution was added dropwise over 3 min. The reaction mixture was then refluxed for an additional 2 h. After cooling the solution, the resulting dark red solid was filtered out and rinsed with cold methanol (10 mL), affording Ga(**Curc**)₃ (32.7 mg, 35%). ¹H NMR (400 MHz, DMSO-d_6) δ = 9.54 (br. s., 6 H, 8'8-OH), 7.42 (d, J = 15.7 Hz, 6 H, 4,4'), 7.2 (br. s., 6 H, 6,6'), 7.03 (d, J = 7.0 Hz, 6 H, 10,10'), 6.77 (d, J = 8.1 Hz, 6H, 9,9'), 6.73 (d, J = 15.7 Hz, 6H, 3,3'), 5.96 (s, 3 H, 1), 3.77 (s, 18 H, 7,7'-O-CH₃). Anal. Calc. (found): $C_{63}H_{57}GaO_{18} \cdot 2H_2O$: C, 62.53 (62.65); H, 4.94 (5.00).

General Synthesis of Lanthanide Curcumin, (Ln(Curc)$_3$); (Ln = La^{3+}, Eu^{3+}, Gd^{3+}, Yb^{3+} and Lu^{3+})

Ln(NO$_3$)$_3$•6H$_2$O (20.0–21.2 mg, 0.045 mmol) was dissolved in hot methanol (2 mL) and added dropwise over 8 minutes to a hot solution of **HCurc** (50.0 mg, 0.136 mmol) in methanol (5 mL). The solution was refluxed for 30 min, upon which time a solution of triethylamine (19 µL, 0.136 mmol) in methanol (0.5 mL) was added dropwise over 8 min and the reaction mixture was then refluxed for an additional 2 h. Upon cooling, the resulting dark red solid was filtered out, rinsed with cold methanol (10 mL) and dried *in vacuo*, affording Ln(**Curc**)$_3$ in a yield of 69–93%.

Lutetium Curcumin (Lu(Curc)$_3$): ^{1}H NMR (400 MHz, DMSO-d_6) δ = 9.49 (br. s, 6 H, 8'8-OH), 7.46 (d, J = 15.4 Hz, 6 H, 4,4'), 7.17 (d, J = 1.4 Hz, 6 H, 6,6'), 6.98 (d, J = 7.5 Hz, 1 H, 10,10'), 6.76 (d, J = 4.1 Hz, 6 H, 9,9'), 6.73 (d, J = 3.4 Hz, 6 H, 3,3'), 5.78 (s, 3 H, 1), 3.76 (s, 18 H, 7,7'-O-CH$_3$).

5.2.5 Cytotoxicity of Curcuminoids with MG-63 Cells

MG-63 cells were obtained from Dr. Rizhi Wang, Materials Engineering, UBC, after their first passage. Cytotoxicity studies were performed in the UBC Chemistry Biological Services Facility. The medium used to culture the cells was minimum essential medium (MEM-α) supplemented with 10% fetal bovine serum (FBS) and 1% penicillin-streptomycin-neomycin 100X (Pen-Strep). The cells were incubated at 37 °C in a humidified atmosphere of 5% CO$_2$ and 95% O$_2$. Cells were cultured in T-75 cm^3 Corning tissue culture flasks.

Cells were revived from a frozen solution containing 500,000 cells in 5% DMSO in medium (1 mL). Upon revival, the cell mixture was thawed to room temperature with 20 mL of medium and incubated at 37 °C in a humidified atmosphere of 5% CO$_2$ and 95% O$_2$ overnight. After 24 h, the medium was exchanged for 12 mL of fresh medium. After 96 h,

188

media was exchanged for treatment with 5 mL of 0.5% trypsin-EDTA in order to lift up the cells. The cells were counted using a haemocytometer, and 1 million cells were divided and passaged into two different culture flasks and incubated with 12 mL of fresh medium. Medium was changed every third day and every 5-6 days the cells were subcultured by trypsination to either new culture flasks or flat bottom 96-well plates. Cells were either passaged to new culture flasks, where 500,000 cells were cultured in each flask and incubated with 12 mL of medium, or to 96-well plates, where 10,000 cells were plated per well in 100 µL of medium.

Toxicity of the three curcuminoids was determined using a modified MTT (2-(4,5-dimethylthiazol-2-yl)-2,5-diphenyltetrazolium bromide) assay.[156] MG-63 cells were seeded into 96-well plates at a density of 10,000 cells/well in 100 µL of medium. After 24 h of incubation, the medium was exchanged for solutions of the three curcuminoids (H**Curc**, H**DMC** and H**BDMC**) affording concentrations of 1, 5, 10, 25, 50, 75, 100, 175 and 250 µM compound dissolved in a 0.25% DMSO/media solution. As a positive control cisplatin (*cis*-diamminedichloroplatinum(II)) was incubated at concentrations of 1, 5, 10, 25, 50, 100, 250, 500 and 1000 µM in 0.25% DMSO/media solution. As a negative control, 0.25% DMSO/medium was incubated with the cells. For each concentration, the assay was performed in triplicate.

After 48 h of treatment a 50 µL aliquot of MTT (2.5 mg/mL in PBS) was added to each well of the plate. The cells were incubated for 3 h with the MTT solution, allowing for the formation of formazan crystals at the bottom of the wells. The MTT/media/compound treatment was aspirated, leaving the formazan crystals, which were subsequently dissolved in 100 µL of DMSO. The absorbance of each well was measured at 570 nm using a Beckman Coulter DTX 800 Multimode Detector.

Cell viability was calculated relative to the negative control (representative of 100% cell viability). EC_{50}, the fifty-percent inhibitory concentration, was determined using Graphpad Prism[TM] software. Absorbance readings were background corrected for DMSO absorbance

and cell viability was calculated by normalizing the absorbance readings relative to the negative control (0.25% DMSO/media) to 100%. A plot of % cell viability versus the log of drug concentration in μM, was plotted and fitted using non-linear regression analysis (a sigmoidal-dose response with a variable slope). The EC_{50} value was determined by finding the concentration at which 50% of the cells were viable, relative to the negative control.

5.3   *Results and Discussion*

5.3.1   Separation of the Curcuminoids

A methodology modified from that developed by Vajragupta *et al.*[251] yielded pure curcumin. However, because of their similar structure and thus polarity, the R_f values of the three curcuminoids are so similar that H**DMC** and H**BDMC** could not be separated by this method. A multitude of chromatographic methods have been reported in the literature for the separation of the curcuminoids.[237-243] All of the chromatographic mixtures listed in Table 5.1 below, with the exception of 100% dichloromethane, would result in pure H**Curc** – this is because it is in such a high abundance compared to H**DMC** and H**BDMC**, and because it is the first compound eluted in the mixture. Unfortunately, column chromatography with a variety of eluent mixtures, did not yield pure H**DMC** or H**BDMC**, even after separating the majority of H**Curc** from the mixture. As a result, preparative thin layer chromatography (prep-TLC) was attempted with a variety of eluents; however, streaking was observed with the mixtures making it difficult to obtain pure H**DMC** or H**BDMC**.

Table 5.1. A comparison of R_f values of different thin layer chromatography (TLC) mobile phases in normal silica TLC plates and phosphate-impregnated silica TLC plates.

TLC mobile phases	Phosphate-impregnated TLC	R_f		
		HCurc	HDMC	HBDMC
Chloroform: methanol: acetic acid (98:5:2)	✘	0.48	0.41	0.30
	✔	0.44	0.34	0.26
Dichloromethane: methanol (99:1)	✘	0.26	0.17	0.10
	✔	0.27	0.17	0.10
Dichloromethane: methanol (99:5)	✘	0.38	0.25	0.19
	✔	0.37	0.27	0.20
Dichloromethane: ethyl acetate (98:2)	✘	0.19	0.07	0.00
	✔	0.19	0.07	0.00
Dichloromethane: ethyl acetate (95:5)	✘	0.60	0.36	0.00-0.33
	✔	0.30	0.21	0.00-0.12
Dichloromethane: ethyl acetate (90:10)	✘	0.44	0.32	0.21
	✔	0.49	0.37	0.27
Dichloromethane	✘	No separation		
	✔	0.15	0	0

Rasmussen *et al.*[252] described a method in which silica impregnated with phosphate ions resulted in much less streaking and better separation of the curcuminoids. Attempts at impregnating silica and trying to separate the curcuminoids with a variety of eluents did not improve the separation of the mixture or result in a noticeable reduction in streaking. It was observed that silica impregnated prep-TLC plates did result in a significant decrease in streaking of the curcuminoids, and thus a large improvement in their separation. As seen in Table 5.1, there is no notable change in the R_f values between the phosphate-impregnated TLC plates and those not impregnated, but significantly less streaking of the compounds was observed.

The best separation method for the isolation of the three curcuminoids was found to be the isolation of **HCurc** by column chromatography, followed by phosphate-impregnated prep-TLC to isolate the remaining **HCurc**, **HDMC** and **HBDMC**. While prep-TLC could have been used to isolate pure **HCurc**, only a small amount of compound (a maximum of 0.05 g of crude mixture) can be loaded on a prep-TLC plate. Thus, using the crude mixture as purchased would have made this method too time consuming for the isolation of **HCurc** and likely resulted in the plate being overloaded with **HCurc**.

5.3.2 Metal Complex Synthesis

While the curcuminoids, which possess a β-diketone functionality, coordinate with a variety of metals,[231,244,246,247,253] there is only one report of a rare earth complexed with curcumin.[249] In this case a mixed ligand lanthanide complex was synthesized, as shown in Figure 5.2. The synthesis of this mixed ligand complex with lanthanum was attempted; however, the reaction yielded a highly insoluble orange solid that could not be characterized by ^{1}H NMR spectroscopy, and was too unstable to characterize by mass spectrometry. Both MALDI-TOF and ESI-MS were employed an attempt to characterize the complex but because of its limited solubility, only MALDI-TOF could be used; the expected mass of 1452.22 m/z was not observed in MALDI-TOF.

The curcuminoids have been successfully coordinated to Ga^{3+} and In^{3+}.[231] It has been demonstrated that group 13 metals have similar coordination preference to those of the lanthanides; we thus attempted the synthesis of Ln^{3+} analogues of Ga(**Curc**)$_3$ and In(**Curc**)$_3$. Unlike most of the other lanthanides, the 5f orbitals of La^{3+} are unoccupied and thus complexes of La^{3+} are diamagnetic and can be characterized by ^{1}H NMR spectroscopy. Hence, synthesis was first attempted with La(NO)$_3$. Unfortunately, while FTIR seems to indicate the majority product was La(**Curc**)$_3$, a clean ^{1}H NMR spectrum could not be obtained. La^{3+} has a much larger ionic radius than Ga^{3+} thus it was postulated that a mixture of La(**Curc**)$_3$ and La(**Curc**)$_4^-$ was synthesized.

As the synthesis of La(**Curc**)$_3$ was not straightforward, the syntheses of Ga(**Curc**)$_3$ and VO(**Curc**)$_3$ were attempted to gain some synthetic experience on working with coordination complexes of **Curc**; the syntheses of both complexes were successful. As the ionic radius of Lu^{3+} (86 pm, CN=6)[60] is closer to that of Ga^{3+} (62 pm, CN=6)[60] than is that of La^{3+} (103 pm, CN=6),[60] the synthesis with Lu^{3+} was attempted. Lu^{3+} is diamagnetic, and thus complexes with this ion can be studied by ^{1}H NMR. Lu(**Curc**)$_3$ was successfully synthesized, but unfortunately this molecule was significantly less soluble than the analogous Ga(**Curc**)$_3$ complex.

While complexes of Eu(**Curc**)$_3$, Gd(**Curc**)$_3$, Yb(**Curc**)$_3$ and Lu(**Curc**)$_3$ were successfully synthesized, the Lu^{3+} and Ga^{3+} complexes are the only ones that contain diamagnetic metal ions and thus, the only complexes that could be analyzed by ^{1}H NMR. As seen in Figure 5.5, the relative shifts of the ^{1}H NMR signals compared to free **Curc** indicate binding of the curcumin ligand to Lu^{3+} or Ga^{3+}. All the curcumin ligand peaks shifted upfield upon coordination to the metal ion. The largest upfield shift was observed for the H_1 hydrogen (Figure 5.5); this is consistent with it being the hydrogen closest to the coordinating metal ion. The chemical shifts of the phenyl ring hydrogens have the smallest upfield shifts, remaining almost the same. Due to the limited solubility, no ^{13}C NMR spectrum was obtained for the Lu^{3+} or Ga^{3+} complexes.
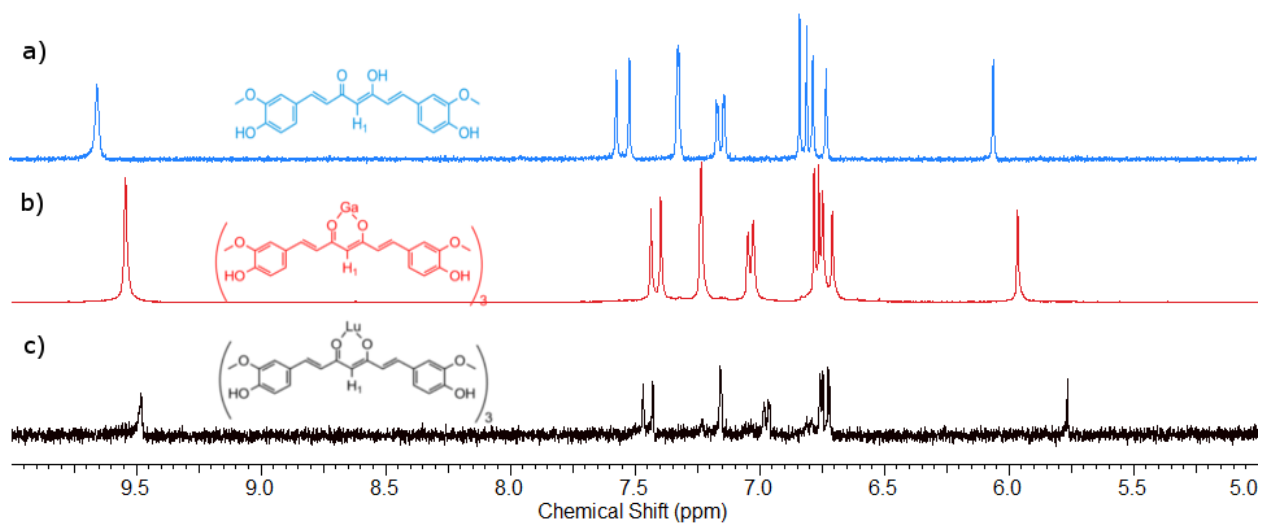
Figure 5.5. ^{1}H NMR (400 MHz, D_2O, RT) spectra of a) HCurc, b) Ga(Curc)$_3$, c) Lu(Curc)$_3$.

The infrared (IR) spectra for all the metal-curcumin complexes are dominated by the peaks corresponding to the curcumin ligand (Table 5.2). As is observed in Figure 5.6, the IR spectra of the metal ion-**Curc** complexes are almost all superimposable indicating that, in the solid state, complexes of Ga^{3+}, Eu^{3+}, Gd^{3+}, Yb^{3+} and Lu^{3+} are all isostructural. The main difference observed between the free ligand and the metal complexes is the appearance of $v_{V=O}$ or v_{M-O} peaks around 965 and 460 cm^{-1} respectively. The replacement of the sharp peak at 3500 cm^{-1} in the free ligand by a broad peak at around 3400 cm^{-1} is due to the coordination of H_2O to the metal ion.

No mass spectrometry data is reported for any of the lanthanide ion-**Curc** complexes, or for the gallium ion-**Curc** complexes, as no evidence of free ligand, or metal complex was observed in the ESI spectra obtained. Further investigation of these Ln(**Curc**)$_3$ complexes by mass spectrometry and elemental analysis need to be carried out to fully characterize this compounds.
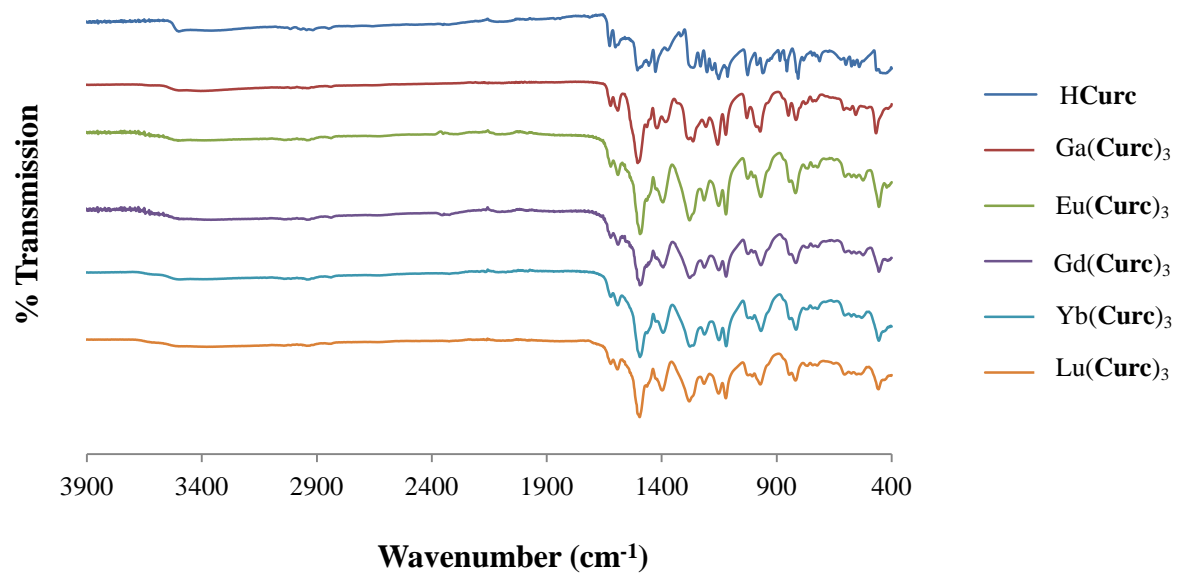
Figure 5.6. Infrared (IR) spectra of H**Curc**, Ga(**Curc**)$_3$, Eu(**Curc**)$_3$, Gd(**Curc**)$_3$, Yb(**Curc**)$_3$ and Lu(**Curc**)$_3$. The FTIR spectra are offset for clarity.

Table 5.2. Selected infrared (IR) stretching frequencies (cm^{-1}) of **HCurc**, VO(**Curc**)$_2$, Ga(**Curc**)$_3$, La(**Curc**)$_3$, Eu(**Curc**)$_3$, Gd(**Curc**)$_3$, Yb(**Curc**)$_3$, and Lu(**Curc**)$_3$.

Compound	ν_{O-H}; H_2O	ν_{C-H}	$\nu_{C=O}$	$\nu_{C=C}$	ν_{C-H}	ν_{C-O}, ν_{C-C-C}	$\nu_{H-C=C-H, \, trans}$	ν_{C-H}, aromatic	$\nu_{V=O}$; ν_{M-O}
HCurc	3500	3016; 2971	1626	1601; 1538	1373	1273 - 1113	985	886	NO
VO(**Curc**)$_2$	~3400	3014; 2643	1625	1592; 1483	1390	1262 - 1152	NO	846	966
Ga(**Curc**)$_3$	~3400	3043; 2869	1622	1590; 1504	1383	1282 - 1121	971	848	467
La(**Curc**)$_3$	~3400	3042; 2874	1621	1588; 1493	1395	1282 - 1121	969	844	455
Eu(**Curc**)$_3$	~3400	3042; 2838	1621	1590; 1494	1394	1278 - 1120	969	844	455
Gd(**Curc**)$_3$	~3400	3041; 2838	1621	1590; 1494	1393	1278 - 1120	968	844	455
Yb(**Curc**)$_3$	~3400	3042; 2838	1621	1591; 1494	1394	1276.4 - 1119	968	842	455
Lu(**Curc**)$_3$	~3400	3042; 2847	1621	1592; 1496	1398	1279.6 - 1120	971	844	457

*NO = Not observed

196

5.3.3   Toxicity of Curcuminoids in MG-63 Cells

The three isolates of the commercially available curcumin mixture were tested for their toxicity against MG-63 cells. MG-63 cells are derived from an osteosarcoma; they are often used as a model for osteoblast cells. Osteoblasts are responsible for the formation of bone; therefore, it is important that there is no toxicity observed with these compounds in this cell line. Due to limited solubility in water and cell-media, only the free ligands were tested. As seen in Table 5.3, they were found to be quite toxic, especially compared to cisplatin (positive control) a known anti-cancer agent.

Table 5.3. $EC_{50} \pm SD$ of curcuminoids in MG-63 cells, n = 3.

Compound	EC_{50} (μM)		
Cisplatin	42.7	±	8.7
Curcumin	22.1	±	5.2
Demethoxycurcumin	32.1	±	8.6
Bisdemethoxycurcumin	50.0	±	7.9

Previous studies by Fuchs and co-workers[254] found that the EC_{50} value of **HCurc** in MG-63 cells was 19.1 μM, which correlates well with our observations; however, they did not study the toxicity of **HDMC** or **HBDMC** in MG-63 cells.

There appears to be a trend in the toxicity of the curcuminoids, with toxicity decreasing in the order of **HCurc**, **HDMC**, and **HBDMC**. The structures of **HCurc**, **HDMC**, and **HBDMC** are quite similar, and the only difference between the three ligands is the number of methoxy

197

groups ortho to the hydroxyl phenol. Thus, the methoxy groups may have an influence on the toxicity of the ligands in MG-63 cells. This could relate to either the change in lipophilicity due to the number of methoxy groups present, or due to the change in intramolecular hydrogen bonding in the molecule as a result of the number of methoxy groups present in the molecule.

From the lipophilicity of the curcuminoids, it is observed that the log P (partition coefficient) of the curcuminoids is H**Curc** (2.56) < H**DMC** (2.69) < **BHDMC** (2.81). T the lipophilicity increases as the number of methoxy groups decreases. The more lipophilic H**DMC** may have decreased uptake by the cell; the same reasoning could be applied to the even more lipophilic H**BDMC**.
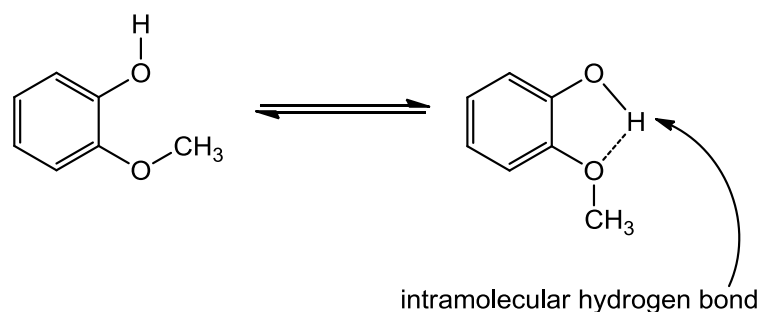
Figure 5.7. Intramolecular hydrogen bond of a methoxy group ortho to a hydroxyl substituent of a phenol ring.[255]

Previous work has demonstrated that the antioxidant activity of the curcuminoids was as follows: H**Curc** > H**DMC** > H**BDMC**.[255,256] These results indicate that the relative potency for suppression of tumor necrosis factor (TNF)-induced nuclear factor κB (NF-κB) activation was H**Curc** > H**DMC** > H**BDMC**, thus suggesting the critical role of a methoxy group on the phenyl ring.[257] It has been demonstrated that the ortho-methoxy group can form a intramolecular hydrogen bond with the phenolic hydrogen (Figure 5.7), making the H-atom abstraction from the ortho-methoxyphenols surprisingly easy.[255] This suggests that the

phenyl methoxy groups could contribute to the toxicity on the osteosarcoma cell line, MG-63.

5.4   *Conclusions*

Optimization of the separation of the three curcuminoids by a combination of conventional column and preparative thin layer chromatographic methods has been realized. Novel lanthanide curcumin complexes with the formula Ln(**Curc**)$_3$ were synthesized and characterized by FTIR and ^{1}H NMR spectroscopies (Lu(**Curc**)$_3$ only). The toxicity using an MTT assay and a MG-63 cell line as a model for osteoblasts was studied, and it was observed that the three isolated curcuminoids have toxicity similar to that of cisplatin. The toxicity observed was in the order of H**Curc** > H**DMC** > H**BDMC**, which can be explained due to the decrease in methoxy substituents from right to left which alters the lipophilicity of the ligands and alters the intramolecular hydrogen bonding in the molecule between the ortho-methoxy and hydroxyl functional groups, resulting in a change in the ability of H-abstraction. While the mechanism of what causes H**Curc** to be more toxic than H**DMC** and H**BDMC** in MG-63 cells is not known, it is clear that the curcuminoids are all quite toxic, and are not good candidates for the treatment of bone density disorders.

Chapter 6. Conclusions, Ongoing and Future Work

6.1   *Conclusions*

A series of 3-hydroxy-4-pyridinone ligands, with a variety of functional groups, was successfully synthesized. The 3-hydroxy-4-pyridinones were rationally designed to incorporate a number of different functional groups that possess differing affinities for hydroxyapatite (HAP), varying lipophilicities and low toxicity profiles. The first reported phosphate functionalized 3-hydroxy-4-pyridinones (H**11**, H**12**, H**13**, H**14** and H**15**) were synthesized and characterized, along with the first example of a 3-hydroxy-4-pyridinone functionalized with a hydroxy-bisphosphonate group (H**10**). H**10** was of particular interest, as it had an almost quantitative binding affinity for HAP after 5 min. H**10** also demonstrated more favourable toxicity profiles compared to alendronate, and a slight proliferative effect in MG-63 cells at low concentrations (<1 μM).

The alcohol and carboxy derivatized 3-hydroxy-4-pyridinone ligands were coordinated to a variety of lanthanides (Ln^{3+}= La, Eu, Gd, Lu). Three ligands (H**4**, H**9** and H**L1**) were studied for their acid dissociation constants (pK_a), all possessing similar pK_as for the 3-hydroxy hydrogen. The stability constants were determined for one ligand, H**L1**, with La^{3+} and Gd^{3+}, confirming the formation of stable *tris*-ligand complexes with 3-hydroxy-4-pyridinones. The metal complexes proved to possess low cytotoxicity profiles in MG-63 cells ($EC_{50} > 100$ μM), and a high affinity for HAP ($> 90\%$). The most promising 3-hydroxy-4-pyridinone complex in this study, La(**4**)$_3$, was 700 times more bioavailable than $La_2(CO_3)_3$ as determined by the apparent permeabilities of the compounds in Caco-2 cells, an assay that mimics the absorption of compounds across the GI tract.

One phosphinate-EDTA ligand (H$_5$**XT**) was synthesized, and coordinated to lanthanide ions (Ln^{3+} = La, Eu, Lu). [La(**XT**)]$^{2-}$ as its potassium salt proved to have the greatest uptake in Caco-2 cells, and was clearly identified as the lead compound from these studies. The cell

200

uptake of [La(**XT**)]$^{2-}$ (15.26 ± 0.17 %) in Caco-2 cells was found to be higher than La(**L1**)$_3$ (9 ± 2 %), the lead compound identified from the first generation studies.[71] Likewise the low toxicity of [La(**XT**)]$^{2-}$ and the high binding affinity for HAP (> 98% after 24 h) warrants further investigation of this complex. Moreover, the slight proliferative effect of [Lu(**XT**)]$^{2-}$ in MG-63 cells also justifies further investigation into the entire series of lanthanide ions coordinated by H$_5$**XT**.

Investigations into the lanthanide ion (Ln^{3+} = La, Gd, Lu) affinity for HAP through isothermal titration calorimetry (ITC) demonstrated a high affinity of Ln^{3+} for bone. Further investigations into the mechanism of this binding (likely ion-exchange) should be carried out.

An effective method for the separation of the three curcuminoids, H**Curc**, H**DMC**, H**BDMC** was identified; the three curcuminoids were found to have high cytotoxic profiles in MG-63 cells. The first reported binary H**Curc** complexes of the rare earths (Ln^{3+}= Eu, Gd, Yb, Lu) were synthesized.

The following sections are devoted to outlining ongoing and potential future work for the further development of this project.

6.2   *Ongoing Studies*

6.2.1   Osteoclast Studies

Osteoclasts are key cells in the bone remodeling process and are responsible for bone resorption. They undergo a differentiation process from monocytes (pre-osteoclasts) to osteoclasts (osteoclastogenesis) when signalled by the RANK ligand (RANKL, Figure 1.5b).[258] Studying the toxicity and the effect on the osteoclastogenesis process of the

201

lanthanide compounds in a pre-osteoclast cell line is necessary to determine whether these compounds are viable for the treatment of osteoporosis.

Studies with a monocyte cell line, RAW 264.7, are currently under investigation in Dr. Michael Cox's laboratory, Vancouver Prostate Centre, Vancouver General Hospital. Studies have demonstrated that the cell line RAW 264.7 can undergo *in vitro* stimulation by the addition of RANKL to generate multinucleated osteoclasts.[259] Current investigations involve studying the toxicity of the lanthanide complexes (La(**L1**)$_3$ and La(**3**)$_3$) on monocytes, as well as the stimulatory or inhibitory effect of the compounds on osteoclast differentiation from monocytes.

6.2.2   Animal Studies

It is well known that the onset of osteoporosis often occurs post-menopause; levels of hormones such as estrogen decline and a perturbation in the bone cycle occurs causing osteoclasts to work faster than osteoblasts resulting in a net loss of bone mass. This postmenopausal osteoporosis can be mimicked by ovariectomized (OVX) rats,[236] in which the ovaries of the rat have been surgically removed in order to imitate the hormonal loss observed in aging patients suffering from osteoporosis.[236,260]

In vivo studies currently ongoing in the Faculty of Pharmaceutical Sciences, UBC are being carried out in aged OVX rats (female, purchased from Sprague Dawley) as a model for osteoporosis.[236,260] The overall goals of the current studies are to 1) determine the pharmacokinetic profiles of the lanthanum compound La(**L1**)$_3$, 2) determine the toxic effects, if any, of the lanthanum compound La(**L1**)$_3$ and 3) determine the efficacy of La(**L1**)$_3$ in the treatment of osteoporosis. These animal studies are based on three previous studies reported by Damment and co-workers[261-263] to investigate the distribution and pharmacokinetics of Fosrenol (lanthanum carbonate).

Investigations into the pharmacokinetic profiles by intravenous (IV) administration of the lanthanum compound, La($L1$)$_3$ are currently underway. The ongoing study involves the intravenous administration of three lanthanum compounds – two controls, LaCl$_3$ and La$_2$(CO$_3$)$_3$, and one test compound, La($L1$)$_3$. Lanthanum chloride will be administered at a constant dosage of 0.03 mg/kg/day, which in previous studies by Damment *et al.*[261] yielded a plasma concentration of 25 ng/mL after 28 d of daily administration. La$_2$(CO$_3$)$_3$ and La($L1$)$_3$ will be administered at three different dosages. The liver, kidney, spleen, brain and bone (femur) will be collected to determine the lanthanum ion concentration by inductively coupled plasma mass spectrometry (ICP-MS), to yield the exact molar concentration of lanthanum distribution in the rat's body. From these studies, not only can the accumulation in organs be determined, but also the half-life elimination parameters and toxicity.

The second study that will be carried out involves determining the pharmacokinetic profiles of the lanthanum compounds La$_2$(CO$_3$)$_3$ and La($L1$)$_3$ administered orally at proposed dosages of 250, 500 and 750 mg/kg over a period of 3 months. The dosing may change as a result of the previous IV studies. Again, the liver, kidneys, spleen, brain and bones (femur) will be collected and analyzed for their lanthanum ion concentration.

Lastly, a long term study will involve orally administering the lead compound La($L1$)$_3$ in OVX rats at three dosage levels over a period of 6 months. The proposed treatment is 2% w/w of food consumed per day, as this is comparable to the dosing previously administered for La$_2$(CO$_3$)$_3$ in experiments carried out by Damment *et al.*[262] To analyze toxicology, serum creatine, calcium and phosphorous levels will be examined throughout the study in order to monitor renal function.[264] Animals will be weighed daily in order to monitor daily dosing requirements.

Bone quality evaluations will be carried out in collaboration with a group in the UBC Materials Engineering. Bone architecture will be assessed on the lumbar spine (for trabecular bone architecture) and femur bone (for cortical bone architecture) with microcomputed tomography (μCT 35 from Scanco Medical, available at the Centre for Hip Health and

Mobility, UBC); μCT has been proven to be a powerful technique in assessing bone architecture in the OVX rat model.[265,266] Bone mineralization (change in the mineral content of the bone matrix) will be assessed by determining the lanthanum and calcium concentrations in the bone mineral by ICP-MS.

6.3   *Future Work*

6.3.1   Further *In Vitro* Bone Studies with Lanthanides and their Complexes

While extensive studies in this thesis have been carried out to examine the binding affinities of the free metal ions, free ligands and metal complexes with synthetic hydroxyapatite (HAP), there are differences between synthetic HAP and biological apatite. Synthetic calcium hydroxyapatite generally has a calcium to phosphorus stoichiometry of 1.67. Biological HAP (isolated from mammalian bone and teeth) does not usually exhibit this exact stoichiometric ratio.[267] Likewise, HAP isolated from animal bones has the advantage of preserving some of the inherent properties of the raw material such as chemical composition (i.e. inclusion of Mg^{2+}), bone defects and structure (i.e. crystal size).[268,269]

Isolation of animal HAP can be performed by obtaining animal bone sludge (deproteinized and defatted bone pulp). In order to remove organic substances, natural HAP is obtained by calcination (950–1050 °C) of the bone sludge to produce free HAP.[267,269] The animal bones can be isolated from food products as reported by Xiaoying *et al.*[269] where they isolated porcine HAP from pig meat obtained at a meat market; as animal HAP is easily accessible, this assay can be performed in the Orvig group laboratory. Analysis of the samples by powder X-ray diffraction (PXRD), Fourier transform infrared spectroscopy (FTIR), surface area analysis by nitrogen adsorption, and ICP-MS can help determine the structural and physical differences between animal and synthetic HAPs.[267-269]

In the studies involving HAP affinity, replacing synthetic HAP with animal HAP as a model for bone will give a more accurate *in vitro* measurement of the affinity of ligands, complexes and free metals.

6.3.2 Other Potential Chelators for the Delivery of Lanthanides to Bone

The lead compound identified in this work was $K_2La(\textbf{XT})$; despite the high log K_{ML} value of $H_5\textbf{XT}$ with La^{3+}, a binding affinity of $> 98\%$ lanthanum ion with HAP was observed. In developing the ideal chelator for the delivery of Ln^{3+} to bone, a balance needs to be found in identifying a chelator that forms a stable complex with the metal ion so that it does not get transchelated *in vivo* by calcium proteins, but conversely is labile enough that the lanthanide ions can be effectively bound by HAP. Moreover, the ideal chelator would also itself have an affinity for the bone mineral. Thus further investigations into hexa- hepta- and octadentate ligands to coordinate lanthanide ions, and deliver them to bone might be of interest.

There is a lot of literature precedent for chelators that form thermodynamically stable complexes with lanthanide(III) ions; a few are listed in Table 6.1 along with their log K_{ML} values. Phosphonate-derivatives of $H_4\textbf{EDTA}$, $H_5\textbf{DTPA}$ and $H_4\textbf{DOTA}$ might be of interest because of their bone seeking properties. Two such ligands, **EDTMP** and **DTPP**, which are phosphinate-derivatives of $H_4\textbf{EDTA}$[270] and $H_5\textbf{DTPA}$,[270] respectively, have successfully been coordinated to lanthanide ions (Figure 6.1). **EDTMP**, is a known bone seeking ligand and when coordinated to $^{153}Sm^{3+}$ is used in to treat bone pain caused by metastatic cancer.[66] Phosphonate-derivatives of $H_4\textbf{DOTA}$ may also be of interest because of their affinity for bone[271] and the high thermodynamic stability of the native ligand (Table 6.1) with lanthanide ions.[63,272]

Once synthesized, the *in vitro* binding affinities with synthetic or natural HAP can be studied, and the *in vitro* cell uptake and apparent permeabilities can be determined in Caco-2 cells, in an effort to establish if the molecule will be orally bioavailable.

Table 6.1. Log K_{ML} values of a variety of multidentate ligands with lanthanide ions (Ln^{3+} = La, Gd, Lu). H$_4$**EDTA** = ethylenediaminetetraacetic acid; H$_5$**DTPA** = diethylenetriaminepentaacetic acid; H$_4$**DOTA** = 1,4,7.10-tetrazacyclododecane-1,4,7,10-tetraacetic acid.
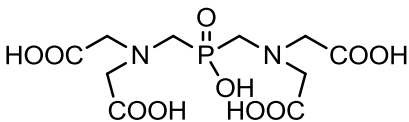
Compound	Log K_{ML} La^{3+}	Log K_{ML} Gd^{3+}	Log K_{ML} Lu^{3+}
H$_5$**XT**	13.0[127]	15.7[127]	n.d.
H$_4$**EDTA**	14.72[273]	17.7[274]	19.06[273]
H$_5$**DTPA**	19.1[275]	22.2[63]	22.6[276]
H$_4$**DOTA**	21.7[272]	25.3[63]	29.2[272]
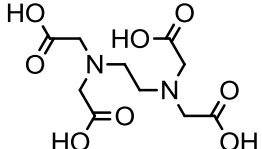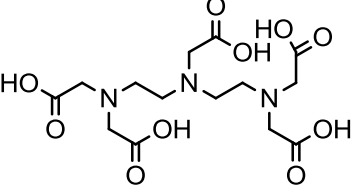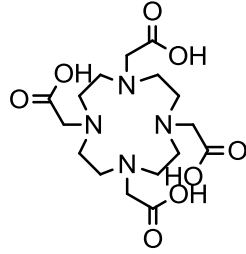
* n.d. – not determined
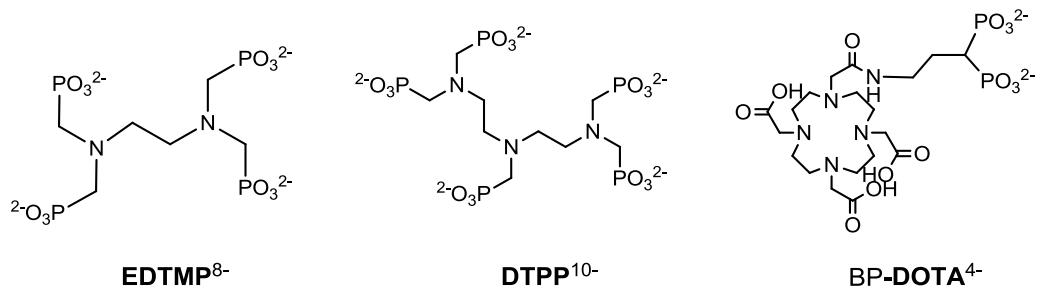
Figure 6.1. Possible acyclic (**EDTMP** and **DTPP**) and macrocyclic (BP-**DOTA**) chelators for Ln^{3+} ions. **EDTMP** = ethylenediaminetetra(methylene phosphonate)[270]; **DTPP** = diethylenetriaminepenta(methylene phosphonate)[270]; BP-**DOTA** = (3-(2-(4,7,10-tris(carboxymethyl)-1,4,7,10-tetraazacyclododecan-1-yl)acetamido)propane-1,1-diyl)bis(phosphonate).[271]

Bibliography

1.   Irnius, A.; Speiciene, D.; Tautkus, S.; Kareiva, A. *Mendeleev Commun.* **2007**, *17*, 216.

2.   Mawani, Y.; Orvig, C. Essential Metal Related Metabolic Disorders. In *Bioinorganic Medicinal Chemistry*; Alessio, E., Ed.; Wiley: New York, 2011; p 311.

3.   Simon, D. B.; Nelson-Williams, C.; Bia, M. J.; Ellison, D.; Karet, F. E.; Molina, A. M.; Vaara, I.; Iwata, F.; Cushner, H. M.; Koolen, M.; Gainza, F. J.; Gitelman, H. J.; Lifton, R. P. *Nat. Genet.* **1996**, *12*, 24.

4.   Baker, S. B.; Worthley, L. I. G. *Crit. Care Resusc.* **2002**, *4*, 307.

5.   Swaminathan, R. *Clin. Biochem. Rev.* **2003**, *24*, 47.

6.   Gassbeek, A.; Meinders, A. E. *Am. J. Med.* **2005**, *118*, 1094.

7.   Gennari, F. J. *Crit. Care Clin.* **2002**, *18*, 273.

8.   Silver, J.; Yalcindag, C.; Sela-Brown, A.; Kilav, R.; Naveh-Many, T. *Kidney Int.* **1999**, *56*, S2.

9.   Poole, K. E.; Reeve, J. *Curr. Opin. Pharm.* **2005**, *5*, 612.

10.   Maeda, S. S.; Fortes, E. M.; Oliveira, U. M.; Borba, V. C. Z.; Lazaretti-Castro, M. *Arq. Bras. Endocrinol. Metabol.* **2006**, *50*, 664.

11.   Bringhurst, F.; Demay, M.; Kronenberg, H. Hormones and Disorders of Mineral Metabolism. In *Williams Textbook of Endocrinology*; 11th Ed.; Kronenberg, H. M.; Melmed, S.; Polonsky, K. S.; Larsen, P. R., Eds.; Saunders/Elsevier: Philadelphia, 2008; p 1203.

12.   Wilson, L. C.; Trembath, R. C. *J. Med. Genet.* **1994**, *31*, 779.

13.   Weinstein, L. S. Albright Hereditary Osteodystrophy, Pseudohypoparathyroidism and G_s Deficiency. In *G Proteins, Receptors, and Disease*; Spiegel, A. M., Ed.; Humana: New Jersey, 1998; p 23.

14.   Ahmad, R.; Hammond, J. M. *Otolaryngol. Clin. North Am.* **2004**, *37*, 701.

15.   Khan, A.; Bilezikian, J. *Can. Med. Assoc. J.* **2000**, *163*, 184.

16.   de Francisco, A. L. M. *Clin. Ther.* **2004**, *26*, 1976.

17.   Lips, P. *Prog. Biophys. Mol. Biol.* **2006**, *92*, 4.

18.   Fordtran, J. S.; Rector, F. C.; Carter, N. W. *J. Clin. Invest.* **1968**, *47*, 884.

19.   Ishikawa, S.; Schrier, R. W. *Clin. Endocrinol. (Oxf).* **2003**, *58*, 1.

20.   Reynolds, R. M.; Padfield, P. L.; Seckl, J. R. *Br. Med. J.* **2006**, *332*, 702.

21.   Bourgognie, J. J.; Oster, J. R.; Perez, G. O.; Green, D. F. Disorders of Potassium Metabolism. In *Therapy of Renal Diseases and Related Disorders*; 2 Ed.; Suki, W. N.; Massry, S. G., Eds.; Kluwer Academic: Norwell, 1991; p 45.

22.   Kratz, A.; Ferraro, M.; Sluss, P. M.; Lewandrowski, K. B. *N. Engl. J. Med.* **2004**, *351*, 1548.

23.   Weisinger, J. R.; Bellorín-Font, E. *Lancet* **1998**, *352*, 391.

24.   Baker, S. B.; Worthley, L. I. G. *Crit. Care Resusc.* **2002**, *4*, 301.

25.   Vormann, J. *Mol. Aspects Med.* **2003**, *24*, 27.

26.   Bugg, N. C.; Jones, J. A. *Anaesthesia* **1998**, *53*, 895.

27.   Stoff, J. S. *Am. J. Med.* **1982**, *72*, 489.

28.   Garg, R. K.; Tandon, N. *Indian J. Pediatr.* **1999**, *66*, 849.

29.   Mornet, E. *Hum. Mutat.* **2000**, *15*, 309.

30.   Whyte, M. P.; Murphy, W. A.; Fallon, M. D. *Am. J. Med.* **1982**, *72*, 631.

31.   Lam, A.; Lam, C.; Tang, M.; Chu, J.; Lam, S. *Hong Kong J. Paediatr.* **2006**, *11*, 341.

32.   Davidson, M. B.; Thakkar, S.; Hix, J. K.; Bhandarkar, N. D.; Wong, A.; Schreiber, M. J. *Am. J. Med.* **2004**, *116*, 546.

33.   Bosch, X.; Poch, E.; Grau, J. M. *N. Engl. J. Med.* **2009**, *361*, 62.

34.   Vanholder, R.; Sever, M. S.; Erek, E.; Lameire, N. *J. Am. Soc. Nephrol.* **2000**, *11*, 1553.

35. Kozack, J. K.; MacIntyre, D. L. *Phys. Ther.* **2001**, *81*, 945.

36. Locatelli, F.; Cannata-Andía, J. B.; Drüeke, T. B.; Hörl, W. H.; Fouque, D.; Heimburger, O.; Ritz, E. *Nephrol. Dial. Transplant.* **2002**, *17*, 723.

37. Kirk, T. S.; Simon, M. A. *J. Bone Joint Surg. Am.* **1981**, *63*, 1167.

38. Watts, N. B. *Endocrinol. Metab. Clin. North Am.* **1998**, *27*, 419.

39. Mohammed, I. A.; Hutchison, A. J. *Ther. Clin. Risk Manag.* **2008**, *4*, 887.

40. Schucker, J. J.; Ward, K. E. *Am. J. Health. Syst. Pharm.* **2005**, *62*, 2355.

41. Hauschka, P. V.; Mavrakos, A. E.; Iafrati, M. D.; Doleman, S. E.; Klagsbrun, M. *J. Biol. Chem.* **1986**, *261*, 2665.

42. Raisz, L. G. *Clin. Chem.* **1999**, *45*, 1353.

43. Sambrook, P. Osteoporosis B. Pathology and Pathophysiology. In *Primer on the Rheumatic Diseases*; Klippel, J. H.; Stone, J. H.; Crofford, L. J.; White, P. H., Eds.; Springer: New York, 2008; p 584.

44. Hadjidakis, D. J.; Androulakis, I. I. Bone Remodelling. In *Women's Health and Disease: Gynecologic, Endocrine, and Reproductive Issues*; Creatsas, G.; Mastorakos, G.; Chrousos, G. P., Eds.; Wiley-Blackwell: Hoboken, 2006; Vol. 1092, p 385.

45. Walsh, J. S.; Fairley, J. A. *J. Am. Acad. Dermatol.* **1995**, *33*, 693.

46. Baker, S. B.; Worthley, L. I. G. *Critical Care and Resuscitation* **2002**, *4*, 307.

47. Jacobs, T. P.; Bilezikian, J. P. *J. Clin. Endocrinol. Metab.* **2005**, *90*, 6316.

48. Eisman, J. A. *Baillieres Clin. Endocrinol. Metab.* **1988**, *2*, 125.

49. Basha, B.; Rao, D. S.; Han, Z.-H.; Parfitt, A. M. *Am. J. Med.* **2000**, *108*, 296.

50. Ralston, S. H.; Langston, A. L.; Reid, I. R. *Lancet* **2008**, *372*, 155.

51. Altman, R. D. Paget's Disease of Bone. In *Primer on the Rheumatic Diseases*; Klippel, J. H.; Stone, J. H.; Crofford, L. J.; White, P. H., Eds.; Springer: New York, 2008; p 573.

52.   Osteoporosis. *Government of Canada* 2008 (Accessed: May 23, 2012, http://www.biobasics.gc.ca/english/view.asp?x=770).

53.   Beall, D. P.; Henslee, H. B.; Webb, H. R.; Scofield, R. H. *Am. J. Med. Sci.* **2006**, *331*, 233.

54.   Caruso, J. B.; Patel, R. M.; Julka, K.; Parish, D. C. *J. Gen. Intern. Med.* **2007**, *22*, 1053.

55.   Hussmann, J.; Russell, R. C.; Kucan, J. O.; Khardori, R.; Steinau, H. U. *Ann. Plast. Surg.* **1995**, *34*, 138.

56.   Hussein, M.-R. A.; Ali, H. O.; Abdulwahed, S. R.; Argoby, Y.; Tobeigei, F. H. *Exp. Mol. Pathol.* **2009**, *86*, 134.

57.   Jakupec, M. A.; Unfried, P.; Keppler, B. K. *Rev. Physiol. Biochem. Pharmacol.* **2005**, *153*, 101.

58.   Holden, N. E.; Coplen, T. *Chem. Int. (IUPAC)* **2004**, *26*.

59.   Kagan, H. B.; Sasaki, M.; Collin, J. *Pure Appl. Chem.* **1988**, *60*, 1725.

60.   Shannon, R. D. *Acta Crystallogr., Sect. A: Found. Crystallogr.* **1976**, *32*, 751.

61.   Evans, C. H. *Trends Biochem. Sci* **1983**, *8*, 445.

62.   Fricker, S. P. *Chem. Soc. Rev.* **2006**, *35*, 524.

63.   Hermann, P.; Kotek, J.; Kubicek, V.; Lukes, I. *Dalton Trans.* **2008**, 3027.

64.   Darrah, T. H.; Prutsman-Pfeiffer, J. J.; Poreda, R. J.; Campbell, M. E.; Hauschka, P. V.; Hannigan, R. E. *Metallomics* **2009**, *1*, 479.

65.   Finlay, O. G.; Mason, M. D.; Shelley, M. *Lancet Oncol.* **2005**, *6*, 392.

66.   Anderson, P. *Expert Opin. Pharmacother.* **2006**, *7*, 1475.

67.   Murrer, B. A.; Powell, N. A. Pharmaceutical Composition Containing Selected Lanthanum Carbonate Hydrates. Canadian Patent 2,221,437, Oct. 3, 1996.

68.   Birnbaum, E. R.; Gomez, J. E.; Darnall, D. W. *J. Am. Chem. Soc.* **1970**, *92*, 5287.

69.   Pidcock, E.; Moore, G. R. *J. Biol. Inorg. Chem.* **2001**, *6*, 479.

70.   Williams, R. J. P. *Quart. Rev. Chem. Soc.* **1970**, *24*, 331.

71.   Barta, C. A.; Sachs-Barrable, K.; Jia, J.; Thompson, K. H.; Wasan, K. M.; Orvig, C. *Dalton Trans.* **2007**, 5019.

72.   Durbin, P. W.; Williams, M. H.; Gee, M.; Newman, R. H.; Hamilton, J. G. *Proc. Soc. Exp. Biol. Med.* **1956**, *91*, 78.

73.   Haley, T. J. Toxicity. In *Handbook on the physics and chemistry of rare earths*; K A Gschneider, J.; Eyring, L., Eds.; North-Holland: Amsterdam, 1979; Vol. 4, p 553.

74.   Magnusson, G. *Acta Pharmacol. Toxicol. (Copenh).* **1963**, *20*, 5.

75.   Eastell, R. *N. Engl. J. Med.* **1998**, *338*, 736.

76.   Kates, S. L.; Kates, O. S.; Mendelson, D. A. *Injury* **2007**, *38*, 17.

77.   Mauck, K. F.; Clarke, B. L. *Mayo Clin. Proc.* **2006**, *81*, 662.

78.   Raisz, L. G. *J. Clin. Invest.* **2005**, *115*, 3318.

79.   Mosca, L.; Grady, D.; Barrett-Connor, E.; Collins, P.; Wenger, N.; Abramson, B. L.; Paganini-Hill, A.; Geiger, M. J.; Dowsett, S. A.; Amewou-Atisso, M.; Kornitzer, M. *Stroke* **2009**, *40*, 147.

80.   Riggs, B. L.; Melton, L. J. *N. Engl. J. Med.* **1992**, *327*, 620.

81.   Sweet, M.; Sweet, J.; Jeremiah, M.; Galazka, S. *Am. Fam. Physician* **2009**, *79*, 193.

82.   Brown, J. P.; Fortier, M. *J. Obstet. Gynaecol. Can.* **2006**, *FEBRUARY*, S95.

83.   Patton, J. S. *Adv. Drug Del. Rev.* **2000**, *42*, 239.

84.   Skarpos, H.; Osipov, S. N.; Vorob'eva, D. V.; Odinets, I. L.; Lork, E.; Roschenthaler, G. V. *Org. Biomol. Chem.* **2007**, *5*, 2361.

85.   Guenin, E.; Monteil, M.; Bouchemal, N.; Prange, T.; Lecouvey, M. *Eur. J. Org. Chem.* **2007**, 3380.

86.   Saag, K. G.; Shane, E.; Boonen, S.; Marín, F.; Donley, D. W.; Taylor, K. A.; Dalsky, G. P.; Marcus, R. *N. Engl. J. Med.* **2007**, *357*, 2028.

87. Hodsman, A. B.; Bauer, D. C.; Dempster, D. W.; Dian, L.; Hanley, D. A.; Harris, S. T.; Kendler, D. L.; McClung, M. R.; Miller, P. D.; Olszynski, W. P.; Orwoll, E.; Yuen, C. K. *Endocr. Rev.* **2005**, *26*, 688.

88. Hoffman, A.; Stepensky, D.; Ezra, A.; Van Gelder, J. M.; Golomb, G. *Int. J. Pharm.* **2001**, *220*, 1.

89. Khosla, S.; Burr, D.; Cauley, J.; Dempster, D. W.; Ebeling, P. R.; Felsenberg, D.; Gagel, R. F.; Gilsanz, V.; Guise, T.; Koka, S.; McCauley, L. K.; McGowan, J.; McKee, M. D.; Mohla, S.; Pendrys, D. G*., et al. J. Bone Miner. Res.* **2007**, *22*, 1479.

90. Boivin, G. Y.; Chavassieux, P. M.; Santora, A. C.; Yates, J.; Meunier, P. J. *Bone* **2000**, *27*, 687.

91. Burr, D. B.; Miller, L.; Grynpas, M.; Li, J. L.; Boyde, A.; Mashiba, T.; Hirano, T.; Johnston, C. C. *Bone* **2003**, *33*, 960.

92. Meunier, P. J.; Boivin, G. *Bone* **1997**, *21*, 373.

93. Mashiba, T.; Turner, C. H.; Hirano, T.; Forwood, M. R.; Johnston, C. C.; Burr, D. B. *Bone* **2001**, *28*, 524.

94. Turner, C. H. *Osteoporos. Int.* **2002**, *13*, 97.

95. Cramer, J. A.; Amonkar, M. M.; Hebborn, A.; Altman, R. *Curr. Med. Res. Opin.* **2005**, *21*, 1453.

96. Cramer, J. A.; Gold, D. T.; Silverman, S. L.; Lewiecki, E. M. *Osteoporos. Int.* **2007**, *18*, 1023.

97. Tanvetyanon, T.; Stiff, P. J. *Ann. Oncol.* **2006**, *17*, 897.

98. Conte, P.; Guarneri, V. *Oncologist* **2004**, *9*, 28.

99. Reid, I. R.; Brown, J. P.; Burckhardt, P.; Horowitz, Z.; Richardson, P.; Trechsel, U.; Widmer, A.; Devogelaer, J.; Kaufman, J.; Jaeger, P.; Body, J.; Meunier, P. J. *N. Engl. J. Med.* **2002**, *346*, 653.

100. Grynpas, M. D.; Hamilton, E.; Cheung, R.; Tsouderos, Y.; Deloffre, P.; Hott, M.; Marie, P. J. *Bone* **1996**, *18*, 253.

101. Marie, P. J. *Bone* **2006**, *38*, S10.

102. Meunier, P. J.; Roux, C.; Seeman, E.; Ortolani, S.; Badurski, J. E.; Spector, T. D.; Cannata, J.; Balogh, A.; Lemmel, E. M.; Pors-Nielsen, S.; Rizzoli, R.; Genant, H. K.; Reginster, J. Y.; Graham, J.; Ng, K. W.*, et al. N. Engl. J. Med.* **2004**, *350*, 459.

103. Atherton, N. D.; Totten, J. W.; Gaitonde, M. D. Treatment of Bone Disorders. US Patent 7,078,059, Jul 18, 2006.

104. Research Rounds: In Europe, Fosrenol Indication Extended to Include Chronic Kidney Disease. *Nephrology Times* Nov. 2009 (Accessed: May 23, 3012, http://journals.lww.com/nephrologytimes/Fulltext/2009/11000/Research_Rounds.10.aspx).

105. Barnato, S.; Sprague, S. *Curr. Rheumatol. Rep.* **2009**, *11*, 185.

106. FDA Experts See Merit in Extending Kidney Drug Use *Reuters* Oct. 16, 2007 (Accessed: May 23, 2012, http://www.reuters.com/article/2007/10/16/fda-phosphate-idUSN1622525820071016).

107. Damment, S. J. P.; Webster, I. *J. Am. Soc. Nephrol.* **2003**, *14*, 204A.

108. Queiros, C.; Amorim, M. J.; Leite, A.; Ferreira, M.; Gameiro, P.; de Castro, B.; Biernacki, K.; Magalhaes, A.; Burgess, J.; Rangel, M. *Eur. J. Inorg. Chem.* **2011**, 131.

109. Burgess, J.; Rangel, M.; Rudi van, E. Hydroxypyranones, hydroxypyridinones, and their complexes. In *Advances in Inorganic Chemistry*; Academic: 2008; Vol. 60, p 167.

110. Zborowski, K.; Gryboś, R.; Proniewicz, L. M. *J. Mol. Struct.-THEOCHEM* **2003**, *639*, 87.

111. Thompson, K. H.; Lichter, J.; LeBel, C.; Scaife, M. C.; McNeill, J. H.; Orvig, C. *J. Inorg. Biochem.* **2009**, *103*, 554.

112. Yokel, R. A. *Coord. Chem. Rev.* **2002**, *228*, 97.

113. Santos, M. A.; Gil, M.; Gano, L.; Chaves, S. *J. Biol. Inorg. Chem.* **2005**, *10*, 564.

114. Hider, R. C.; Zhou, T. *Ann. N. Y. Acad. Sci.* **2005**, *1054*, 141.

115. FDA approves Ferriprox to treat patients with excess iron in the body. *U.S. Food and Drug Administration* Oct. 14, 2011.

116. Cohen, S. M.; Xu, J.; Radkov, E.; Raymond, K. N.; Botta, M.; Barge, A.; Aime, S. *Inorg. Chem.* **2000**, *39*, 5747.

117. Doble, D. M. J.; Melchior, M.; O'Sullivan, B.; Siering, C.; Xu, J. D.; Pierre, V. C.; Raymond, K. N. *Inorg. Chem.* **2003**, *42*, 4930.

118. Gorden, A. E. V.; Xu, J.; Raymond, K. N.; Durbin, P. *Chem. Rev.* **2003**, *103*, 4207.

119. Porter, J. B.; Gyparaki, M.; Burke, L. C.; Huehns, E. R.; Sarpong, P.; Saez, V.; Hider, R. C. *Blood* **1988**, *72*, 1497.

120. Russell, R. G. G. *Ann. N. Y. Acad. Sci.* **2006**, *1068*, 367.

121. Zhang, S. F.; Gangal, G.; Uludag, H. *Chem. Soc. Rev.* **2007**, *36*, 507.

122. Epstein, N. A.; Horton, J. L.; Vogels, C. M.; Taylor, N. J.; Westcott, S. A. *Aust. J. Chem.* **2000**, *53*, 687.

123. Zhang, Z.; Rettig, S. J.; Orvig, C. *Can. J. Chem.* **1992**, *70*, 763

124. Kontoghiorghes, G. J.; Sheppard, L. *Inorg. Chim. Acta* **1987**, *136*, L11.

125. Nelson, W. O.; Karpishin, T. B.; Rettig, S. J.; Orvig, C. *Can. J. Chem.* **1988**, *66*, 123.

126. Dobbin, P. S.; Hider, R. C.; Hall, A. D.; Taylor, P. D.; Sarpong, P.; Porter, J. B.; Xiao, G.; van der Helm, D. *J. Med. Chem.* **1993**, *36*, 2448.

127. Xu, L.; Rettig, S. J.; Orvig, C. *Inorg. Chem.* **2001**, *40*, 3734.

128. Gran, G. *Analyst* **1952**, *77*, 661.

129. Barnum, D. W. *Inorg. Chem.* **1983**, *22*, 2297.

130. Baes, C. F.; Mesmer, R. E. *The Hydrolysis of Cations*. Wiley: 1976.

131. Gans, P.; Sabatini, A.; Vacca, A. *Talanta* **1996**, *43*, 1739.

132. Elkaschef, M. A.-F.; Nosseir, M. H. *J. Am. Chem. Soc.* **1960**, *82*, 4344.

133. Widler, L.; Jaeggi, K. A.; Glatt, M.; Muller, K.; Bachmann, R.; Bisping, M.; Born, A. R.; Cortesi, R.; Guiglia, G.; Jeker, H.; Klein, R.; Ramseier, U.; Schmid, J.; Schreiber, G.; Seltenmeyer, Y.*, et al. J. Med. Chem.* **2002**, *45*, 3721.

134. Kieczykowski, G. R.; Jobson, R. B.; Melillo, D. G.; Reinhold, D. F.; Grenda, V. J.; Shinkai, I. *J. Org. Chem.* **1995**, *60*, 8310.

135. Egorov, M.; Fortun, Y.; Heymann, D.; Lebreton, J.; Mathe, M.; Padrines, M.; Redini, F. Procede de synthese de derives d'Acide hydroxy-bisphosphonique. European Patent 2,240,500, Oct. 20, 2010.

136. Mehdipour-Ataei, S.; Babanzadeh, S. *Appl. Organomet. Chem.* **2007**, *21*, 360.

137. Mukherjee, S.; Song, Y.; Oldfield, E. *J. Am. Chem. Soc.* **2008**, *130*, 1264.

138. Kotsikorou, E.; Song, Y.; Chan, J. M. W.; Faelens, S.; Tovian, Z.; Broderick, E.; Bakalara, N.; Docampo, R.; Oldfield, E. *J. Med. Chem.* **2005**, *48*, 6128.

139. Montserat, J.; Chen, L.; Lawrence, D. S.; Zhang, Z.-Y. *J. Biol. Chem.* **1996**, *271*, 7868.

140. Frenkel, S. R.; Jaffe, W. L.; Valle, C. D.; Jazrawi, L.; Maurer, S.; Baitner, A.; Wright, K.; Sala, D.; Hawkins, M.; Di Cesare, P. E. *J. Biomed. Mater. Res.* **2001**, *58*, 645.

141. Daniel, R., Update: Teva: 2 courts revoke Merck alendronate patent. *The Wall Street Journal* February 25, 2008.

142. Yamauchi, K.; Tanabe, T.; Kinoshita, M. *J. Org. Chem.* **1976**, *41*, 3691.

143. McGuigan, C.; Pathirana, R. N.; Migliore, M.; Adak, R.; Luoni, G.; Jones, A. T.; Díez-Torrubia, A.; Camarasa, M.-J.; Velázquez, S.; Henson, G.; Verbeken, E.; Sienaert, R.; Naesens, L.; Snoeck, R.; Andrei, G.*, et al. J. Antimicrob. Chemother.* **2007**, *60*, 1316.

144. Bello, A. M.; Poduch, E.; Liu, Y.; Wei, L.; Crandall, I.; Wang, X.; Dyanand, C.; Kain, K. C.; Pai, E. F.; Kotra, L. P. *J. Med. Chem.* **2008**, *51*, 439.

145. Aguilar-Pérez, F.; Gómez-Tagle, P.; Collado-Fregoso, E.; Yatsimirsky, A. K. *Inorg. Chem.* **2006**, *45*, 9502.

146. Nelson, W. O.; Karpishin, T. B.; Rettig, S. J.; Orvig, C. *Inorg. Chem.* **1988**, *27*, 1045.

147. Katritzky, A. R.; Jones, R. A. *J. Chem. Soc.* **1960**, 2947.

148. Cook, D. *Can. J. Chem.* **1963**, *41*, 2575.

149. Mazdiyasni, K. S.; Brown, L. M. *Inorg. Chem.* **1970**, *9*, 2783.

150.	Clevette, D. J.; Lyster, D. M.; Nelson, W. O.; Rihela, T.; Webb, G. A.; Orvig, C. *Inorg. Chem.* **1990**, *29*, 667.

151.	Motekaitis, R. J.; Martell, A. E. *Inorg. Chim. Acta* **1991**, *183*, 71.

152.	Kline, M. A.; Orvig, C. *Clin. Chem.* **1992**, *38*, 562.

153.	Epstein, M.; Levitzki, A.; Reuben, J. *Biochemistry* **1974**, *13*, 1777.

154.	Zhang, J. C.; Xu, S. J.; Wang, K.; Yu, S. F. *Chin. Sci. Bull.* **2003**, *48*, 2170.

155.	Zhang, J.; Liu, C.; Li, Y.; Sun, J.; Wang, P.; Di, K.; Zhao, Y. *J. Rare Earth* **2010**, *28*, 138.

156.	Mosmann, T. *J. Immunol. Methods* **1983**, *65*, 55.

157.	Buttke, T. M.; McCubrey, J. A.; Owen, T. C. *J. Immunol. Methods* **1993**, *157*, 233.

158.	Lajeunesse, D. *Bone Miner.* **1994**, *24*, 1.

159.	Wohnsland, F.; Faller, B. *J. Med. Chem.* **2001**, *44*, 923.

160.	Wenlock, M. C.; Austin, R. P.; Barton, P.; Davis, A. M.; Leeson, P. D. *J. Med. Chem.* **2003**, *46*, 1250.

161.	Lipinski, C. A. *J. Pharmacol. Toxicol. Methods* **2000**, *44*, 235.

162.	Bhal, S. K.; Kassam, K.; Peirson, I. G.; Pearl, G. M. *Mol. Pharm.* **2007**, *4*, 556.

163.	Meunier, V.; Bourrié, M.; Berger, Y.; Fabre, G. *Cell Biol. Toxicol.* **1995**, *11*, 187.

164.	Rubas, W.; Cromwell, M. E. M. *Adv. Drug Del. Rev.* **1997**, *23*, 157.

165.	OECD Test No. 107: Partition Coefficient (n-octanol/water): Shake Flask Method. In *OECD Guidelines for the Testing of Chemicals, Section 1*; OECD Publishing: 1995; p 1.

166.	Walker, J. M. The Bicinchoninic Acid (BCA) Assay for Protein Quantitation. In *The Protein Protocols Handbook*; 2nd Ed.; Walker, J. M., Ed.; Humana: Totawa, 2002; p 11.

167.	Xue, Z.; Lin, M.; Zhu, J.; Zhang, J.; Li, Y.; Guo, Z. *Chem. Commun.* **2010**, *46*, 1212.

168. Huang, C.-Y.; Lee, C.-Y.; Chen, M.-Y.; Tsai, H.-C.; Hsu, H.-C.; Tang, C.-H. *J. Cell. Physiol.* **2010**, *224*, 475.

169. Product Information Sheet for CRL-11372. http://www.atcc.org/attachments/17494.pdf.

170. Ezra, A.; Hoffman, A.; Breuer, E.; Alferiev, I. S.; Mönkkönen, J.; El Hanany-Rozen, N.; Weiss, G.; Stepensky, D.; Gati, I.; Cohen, H.; Törmälehto, S.; Amidon, G. L.; Golomb, G. *J. Med. Chem.* **2000**, *43*, 3641.

171. Huang, X.-P.; Spino, M.; Thiessen, J. *Pharm. Res.* **2006**, *23*, 280.

172. Artursson, P.; Karlsson, J. *Biochem. Biophys. Res. Commun.* **1991**, *175*, 880.

173. Yan, Z.; Sun, J.; Chang, Y.; Liu, Y.; Fu, Q.; Xu, Y.; Sun, Y.; Pu, X.; Zhang, Y.; Jing, Y.; Yin, S.; Zhu, M.; Wang, Y.; He, Z. *Mol. Pharm.* **2011**, *8*, 319.

174. Yazdanian, M.; Glynn, S. L.; Wright, J. L.; Hawi, A. *Pharm. Res.* **1998**, *15*, 1490.

175. Baranov, V. I.; Quinn, Z. A.; Bandura, D. R.; Tanner, S. D. *J. Anal. At. Spectrom.* **2002**, *17*, 1148.

176. Steele, D. G.; Bramblett, C. A. Indroduction to the Study of Human Skeletal Anatomy. In *The Anatomy and Biology of the Human Skeleton*; Texas A&M University: 1988; p 3.

177. Clarke, B. *Clin. J. Am. Soc. Nephro.* **2008**, *3*, S131.

178. Seeman, E.; Delmas, P. D. *N. Engl. J. Med.* **2006**, *354*, 2250.

179. Steele, D. G.; Bramblett, C. A. Bone Biology. In *The Anatomy and Biology of the Human Skeleton*; Texas A&M University: 1988; p 10.

180. Miller, A.; Parker, S. B. *Philos. Trans. R. Soc. Lond., Ser. B: Biol. Sci.* **1984**, *304*, 455.

181. Viguet-Carrin, S.; Garnero, P.; Delmas, P. *Osteoporos. Int.* **2006**, *17*, 319.

182. Hernandez, C. J.; Keaveny, T. M. *Bone* **2006**, *39*, 1173.

183. Malluche, H. H.; Mawad, H.; Monier-Faugere, M.-C. *Clin. J. Am. Soc. Nephro.* **2008**, *3*, S157.

184. D'Haese, P. C.; Spasovski, G. B.; Sikole, A.; Hutchison, A.; Freemont, T. J.; Sulkova, S.; Swanepoel, C.; Pejanovic, S.; Djukanovic, L.; Balducci, A.; Coen, G.; Sulowicz, W.; Ferreira, A.; Torres, A.; Curic, S., *et al. Kidney Int.* **2003**, *63*, S73.

185. Malluche, H. H.; Siami, G. A.; Swanepoel, C.; Wang, G. H.; Mawad, H.; Confer, S.; Smith, M.; Pratt, R. D.; Monier-Faugere, M.-C. *Clin. Nephrol.* **2008**, *70*, 284.

186. Tanizawa, Y.; Sawamura, K.; Suzuki, T. *J. Chem. Soc., Faraday Trans.* **1990**, *86*.

187. Collys, K.; Slop, D.; Delanghe, L.; Coomans, D. *J. Dent. Res.* **1990**, *69*, 458.

188. Wegehaupt, F. J.; Sener, B.; Attin, T.; Schmidlin, P. R. *Arch. Oral Biol.* **2010**, *55*, 441.

189. Murphy, M. B.; Hartgerink, J. D.; Goepferich, A.; Mikos, A. G. *Biomacromolecules* **2007**, *8*, 2237.

190. Diegmueller, J. J.; Cheng, X.; Akkus, O. *Cryst. Growth Des.* **2009**, *9*, 5220.

191. Ogawa, K.; Mukai, T.; Inoue, Y.; Ono, M.; Saji, H. *J. Nucl. Med.* **2006**, *47*, 2042.

192. Sing, K. S. W.; Everett, D. H.; Haul, R. A. W.; Moscou, L.; Pierotti, R. A.; Rouquérol, J.; Siemieniewska, T. *Pure Appl. Chem.* **1985**, *57*, 603.

193. Spasovski, G. B.; Sikole, A.; Gelev, S.; Masin-Spasovska, J.; Freemont, T.; Webster, I.; Gill, M.; Jones, C.; De Broe, M. E.; D'Haese, P. C. *Nephrol. Dial. Transplant.* **2006**, *21*, 2217.

194. Behets, G. J.; Verberckmoes, S. C.; Oste, L.; Bervoets, A. R.; Salome, M.; Cox, A. G.; Denton, J.; De Broe, M. E.; D'Haese, P. C. *Kidney Int.* **2005**, *67*, 1830.

195. Hulanicki, A.; Glab, S.; Ackermann, G. *Pure Appl. Chem.* **1983**, *55*, 1137.

196. Ali, M.; Woods, M.; Suh, E.; Kovacs, Z.; Tircsó, G.; Zhao, P.; Kodibagkar, V.; Sherry, A. *J. Biol. Inorg. Chem.* **2007**, *12*, 855.

197. Gaidamauskas, E.; Parker, H.; Kashemirov, B. A.; Holder, A. A.; Saejueng, K.; McKenna, C. E.; Crans, D. C. *J. Inorg. Biochem.* **2009**, *103*, 1652.

198. Lyle, S. J.; Rahman, M. M. *Talanta* **1963**, *10*, 1177.

199. Wang, D.; Miller, S.; Sima, M.; Kopekova, P.; Kopecek, J. *Bioconj. Chem.* **2003**, *14*, 853.

200. Marma, M. S.; Xia, Z.; Stewart, C.; Coxon, F.; Dunford, J. E.; Baron, R.; Kashemirov, B. A.; Ebetino, F. H.; Triffitt, J. T.; Russell, R. G. G.; McKenna, C. E. *J. Med. Chem.* **2007**, *50*, 5967.

201. Freire, E.; Mayorga, O. L.; Straume, M. *Anal. Chem.* **1990**, *62*, 950A.

202. Freyer, M. W.; Lewis, E. A. Isothermal Titration Calorimetry: Experimental Design, Data Analysis, and Probing Macromolecule/Ligand Binding and Kinetic Interactions. In *Methods Cell Biol.*; Correia, J. J.; Detrich, c. W., Eds.; Academic: Salt Lake City, 2008; Vol. 84, p 79.

203. Mukherjee, S.; Huang, C.; Guerra, F.; Wang, K.; Oldfield, E. *J. Am. Chem. Soc.* **2009**, *131*, 8374.

204. Hughes, J. M.; Cameron, M.; Crowley, K. D. *Am. Mineral.* **1989**, *74*, 870.

205. Bigi, A.; Boanini, E.; Capuccini, C.; Gazzano, M. *Inorg. Chim. Acta* **2007**, *360*, 1009.

206. Wakamura, M.; Kandori, K.; Ishikawa, T. *Colloids Surf. Physicochem. Eng. Aspects* **1998**, *142*, 107.

207. Serret, A.; Cabañas, M. V.; Vallet-Regí, M. *Chem. Mater.* **2000**, *12*, 3836.

208. Zhu, K.; Yanagisawa, K.; Shimanouchi, R.; Onda, A.; Kajiyoshi, K. *J. Eur. Ceram. Soc.* **2006**, *26*, 509.

209. Verbeeck, R.; Lassuyt, C.; Heijligers, H.; Driessens, F.; Vrolijk, J. *Calcif. Tissue Int.* **1981**, *33*, 243.

210. Get'man, E. I.; Loboda, S. N.; Tkachenko, T. V.; Ignatov, A. V.; Zabirko, T. F. *Functional Materials* **2005**, *12*, 6.

211. Suzuki, T.; Hatsushika, T.; Hayakawa, Y. *J. Chem. Soc., Faraday Trans. 1* **1981**, *77*.

212. Suzuki, T.; Hatsushika, T.; Miyake, M. *J. Chem. Soc., Faraday Trans. 1* **1982**, *78*.

213. Takeuchi, Y.; Arai, H. *J. Chem. Eng. Japan* **1990**, *23*, 75.

214. Lazić, S.; Vuković, Ž. *J. Radioanal. Nucl. Chem.* **1991**, *149*, 161.

215. Jeanjean, J.; Vincent, U.; Fedoroff, M. *J. Solid State Chem.* **1994**, *108*, 68.

216. Matsunaga, K.; Inamori, H.; Murata, H. *Phys. Rev. B: Condens. Matter* **2008**, *78*.

217. Li, Y.; Ooi, C. P.; Cheang, P. H. N.; Aik Khor, K. *Int. J. Appl. Ceram. Technol.* **2009**, *6*, 501.

218. Feng, Z. D.; Liao, Y. M.; Ye, M. *J. Mater. Sci. Mater. Med.* **2005**, *16*, 417.

219. Assaaoudi, H.; Ennaciri, A.; Rulmont, A. *Vib. Spectrosc* **2001**, *25*, 81.

220. Hikichi, Y.; Hukuo, K. I.; Shiokawa, J. *Bull. Chem. Soc. Jpn.* **1978**, *51*, 3645.

221. Patra, C. R.; Alexandra, G.; Patra, S.; Jacob, D. S.; Gedanken, A.; Landau, A.; Gofer, Y. *New J. Chem.* **2005**, *29*, 733.

222. Lucas, S.; Champion, E.; Bregiroux, D.; Bernache-Assollant, D.; Audubert, F. *J. Solid State Chem.* **2004**, *177*, 1302.

223. Fleet, M. E.; Liu, X. Y.; Pan, Y. M. *Am. Mineral.* **2000**, *85*, 1437.

224. Mooney, R. C. L. *Acta Crystallogr.* **1950**, *3*, 337.

225. Hatcher, H.; Planalp, R.; Cho, J.; Tortia, F. M.; Torti, S. V. *Cell. Mol. Life Sci.* **2008**, *65*, 1631.

226. Chattopadhyay, I.; Biswas, K.; Bandyopadhyay, U.; Banerjee, R. K. *Curr. Sci.* **2004**, *87*, 44.

227. Aggarwal, B. B.; Bhatt, I. D.; Ichikawa, H.; Ahn, K. S.; Sethi, G.; Santosh K. Sandur; Natarajan, C.; Seeram, N.; Shishodia, S. Curcumin — Biological and Medicinal Properties. In *Turmeric: The Genus Curcuma*; Ravindran, P. N.; Babu, K. N.; Sivaraman, K., Eds.; Taylor & Francis Group: Boca Ranton, 2007; p 297.

228. Payton, F.; Sandusky, P.; Alworth, W. L. *J. Nat. Prod.* **2007**, *70*, 143.

229. Bernabé-Pineda, M.; Ramírez-Silva, M. T.; Romero-Romo, M.; González-Vergara, E.; Rojas-Hernández, A. *Spectrochim. Acta, Part A* **2004**, *60*, 1091.

230. Mancuso, C.; Bates, T. E.; Butterfield, D. A.; Calafato, S.; Cornelius, C.; De Lorenzo, A.; Kostova, A. T. D.; Calabrese, V. *Expert Opin. Investig. Drugs* **2007**, *16*, 1921.

231. Mohammadi, K.; Thompson, K. H.; Patrick, B. O.; Storr, T.; Martins, C.; Polishchuk, E.; Yuen, V. G.; McNeill, J. H.; Orvig, C. *J. Inorg. Biochem.* **2005**, *99*, 2217.

232. Ozaki, K.; Takeda, H.; Iwahashi, H.; Kitano, S.; Hanazawa, S. *FEBS Lett.* **1997**, *410*, 297.

233. Ozaki, K.; Kawata, Y.; Amano, S.; Hanazawa, S. *Biochem. Pharmacol.* **2000**, *59*, 1577.

234. Singh, S.; Aggarwal, B. B. *J. Biol. Chem.* **1995**, *270*, 24995.

235. Bharti, A. C.; Takada, Y.; Aggarwal, B. B. *J. Immunol.* **2004**, *172*, 5940.

236. French, D. L.; Muir, J. M.; Webber, C. E. *Phytomedicine* **2008**, *15*, 1069.

237. Péret-Almeida, L.; Cherubino, A. P. F.; Alves, R. J.; Dufossé, L.; Gloria, M. B. A. *Food Res. Int.* **2005**, *38*, 1039.

238. Smith, R. M.; Witowska, B. A. *Analyst* **1984**, *109*.

239. Jayaprakasha, G. K.; Jagan Mohan Rao, L.; Sakariah, K. K. *J. Agric. Food Chem.* **2002**, *50*, 3668.

240. Gupta, A. P.; Gupta, M. M.; Kumar, S. *J. Liq. Chromatogr. Rel. Technol.* **1999**, *22*, 1561.

241. Paramasivam, M.; Poi, R.; Banerjee, H.; Bandyopadhyay, A. *Food Chem.* **2009**, *113*, 640.

242. Patel, K.; Krishna, G.; Sokoloski, E.; Ito, Y. *J. Liq. Chromatogr. Rel. Technol.* **2000**, *23*, 2209.

243. Nhujak, T.; Saisuwan, W.; Srisa-Art, M.; Petsom, A. *J. Sep. Sci.* **2006**, *29*, 666.

244. Borsari, M.; Ferrari, E.; Grandi, R.; Saladini, M. *Inorg. Chim. Acta* **2002**, *328*, 61.

245. Bernabé-Pineda, M.; Ramírez-Silva, M. T.; Romero-Romo, M. A.; González-Vergara, E.; Rojas-Hernández, A. *Spectrochim. Acta, Part A* **2004**, *60*, 1105.

246. Barik, A.; Mishra, B.; Kunwar, A.; Kadam, R. M.; Shen, L.; Dutta, S.; Padhye, S.; Satpati, A. K.; Zhang, H.-Y.; Indira Priyadarsini, K. *Eur. J. Med. Chem.* **2007**, *42*, 431.

247. Kühlwein, F.; Polborn, K.; Beck, W. *Z. Anorg. Allg. Chem.* **1997**, *623*, 1211.

248. Dutta, S.; Murugkar, A.; Gandhe, N.; Padhye, S. *Met.-Based Drugs* **2001**, *8*, 183.

249. Seltzer, M.; Fallis, S.; Hollins, R.; Prokopuk, N.; Bui, R. *J. Fluoresc.* **2005**, *15*, 597.

250. Song, Y. M.; Xu, J. P.; Ding, L.; Hou, Q.; Liu, J. W.; Zhu, Z. L. *J. Inorg. Biochem.* **2009**, *103*, 396.

251. Vajragupta, O.; Boonchoong, P.; Berliner, L. J. *Free Radic. Res.* **2004**, *38*, 303.

252. Rasmussen, H. B.; Christensen, S. B.; Kvist, L. P.; Karazmi, A. *Planta Med.* **2000**, *66*, 396.

253. Thompson, K. H.; Böhmerle, K.; Polishchuk, E.; Martins, C.; Toleikis, P.; Tse, J.; Yuen, V.; McNeill, J. H.; Orvig, C. *J. Inorg. Biochem.* **2004**, *98*, 2063.

254. Walters, D.; Muff, R.; Langsam, B.; Born, W.; Fuchs, B. *Invest. New Drugs* **2008**, *26*, 289.

255. Chen, W.-F.; Deng, S.-L.; Zhou, B.; Yang, L.; Liu, Z.-L. *Free Radic. Biol. Med.* **2006**, *40*, 526.

256. Ahsan, H.; Parveen, N.; Khan, N. U.; Hadi, S. M. *Chem. Biol. Interact.* **1999**, *121*, 161.

257. Sandur, S. K.; Pandey, M. K.; Sung, B.; Ahn, K. S.; Murakami, A.; Sethi, G.; Limtrakul, P.; Badmaev, V.; Aggarwal, B. B. *Carcinogenesis* **2007**, *28*, 1765.

258. Hogan, P. G.; Chen, L.; Nardone, J.; Rao, A. *Genes Dev.* **2003**, *17*, 2205.

259. Collin-Osdoby, P.; Yu, X.; Zheng, H.; Osdoby, P. RANKL-Mediated Osteoclast Formation from Murine RAW 264.7 Cells. In *Methods in Molecular Medicine: Bone Research Protocols*; Helfrich, M. H.; Ralston, S., Eds.; Humana Press: Totowa, 2003; Vol. 80, p 153.

260. Kalu, D. N. *Bone Miner.* **1991**, *15*, 175.

261. Damment, S. J. P.; Cox, A. G.; Secker, R. *Toxicol. Lett.* **2009**, *188*, 223.

262. Damment, S. J. P.; Secker, R.; Shen, V.; Lorenzo, V.; Rodriguez, M. *Nephrology Dialysis Transplantation* **2011**, *26*, 1803.

263. Pennick, M.; Dennis, K.; Damment, S. J. P. *J. Clin. Pharmacol.* **2006**, *46*, 738.

264. Levey, A. S.; Bosch, J. P.; Lewis, J. B.; Greene, T.; Rogers, N.; Roth, D.; for the Modification of Diet in Renal Disease Study, G. *Ann. Intern. Med.* **1999**, *130*, 461.

265. Bain, S. D.; Jerome, C.; Shen, V.; Dupin-Roger, I.; Ammann, P. *Osteoporos. Int.* **2009**, *20*, 1417.

266. McManus, J. F.; Davey, R. A.; MacLean, H. E.; Doust, E. A.; Chiu, W. S. M.; Sims, N. A.; Bouxsein, M. L.; Glatt, V.; Zajac, J. D.; Danks, J. A. *Bone* **2008**, *42*, 1164.

267. Sobczak, A.; Kowalski, Z.; Wzorek, Z. *Acta Bioeng. Biomech.* **2009**, *11*, 23.

268. Haberko, K.; Bućko, M. M.; Brzezińska-Miecznik, J.; Haberko, M.; Mozgawa, W.; Panz, T.; Pyda, A.; Zarębski, J. *J. Eur. Ceram. Soc.* **2006**, *26*, 537.

269. Xiaoying, L.; Yongbin, F.; Dachun, G.; Wei, C. *Key Eng. Mater.* **2007**, *213*, 342.

270. Galezowska, J.; Gumienna-Kontecka, E. *Coord. Chem. Rev.* **2012**, *256*, 105.

271. Vitha, T.; Kubíček, V. c.; Hermann, P.; Elst, L. V.; Muller, R. N.; Kolar, Z. I.; Wolterbeek, H. T.; Breeman, W. A. P.; Lukeš, I.; Peters, J. A. *J. Med. Chem.* **2008**, *51*, 677.

272. Song, B.; Kurokawa, G. S.; Liu, S.; Orvig, C. *Can. J. Chem.* **2001**, *79*, 1058.

273. Wheelwright, E. J.; Spedding, F. H.; Schwarzenbach, G. *J. Am. Chem. Soc.* **1953**, *75*, 4196.

274. Kumar, K.; Chang, C. A.; Francesconi, L. C.; Dischino, D. D.; Malley, M. F.; Gougoutas, J. Z.; Tweedle, M. F. *Inorg. Chem.* **1994**, *33*, 3567.

275. Holloway, J. H.; Reilley, C. N. *Anal. Chem.* **1960**, *32*, 249.

276. Byegard, J.; Skarnemark, G.; Skalberg, M. *J. Radioanal. Nucl. Chem.* **1999**, *241*, 281.

Appendix

Table A.1. ^{1}H NMR shifts of alkylhydroxyl-3-hydroxy-4-pyridinones compared to dihydrogenphosphate-3-hydroxy-4-pyridinones.

Compound	Solvent	H_a	H_b	Ring CH_3	CH_2-OH or CH-OH	Alkyl protons		
H1	D_2O	7.62	6.49	2.40	4.20	3.85		
H11	D_2O	7.41	6.36	2.37	4.22	3.98		
H2•HCl	D_2O	8.02	7.07	2.58	3.63	4.40	2.05	
H12	0.1M NaOD	7.40	6.37	2.38	4.09 - 4.19	3.73 - 3.80	2.00	
H3•HCl	D_2O	8.00	7.05	2.55	3.57	4.31	1.76 - 1.91	1.48 - 1.62
H13	D_2O	7.68	6.40	2.46	4.07 - 4.18	3.92	1.99	1.58 - 1.77
H4	D_2O	7.62	6.50	2.42	4.20 3.88 - 4.23	3.91 - 4.23	1.23	
H14	D_2O	8.13	7.24	2.70	4.60	4.46	1.46	
H6	D_2O	7.74	6.60	2.45	3.74 - 3.92	4.53	1.64 - 1.94	0.78
H15	D_2O	7.76	6.59	2.48	3.99; 3.87 - 3.96	4.52 - 4.70	1.88 - 2.00; 1.73 - 1.86	0.78

Table A.2. Isotopic distribution observed in the ESI-MS spectra of Ln(**L**)$_3$ metal complexes.

	Formula	Fragment	*m/z*								
La(**1**)$_3$	C$_{24}$H$_{30}$LaN$_3$O$_9$	[M+H]$^+$	644.1;	645.1	646.2						
Calculated mass			644.11	645.12; 645.11	646.12						
Intensity (%)			100.0	26.7; 1.1	5.3						
Eu(**1**)$_3$	C$_{24}$H$_{30}$EuN$_3$O$_9$	[M+H]$^+$	656.3	657.2	658.2	659.2	660.2				
Calculated mass			656.13	657.13	658.13	659.13; 659.12	660.13				
Intensity (%)			87.2	23.3	100.0	25.9; 1.1	5.2				
Lu(**1**)$_3$	C$_{24}$H$_{30}$LuN$_3$O$_9$	[M+H]$^+$	680.1	681.2	682.1						
Calculated mass			680.15	681.15; 682.14	682.15						
Intensity (%)F			100.0	29.3; 1.1	6.2						
La(**2**)$_3$	C$_{27}$H$_{36}$LaN$_3$O$_9$	[M+H]$^+$	686.2	687.2	688.3						
Calculated mass			686.16	687.16	688.17; 688.16						
Intensity (%)			100.0	30.6	4.3; 2.2						
Eu(**2**)$_3$	C$_{27}$H$_{36}$EuN$_3$O$_9$	[M+H]$^+$	698.3	699.3	700.3	701.2	702.3				
Calculated mass			698.17	699.18; 699.17	700.17; 700.18	701.18 701.17	702.18				
Intensity (%)			91.3	27.4; 1.0	100.0; 5.7	30.8; 1.1	6.3				
Gd(**2**)$_3$	C$_{27}$H$_{36}$GdN$_3$O$_9$	[M+Na]$^+$	723.0	724.2	725.2	726.2	727.2	728.2	729.2	730.1	
Calculated			723.16	724.16	725.16	726.16	727.16	728.16;	729.16;	730.17	731.17

	Formula	Fragment	*m/z*								
mass									728.17	729.17	
Intensity (%)			7.1	49.9	80.9	734	100.0	26.1; 2.9	72.4; 4.0	22.0	4.5
Lu(**2**)₃	C₂₇H₃₆LuN₃O₉		722.3	723.2	724.3						
Calculated mass			722.19	723.20; 723.19	724.20	725.20					
Intensity (%)			100.0	32.6; 1.1	7.0	1.2					
La(**3**)₃	C₃₀H₄₂LaN₃O₉	[M+H]⁺	728.2	729.2	730.2						
Calculated mass			728.21	729.21; 729.20	730.21						
Intensity (%)			100.0	33.3; 1.1	7.4						
Eu(**3**)₃	C₃₀H₄₂EuN₃O₉	[M+H]⁺	740.4	741.3	742.3	743.3	744.3				
Calculated mass			740.22	741.22	742.22; 742.23	743.22;743.23	744.23	745.23			
Intensity (%)			89.8	30.4	100.0; 4.8	33.0; 1.9	7.2	1.2			
Lu(**3**)₃	C₃₀H₄₂LuN₃O₉	[M+H]⁺	764.4	765.3	766.4						
Calculated mass			764.24	765.24	766.25; 766.24	767.25					
Intensity (%)			100.0	36.6	6.2; 2.2	1.4					
La(**4**)₃	C₂₇H₃₆LaN₃O₉	[M+H]⁺	686.2	687.2	688.3						
Calculated mass			686.16	687.16	688.17; 688.16						
Intensity (%)			100.0	30.6	4.3; 2.2						
Eu(**4**)₃	C₂₇H₃₆EuN₃O₉	[M+H]⁺	698.3	699.3	700.3	701.2	702.3	703.4			
Calculated mass			698.17	699.18; 699.17	700.17; 700.18	701.18; 701.17	702.18				
Intensity (%)			91.3	27.4; 1.0	100.0; 5.7	30.8; 1.1	6.3				
Gd(**4**)₃	C₂₇H₃₆GdN₃O₉	[M+H]⁺	701.4	702.4	703.4	704.4	705.4	706.3	707.3	708.3	709.3

227

	Formula	Fragment	*m/z*								
Calculated mass			701.17	702.18	703.18	704.18	705.18	706.18	707.18	708.18	709.19; 709.18
Intensity (%)			7.0	49.9	80.9	73.5	100.0	27.7	76.1	22.1	3.2; 1.5
Lu(**4**)₃	C₂₇H₃₆LuN₃O₉	[M+H]⁺	722.4	723.2	724.3	725.4					
Calculated mass			722.19	723.20; 723.19	724.20	725.20					
Intensity (%)			100.0	32.6; 1.1	7.0	1.2					
La(**5**)₃	C₃₃H₄₈LaN₃O₉	[M+Na]⁺	792.2	793.2	794.2						
Calculated mass			792.24	793.24; 793.23	794.24						
Intensity (%)			100.0	36.6%; 1.1%	8.7%						
La(**6**)₃	C₃₀H₄₂LaN₃O₉	[M+H]⁺	728.3	729.2	730.2						
Calculated mass			728.21	729.21	730.21	729.20					
Intensity (%)			100.0	33.3	7.4	1.1					
Eu(**6**)₃	C₃₀H₄₂EuN₃O₉	[M+H]⁺	740.5	741.4	742.4	743.3	744.4	745.4	746.3		
Calculated mass			740.22	741.22	742.22; 742.23	743.22;743.23	744.23	745.23			
Intensity (%)			89.8	30.4	100.0; 4.8	33.0; 1.9	7.2	1.2			
Gd(**6**)₃	C₃₀H₄₂GdN₃O₉	[M+H]⁺	743.2	744.4	745.4	746.4	747.3	748.3	749.3	750.3	751.3
Calculated mass			743.22	744.22	745.22; 745.23	746.22 ;746.23	747.2;2 747.23	748.23; 748.22	749.23	750.23	751.23
Intensity (%)			8.7	61.9	82.3; 20.3	63.5; 31.5	100.0; 27.4	38.5; 1.3	95.1	30.3	6.6
Lu(**6**)₃	C₃₀H₄₂LuN₃O₉	[M+H]⁺	764.4	765.4	766.3	767.3					
Calculated mass			764.24	765.24	766.25; 766.24	767.25					
Intensity (%)			100.0	36.6	6.2; 2.2	1.4					

	Formula	Fragment	m/z								
Na₃La(**8**)₃	Na₃C₂₄H₂₁LaN₃O₁₂	[M-2Na+H]⁻	706.0	707.0	708.0						
Calculated mass			706.02	707.02; 707.01	0708.02						
Intensity (%)			100.0	26.7; 1.1	6.1						
Na₃Eu(**8**)₃	Na₃C₂₄H₂₁EuN₃O₁₂	[M-2Na+H]⁻	718.0	719.0	720.0	721.0	722.7				
Calculated mass			718.03	719.03	720.03; 720.04	721.03; 721.04	722.04				
Intensity (%)			89.3	24.6	100.0; 3.1	26.5; 1.5	5.9				
Na₃Gd(**8**)₃	Na₃C₂₄H₂₁GdN₃O₁₂	[M-2Na+H]⁻	721.0	722.0	723.0	724.0	725.0	726.0	727.1	728.0	729.0
Calculated mass			721.03	722.03	723.03; 723.04	724.03; 724.04	725.03; 725.04	726.04; 726.03	727.04	728.04	729.04
Intensity (%)			8.7	61.4	82.3; 16.3	63.5; 25.3	100.0; 22.0	30.9; 1.3	93.7	24.2	5.4
Na₃Lu(**8**)₃	Na₃C₂₄H₂₁LuN₃O₁₂	[M-3Na+2H]⁻	720.1	721.1	722.1	723.1					
Calculated mass	m/z:, , ,		720.07	721.07	722.07; 722.08	723.08					
Intensity (%)			100.0	30.2	3.5; 3.4	1.1					
Na₃La(**9**)₃	Na₃C₂₇H₂₇LaN₃O₁₂	[M-2Na+H]⁻	748.1	749.1	749.2	750.1					
Calculated mass			748.06	749.07; 749.06	750.07	751.07					
Intensity (%)			100.0	30.0; 1.1	6.8	1.2					
Na₃Eu(**9**)₃	Na₃C₂₇H₂₇EuN₃O₁₂	[M-3Na+2H]⁻	738.1	739.1	740.1	741.1	742.1				
Calculated mass			738.09	739.10	740.10; 741.09	741.10	742.10				
Intensity (%)			86.0	25.8	100.0; 1.0	28.8	6.6				
Na₃Gd(**9**)₃	Na₃C₂₇H₂₇GdN₃O₁₂	[M-3Na+2H]⁻	741.1	742.1	743.1	744.1	745.1	746.1	747.1	748.1	749.1
Calculated mass	m/z:, ,), , , ,		741.10	742.10	743.10	744.10	745.10	746.10; 746.11	747.10; 747.11	748.11	749.11

	Formula	Fragment	*m/z*								
Intensity (%)			7.1	49.7	80.6	73.4	100.0	26.5; 2.8	72.6; 4.2	22.1	4.9
Na$_3$Lu(**9**)$_3$	Na$_3$C$_{27}$H$_{27}$LuN$_3$O$_{12}$	[M-2Na+H]$^-$	784.1	785.1	786.1	787.1					
Calculated mass			784.10	785.10; 785.09	786.10	787.11					
Intensity (%)			100.0	32.6; 1.1	7.7	1.3					

Figure A.1. Speciation diagrams for solutions containing 1 mM M^{3+} and 3 mM $HL1$: a) La^{3+}; b) Gd^{3+}.

a)
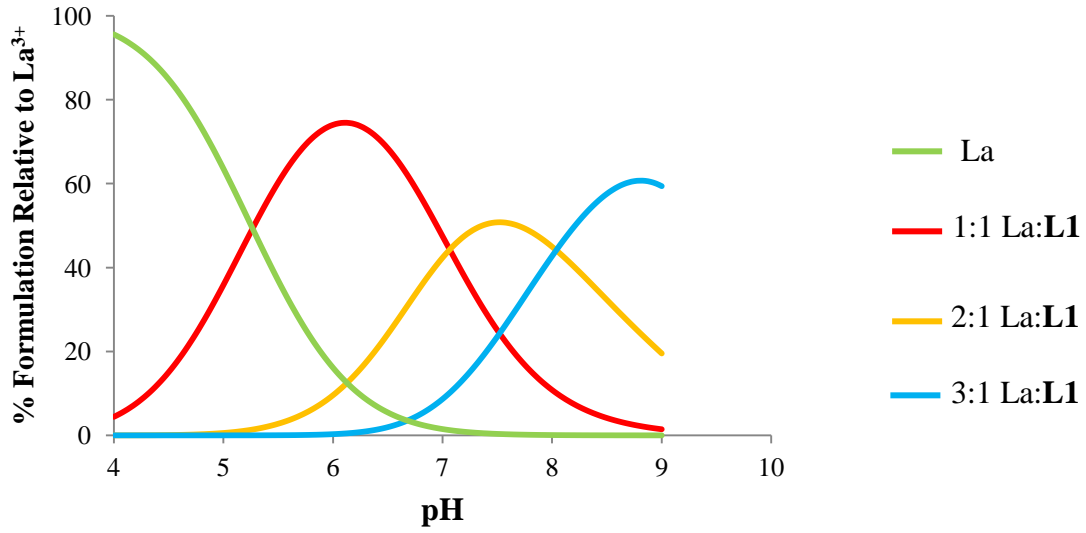
b)
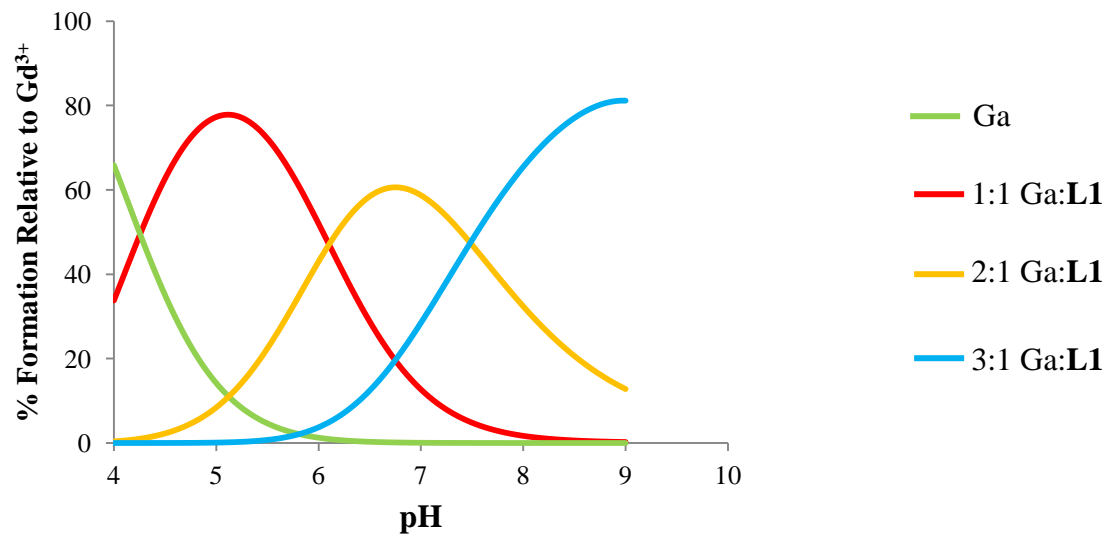
Table A.3. Mean percentage ± SD of Ln(III) bound to HAP, n = 3.

Compound Time	La(4)$_3$			Eu(8)$_3$			La(9)$_3$			LaXT		
	% Ln(III) Bound			% Ln(III) Bound			% Ln(III) Bound			% Ln(III) Bound		
5 min	91.6	±	8.7	97.4	±	0.6	99.3	±	0.5	99.5	±	0.1
15 min	92.7	±	7.7	97.2	±	0.7	98.6	±	0.5	99.8	±	0.1
3 hr	91.8	±	8.9	96.6	±	0.9	99.5	±	0.5	99.7	±	0.1
24 hr	91.2	±	9.4	97.0	±	0.7	99.0	±	0.4	99.7	±	0.1

Figure A.2. Speciation diagrams for solutions containing 1 mM La^{3+} and 1 mM H$_5$**XT**.